Université Libre de Bruxelles
Département de Physique

Università degli Studi di Torino
Dipartimento di Fisica

MATRIX MODELS FOR HOLOGRAPHY AND SUPERSYMMETRIC LOCALIZATION

Submitted by:
Paolo Gregori

Supervisors:
Prof. Marco Billò
Prof. Frank Ferrari

Academic year
2017-2018

Contents

I Introduction and Background **1**

1 Introduction **2**
1.1 General context 2
1.2 Outline of the thesis 4

2 The gauge/gravity correspondence **7**
2.1 D-branes 7
2.1.1 Chan-Paton factors 9
2.2 The correspondence 10
2.2.1 The example of $\mathcal{N} = 4$ SYM 11
2.2.2 The example of D0-brane quantum mechanics 12
2.3 Take-home message 13

II Simple models of Holography **14**

3 Simple models of Holography **15**
3.1 General properties 15
3.1.1 Chaotic behaviour of correlators 16
3.1.2 Models with probes 17
3.2 The IP and IOP models 19
3.2.1 Introduction 19
3.2.2 Definition of the IP model 20
3.2.3 Large M computation 20
3.2.4 Bose-Einstein condensation 22
3.2.5 Definition of the IOP model 25
3.2.6 Large M computation 25
3.2.7 Concluding remarks 27
3.3 Melonic models 27
3.3.1 The Sachdev-Ye-Kitaev model 28
3.3.2 The Gurau-Witten model 30
3.3.3 Quartic matrix-vector model 31

4 Diagrammatics and bilocal structure of melonic models **33**
4.1 SYK diagrammatics . . . 33
4.2 Large D matrix model diagrammatics . . . 35
4.2.1 Models . . . 35
4.2.2 Genus of a vertex . . . 35
4.2.3 Standard scaling vs. new scaling . . . 36
4.2.4 Proof . . . 37
4.3 More on the new large D limit of matrix models . . . 39
4.3.1 Multi-trace models . . . 39
4.3.2 Models with reduced symmetry . . . 39
4.3.3 Correlation functions . . . 40
4.3.4 Model building . . . 40
4.4 Bilocal structure . . . 41
4.4.1 An instructive computation . . . 41

5 Physical properties of melonic models **44**
5.1 Two-point functions and emergent symmetry . . . 44
5.2 Low temperature entropy . . . 47
5.3 Four-point functions and chaos . . . 47
5.4 Phase structure of complex melonic models . . . 50

6 Quartic matrix-vector models **52**
6.1 Definition and properties of the model . . . 52
6.1.1 Leading diagrams for $\lambda_1 = 0$ . . . 53
6.1.2 Including the $I_{4,1}$ interaction term . . . 55
6.1.3 Two-point functions . . . 56
6.1.4 Writing the free energy in terms of the Matsubara coefficients G_k . . . 57
6.2 Probe analysis . . . 61
6.2.1 Generalities . . . 62
6.2.2 A toy example . . . 63
6.2.3 Probe analysis of the quartic matrix-vector model . . . 65
6.2.4 Test of the fundamental relation for the on-shell probe action 71

III Localization in $\mathcal{N} = 2$ SQCD **74**

7 Models and observables **75**
7.1 Introduction . . . 75
7.2 $\mathcal{N} = 4$ SYM and $\mathcal{N} = 2$ SCQCD . . . 76
7.3 Supersymmetric Wilson loops . . . 80
7.3.1 The circular 1/2 BPS Wilson loop in $\mathcal{N} = 2$ SYM . . . 81

8 Localization **83**
8.1 Overview . . . 83
8.1.1 Super Yang-Mills on S^4 . . . 84
8.2 Correlators of chiral operators . . . 89
8.2.1 From S^4 to $\mathbb{R}_4$ . . . 89
8.2.2 Localization results . . . 91
8.2.3 Perturbative checks . . . 93
8.3 1/2-BPS circular Wilson loops . . . 96
8.3.1 Localization results in $\mathcal{N} = 4$ SYM and their interpretation 96
8.3.2 Localization results in $\mathcal{N} = 2$ SCQCD and their interpretation 99
8.4 Correlators between Wilson loop and chiral operators in $\mathcal{N} = 2$ conformal gauge theories . . . 101
8.4.1 Wilson loop and its correlators with chiral operators . . . 101
8.4.2 The matrix model approach . . . 102
8.4.3 Perturbative checks in field theory . . . 102

A Publication I:
More on the new large D limit of matrix models **103**

B Publication II:
Correlators between Wilson loop and chiral operators in $\mathcal{N} = 2$ conformal gauge theories **123**

Bibliography **162**

Part I

Introduction and Background

Chapter 1

Introduction

1.1 General context

Our current understanding of the four fundamental interactions relies mainly on two theories that do not seem to have much in common: the Standard Model and General Relativity. The first is a quantum field theory (QFT) that describes electromagnetic, weak and strong interactions with excellent agreement with the experimental results. To be more precise, it is a gauge theory and all the fields that appear in its Lagrangian are associated to the well-known fundamental particles (electrons, quarks, photons, etc.). General Relativity (GR) on the other hand is a classical theory that provides a geometrical interpretation to all gravitational phenomena. Gravitation is described in terms of the curvature of spacetime, whose metric encodes the fundamental degrees of freedom of the theory. As in the case of the Standard Model, also the theoretical predictions of GR are confirmed by experiments and observations with extreme accuracy, with the recent obervation of gravitational waves being perhaps one of its most striking successes.

Nevertheless, theoretical physicists are unsatisfied with this picture. The scales at which we are able to test GR are very far from the Planck scale, at which quantum effects are expected to become important for gravitational interactions, and GR would stop being reliable. The idea that GR should be regarded just as an effective theory, in the sense that it represents only the classical limit of a quantum theory of gravity, is substantiated by several arguments. One of them is the breakdown of GR near curvature singularities like black holes, which are expected to be "resolved" by quantum effects. Moreover, paradoxes arise when one tries to combine quantum mechanics and GR, showing a superficial incompatibility. For example, one of the results of GR are the classical no-hair theorems, which state that black hole solutions in four dimensions can be characterized by only three parameters (mass, electric charge and angular momentum), thus suggesting they can only have a single microstate. This is in sharp contrast with the computation of the Bekenstein-Hawking entropy $S_{BH} \propto A/4l_p^2$ [3, 4, 5], which implies that black holes have a number of microstates proportional to the area of their event horizon. Similarly, another semi-classical result by Hawking states that black holes

evaporate by emitting thermal radiation [6]. The outcome is that all information carried by a quantum state (which could in principle be a pure state) that falls into a black hole is lost after the black hole has evaporated into a thermal bath of radiation: this seems to contradict unitarity, one of the governing principles of quantum mechanics.

Such considerations make the search for a theory of quantum gravity one of the main goals of theoretical physics, but the task proved to be far from trivial. Any attempt to directly quantize gravity using standard QFT techniques results in untamable divergencies as the theory is perturbatively non-renormalizable [7, 8]. A different framework that initially gave hope for a solution of the problem is that of Superstring Theory. As a well-defined, UV-complete quantum theory that contains both the ingredients of gauge theories like the Standard Model and a massless spin-2 field with the same properties of the graviton (the mediator of the gravitational interaction in quantum gravity), Superstring Theory seemed like a good candidate for the long-sought Theory of Everything. Although this program has not produced yet the wished results, string theory served and serves today as an amazing playground for the study of both gauge theories and gravity, and it produced an extremely powerful duality: the AdS/CFT correspondence. On one side of this duality we have string theory defined on a ten-dimensional spacetime which is the product of five-dimensional Anti de Sitter (AdS) space and a five-sphere. On the other side we have an SU(N) gauge theory called super Yang-Mills theory (SYM), which is also a conformal field theory (CFT), defined on a four-dimensional Minkowski spacetime (for reviews on the AdS/CFT correspondence, see [9, 10]). Since superstring theory contains quantum gravity (in particular it reduces to supergravity (SUGRA) in the low energy limit), this correspondence is a concrete realization of the gauge/gravity duality. Also, it relates a theory of gravity in ten dimensions, which is often referred to as the "bulk theory", to a QFT which can be seen as being defined on the four-dimensional boundary of AdS_5, hence, the "boundary theory". Therefore, this correspondence is the first precise and well-defined realization of the holographic principle, an idea already envisioned by 't Hooft and Susskind [11, 12].

Therefore, the gauge/gravity duality seems like the perfect framework for addressing in a completely unitary and well-defined setup some of the above-mentioned puzzles. More precisely, the correspondence is best understood when superstring theory can be reliably approximated by supergravity, which corresponds to suppressing all quantum and higher-derivative effects on the gravity side. On the QFT side of the duality, this typically corresponds to taking the limit in which the rank N of the gauge symmetry group is large and the theory is strongly coupled. This regime of parameter space is notoriously hard to study: although the $N \to \infty$ limit reduces the Feynman diagrams that contribute to the gauge theory to just those that can be drawn on a sphere [13] (the so-called planar diagrams), the complete sum over such diagrams which is required to study the theory at strong coupling is not yet computable for the most interesting cases. This is not the only difficulty one encounters when trying to apply

the gauge/gravity duality: while the correspondence itself has passed many convincing tests, some aspects of the dictionary between the two theories it relates are still to be completely understood. This is also due to the general scarcity of concrete realizations of the correspondence.

Therefore, in order to improve our understanding of the inner workings of the gauge/gravity correspondence and exploit it to understand the deep questions associated with both classical and quantum gravity there are two main topics which need to be addressed:

- the development of tools for the study of strongly coupled gauge theories,
- the formulation of more tractable, yet interesting, examples of realizations of the gauge/gravity correspondence.

The first line of research has received a great boost in recent years thanks to the development of the powerful techniques offered by supersymmetric localization. Localization is a method that allows to obtain exact results in supersymmetric gauge theories by reducing the infinite-dimensional path integral of the theory to finite integrals localized on a set of fixed points. This allows for the computation of the partition function and of several observables for any value of the coupling constant in a number of supersymmetric theories. The third part of this thesis will be devoted to this approach, with particular emphasis on the computation of Wilson loops and correlators of chiral operators in $\mathcal{N} = 2$ super Yang-Mills using localization techniques. Regarding the second line of research, which concerns the formulation of new simple examples of the gauge/gravity duality, a lot of progress has been made in the past few years by engineering quantum mechanical models, usually defined in 0+1 dimensions, which are simplified versions of boundary gauge theories. Several examples of such models have been proposed over the years, many of which featuring non-trivial characteristics which indeed correspond to expected properties of a putative gravitational bulk dual. They are typically engineered in such a way that they should be simple enough to be solvable or at least tractable in the strongly coupled regime but non-trivial enough to reproduce the interesting physics of holography. The general properties of such models and some explicit examples will be discussed in the second section of the thesis.

1.2 Outline of the thesis

This thesis is based on the original research work presented in:

- T. Azeyanagi, F. Ferrari, P.G., L. Leduc, and G. Valette, "More on the New Large D Limit of Matrix Models", *Annals Phys.* **393** (2018) 308 326, arXiv:1710.07263 [hep-th] [1]
- M. Billò, F. Galvagno, P.G. and A. Lerda, "Correlators between Wilson loop and chiral operators in N=2 conformal gauge theories", *JHEP* **03**, 193 (2018), arXiv:1802.09813 [hep-th] [2]

The former concerns the study of a new large D limit developed in the study of U(N) matrix models which also feature an additional global O(D) symmetry. The latter focuses on the computation of one-point correlation functions of chiral operators in presence of a 1/2-BPS Wilson loop in conformal $\mathcal{N} = 2$ super Yang-Mills theory. The thesis is organized as follows: the first part serves as a brief review of the gauge/gravity correspondence. In the second part, after a review of the main properties we expect to find in models of holography, several such models are presented. Among them, we define precisely matrix-vector models, which are then studied in detail in [1]. Finally, the third part is devoted to a review of the localization techniques and the main results of their application, including those contained in [2].

Part one

The aim of this part is to provide a justification to the research work this thesis is based on by placing it in the context of the gauge/gravity correspondence. First, an introductory section briefly reviews the current challenges one has to face in the quest for a theory of quantum gravity and emphasizes the role of the gauge/gravity correspondence as a suitable framework for addressing such non-trivial questions. Moreover, we present some obstacles in the application of the correspondence which serve as a motivation for the research carried out by the author. Then, a chapter is devoted to a more precise definition of the correspondence, with particular emphasis on how the boundary gauge theories arise from D-brane constructions. Two explicit realizations of the duality which are especially relevant to the research of the author are presented. The first one is the case of four-dimensional $\mathcal{N} = 4$ super Yang-Mills theory, which is dual to string theory defined in $\mathrm{AdS}_5 \times S^5$. This gauge theory will appear again in Part III, as it is instrumental in the study of the closely related $\mathcal{N} = 2$ super Yang-Mills. The second example is D0-brane quantum mechanics. As a simple, albeit non-solvable, quantum mechanical model in 0+1 dimensions, it shares some of the features of the models which will be presented in Part II. A brief summary of the main ingredients that will play a role in the rest of the thesis serves as a conclusion to Part I.

Part two

The second part is devoted to a possible approach to the scarcity of realizations of the gauge/gravity correspondence which are solvable on both sides of the duality, namely the construction and study of simple models of holography. In the first chapter, we initially review the general properties one should look for in simplified versions of the boundary gauge theories. These are properties that are connected to specific features of gravitational bulk theories, especially those which contain black holes. Among them, we have the quasi-normal behaviour of two-point functions, a continuous energy spectrum and, in the case of extremal black holes, a

non-vanishing entropy at zero temperature. Moreover, a non-trivial property that has received a lot of interest in the recent literature is the chaotic behaviour of out-of-time-order correlators (OTOC), which is treated in more detail in this section. Then, several models are introduced with their most interesting properties. The models are divided essentially in two classes: first the Iizuka-Polchinski and Iizuka-Okuda-Polchinski models, which are inspired by probe brane systems. Such systems feature both vector and matrix degrees of freedom interacting with each other. Secondly, melonic models are introduced: the Sachdev-Ye-Kitaev model, the Gurau-Witten model and U(N) matrix models with global O(D) symmetry. These models are apparently very different from each other but in a suitable limit they display the same Feynman diagram structure, which eventually leads to the same physical properties. The second chapter of Part II is devoted to the study of the diagrammatics of melonic models, and how it is related to the property of bilocality. The subtleties associated with the large D limit of planar diagrams of $U(N)$ matrix models are developed in detail, as this serves as an introduction to the original contributions contained in [1], where generalizations of such models were studied, including multi-trace interactions, as well as bosonic and supersymmetric models. Then, it is shown how the diagrammatic structure (and therefore bilocality) of melonic models translates into their many non-trivial properties, all of which were introduced in the first chapter. The final chapter of Part II is entirely devoted to the study of quartic matrix-vector models and contains several original results, including a computation of the free energy of the model through a probe analysis.

Part three

The final part of the thesis focuses entirely on supersymmetric localization, which provides useful tools for the study of gauge theories in the strongly coupled regime and has been used to test and improve the understanding of the AdS/CFT correspondence. One chapter is devoted to presenting the two supersymmetric theories which are relevant to the author's research: $\mathcal{N} = 4$ and $\mathcal{N} = 2$ super Yang-Mills (SYM) in four dimensions. The two models are presented using the $\mathcal{N} = 1$ superfield formalism, and a few comments are made on the superconformal limit of $\mathcal{N} = 2$ SYM. The second chapter starts with an overview of the localization technique applied to $\mathcal{N} = 2$ SYM defined on S^4. It is shown how the full field theory path integral in $\mathcal{N} = 4$ and $\mathcal{N} = 2$ SYM reduces to a matrix model integration, and the differences between the two matrix models are explored. Some subtleties associated with the computation of observables through localization are presented, in particular those related to operator mixing, which leads to a non-trivial normal ordering prescription in matrix model computations. Moreover, the main observables which can be computed through localization are presented: correlators of chiral operators, Wilson loops and finally one-point functions of chiral operators in presence of Wilson loops, whose computation is at the core of [2].

Chapter 2

The gauge/gravity correspondence

The gauge/gravity correspondence is a powerful tool which can be used to gain insight on both sides of the duality. The main difficulty in this approach is that the best understood formulations of the duality involve the strongly coupled regime and the planar limit of the boundary gauge theory. Since the gauge/gravity correspondence was originally formulated in the context of Dirichlet-branes (D-branes) dynamics, it is instructive to review some of their basic properties. We will in particular emphasize the role played by the gauge theories that live on D-branes worldvolumes, their properties and their field content. After a general definition of the gauge/gravity duality, we will present two of its explicit realizations that are particularly relevant to this thesis: the case of $\mathcal{N} = 4$ super Yang-Mills (SYM) theory and the case of D0-brane quantum mechanics.

2.1 D-branes

In this section, for the sake of simplicity and in order to avoid heavy notations we will restrict ourselves to the case of 26-dimensional bosonic string theory, keeping in mind that the key concepts that will be addressed still apply in superstring theory, unless explicitly specified. Most of the concepts which will be introduced in this section can be found in the reviews [14, 15]. In this framework, the string worldsheet is a two-dimensional surface which can be parameterized by a spatial coordinate σ_1 and by a time coordinate σ_0 and which moves in 26-dimensional Minkowski spacetime. The position of the worldsheet in this ambient spacetime is given by $X_M(\sigma_0, \sigma_1)$, with M running from 0 to 25. The X_M are the fundamental degrees of freedom of bosonic string theory and their equations of motion are derived from the Nambu-Goto action

$$S_{NG} = -\frac{1}{2\pi\alpha'} \int d^2\sigma \sqrt{(\dot{X} \cdot X')^2 - (\dot{X}^2)(X'^2)}\,, \tag{2.1.1}$$

where $\dot{X}_M$ and X'_M are respectively the derivatives of X_M with respect to σ_0 and σ_1. The constant α' is called the universal Regge slope and has the units of a length squared. What distinguishes open strings from closed strings is the fact that for the first ones one has to impose a periodicity condition on σ_1, while for the second kind the endpoints do not coincide, and one has to assign boundary conditions to them. Let us now consider an open string and let σ_1 go from 0 to π. There are two kinds of boundary conditions one can impose on the X_M which are consistent with the equations of motion obtained from (2.1.1):

- Neumann boundary conditions: $\partial_{\sigma_1} X_M(0, \sigma_0) = \partial_{\sigma_1} X_M(\pi, \sigma_0) = 0$
- Dirichlet boundary conditions: $X_M|_{\sigma_1=0,\pi} = \text{constant}$

Note that imposing Dirichlet boundary conditions on $q = 25 - p$ of the 26 directions breaks the original $\mathrm{SO}(1, 25)$ Lorentz symmetry of the theory down to $\mathrm{SO}(q)\times\mathrm{SO}(1, p)$. This is how D$p$-branes made their first appearance in string theory: they are the p-dimensional hypersurfaces to which the endpoints of open strings are attached when one imposes Dirichlet boundary conditions on them. From now on, we will distinguish two kinds of indices associated to the coordinates in the ambient spacetime: μ, ν indices will go from 0 to p and will denote the directions in which Neumann boundary conditions are imposed, while i, j indices will go from $p + 1$ to 25 and denote the directions in which Dirichlet boundary conditions are imposed. By doing a mode expansion of the most general solution of the X_M equations of motion and performing the canonical quantization procedure we obtain, on top of the usual position and momentum operators, two infinite sets of creation and annihilation operators obeying

$$\begin{aligned} [\alpha^\mu_n, \alpha^\nu_{-m}] =& n\delta_{n,m}\delta^{\mu\nu} \\ [\alpha^i_n, \alpha^j_{-m}] =& n\delta_{n,m}\delta^{ij} \end{aligned} \tag{2.1.2}$$

which create and annihilate excitations on the string. Using these operators we can build the spectrum of excitations of open strings attached to a Dp-brane. Given the Fock vacuum state $|k\rangle$, which corresponds to a string with momentum k^μ and no excitations, one can act upon it with the two kinds of creation operators α^μ_{-m} and α^i_{-m} (with $m < 0$) to obtain excited states. The lightest states one can get through this procedure are:

- tachyon $\quad |k\rangle \quad M^2 = -1/\alpha'$
- vector $\quad \alpha^\mu_{-1}|k\rangle \quad M^2 = 0$
- scalars $\quad \alpha^i_{-1}|k\rangle \quad M^2 = 0$

where we also specified their mass squared. The tachyon is just an illness of 26-dimensional bosonic string theory which is solved in ten-dimensional superstring theory. We have two kinds of massless states: a spin-one particle, which is a $\mathrm{SO}(1, p)$ vector, and a set of $25 - p$ states which are scalars under the $\mathrm{SO}(1, p)$

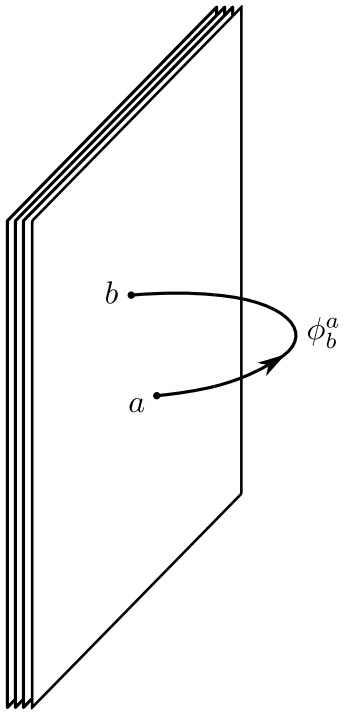

Figure 2.1: Sketchy representation of an open string attached to a stack of D-branes with Chan-Paton factors associated to its endpoints.

Lorentz symmetry of the $(p+1)$-dimensional spacetime spanned by the Dp-brane as the system evolves in time, which is also called the worldvolume of the D-brane. The scalars transform in the fundamental representation of $\mathrm{SO}(25-p)$, which is now a global symmetry of the worldvolume theory. These vector and scalar particle states we just introduced can be seen as quanta of fields and ϕ^i and A^μ respectively. The latter acts as the gauge connection of a U(1) gauge theory that lives on the $(p+1)$-dimensional brane worldvolume, while the former can be associated to fluctuations of the position of the D-brane in its transverse directions, making it a dynamical object, rather than just a static hyperplane to which open string endpoints can be attached.

2.1.1 Chan-Paton factors

So far we have dealt with open strings attached to a single Dp-brane, but this scenario can be easily generalized to the case of N parallel Dp-branes. Now we can associate additional non-dynamical degrees of freedom to the endpoints of open strings attached to the D-branes. They are called Chan-Paton factors and take the form of indices a and b running from 1 to N, which label the branes to which each endpoint is attached. The aforementioned scalar and vector fields will

therefore carry two indices:

$$\begin{array}{ccc} \phi^i & \rightarrow & (\phi^i)^a_b \\ A^\mu & \rightarrow & (A^\mu)^a_b \end{array} \tag{2.1.3}$$

In the case of coinciding D-branes, these fields remain massless: they now transform in the adjoint representation of U(N), with the vector being the gauge connection of the U(N) gauge theory that lives on the brane worldvolume. A schematic depiction of such a set-up is shown in Figure 2.1. As a side note, it should be pointed out that U(N) can be written as the product SU(N)×U(1), and it can be shown that the fields associated with the generator of the U(1) factor decouple from the theory [16]. That is why in the following we will always refer to the brane worldvolume gauge theories as SU(N) theories. As it will be explained in the next section, however, in the context of the gauge/gravity correspondence we are typically interested in the large N limit (or the planar limit) of such theories, therefore for our purposes the U(N) and SU(N) symmetry groups are interchangeable.

2.2 The correspondence

We have seen how gauge theories arise naturally in D-brane constructions, and that D-branes are in fact dynamical objects. Let us make this statement a bit more precise. In a similar way to how the scalar and vector fields arise from the open string spectrum, one can show that the massless states of the closed string spectrum are the quanta of three fields: a dilaton Φ, a graviton G_{MN} and an antisymmetric tensor B_{MN} (where the M and N indices run from 0 to 25). These objects are the same that we encounter in Einstein's gravity and indeed they are associated to the geometry of the ambient spacetime. The coupling between these gravitational fields and a D-brane is proportional to the string coupling g_s which is in turn determined by the expectation value of the dilaton

$$g_s = e^{\langle \Phi \rangle} .$$

The effect a stack of N D-branes has on the geometry of the ambient spacetime is therefore parameterized by $g_s N$: when its value is very small we can do perturbation theory around flat spacetime, but as it grows the backreaction of the D-branes on the bulk geometry becomes no longer negligible. More precisely, in the strong coupling limit $g_s N \gg 1$, the D-branes source a black-brane geometry, which corresponds to a specific supergravity solution. In the $g_s N \ll 1$ regime, taking a low energy limit amounts to decoupling the closed strings that propagate in the bulk from the open strings attached to the branes: we are left with a SU(N) gauge theory defined on a $(p+1)$-dimensional flat spacetime. On the other hand, taking the same low energy limit in the $g_s N \gg 1$ regime amounts to decoupling the modes that propagate in the asymptotic region of the black brane solution, leaving us only with those that live near the horizon of the background

geometry. So far we have described two regimes of the low energy limit of string theory which do not seem to overlap: a weak string coupling regime described by a SU(N) gauge theory in $p+1$-dimensions and a strong string coupling regime corresponding to string theory in the near-horizon limit of a black brane background. One can move from one regime to the other by continuously varying g_sN, and if we assume that this continuous change of g_sN commutes with taking the low energy limit we obtain an equivalence between the two regimes, given that the gauge theory is well-defined for all values of g_sN and not only in the weak string coupling regime. This equivalence between a SU(N) gauge theory and the full string theory on the near-horizon region of the black brane geometry is a formulation of the gauge/gravity correspondence. We cannot however trust the black brane supergravity solution for all values of the string theory parameters: it is valid only if we can neglect quantum corrections (which are parameterized by Newton's constant G_N) and higher derivative corrections (which in string theory are parameterized by α'). We will see in a couple of explicit examples how these prescriptions are implemented and how they translate in terms of the rank of the gauge group N and of its 't Hooft coupling λ.

2.2.1 The example of $\mathcal{N}=4$ SYM

Let us give a concrete example of the duality by showing some details of the first realization of the gauge/gravity correspondence as it was proposed by Maldacena in [17]. The framework is that of ten-dimensional superstring theory in the presence of N coinciding D3-branes. The near-horizon region of the black 3-brane geometry is given by the following metric

$$ds^2 = \frac{r^2}{L^2}\eta_{\mu\nu}dx^\mu dx^\nu + \frac{L^2}{r^2}dr^2 + L^2 d\Omega^2_{S^5}\,,$$

with $L^4 = 4\pi g_s N \alpha'^2$. We recognize immediately the AdS_5 metric in the first two terms, times an S^5 factor. The gauge theory living on the D3-branes worldvolume is four-dimensional $\mathcal{N}=4$ super Yang-Mills theory with coupling constant g_{YM} and 't Hooft coupling λ given by the following relation

$$4\pi g_s = g^2_{YM} = \frac{\lambda}{N}\,.$$

The theory can be obtained by dimensional reduction of $\mathcal{N}=1$ SYM from ten to four dimensions. First of all it is interesting to look at the field content of the theory. As expected from the previous considerations, the bosonic field content consists of a four-dimensional gauge vector A_μ and six scalars ϕ_I. The latter are precisely the aforementioned fields associated to transverse fluctuations of the D3-branes, and they transform in the fundamental of a global SO(6) symmetry which is the R-symmetry of $\mathcal{N}=4$ SYM. All the fermionic degrees of freedom can be packaged into a single ten-dimensional Majorana-Weyl spinor. The resulting

Euclidean action is

$$S_{\mathcal{N}=4} = \frac{1}{g_{YM}} \int d^4x \, \mathrm{tr} \Big\{ -\frac{1}{2} F_{\mu\nu}^2 + (D_\mu \phi^I)^2 + \frac{1}{2}[\phi_I,\, \phi_J]^2 + i\bar{\Psi}\gamma^\mu D_\mu \Psi + \bar{\Psi}\gamma^I [\phi_I,\, \Psi] \Big\} , \tag{2.2.1}$$

where $F_{\mu\nu}$ and D_μ are the usual field strength and covariant derivative respectively. The Dirac matrices $(\gamma^\mu,\, \gamma^I)$ form the ten-dimensional Clifford algebra. As it was anticipated, we can only trust the supergravity solution in the limit in which both the stringy (higher derivative) and the quantum corrections to classical gravity are suppressed. This is achieved by keeping the curvature radius L large in string length units and by taking g_s to be small (since $G_N \propto g_s^2$). Considering that $L/\sqrt{\alpha'} = \lambda^{1/4}$, this corresponds to the large N, large λ limit: the planar and strongly coupled limit of the gauge theory. It is also important to note the matching of symmetries between the two sides of the correspondence. The global SO(6) R-symmetry of the gauge theory corresponds to the isometries of the S^5 piece of the bulk geometry. Moreover, $\mathcal{N} = 4$ super Yang-Mills theory in four dimensions is a conformal theory, and the conformal group of flat four-dimensional Minkowski space is $\mathrm{SO}(4,2)$, which corresponds exactly to the isometry group of AdS_5. Another important aspect of the correspondence is that finite temperature configurations in the boundary gauge theory are dual to black hole solutions in the bulk AdS spacetime: this will be seen in the next example.

2.2.2 The example of D0-brane quantum mechanics

Another example, which will be particularly relevant in relation to the second part of this thesis is given by D0-brane quantum mechanics [18, 19, 20]. This is a supersymmetric model defined in 0+1 dimensions which at finite temperature, in the strongly coupled regime is dual to the near-horizon region of a type IIA supergravity charged black hole solution, whose metric is

$$\frac{ds^2}{\alpha'} = -\frac{f(r) r^{7/2}}{\sqrt{\Lambda}} dt^2 + \sqrt{\frac{\Lambda}{r^3}} \left(\frac{1}{f(r) r^2} dr^2 + d\Omega_8^2 \right) , \tag{2.2.2}$$

with

$$f(t) \equiv 1 - \frac{r_0^7}{r^7}, \qquad \Lambda \equiv 240\pi^5 \lambda = 240\pi^5 g^2 N \, .$$

The dilaton ϕ and radius of the horizon r_0 are given by

$$e^\phi = \frac{1}{60\pi^3 N} \left(\frac{\Lambda}{r^3} \right)^{7/4}, \qquad r_0 = \left(\frac{7\beta}{4\pi\sqrt{\Lambda}} \right)^{-2/5} , \tag{2.2.3}$$

where $\beta = 1/T$ is the inverse temperature. From the metric (2.2.2) one can read off the effective curvature radius of the geometry, which is given by the radius of the S^8 factor:

$$\frac{R_{eff}^2}{\alpha'} = \sqrt{\frac{\Lambda}{r^3}} \, . \tag{2.2.4}$$

By demanding that the effective radius of curvature is large in units of the string length we obtain a constraint on the region of validity of the supergravity solution in terms of the 't Hooft coupling of the dual gauge theory, namely $r \ll \lambda^{1/3}$. In particular, by imposing this at the horizon $r = r_0$ we get

$$1 \ll \lambda\beta^3 \,. \tag{2.2.5}$$

However, since from (2.2.3) we get that, at the horizon

$$e^{\phi} \propto \frac{1}{N}(\lambda\beta^3)^{7/10} \,, \tag{2.2.6}$$

we also have to impose the additional constraint $\lambda\beta^3 \lesssim N^{10/7}$, in order to prevent the dilaton from getting too big at the horizon. The dual quantum mechanical model can be obtained by dimensional reduction of super Yang-Mills from 10 to 1 dimension, which results in the following Lagrangian

$$L = \frac{1}{2g}\left[\mathrm{tr}\dot{X}^i\dot{X}^i + 2\theta^T\dot{\theta} - \frac{1}{2}\mathrm{tr}\left[X^i, X^j\right]^2 - 2\theta^T\gamma_i\left[\theta, X^i\right]\right] . \tag{2.2.7}$$

Focusing solely on the bosonic sector, the degrees of freedom are the fields X^i which transform in the adjoint of gauge group SU(N) and in the fundamental of a global SO(9) symmetry. This is precisely what we would have guessed from a D0-brane construction in light of all the previous considerations. Note also that the quartic interaction term in the Lagrangian has exactly the same form of the one we find in (2.2.1). Inspite of the simplifications that occur when one studies quantum mechanical models with respect to full-blown QFTs in higher dimensions, analytical control over D0-brane quantum mechanics is still out of reach. At the level of the numerics, instead, a lot of progress in the understanding of its properties has been made through lattice Monte Carlo simulations [21, 22]. Finally, we will see later that several simple models of holography (e.g. IP, IOP, and matrix-vector models) have been inspired by it in terms of field content and kinds of interactions.

2.3 Take-home message

As it was seen from general considerations on D-brane constructions, and in two explicit examples, SU(N) (or equivalently, for our purposes U(N)) gauge theories appear naturally in the context of holography as duals of higher-dimensional gravitational theories, and it is natural for them to feature an additional global SO(D) symmetry. The typical degrees of freedom that appear in such boundary theories, are therefore D fields which transform in the adjoint representation of SU(N) (i.e. $N \times N$ matrices) and in the fundamental representation of SO(D). Such fields are typically coupled through quartic interaction terms of the form shown in (2.2.1) and (2.2.7). Moreover, if one wants to stay in the regime in which the dual supergravity solution is reliable, and therefore suppress all stringy and quantum effects in the bulk, all computations in the boundary gauge theories need to be carried out in the planar limit and in the strong coupling regime.

Part II

Simple models of Holography

Chapter 3

Simple models of Holography

3.1 General properties

We have seen that in the context of the gauge/gravity correspondence (at least in its well-understood realizations) the theory that lives in lower dimensions is a U(N) gauge theory. Moreover, the duality relates the planar, strongly coupled regime of the gauge theory to classical gravity in the bulk. Therefore, if one wants to engineer a quantum mechanical model that captures some interesting physics and possibly helps in answering deep questions about gravity, the starting point is already a non-trivial one: constructing a model of interacting U(N) adjoint fields which is solvable in the large N limit and at strong coupling. In order to keep things as simple as possible, we will restrict ourselves to 0+1 spacetime dimensions, i.e. to models of quantum mechanics. Moreover, what we are mostly interested in is black hole physics, and requiring the presence of (possibly extremal) black holes in the bulk theory imposes more properties on the boundary model. Here we review some of them:

- Continuous energy spectrum: In the presence of a black hole, any gap in the energy spectrum gets infinitely red-shifted near the horizon, resulting in a continuous spectrum. This property is intimately related to the information loss at the horizon [23, 24]. Such a feature is far from trivial in compact quantum systems, where the energy spectrum is always discrete and unitarity guarantees that no information is lost. A continuous spectrum must therefore arise in the $N \to \infty$ limit.

- Non-zero entropy at $T = 0$: Extremal black holes have the remarkable property of having a large finite entropy at zero temperature, which is proportional to the area of their event horizon [3, 4, 5]. Again, this is a non-trivial property for a quantum mechanical model, which is typically in its ground state at $T = 0$.

- Quasi-normal behaviour of two-point functions: The behaviour of a black hole geometry when it is perturbed out of equilibrium is described by damped

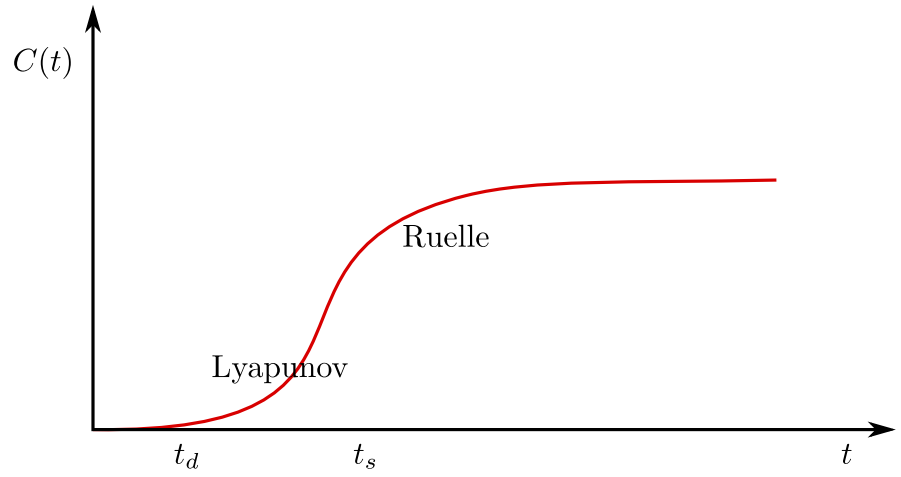

Figure 3.1: Typical behaviour of the thermal expectation value of the commutator-squared versus time in a chaotic system.

oscillations called quasi-normal modes [25, 26, 27, 28]. In the dual QFT, this phenomenon is equivalent to a thermalization process, hence the exponential decay of quasi-normal modes in the bulk must correspond to a late time exponential decay of finite-temperature two-point functions in the boundary theory. Standard quantum models do not exhibit such a behaviour: two-point functions undergo Poincaré recurrences after a time proportional to the exponential of the entropy [29]. This time scale must therefore be pushed to infinity in the large N limit in order to achieve quasi-normal behaviour.

3.1.1 Chaotic behaviour of correlators

In addition to the above properties, there is an additional very sharp and non-trivial criterion which the gauge dual of a bulk theory containing a black hole must satify: the chaotic behaviour of out-of-time-order four-point functions. This criterion is based on a definition of chaos that we will briefly sketch. In classical chaos, we define chaotic behaviour as extreme sensitivity of a system with respect to changes of initial conditions. This property can be formalized as an exponential growth of the separation of two trajectories which were initially separated by $\delta x(0)$:

$$\delta x(t) = \delta x(0) e^{\kappa t} \,, \tag{3.1.1}$$

where κ is called the Lyapunov exponent. We can rewrite (3.1.1) making use of the Poisson bracket

$$\frac{\partial x(t)}{\partial x(0)} = \{x(t), p(0)\} \,. \tag{3.1.2}$$

In the semiclassical regime we can substitute the bracket by a commutator and take its thermal expectation value [30]. However such a quantity will in general vanish because of phase cancellations, therefore a more appropriate quantity to

consider is the thermal expectation value of the square of the commutator

$$\langle [x(t), p(0)]^2 \rangle_\beta \sim \hbar^2 e^{2\kappa t} \,, \tag{3.1.3}$$

where the factor of 2 in the exponent is due to having taken the square of the commutator. When dealing with U(N) gauge theories, the classical limit corresponds to $N \to \infty$, therefore we can replace $\hbar$ by $1/N$. Also, we can generalize the discussion to any couple of Hermitian operators V and W obtaining

$$\langle [V(t), W(0)]^2 \rangle_\beta \sim \frac{1}{N^2} e^{2\kappa t} \,. \tag{3.1.4}$$

In holographic models, such an object typically features two distinct regimes, as depicted in Figure 3.1. The late time saturation, also known as Ruelle behaviour, happens at time scales of order $\ln N$ and cannot be seen in the large N limit. The early time exponential growth instead is associated with chaos in the way we have just defined and is a direct hint of the presence of a horizon in the bulk theory. Intuitively, this exponential growth can be related to the exponential blueshift of a source of fixed frequency which is thrown into the black hole [32]. According to the asymptotic observer, this effect will be proportional to

$$\frac{1}{M} e^{2\pi t/\beta} \,, \tag{3.1.5}$$

where M and β are the mass and the inverse temperature of the black hole respectively. In [33] it was conjectured that this value of the Lyapunov exponent is the maximum one, and arguments were given to show that quantum corrections can only lower it. Therefore, if a quantum system displays an exponential growth in observables of the kind defined in (3.1.4) with a Lyapunov exponent which saturates the conjectured bound, this is a strong hint that the dual bulk theory contains classical black hole solutions.

3.1.2 Models with probes

A typical analysis that has been shown to provide useful insight about both sides of the gauge/gravity correspondence is done through the use of probe branes [34, 35, 36, 37]. In the holographic picture, one can imagine starting from a stack of $N+1$ coinciding D-branes and separating one of them from the rest. Studying the dynamics of this probe can give us insight on the gravitational background induced by the remaining stack of N branes. From the point of view of the open strings attached to the D-branes, separating the probe from the background amounts to distinguishing three kinds of objects: those with both endpoints on the background, those that go from the background to the probe, and those attached only to the probe. To understand what this means in terms of the gauge theory that lives on the brane worldvolume, let us use a zero-dimensional toy example [38] in which the adjoint degrees of freedom are $(N+1) \times (N+1)$ matrices M

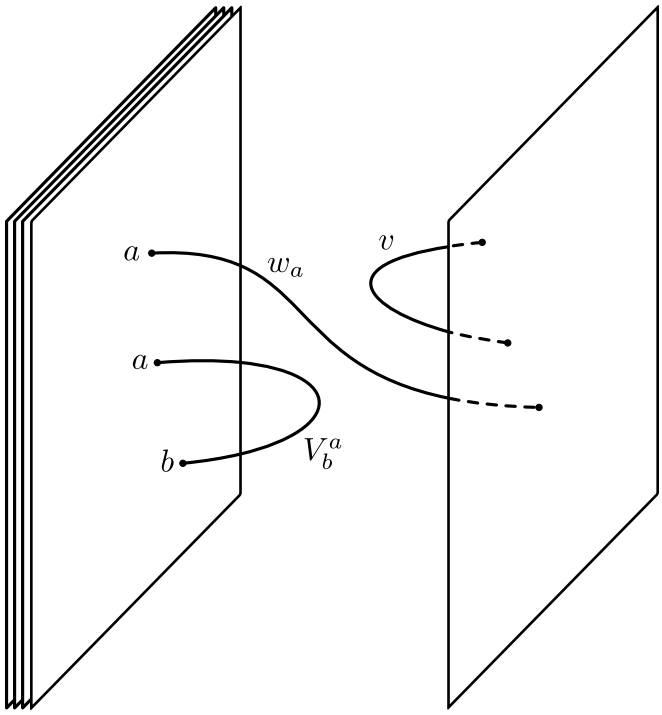

Figure 3.2: Sketchy representation of a system of N background branes and one probe, after the decomposition performed in (3.1.6).

with some action $S_{N+1}(M)$. Splitting the probe from the background amounts to a distinction between various pieces that compose the M matrices:

$$M = \begin{pmatrix} V_b^a & \bar{w}^a \\ w_b & v \end{pmatrix} . \tag{3.1.6}$$

The interpretation of the various pieces is clear: the $N \times N$ matrix V is associated to background-background open strings, the vectors w and $\bar{w}$ to probe-background strings, and the scalar v to probe-probe strings. The original $\mathrm{U}(N+1)$ symmetry of the model is broken down to $\mathrm{U}(N)\times\mathrm{U}(1)$. To understand the effect this splitting has on the action of the model, let us consider the following explicit example:

$$S_{N+1}(M) = \frac{N+1}{\lambda}\mathrm{tr}\left(\frac{1}{2}M^2 + \frac{1}{4}M^4\right) . \tag{3.1.7}$$

In terms of the new variables we get

$$S_{N+1}(M) \to S_{N+1}(V,\, w,\, \bar{w},\, v) = (N+1)\left[\frac{1}{N}S_N(V) + S_1(v) + \hat{S}(V,\, w,\, \bar{w},\, v)\right] , \tag{3.1.8}$$

with

$$\hat{S}(V,\, w,\, \bar{w},\, v) = \frac{1}{\lambda}\left(\bar{w}w + wV^2\bar{w} + v^2\bar{w}w + vwV\bar{w} + \frac{1}{2}\bar{w}w\bar{w}w\right) , \tag{3.1.9}$$

which, on top of the original action for the matrix and the scalar fields, contains completely new couplings involving the vectors. Now, let us introduce the partition function of this background plus probe system

$$Z = \int \mathcal{D}V\mathcal{D}w\mathcal{D}\bar{w}\mathcal{D}v\, e^{-S_{N+1}(V,w,\bar{w},v)}\,. \tag{3.1.10}$$

The gauge/gravity correspondence postulates that performing this path integral should be equivalent to the path integral of the probe brane gauge theory in the non-trivial near-horizon geometry generated by the N background branes [39]:

$$Z = \int \mathcal{D}v\, e^{-S_p(v,g_{\mu\nu},\phi,...)}\,, \tag{3.1.11}$$

where the probe action depends on all the properties of the background geometry (metric, dilaton, and so on). If we integrate out all the background fields in (3.1.10) we obtain an effective action for the probe brane variables, defined by

$$e^{-S_{\rm eff}(v)} = \int \mathcal{D}V\mathcal{D}w\mathcal{D}\bar{w}\, e^{-S_{N+1}(V,w,\bar{w},v)}\,, \tag{3.1.12}$$

which, by comparing (3.1.10) and (3.1.11), must be equivalent to $S_{\rm p}$. Therefore, the effective action $S_{\rm eff}$, obtained entirely through a gauge theory computation in flat spacetime, contains all the information on the curved bulk geometry in the gravitational picture. The procedure we just sketched can in principle be carried out for any gauge theory [40, 38], and has been successfully tested in several examples in which both the gravitational and the gauge theory sides of the correspondence are known. For example, the $AdS_5 \times S^5$ geometry generated by a stack of D3-branes can be obtained through a field theoretic computation performed using D-instantons as probes [34].

3.2 The IP and IOP models

3.2.1 Introduction

As it was emphasized in the previous section, U(N) matrix models appear naturally in the framework of string theory and holography, and in order to make contact with classical gravity, we have to study their planar limit at strong coupling. This is not always easy, as we are in general not able to resum all the planar diagrams of a generic non-Gaussian matrix model. Also, we mentioned that models involving vector-matrix interactions are associated with probe analysis in brane constructions. This idea is what prompted Iizuka and Polchinski [41] and Iizuka, Okuda and Polchinski [42] to study two simple models which from now on we will refer to as IP and IOP models respectively. Their strategy was to start from a very simple Hamiltonian: a harmonic oscillator in the adjoint of U(N) plus one in the fundamental, coupled though a cubic and a quartic interaction. This allows for complete planar diagram resummation.

3.2.2 Definition of the IP model

The Iizuka-Polchinski Hamiltonian is the following:

$$H = \frac{1}{2}\mathrm{tr}\left(\Pi^2 + m^2 s X^2\right) + M a_i^\dagger a^i + \frac{\mu}{N} a_i^\dagger a_j^\dagger a^i a^j + g a_i^\dagger X_j^i a^j \,, \tag{3.2.1}$$

where X and Π are $N \times N$ matrix operators satisfying

$$(X_j^i)^\dagger = X_i^j \qquad (\Pi_j^i)^\dagger = \Pi_i^j \,, \tag{3.2.2}$$

and the canonical commutation relation

$$[X_j^i, \Pi_l^k] = i\delta_l^i \delta_j^k \,. \tag{3.2.3}$$

The $a^\dagger$ and a and are vector operators and satisfy the usual creation-annihilation commutation relation

$$[a^i, a_j^\dagger] = \delta_j^i \,. \tag{3.2.4}$$

Since the coupling between the matrix and the vectors is cubic, the quartic vector coupling is necessary to make the model stable. In the probe picture described in the previous section, one can imagine the adjoint fields as being associated to background-background open strings, while the $a^\dagger$ and a respectively create and annihilate open strings that go from the background to the probe. Since in string theory the mass of open strings is proportional to the distance between the branes they are attached to, the mass parameter M of the vector fields can be associated to the distance of the probe from the background in this picture. In [41] the model is studied in a regime corresponding to a probe at infinite distance from the black hole, while an analysis at finite distance is carried out in [43].

3.2.3 Large M computation

The simplicity of the adjoint sector of the Hamiltonian allows for the complete summation of the planar diagrams of the model. As it is common in probe set-ups, all the contributions to correlators of the adjoint fields coming from the interactions with the probes are subleading in the large N limit. Therefore, the real-time two-point function of the adjoint fields is just the harmonic oscillator one, which at finite temperature $T = 1/\beta$ and in frequency domain is given by

$$K_0(\omega) = \frac{i}{1 - e^{-\beta m}} \left(\frac{1}{\omega^2 - m^2 + i\epsilon} - \frac{e^{-\beta m}}{\omega^2 - m^2 - i\epsilon} \right) . \tag{3.2.5}$$

Let us now turn to the computation of the real-time, finite temperature propagator of the fundamentals defined in the following way

$$G^P(t) \equiv \frac{1}{N} e^{iMt} \langle \mathrm{T} a^i(t) a_i^\dagger(0) \rangle \,, \tag{3.2.6}$$

which, on the other hand, receives contributions because of the cubic vector-matrix vertex. The choice to define it with the phase factor e^{iMT} makes it loose

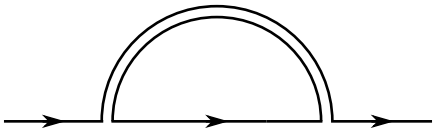

Figure 3.3: The one-loop diagrammatic unit whose iteration generates all the planar contributions to the vector two-point function in the IP model.

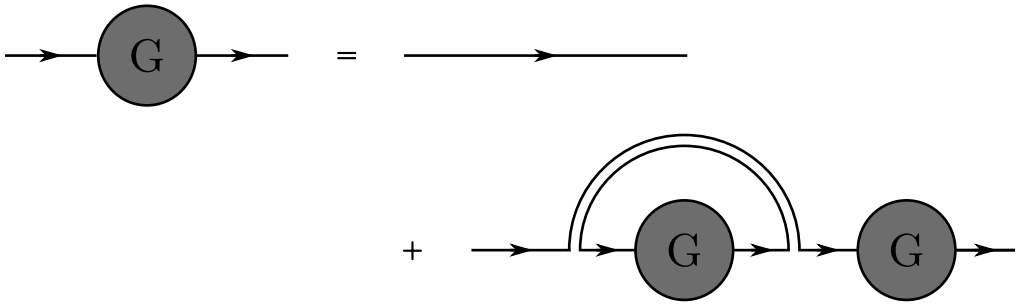

Figure 3.4: Graphical representation of the Schwinger-Dyson equation for the two-point function of the fundamentals in the IP model.

the dependence on M in the $M \gg T$ limit, which is the regime we are going to initially focus on. It is important to point out that in this limit, the quartic stabilizing term $a_i^\dagger a_j^\dagger a^i a^j$ plays no role and for the moment we can neglect it. All the planar diagrams which contribute to the vector two-point function can be obtained by iteration of the diagrammatic unit shown in Figure 3.3. The sum over all such diagrams can be performed and packaged in the following Schwinger-Dyson equation

$$G^P(\omega) = G_0^P(\omega) + \lambda G_0^P(\omega) G^P(\omega) \int_{-\infty}^{\infty} \frac{d\omega'}{2\pi} G^P(\omega') K_0(\omega - \omega') \,, \tag{3.2.7}$$

where $\lambda = g^2 N$ is the 't Hooft coupling. A graphical representation of the Schwinger-Dyson equation is depicted in Figure 3.4. The bare finite temperature fundamental two-point function $G_0^P(t)$ is the same as the zero temperature one because of the $M \gg T$ limit:

$$G_0^P(\omega) = \frac{i}{\omega + i\epsilon} \,. \tag{3.2.8}$$

The Schwinger-Dyson equation (3.2.7) can in general be treated only numerically, but if one takes the $m \to 0$ limit while holding $\nu^2 \equiv 2\lambda/[m(1 - e^{-\beta m})]$ fixed it can be solved analytically, yielding the following result

$$G^P(\omega) = \frac{2i}{\omega + \sqrt{\omega^2 - 2\nu^2}} \,. \tag{3.2.9}$$

It is important to notice how the presence of a branch cut in (3.2.9) implies a continuous spectrum for the fundamental fields: the interaction with the adjoint fields

has the effect of broadening the spectral density of the fundamentals, which in the free theory would just be a Dirac delta centered at M. The Fourier transform of (3.2.9) can be written in terms of a Bessel function

$$G^P(t) = \frac{\sqrt{2}}{\nu t} J_1(\sqrt{2}\nu t)\theta(t)\,. \tag{3.2.10}$$

3.2.4 Bose-Einstein condensation

We have shown that in the large M limit, the IP model already features some interesting properties but, since in the probe picture it corresponds to placing the probe at an infinite distance from the black hole, it is not the best regime for studying the near-horizon physics or, possibly, phenomena like the crossing of the horizon. The IP model can however be studied at finite M, both analytically and numerically [43]. In order to obtain analytical results, we need to take the $m/T \ll 1$ first, which amounts to "freezing" the adjoint field X. In this limit, in fact, only its zero mode X_0 contributes, while all the higher modes decouple from the theory. The path integral which determines the partition function of the model at finite temperature is therefore given by

$$\begin{aligned} Z = \int \mathcal{D}X_0 \mathcal{D}a \mathcal{D}a^\dagger \exp\Big[-\frac{m^2}{2\beta} X_0^2 - \int_0^\beta d\tau \big(a^\dagger(\partial_\tau + M)a + \frac{g}{\beta} a^\dagger X_0 a \\ + \frac{\mu}{N}(a^\dagger a)^2 \big) \Big]\,, \end{aligned} \tag{3.2.11}$$

where X_0 appears only quadratically and can be integrated out, leaving a bilocal action for the probe fields

$$\begin{aligned} Z = \int \mathcal{D}a \mathcal{D}a^\dagger \exp\Big\{ -\int_0^\beta d\tau \Big[a^\dagger(\partial_\tau + M)a + \frac{\mu}{N}(a^\dagger a)^2 \Big] \\ + \frac{g^2}{2\beta m^2} \int_0^\beta d\tau_1 d\tau_2 \Big[(a^\dagger(\tau_1)a(\tau_2))(a^\dagger(\tau_2)a(\tau_1)) \Big] \Big\}\,. \end{aligned} \tag{3.2.12}$$

The action contains quartic terms in the fundamental fields, but it can be made quadratic by introducing two Hubbard-Stratonovich auxiliary fields ϕ and σ, the former being a local field, while the latter being bi-local. We obtain

$$\begin{aligned} Z = \int \mathcal{D}a \mathcal{D}a^\dagger \mathcal{D}\sigma \mathcal{D}\phi \exp\Big\{ -\int_0^\beta d\tau \Big[a^\dagger(\partial_\tau + M + \phi)a - \frac{N}{4\mu}\phi^2 \Big] \\ - \frac{1}{\beta m^2} \int_0^\beta d\tau_1 d\tau_2 \Big[\sigma(\tau_2,\tau_1)(a^\dagger(\tau_2)a(\tau_1)) \\ + \frac{N}{2\lambda}\sigma(\tau_1,\tau_2)\sigma(\tau_2,\tau_1) \Big] \Big\}\,, \end{aligned} \tag{3.2.13}$$

where we introduced the 't Hooft coupling $\lambda \equiv g^2 N$. We can finally integrate out the fundamental fields, obtaining an effective action for the auxiliary fields:

$$Z = \int \mathcal{D}\sigma\mathcal{D}\phi \exp\Bigg(- N \Bigg[\mathrm{lnDet}(\partial_\tau + M + \phi + \frac{\sigma}{\beta m^2}) - \int_0^\beta d\tau \frac{\phi^2}{4\mu} + \int_0^\beta d\tau_1 d\tau_2 \frac{1}{2\lambda m^2} \sigma(\tau_1, \tau_2)\sigma(\tau_2, \tau_1) \Bigg] \Bigg) . \tag{3.2.14}$$

Since they do not carry $\mathrm{U}(N)$ indices and their action is proportional to N, in the $N \to \infty$ limit the path integral over the auxiliary fields localizes at their saddle point values ϕ_* and σ_* which are given by the solutions of the equations of motion for ϕ and σ respectively:

$$\begin{aligned} \phi_* &= \frac{2\mu}{N} \left\langle a^\dagger a \right\rangle , \\ \sigma_*(\tau) &= -\lambda G_E(\tau) = -\lambda \left(\partial_\tau + M + \phi_* + \frac{\sigma_*}{\beta m^2} \right)^{-1} , \end{aligned} \tag{3.2.15}$$

where G_E is the imaginary time, finite temperature correlator of the fundamental fields:

$$G_E(\tau) = \frac{1}{N} \left\langle \mathrm{T} a(\tau) a^\dagger(0) \right\rangle = \frac{1}{\beta} \sum G_k e^{-i\omega_k \tau} , \tag{3.2.16}$$

and the $\omega_k = 2\pi/\beta$ are the usual Matsubara frequencies. We can rewrite the saddle point equations (3.2.15) as an equation for the Matsubara coefficients G_k:

$$G_k^{-1} = -i\omega_k + M_* - \frac{\Lambda G_k}{\beta} , \tag{3.2.17}$$

where we have introduced two new quantities

$$M_* \equiv M + \phi_* \qquad \Lambda \equiv \lambda m^2 . \tag{3.2.18}$$

Equation (3.2.17) is a quadratic equation in the G_k and is just the $m\beta \ll 1$ limit of the imaginary-time version of the Schwinger-Dyson equation (3.2.7). It can easily be solved for $k \neq 0$, giving

$$G_k = \frac{2}{M_* - i\omega_k + \sqrt{(M_* - i\omega_k)^2 - 4\frac{\Lambda}{\beta}}} , \tag{3.2.19}$$

which is analogous to (3.2.9), but this time for finite values of M. Now, from the G_k one can obtain the resolvent of the model, which is an analytic function in the upper and lower half complex plane, related to the spectral density $\rho(\omega)$ by

$$R(z) = \int_{-\infty}^{+\infty} \frac{\rho(\omega)}{z - \omega} d\omega . \tag{3.2.20}$$

The resolvent satisfies the two relations

$$\begin{aligned} G_k &= -R(i\omega_k)\,, \qquad k \neq 0\,, \\ \rho_{\text{smooth}}(\omega) &= \frac{i}{2\pi}\left(R(\omega+i\epsilon) - R(\omega-i\epsilon)\right)\,, \end{aligned} \tag{3.2.21}$$

where $\rho_{\text{smooth}}(\omega)$ is the smooth part of the spectral function, which is in general a positive (negative) function for positive (negative) values of ω. Note that, from the first equation, the zero-mode G_0 cannot be read off the resolvent. Moreover, only the smooth part of the spectral density can be obtained from the resolvent: this allows for the presence of a term proportional to $\omega\delta(\omega)$ in the full spectral density which is not captured by the discontinuity of the resolvent across the real axis. From (3.2.19) we can determine the expression for the resolvent:

$$R(z) = \frac{1}{2\Lambda T}\left[z - M_* - \sqrt{(z-M_+)(z-M_-)}\right]\,, \tag{3.2.22}$$

where

$$M_\pm = M_* \pm 2\sqrt{\Lambda T}\,. \tag{3.2.23}$$

It has a branch cut on the real axis from M_- to M_+, from which, using (3.2.21) we obtain

$$\rho_{\text{smooth}}(\omega) = \frac{1}{2\pi\Lambda T}\sqrt{(M_+-\omega)(\omega-M_-)} \quad \text{for} \quad M_- \leq \omega \leq M_+\,. \tag{3.2.24}$$

Let us now consider the Matsubara zero mode G_0, whose analysis requires more care than the higher modes. At low temperature, when the effective coupling $\sqrt{\Lambda T}$ is small, we can trust the perturbative result (3.2.17) for $k=0$ and write

$$G_0 = \frac{1}{2\Lambda T}\left[M_- + 2\sqrt{\Lambda T} - \sqrt{M_-(M_- + 4\sqrt{\Lambda T})}\right] = -R(0)\,, \tag{3.2.25}$$

as T increases, however, M_- decreases monotonically and reaches its minimum $M_- = 0$ for a critical value of the temperature T_c. This corresponds to the branching point of (3.2.25). Now, if we further increase the temperature, G_0 should be analytically continued to

$$G_0 = \frac{1}{2\Lambda T}\left[M_- + 2\sqrt{\Lambda T} + \sqrt{M_-(M_- + 4\sqrt{\Lambda T})}\right]\,. \tag{3.2.26}$$

This means that for $T > T_c$ the relation $G_0 = -R(0)$ no longer holds, instead we have

$$G_0 + R(0) = \beta n_0 \qquad \text{with} \qquad n_0 = \frac{1}{\Lambda}\sqrt{M_-(M_- + 4\sqrt{\Lambda T})}\,, \tag{3.2.27}$$

where one can show that n_0 is the proportionality constant in front of the aforementioned $\delta(\omega)$ term in the full spectral density. Since the total number n of fundamentals is given in terms of $\rho(\omega)$ by

$$n = \int_{-\infty}^{+\infty}\frac{\rho(\omega)}{e^{\beta\omega}-1}d\omega = n_0 + \int_{-\infty}^{+\infty}\frac{\rho_{\text{smooth}}(\omega)}{e^{\beta\omega}-1}d\omega\,, \tag{3.2.28}$$

this analytic continuation procedure can be seen as a Bose-Einstein condensation of massless fundamentals [43]. This discussion can be carried out in an analogous way by keeping T fixed and varying the mass parameter M. As M is decreased below a critical value M_c, the same condensation phenomenon is observed. In the introduction, we associated the fundamental fields to open strings attached to the probe and the black hole, their mass M being related to the distance between the two. It is very tempting to associate the value M_c to the position of the horizon of the black hole. In this sense, the presence of a non-perturbative phase transition at a critical value of the distance between the probe and the black hole seems to suggest that even simple models like IP and IOP can be used to study the non-trivial physics associated to the crossing of the horizon.

3.2.5 Definition of the IOP model

The Iizuka-Okuda-Polchinski (IOP) model is a close relative of the IP model. It has the same field content, and its Hamiltonian is

$$H = m \operatorname{tr}\left(A^\dagger A\right) + M a_i^\dagger a^i + \frac{\mu}{N} a_i^\dagger a_j^\dagger a^i a^j + \sqrt{\frac{\lambda}{N}} a_i^\dagger A_j^{\dagger i} A_l^j a^l \,, \tag{3.2.29}$$

which is written, for convenience, in terms of the adjoint creation and annihilation operators, satisfying $X = \left(A + A^\dagger\right)/\sqrt{2m}$. This model can be obtained from the IP model by keeping only the most singular planar graphs in frequency space. Although the vector-matrix coupling is of higher order, and the resulting Schwinger-Dyson equations for the fundamental two-point function are more complicated, the model is more tractable analytically [42]. This is due to the fact that the vector-matrix coupling is really a quadratic coupling in terms of the fundamental and adjoint U(N) charges

$$q_i^l = a_i^\dagger a^l \qquad Q_l^i = A_j^{\dagger i} A_l^j \,. \tag{3.2.30}$$

3.2.6 Large M computation

In order to solve the model, one can proceed along the same lines as the IP model and take the limit for large mass of the fundamental $M \gg T$. Again, the propagator for the adjoint fields does not receive corrections from their interactions with the fundamentals, it is therefore just given by the harmonic oscillator one. We define it in the following way

$$L_0(t)\delta_{il}\delta_{jk} = \left\langle \mathrm{T} A_{ij}(t) A_{kl}^\dagger(0) \right\rangle \,. \tag{3.2.31}$$

At finite temperature, in frequency domain it gives

$$L_0(\omega) = \frac{i}{1 - e^{-\beta m}} \left(\frac{1}{\omega - m + i\epsilon} - \frac{e^{-\beta m}}{\omega - m - i\epsilon} \right) \,. \tag{3.2.32}$$

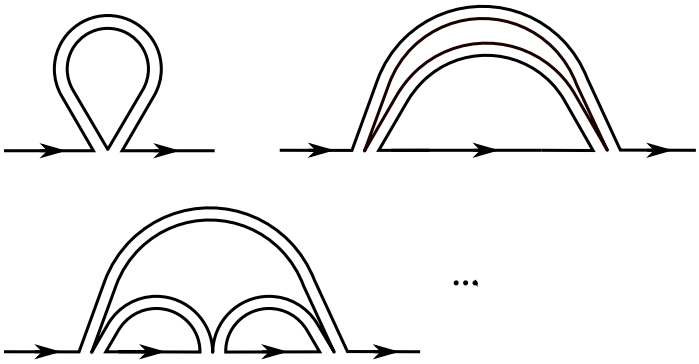

Figure 3.5: The first few diagrammatic units whose iteration generates all the planar contributions to the vector two-point function in the IOP model.

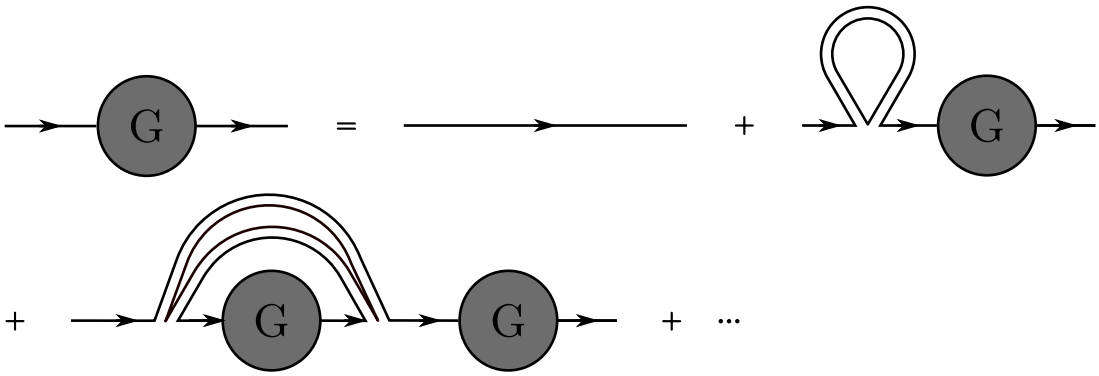

Figure 3.6: Graphical representation of the Schwinger-Dyson equation for the two-point function of the fundamentals in the IOP model.

The fundamental full and bare two-point functions are again defined by (3.2.6) and (3.2.8) respectively. Because of the quartic coupling, the class of planar diagrams which contributes to the fundamental two-point function is larger with respect to the IP model. It contains all the diagrams which can be obtained by iterating the family of structures depicted in Figure 3.5. The resulting Schwinger-Dyson equations for $G^P(t)$ take the following form

$$\begin{aligned} G^P(\omega) =& G_0^P(\omega) + G_0^P(\omega) G^P(\omega) \sum_{n=0}^{\infty} S_n(\omega)\,, \\ S_n(\omega) =& (-ihN)^{n+1} \int \frac{d\omega_1}{2\pi} L_0(-\omega_1) \prod_{l=1}^{n} \frac{d\omega_l}{2\pi} G^P(\omega - \omega_{l+1} - \omega_1) L_0(\omega_{l+1})\,. \end{aligned} \tag{3.2.33}$$

These equations, which are depicted graphically in Figure 3.6 for $n = 0$, 1 and 2, look more complicated than the IP ones but are actually more tractable. The $M \gg T$ is in fact sufficient for reducing them to a solvable algebraic solution for

$G^P(\omega)$ with solution

$$G^P(\omega) = \frac{2i}{\lambda + \omega + \sqrt{(\omega - \omega_+)(\omega - \omega_-)}}, \qquad \omega_\pm = \lambda \frac{1 \pm e^{-\beta m/2}}{1 \mp e^{-\beta m/2}} \tag{3.2.34}$$

where $\lambda = hN$ is the 't Hooft coupling. Similarly to the IP case, but without having to take the small adjoint mass limit, we obtain a propagator with a branch cut, indicating a continuous energy spectrum.

3.2.7 Concluding remarks

The computation of the thermal two-point functions of the fundamental fields in the IP and IOP model has shown the presence of a continuous spectrum, a physical property associated with the presence of a horizon in the bulk dual. Through similar, though more involved, computations one can also compute the thermal four-point functions of the fundamentals, both in the IP and IOP model. As it was already pointed out, an exponential growth of the connected out-of-time-order four-point function is a non-trivial criterion for determining the viability of a model of holography. However, neither the IP nor the IOP model exhibit such an exponential growth. Although the computation of the four-point function was performed in [44], like the two-point one, in the $M \gg T$ limit, it is unlikely that relaxing this condition would lead to the wanted chaotic behaviour. The problem lies most likely in the simplicity of the models, which lack self-interactions between the adjoint fields. On the other hand, the Bose-Einstein condensation phenomenon observed in the IP model could be a very general property of bosonic models of interacting vectors and matrices.

3.3 Melonic models

In [45] Kitaev proposed a simplified version the Sachdev-Ye model [46], which was originally introduced for the study of spin glass/spin fluid phase transitions. This new model, called the Sachdev-Ye-Kitaev (SYK) model, features many interesting properties that make it a good candidate for a simple model of holography. Since Kitaev's proposal, several other models with the same properties have been constructed: what connects them, despite evident differences in terms of field content, symmetries, etc., is a similar Feynman diagram structure, which is dominated by so-called *melon diagrams*. This class of diagrams is obtained by iterating a two-loop structure (shown in Figure 3.7 along with an example of a vacuum diagram constructed by iteration of said structure) and is simple enough to allow for complete summation, and therefore solvability at any value of the coupling. Although summable, this class of diagrams is non-trivial enough to result in the remarkable properties of these models, among which we find a continuous spectrum, the quasi-normal behaviour of thermal two point functions and the maximally chaotic behaviour of out-of-time-order four-point functions in the strong coupling limit.

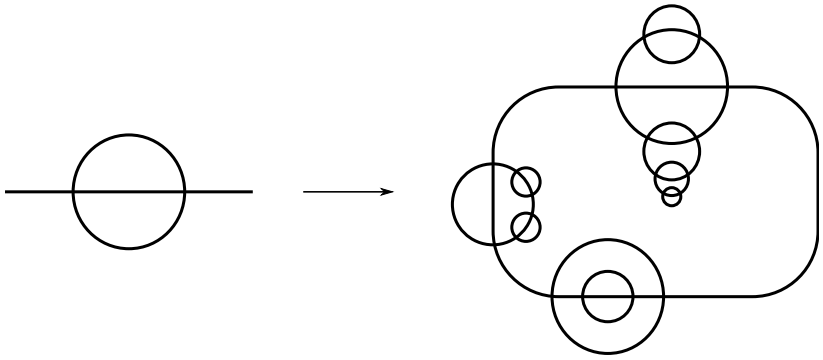

Figure 3.7: The basic graphical unit of melonic models (left) and an example of melon diagram (right)

In the remainder of this section will introduce three models which belong to this class: the SYK model, the Gurau-Witten model and a matrix-vector model with $\mathrm{U}(N)^2 \times \mathrm{O}(D)$ symmetry.

3.3.1 The Sachdev-Ye-Kitaev model

The Sachdev-Ye model [46] is model a of $\mathrm{SU}(M)$ spins on N sites, coupled through a Gaussian random interaction. The model is studied by taking the $N \to \infty$ followed by the $M \to \infty$ limit and exhibits a spin glass phase. In [45] it was simplified by introducing a similar model which only features the parameter N, and in which the spin glass order is suppressed. The resulting SYK model is a model of N Majorana fermions χ_i satisfying $\{\chi_i, \chi_j\} = \delta_{ij}$, coupled through a quartic all-to-all interaction:

$$H = \frac{1}{4!} \sum_{i,j,k,l=1}^{N} J_{ijkl} \chi_i \chi_j \chi_k \chi_l \,. \tag{3.3.1}$$

The couplings J_{ijkl} are random and drawn from a Gaussian distribution with the following properties:

$$\overline{J_{ijkl}^2} = \frac{3! \lambda^2}{N^3} \,, \qquad \overline{J_{ijkl}} = 0 \,, \tag{3.3.2}$$

where the bar denotes the average over the Gaussian distribution. Each observable is computed by taking the average over the disorder in the following way

$$\overline{\langle O \rangle} = \int D J_{ijkl} e^{-J_{ijkl}^2 N^3 / 12 \lambda^2} \frac{\int D\chi_i O e^{-\int dt L}}{\int D\chi_i e^{-\int dt L}} \,. \tag{3.3.3}$$

The presence of such a random, time-independent coupling is known in the Condensed Matter literature as quenched disorder. The idea behind it is that, although one is typically interested in the study of one specific realization of the

system, studying the average over all realizations is easier. Certain physical quantities, called self-averaging quantities, have the property that in the $N \to \infty$ limit their value in a typical realization of the model tends to their average value. Therefore, if one restricts oneself to considering only self-averaging quantities in the large N limit, studying the average over all realizations is equivalent to studying a typical realization of the model [47]. The free energy F is one such quantity and, as a consequence, all connected correlation functions.

Generalizations

The SYK model can be generalized in several ways, here we review a few of them. A natural generalization of the SYK model is the complex SYK model [48, 49], which makes use of complex fermions instead of Majorana fermions and is defined by the Hamiltonian

$$H_{\text{complex}} = \sum_{i,j,k,l=1}^{N} J_{ijkl} \chi_i^\dagger \chi_j^\dagger \chi_k \chi_l + m \chi_i^\dagger \chi_i \,. \tag{3.3.4}$$

To ensure the Hermiticity of the Hamiltonian, we also have to impose the following condition on J_{ijkl}:

$$J_{klij} = J_{ijkl}^* \,. \tag{3.3.5}$$

Notice how the use of complex fermions allows for a mass term: while all the interesting properties of SYK remain untouched, the extra parameter m allows for a richer phase space, as it will be discussed in Chapter 5. One can also modify the SYK Hamiltonian to allow for interaction terms involving any even number q of fermions instead of just four [50]:

$$H_q = \frac{i^{q/2}}{q!} \sum_{i_1 i_2 \cdots i_q = 1}^{N} J_{i_1 i_2 \cdots i_q} \chi_{i_1} \chi_{i_2} \cdots \chi_{i_q} \,. \tag{3.3.6}$$

where the $i^{q/2}$ factor ensures Hermiticity for odd $q/2$. There are two interesting limits that one can consider, which both lead to solvable models: $q = 2$ and $q = \infty$. The former can be seen as a close relative of the $m\beta \ll 1$ limit of the IP model. For $q = 2$, in fact, the random coupling reduces to a matrix J_{ij} and plays an analogous role to the zero mode of the adjoint field X in (3.2.11). However, since the vector degrees of freedom in $q = 2$ SYK are fermions, the peculiar condensation phenomenon observed in the IP model cannot occur. Moreover, much like in the IP model, no chaotic behaviour is observed in out-of-time-ordered four-point functions. Therefore, albeit being completely solvable, the $q = 2$ case is much less interesting than its $q > 2$ relatives. Interestingly, also taking the $q = \infty$ limit leads to simplifications. This is particularly useful when one has to compute quantities that do not depend on q, or study the qualitative features of the model. Finally, we briefly present a supersymmetric generalization of the SYK model which was proposed in [51]. In its $\mathcal{N} = 1$ version, it is obtained

by constructing a Hermitian supercharge Q out of the fermions and the random coupling:

$$Q = i \sum_{i,j,k=1}^{N} J_{ijk}\chi_i\chi_j\chi_k \,. \tag{3.3.7}$$

As it is customary, the Hamiltonian is obtained by taking the square of the supercharge

$$H_{\text{SUSY}} = Q^2 \,. \tag{3.3.8}$$

It should be noted that as it is, the model does not contain any bosonic degrees of freedom: the superpartners of the fermions arise as non-dynamical auxiliary fields, that are introduced in order to linearize the action of the supercharge on the fermions.

3.3.2 The Gurau-Witten model

The SYK model, due to the quenched disorder, is not a quantum system per se, but rather an average over an ensemble of quantum systems. This fact, combined with the unclear interpretation of $1/N$ corrections, prompted the search for models that reproduced the same interesting features of the SYK model, but without the random coupling. The first proposal in this direction came from Witten [52], who pointed out that one could reproduce the same diagrammatic structure of SYK (and therefore the same properties) by using a tensor model with the following action:

$$S_{G-W} = \int dt \left(\frac{i}{2}\psi_A^{abc}\partial_t\psi_A^{abc} + \frac{\lambda}{N^{3/2}}\psi_0^{abc}\psi_1^{ade}\psi_2^{fbe}\psi_3^{fdc} \right). \tag{3.3.9}$$

Here the ψ_A^{abc} are 4 real fermionic tensors and the model has a $O(N)^6$ symmetry. Similar models had been introduced by Gurau and collaborators [53, 54, 55, 56, 57] and are studied in the tensor model literature with the aim of generalizing to higher dimensions the correspondence between matrix models and two-dimensional geometries. The factor of $N^{-3/2}$ in front of the quartic coupling ensures that the large N limit of the model is well-defined, as the coupling constant λ is held fixed. It can be shown that the leading diagrams in the large N limit have exactly the same structure as the SYK model, thus reproducing the same physical properties. Much like the SYK model, these tensor models can be easily generalized to feature a q-fold interaction. In order to do so, however, one needs q distinct tensors and the resulting model will enjoy a $\mathrm{O}(N)^{q(q-1)/2}$ symmetry. For the case $q = 4$, Klebanov and Tarnopolsky [58], basing their work on ideas developed in [59], showed that it is not necessary to have four distinct fermionic tensors in order to reproduce the SYK diagrammatics, but just one (an *uncolored* model in tensor model terminology) is enough. The resulting action is

$$S_{\text{unc.}} = \int dt \left(\frac{i}{2}\psi^{abc}\partial_t\psi^{abc} + \frac{\lambda}{N^{3/2}}\psi^{abc}\psi^{ade}\psi^{fbe}\psi^{fdc} \right), \tag{3.3.10}$$

and the model has a $\mathrm{O}(N)^3$ symmetry.

3.3.3 Quartic matrix-vector model

A close relative of the aforementioned uncolored tensor model was introduced in [60] as a model of D U(N) matrices. Such models enjoy a U(N)$^2\times$O(D) symmetry (or U(N)$\times$O(D) in the case of Hermitian matrices) and it is possible to define a non-trivial scaling of their couplings which leads to a new, well-defined large N, large D limit. The limit has several interesting features which will be explored in detail in Chapter 4, while more details on the properties of this specific model, which will be referred to as the *quartic matrix-vector model*, will be given in Chapter 6. For the moment we will limit ourselves to the definition of a model that in the large N, large D limit reproduces the diagrammatic structure of the SYK model, using U(N) matrices as fundamental degrees of freedom. Let us consider the following Hamiltonian:

$$H = ND\,\mathrm{tr}\left(m\psi_\mu^\dagger\psi_\mu + \frac{1}{2}\lambda\sqrt{D}\,\psi_\mu\psi_\nu^\dagger\psi_\mu\psi_\nu^\dagger\right), \tag{3.3.11}$$

where the greek indices run from 1 to D. The ψ_μ and $\psi_\mu^\dagger$ are complex fermionic $N\times N$ matrices obeying

$$\left\{\psi^a_{\mu\,b}, \left(\psi^\dagger_\nu\right)^c_d\right\} = \frac{1}{ND}\delta_{\mu\nu}\delta^a_d\delta^c_b\,, \tag{3.3.12}$$

with latin indices running from 1 to N. The trace is taken over the U(N) indices. Note that we have defined the model's Hamiltonian with a mass term, just like we did for the SYK model with complex fermions defined in (3.3.4). We can always set $m=0$ to recover the properties of the SYK model with real fermions. It should also be stressed that the $\sqrt{D}$ factor in front of the quartic interaction term is crucial for reproducing the melonic structure in the large N, large D limit. As it will be explained in the following, such an interaction term would produce subleading diagrams in the large D limit if one were to use the standard scaling of the coupling constant. From a holographic perspective, the field content of this model is very similar to the one we encounter in the D-brane constructions which were presented in Chapter 2. In that context we had D scalar fields in the adjoint of SU(N), where D parameterized the number of transverse directions to the D-branes. Moreover, we recognize in the Hamiltonian (3.3.11) a quartic interaction term which is also present both in $\mathcal{N}=4$ SYM theory and in D0-brane quantum mechanics. In those explicit realizations of the gauge/gravity duality, we have $D=6$ and $D=9$ respectively. The fact that we have two distinct parameters N and D is very convenient since, from a holographic point of view, the two symmetries they are associated to distinct physical properties. While the O(D) symmetry should be a global symmetry of the theory, associated to the rotation symmetry of the transverse directions, the U(N) is associated to a local symmetry of the boundary theory, and should in principle be gauged. It is also important to stress that in these models the large N and large D do not commute, as it will be shown in Chapter 4. In order to obtain a well-defined limit, one needs to take the large N limit first, and then the large D limit. In the holographic picture,

this corresponds to taking the classical limit of bulk gravity, and then its limit for a high number of spacetime dimensions. As it was shown by Emparan and others [61, 62, 63], such a limit of general relativity can be taken in a meaningful way, capturing many non-trivial features of gravity and in particular of black hole solutions. On top of the striking similarities, in terms of field content, interactions and symmetries, to explicit examples of boundary gauge theories, such models also have the nice feature that their basic degrees of freedom are matrices: they can have therefore a stringy interpretation and can be used to perform a probe analysis along the lines of the one sketched in Section 3.1.2, in order to try and reconstruct the properties of the gravitational bulk dual in a well-defined framework.

Chapter 4

Diagrammatics and bilocal structure of melonic models

4.1 SYK diagrammatics

Although the fundamental degrees of freedom of the SYK model are fermionic U(N) vectors , its diagrammatic structure in the large N limit differs substantially from that of standard vector models and this is what makes the model interesting from the holographic point of view. The structural difference from the usual vector models comes essentially from the random coupling: the fact that is averages to zero suppresses all diagrams with an odd number of vertices and results in the melonic structure at $N \to \infty$. To illustrate this, we perform the first two corrections to the bare propagator of the fermions in perturbation theory. The fermion two-point function is defined as

$$G(t) = \frac{1}{N}\langle \mathrm{T}\chi_m(t)\chi_m(0)\rangle \,. \tag{4.1.1}$$

In perturbation thory, the first correction it gets is given by

$$\frac{1}{N}J_{ijkl}\langle \chi_m(t)\chi_m(0)\chi_i\chi_j\chi_k\chi_l(\tau)\rangle \,, \tag{4.1.2}$$

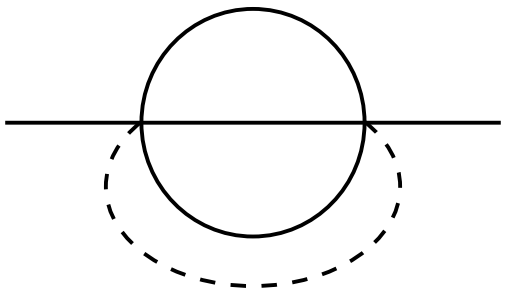

Figure 4.1: The basic graphical unit of the SYK model. The solid lines are fermions χ_i, the dotted line is the coupling J_{ijkl}.

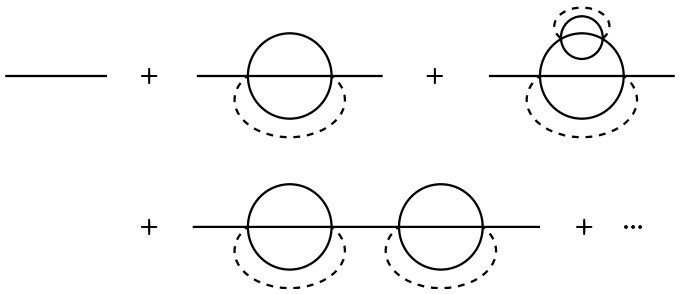

Figure 4.2: The first few corrections to the bare two-point function in the SYK model.

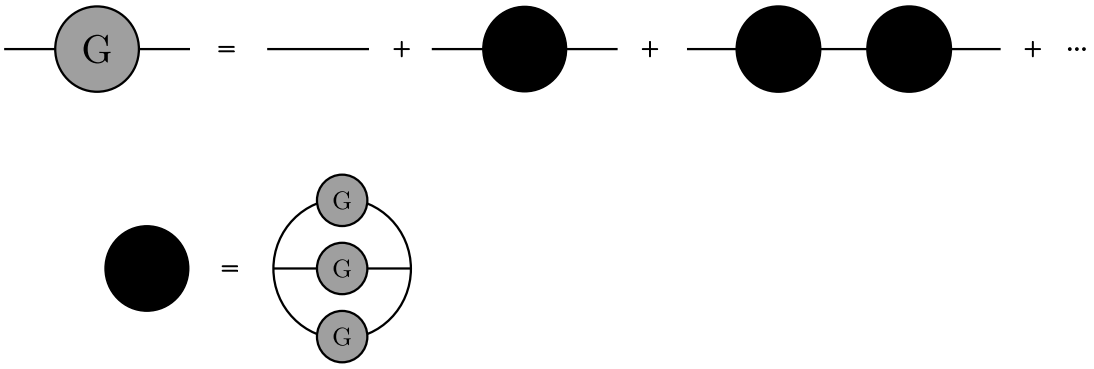

Figure 4.3: Graphical representation of the Schwinger-Dyson equations for the SYK model. The solid circle corresponds to the one-particle irreducible self-energy of the fermions.

but since the random couplings average to zero, it does not contribute. One can then consider the second order contribution:

$$\frac{1}{N}\frac{1}{2}J_{ijkl}J_{i'j'k'l'}\langle\chi_m(t)\chi_m(0)\chi_i\chi_j\chi_k\chi_l(\tau_1)\chi_{i'}\chi_{j'}\chi_{k'}\chi_{l'}(\tau_2)\rangle\,, \tag{4.1.3}$$

Taking the average over the disorder gives

$$\frac{1}{2}\frac{3!\lambda^2}{N^4}\delta_{ii'}\delta_{jj'}\delta_{kk'}\delta_{ll'}\langle\chi_m(t)\chi_m(0)\chi_i\chi_j\chi_k\chi_l(\tau_1)\chi_{i'}\chi_{j'}\chi_{k'}\chi_{l'}(\tau_2)\rangle\,. \tag{4.1.4}$$

It becomes clear that in order to recover the necessary number of factors of N, the only allowed Wick contractions are the ones that pair three fermions of the τ_1 vertex with the corresponding three fermions with primed indices in τ_2 (e.g. i, j, k paired with i', j', k' respectively). The resulting diagram is the melon depicted in Figure 4.1, where also the pairing of the vertices in shown with a dashed line. This structure can be iterated to generate all the leading large N diagrams which contribute to the propagator, the first few of which are illustrated in Figure 4.2. The simple structure we showed, results in the summability of the leading large N diagrams, and therefore allows us to write compact Schwinger-Dyson equations

for the correlators of the model. For the two-point function defined in (4.1.1), the result of summing over all melon diagrams can be graphically depicted as in Figure 4.3, which is equivalent to the following Schwinger-Dyson equations

$$\frac{1}{G(\omega)} = -i\omega - \Sigma(\omega), \qquad \Sigma(\tau) = \lambda^2 \left[G(\tau)\right]^3 , \tag{4.1.5}$$

where Σ is the one-particle irreducible self-energy of the fermions. The same Schwinger-Dyson equation, with slight modifications if we consider models with a mass term in the Hamiltonian, is shared by all melonic models presented in the previous chapter, and is at the core of many of the interesting properties they have in common.

4.2 Large D matrix model diagrammatics

4.2.1 Models

The melonic matrix-vector model defined in Section 3.3.3 belongs to a class of matrix field theories which can be defined in any number of spacetime dimensions and which can be models of either bosonic or fermionic matrices. Such models were presented and studied in [60] and the rest of the section is largely based on it. For simplicity we will stick to 0+1 dimensions, and bosonic matrices since the following diagrammatic considerations are not affected by the dimensionality or the commuting/anticommuting nature of the matrices. We study Lagrangians of the form

$$L = ND\left(\mathrm{tr}\left(\dot{X}^\dagger_\mu \dot{X}_\mu + m^2 X^\dagger_\mu X_\mu\right) - \sum_B t_B I_B(X)\right), \tag{4.2.1}$$

where the t_B are coupling constants and the I_B are single-trace interaction terms of the form

$$I_B = \mathrm{tr}\left(X_{\mu_1} X^\dagger_{\mu_2} X_{\mu_3} \cdots X^\dagger_{\mu_{2s}}\right) , \tag{4.2.2}$$

such that the μ_i are contracted pairwise to ensure the $\mathrm{O}(D)$ symmetry of the model. For example, the quartic vertex in (3.3.11) is one of the two possible $\mathrm{O}(D)$-symmetric, single-trace vertices, the other being

$$I_{4,1} = \mathrm{tr}\left(X_\mu X^\dagger_\mu X_\nu X^\dagger_\nu\right) . \tag{4.2.3}$$

We will see in the next section that all the following derivations can be generalized to multi-trace interaction terms.

4.2.2 Genus of a vertex

We can represent graphically each interaction term I_B in several different ways. Three of them, namely the colored, ribbon and stranded graph representations, are depicted in Figure 4.4. The colored graph (c-graph) associated to an interaction

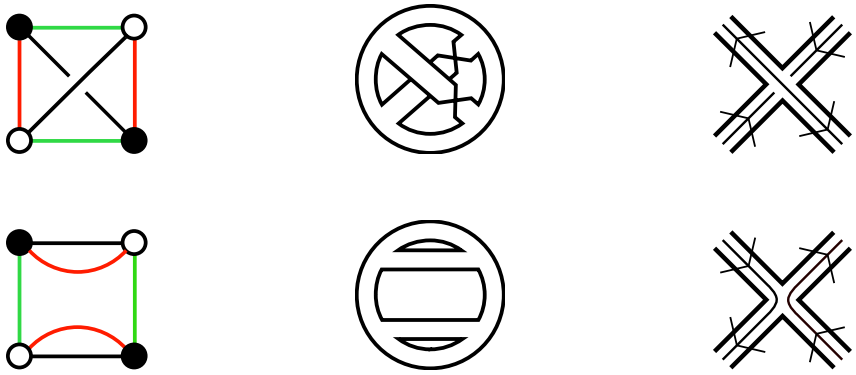

Figure 4.4: Colored (left), ribbon (center) and stranded (right) graphs associated to the two quartic vertices $\mathrm{tr}\left(X_\mu X_\mu^\dagger X_\nu X_\nu^\dagger\right)$ (up) and $\mathrm{tr}\left(X_\mu X_\nu^\dagger X_\mu X_\nu^\dagger\right)$ (down). The two vertices have genus zero and one-half respectively.

term I_B is obtained in the following way: first we associate to each X ($X^\dagger$) an unfilled (filled) vertex. Then we associate indices a, b and μ to green, red and black lines respectively: we connect the vertices with such lines, according to the index contractions prescribed by the form of I_B. It is important to notice that, while green and red lines can only link unfilled vertices with filled ones, black lines can connect vertices of the same kind. In other words, the red and the green lines respect the bipartite structure of the graph, while the black ones do not. One can easily obtain the ribbon graph (r-graph) from the colored one by choosing a cyclic clockwise (anticlockwise) ordering of the black, red and green lines around each unfilled (filled) vertex. The number of faces in the c-graph is determined by the number of cycles made of lines of alternating color: this is equal to the number of faces of the r-graph if we twist the ribbon corresponding to a black line connecting two vertices of the same same type, as shown in Figure 4.4. We can now associate to each interaction term a quantity $g(B)$ called genus of the interaction B, which is defined as the genus of the ribbon graph associated to B. Finally, the stranded graph (s-graph) is simply obtained taking the standard fat graph for the $\mathrm{U}(N)$ indices, and adding an internal line for the $\mathrm{O}(D)$ ones.

4.2.3 Standard scaling vs. new scaling

Taking the large N and large D limit in the standard way consists in treating the model as a matrix model with respect to the $\mathrm{U}(N)$ symmetry and as a vector model with respect to the $\mathrm{O}(D)$ symmetry. With a Lagrangian written as in 4.2.1, with a factor of ND in front of it, the standard scaling amounts to keeping all the couplings t_B fixed. In the melonic example (3.3.11) the standard scaling would be obtained by removing the $\sqrt{D}$ factor in front of the quartic coupling. When this scaling is used the large N and large D limits commute, and only genus zero interaction terms contribute to the leading order N^2D. In particular, all diagrams containing the interaction term (3.3.11) would be subleading. In

the standard scaling, this family of models behaves more like vector models than matrix models: the class of leading diagrams is too small to contain the non-trivial physics of holographic models. The new scaling consists in keeping $\lambda_B = D^{-g(B)} t_B$ fixed instead of t_B. This produces an enhancement of the couplings of interaction terms with $g(B) > 1$ which in turn results in a larger number of diagrams contributing at each order in the large N and large D limits. In (3.3.11), this enhancement corresponds to the $\sqrt{D}$ factor in front of the quartic coupling. Since this enhancement involves only D, the expansion in powers of $1/N$ for each physical quantity is the usual one. For example, for the free energy F we have

$$F = \sum_{g \in \mathbb{N}} F_g(D) N^{2-2g} \,, \tag{4.2.4}$$

where g is as usual associated to the genus of the fat graphs which contribute to the free energy. Clearly, the coefficients F_g now depend on D and, in fact, they can be expanded in powers of $1/\sqrt{D}$ in the following way

$$F_g = \sum_{\ell \in \mathbb{N}} F_{g,\ell} D^{1+g-\ell/2} \,. \tag{4.2.5}$$

It is clear from this expression that a Feynman diagram contributing to the free energy can be proportional to an arbitrary power of D but, at fixed fat graph genus g, its power of D cannot exceed D^{1+g}. Hence, when we use the new scaling, the large N limit must be taken before the large D limit: the two limits do not commute.

4.2.4 Proof

We will now provide a proof for the expression (4.2.5), in the case of complex matrices, keeping in mind that these results do not apply just to the free energy, but can be generalized to connected correlation functions as well. Similarly to the vertices depicted in Figure 4.4, each vacuum Feynman diagram which contributes to the free energy can be represented both as an s-graph and as a c-graph. The s-graph is obtained straighforwardly: the vertices in the s-graph representation are connected with each other by propagators, represented by two lines for the U(N) indices and one for the O(D) index which runs through it. The corresponding c-graph representation is obtained replacing each vertex by its 3-colored c-graph and by joining each vertex by a line of a new color (violet), representing the propagators. An example of s-graph and c-graph representations for the same vacuum diagram is depicted in Figure 4.5. Since propagators always connect X with $X^\dagger$, the violet lines always respect the bipartite structure of the c-graph. Now we need to introduce some terminology for the resulting 4-colored graph. First of all, we denote colors (violet, green, red, black) by numbers (0, 1, 2, 3). We call a face of colors (i, j), with $i \neq j$, a closed cycle of alternating colors i and j. For our 4-colored graphs, the sum of the numbers of (0, 1) and (0, 2) faces corresponds to the number of closed loops of U(N) indices, while the (0, 3) faces

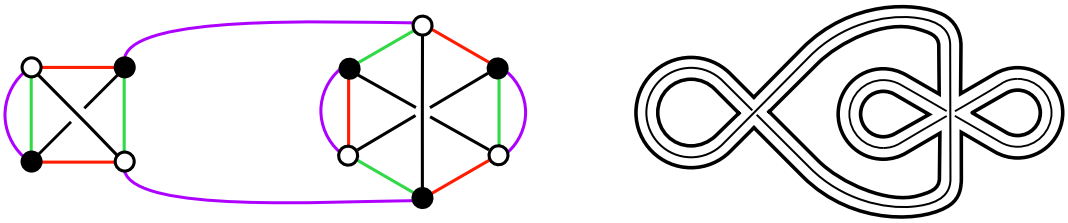

Figure 4.5: Example of vacuum diagram in the c-graph (left) and s-graph (right) representations.

correspond to loops of $\mathrm{O}(D)$ indices. Each Feynman diagram is characterized by the following quantities in the s-graph: number of $\mathrm{U}(N)$ loops f, number of $\mathrm{O}(D)$ loops φ, number of propagators p, total number of vertices v and number of $2s$-valent vertices v_{2s}. To the c-graph, instead, we can associate the number of $(i\,,j)$-faces F_{ij} and the number of vertices V. All these quantities satisfy

$$f = F_{01} + F_{02}\,, \qquad \varphi = F_{03}\,, \qquad V = 2\sum_s s v_{2s} = 2p\,. \tag{4.2.6}$$

Now, the N dependence of a Feynman diagram of a model defined by the Lagrangian (4.2.1) is just the usual matrix model dependence N^{2-2g} where g is the genus of the fat graph obtained by removing the $\mathrm{O}(D)$ lines from the s-graph and is given by

$$g = 1 + \frac{1}{2}(p - v - f)\,. \tag{4.2.7}$$

On the other hand the D dependence, keeping in mind that in the new scaling each interaction vertex B_a is enhanced by a factor of $D^{g(B_a)}$, is given by

$$D^{-p+v+\varphi+\sum_a g(B_a)}\,. \tag{4.2.8}$$

Matching (4.2.5) with (4.2.8) gives

$$\ell = 4 - 3v + 3p - f - 2\varphi - 2\sum_{a=1}^{v} g(B_a)\,. \tag{4.2.9}$$

Now, in order to show that $\ell \geq 0$, we proceed in the following way: from the 4-colored graph we remove all lines of color i, obtaining $B^{(i)}$ connected 3-colored graphs which we name $B_a^{(i)}$, with $1 \leq a \leq B^{(i)}$. Just like we did for the graphs associated to the interaction vertices, we can associate a ribbon graph to each of these connected components, and therefore a genus $g(B_a^{(i)})$. We can then define

$$g_i = \sum_a g(B_a^{(i)})\,. \tag{4.2.10}$$

Similarly, one can remove two colors i and j from the c-graph, obtaining a set of $B^{(ij)}$ connected 2-colored graphs which we name $B_a^{(ij)}$, with $1 \leq a \leq B^{(ij)}$. In

terms of these quantities, ℓ can be rewritten in the following way

$$\frac{\ell}{2} = g_1 + g_2 + \left(B^{(01)} - B^{(0)} - B^{(1)} + 1\right) + \left(B^{(02)} - B^{(0)} - B^{(2)} + 1\right) . \quad (4.2.11)$$

Written in this form, it is clear that $\ell \geq 0$, if we are able to prove that

$$B^{(ij)} - B^{(i)} - B^{(j)} + 1 \geq 0 . \quad (4.2.12)$$

This is actually a general property of the diagrams we encounter in our models. Let us call $\mathcal{B}^{(ij)}$ the graph which is obtained by removing both the i and the j lines from the original graph, and which has $B^{(ij)}$ connected components. Since erasing only the j lines from the orginal graph produces $B^{(j)}$ connected components, this means that redrawing the j-lines in $\mathcal{B}^{(ij)}$ should reduce the number of connected components by at least $B^{(j)} - 1$.

4.3 More on the new large D limit of matrix models

This new scaling opens the door to the study of a whole new class of $\mathrm{U}(N)^2\times$ $\mathrm{O}(D)$ (or $\mathrm{U}(N)\times$ $\mathrm{O}(D)$ in the case of Hermitian matrices) matrix models which was not tractable before. Since this is a completely new developement in the study of matrix models and it has potentially interesting applications in the context of holography, it is worth trying to get into the details of the properties of the large D limit of the models defined in [60] and of generalizations thereof. In [1], which can be found attached in its entirety in Appendix A, the analysis of [60] is extended in several ways.

4.3.1 Multi-trace models

One obvious generalization consists in considering models with multi-trace interactions, rather than just the single-trace ones defined in (4.2.2). Once multi-trace interaction terms are introduced, as well as their stranded and colored graph representations along the lines of Figure 4.4; it is necessary to introduce an appropriate scaling in powers of N and D of the coupling constants in order to obtain a well-defined large N, large D limit of the model. Such scalings are defined, and it is proved that they give rise to a well-defined large N, large D limit by counting the powers of N and D of a generic Feynman diagram contributing to the free energy of the model. It is moreover shown what kinds of diagrams contribute to the leading order in that limit.

4.3.2 Models with reduced symmetry

In the framework of tensor models, attempts were made to study models with reduced symmetry [58, 65, 66]. This amounts to imposing symmetry constraints

on the tensors, which result in a reduction of the symmetry of the model from $\mathrm{O}(N)^3$ to $\mathrm{O}(N)^2$ or even just $\mathrm{O}(N)$. However, if one does not impose additional constraints on the tensors (like a tracelessness condition), it can be shown that their large N limit cannot be well-defined. A similar problem appears when one tries to reduce the symmetry of matrix-vector models from $\mathrm{U}(N)^2\times\mathrm{O}(D)$ to $\mathrm{U}(N)\times\ \mathrm{O}(D)$ by considering Hermitian matrices. While it was shown in [60] that the planar limit of such models admits a well-defined large D limit, a specific class of genus one diagrams can be constructed, which is proportional to arbitrary powers of D, thus spoiling the good behaviour of the large D limit. However, by imposing the condition of tracelessness to the matrices, this particular class of diagrams becomes well-behaved, leading us to conjecture that the model with traceless Hermitian matrices admits a large D limit for each genus of the large N expansion.

4.3.3 Correlation functions

Since all the proofs and derivations so far, both in the single-trace and multi-trace cases, involved only Feynman diagrams contributing to the free energy, we now focus on the N and D power counting for correlation functions. We focus on connected $2n$-point correlators and show how they have well-defined large N and large D limit, as well as which diagrams contribute to them at leading order.

4.3.4 Model building

The diagrammatic considerations we made so far apply to a large class of matrix-vector models, whose strongly coupled physics can in principle be accessed with this new truncation of the planar expansion. These models can be defined in different numbers of spacetime dimensions, they can be models of fermionic and bosonic matrices, and there is a large variety of possible interaction terms which can be studied in this framework. Since the fermionic model defined in (3.3.11) leads to the same non-trivial properties as the SYK model, it is natural to ask oneself if also bosonic models can feature such interesting properties. As it turns out, a careful analysis for the Schwinger-Dyson equations of two bosonic models shows that such models indeed have crucially different properties with respect to their fermionic counterparts. A more in-depth analysis of this phenomenon can be found in [64]. Another natural question is whether the new large D limit is consistent with supersymmetry. Indeed, one can construct supersymmetric matrix-vector models with two or four supercharges, but it is not obvious that supersymmetry is preserved as one takes D to infinity. Interestingly, supersymmetry is shown to be consistent with the new large D limit. It is also important to stress that, unlike the supersymmetric version of SYK we defined in (3.3.7) and (3.3.8), in matrix-vector models the supersymmetry is linearly realized.

4.4 Bilocal structure

As it was shown in the previous section, three apparently very different classes of models share a similar diagrammatic structure in a specific limit ($N \to \infty$ for SYK and tensor models, $N, D \to \infty$ for O(D) matrix models [1]). This ultimately leads to them describing the same non-trivial physics, as it will be shown in the next chapter. In this section we will see how the diagrammatic structure of such models is related to bilocality [67] and how this property sets them apart from vector models, whose large N behaviour has none of the properties we look for in holographic models.

4.4.1 An instructive computation

In order to better understand the link between the melonic structure of the leading diagrams of the aforementioned models and bilocality, we reproduce here a simple computation that can be performed in the SYK model. If instead of performing the average over the disorder as it was defined in (3.3.3), we treat the random couplings J_{ijkl} as quantum variables on the same footing as the fermions χ_i, the expectation value of an operator O becomes

$$\langle O \rangle = Z^{-1} \int \mathcal{D}J_{ijkl} \mathcal{D}\chi_i \, O \exp\left(-J_{ijkl}^2 N^3/12\lambda^2 - \int dt L \right) , \tag{4.4.1}$$

which is a clearly diffrent expression from (3.3.3). In the Condensed Matter literature, this way of taking the average over the random coupling is called annealed disorder, in contrast with the quenched disorder which is featured in the SYK model. In general, these two kinds of disorder lead to very different physics, however it can be shown that in the large N limit, if we restrict ourselves to the computation of connected correlation functions, this way of integrating out the random couplings is equivalent to the quenched one. Using this technique, the partition function can be computed in the following way:

$$Z = \int \mathcal{D}J_{ijkl} \mathcal{D}\chi_i \, O \exp\left(-J_{ijkl}^2 N^3/12\lambda^2 - \int dt \frac{1}{2} \chi_i \dot{\chi}_i - J_{ijkl} \chi_i \chi_j \chi_k \chi_l \right) , \tag{4.4.2}$$

The J_{ijkl} appear only quadratically and can therefore be integrated out right away, leaving us with a non-local action for the fermions.

$$Z = \int \mathcal{D}\chi_i \exp\left(- \int dt \frac{1}{2} \chi_i \dot{\chi}_i - \int dt_1 dt_2 \frac{\lambda^2}{4N^3} \chi_i \chi_j \chi_k \chi_l(t_1) \chi_i \chi_j \chi_k \chi_l(t_2) \right) . \tag{4.4.3}$$

This rewriting of the SYK model makes it appearent how its properties are so different from an ordinary vector model: the fermions are now coupled through a

[1] It is important to stress that if one considers subleading diagrams, the three kinds of models have a very different structure. In particular, the SYK model has a much simpler structure than the other two.

bi-local octic coupling. One can now use the standard vector model technique of introducing auxiliary fields $\tilde{G}$ and $\tilde{\Sigma}$ that allow us to perform the integration over the fermions, leaving us with

$$Z = \int \mathcal{D}\tilde{G}\mathcal{D}\tilde{\Sigma}\exp\Bigg\{N\Bigg[\log \mathrm{Pf}(\partial_t - \tilde{\Sigma}) - \frac{1}{2}\int dt_1 dt_2 \Bigg(\tilde{\Sigma}(t_1,t_2)\tilde{G}(t_1,t_2) - \frac{\lambda^2}{4}\tilde{G}(t_1,t_2)^4\Bigg)\Bigg]\Bigg\} . \tag{4.4.4}$$

Notice that since $\tilde{G}$ and $\tilde{\Sigma}$ do not carry $\mathrm{U}(N)$ indices, and there is a factor N in front of their action, in the $N \to \infty$ limit we can perform the path integral by setting the two fields to their saddle point values, which we will call G and Σ respectively. This is done by solving their equations of motion, which turn out to be the Schwinger-Dyson equations for the two-point function and the self-energy we derived from diagrammatic considerations at the beginning of the chapter. In fact, varying the effective action with respect to $\tilde{\Sigma}$ and $\tilde{G}$ we obtain respectively

$$\frac{1}{G(\omega)} = -i\omega - \Sigma(\omega)\,, \qquad \Sigma(\tau) = \lambda^2\left[G(\tau)\right]^3 . \tag{4.4.5}$$

It can be shown that analogous rewritings of the partition function in terms of bilocal fields $\tilde{G}$ and $\tilde{\Sigma}$ can be used also for the other two classes of models which share the same Schwinger-Dyson equations as the SYK model, even though in those cases it cannot be straightforwardly obtained from a path integral computation as the above one. It is important to stress that if we had had a local action for the fermions, instead of the one in (4.4.3), we would have ended up with completely different, and much less interesting, physical properties. This can be easily shown computing the following partition function

$$Z = \int \mathcal{D}\chi_i \mathcal{D}\bar{\chi}_i \exp\left(-\int dt \bar{\chi}_i \partial_t \chi_i + \frac{\lambda^2}{4N^3}\bar{\chi}_i\bar{\chi}_j\bar{\chi}_k\bar{\chi}_l\chi_i\chi_j\chi_k\chi_l\right) , \tag{4.4.6}$$

which is just the local analogue of (4.4.3), and we used complex fermions in order to have a non-zero interaction term. This model is easily solvable through the introduction of an auxiliary field ϕ and a Lagrange multiplier L:

$$Z = \int \mathcal{D}\chi_i \mathcal{D}\bar{\chi}_i \mathcal{D}\phi \mathcal{D}L \exp\left(-\int dt \bar{\chi}_i \partial_t \chi_i + L(\bar{\chi}_i\chi_i - N\phi) + \frac{N\lambda^2}{4}\phi^4\right) . \tag{4.4.7}$$

Similarly to the non-local case, in the large N limit the auxiliary fields settle to their saddle point values ϕ_* and L_*, which satisfy the following equations

$$\phi_* = 1 - G(0^+)\,, \qquad L_* = \lambda^2\phi_*^3\,, \tag{4.4.8}$$

with

$$G(t) = \frac{1}{N}\left\langle \chi_i(t)\bar{\chi}_i(0)\right\rangle , \qquad G(\omega) = \frac{1}{-i\omega + L_*}\,. \tag{4.4.9}$$

However now the properties of the model are much more trivial with respect to the non-local case. In the large N limit, the effect of the interaction term in (4.4.6) is just to introduce a mass term for the fermions. The resulting effective action is just that of a fermionic harmonic oscillator, which clearly features none of the interesting properties (continuous spectrum, quasi-normal behaviour, chaos, etc.) we look for in a model of holography.

Chapter 5

Physical properties of melonic models

5.1 Two-point functions and emergent symmetry

We have seen that the melonic models we presented in Section 3.3 all share the same diagrammatic structure in some appropriate limit. Since they are all defined in 0+1 dimensions and describe fermionic variables, this results in the zero-temperature Schwinger-Dyson equations for the two-point functions of the fermions being the same for all three models :

$$\frac{1}{G(\omega)} = -i\omega - \Sigma(\omega)\,, \qquad \Sigma(\tau) = \lambda^2 \left[G(\tau)\right]^3 \,. \tag{5.1.1}$$

In the strong coupling regime $\lambda|\tau| \gg 1$ the $-i\omega$ term on the right hand side of the first equation can be neglected, yielding

$$G(\omega)\Sigma(\omega) = -1\,, \qquad \Sigma(\tau) = \lambda^2 \left[G(\tau)\right]^3 \,, \tag{5.1.2}$$

and the two equations can be combined into a single integral equation

$$\lambda^2 \int d\tau' G(\tau,\tau') G(\tau',\tau'')^3 = -\delta(\tau - \tau'')\,. \tag{5.1.3}$$

This equation is invariant under time reparameterizations in the following sense. Given a solution of (5.1.3) $G(\tau)$ we can always construct another solution $\tilde{G}(\sigma)$ through a time reparameterization $\tau \to \sigma(\tau)$:

$$\tilde{G}(\sigma_1,\sigma_2) \equiv G(\tau(\sigma_1) - \tau(\sigma_2)) \left|\tau'(\sigma_1)\tau'(\sigma_2)\right|^{\frac{1}{4}} \,. \tag{5.1.4}$$

It can be verified, by making use of the relation

$$\int_{-\infty}^{\infty} d\tau e^{i\omega\tau} \frac{\mathrm{sgn}(\tau)}{|\tau|^{\Delta}} = i 2^{1-\Delta}\sqrt{\pi} \frac{\Gamma\left(1-\frac{\Delta}{2}\right)}{\Gamma\left(\frac{1}{2}+\frac{\Delta}{2}\right)} |\omega|^{1-\Delta} \mathrm{sgn}(\omega)\,, \tag{5.1.5}$$

that the power-law ansatz

$$G(\tau) = \frac{b}{|\tau|^{\frac{1}{2}}} \mathrm{sgn}(\tau)\,, \tag{5.1.6}$$

solves the IR Schwinger-Dyson equation (5.1.2) with b satisfying $\lambda^2 b^4 \pi = 1/4$. From these considerations, we see that melonic models flow to a conformal IR fixed point, with the fermions aquiring a scaling dimension of 1/4.

From zero to finite temperature

Obtaining the finite temperature IR propagator of the fermions from the zero temperature one given by (5.1.6) is not trivial. In two-dimensional conformal field theories, one can exploit the fact that there is only one analytic map from the cylinder to the plane, namely the exponential function. However in one dimension, as is the case for the melonic models we are considering, one has an infinite number of analytic maps from the circle to the line. In the literature [50, 48], however, the tangent map is chosen to obtain the finite temperature result, with no justification regarding that choice. We propose instead that a criterion needs to be found to obtain the correct time reparameterization which can be used to get the finite temperature result. When we look at (5.1.4), we notice that the new solution of the IR Schwinger-Dyson equation $\tilde{G}(\sigma_1, \sigma_2)$, obtained from another solution $G(t)$ through a time reparameterization $\sigma(t)$, is not in general invariant under translations of the new time coordinate σ. This is however a necessary requirement for the two-point function of a quantum mechanical model with a time independent Hamiltonian. Such a requirement restricts the class of admissible time reparameterizations which can be performed on a given solution $G(\tau)$. In particular, if $G(\tau)$ is the power law ansatz (5.1.6), we have:

$$\tilde{G}(\sigma_1, \sigma_2) = \frac{b}{|\tau(\sigma_1) - \tau(\sigma_2)|^{\frac{1}{2}}} \mathrm{sgn}(\tau(\sigma_1) - \tau(\sigma_2)) \, |\tau'(\sigma_1)\tau'(\sigma_2)|^{\frac{1}{4}}\,. \tag{5.1.7}$$

We want the new solution to be time translation invariant, therefore we impose

$$\left(\frac{d}{d\sigma_1} + \frac{d}{d\sigma_2}\right) \tilde{G}(\sigma_1, \sigma_2) = 0\,. \tag{5.1.8}$$

Combining (5.1.7) and (5.1.8) we obtain a differential equation for $\tau(\sigma)$:

$$2\left(\tau'(\sigma_1) - \tau'(\sigma_2)\right) = \left(\tau(\sigma_1) - \tau(\sigma_2)\right)\left(\frac{\tau''(\sigma_1)}{\tau'(\sigma_1)} + \frac{\tau''(\sigma_2)}{\tau'(\sigma_2)}\right)\,. \tag{5.1.9}$$

We can moreover impose $\tau(0) = 0$, since also the new solution needs to be odd. The resulting differential equation takes the form

$$-2\left(\tau'\right)^2 + 2a\tau' + \tau\tau'' + b\tau\tau' = 0\,, \tag{5.1.10}$$

with $a = \tau'(0)$ and $b = \tau''(0)$. We can rewrite it in terms of $u(\tau) \equiv \dot{\sigma}(\tau)^{-1}$, where the dotted notation corresponds to taking the derivative with respect to τ. The differential equation for u is

$$\dot{u} - 2\frac{u}{\tau} = -2\frac{a}{\tau} - b\,, \tag{5.1.11}$$

which is solved by $u(\tau) = a + bt + kt^2$, with k being an integration constant. This results in the following expression for $\sigma(\tau)$:

$$\sigma(\tau) = \frac{2}{\sqrt{4ak - b^2}} \arctan\left(\frac{b + 2k\tau}{\sqrt{4ak - b^2}}\right) . \tag{5.1.12}$$

This solution is consistent with initial conditions $\sigma(0) = 0$, $\dot{\sigma}(0) = 1/a$ and $-\left(\dot{\sigma}(0)\right)^{-3} \ddot{\sigma}(0) = b$ only if $b = 0$. This results in the most general form $\sigma(\tau)$ can take

$$\sigma(\tau) = k_1 \arctan\left(k_2 \tau\right) , \tag{5.1.13}$$

where k_1 and k_2 are arbitrary constants. By imposing time translation invariance on the transformed correlator, we have obtained a very strict prescription on the admissible time reparameterizations which can be performed on the power law solution of the IR Schwinger-Dyson equation. More specifically, there is only one map from the circle to the line which preserves time translation invariance: the tangent map. Therefore, in order to obtain the finite temperature IR propagator, we have to use $\tau(\sigma) = \tan\frac{\sigma\pi}{\beta}$. By plugging it into (5.1.7), we obtain

$$G_\beta(\tau) = b\left[\frac{\pi}{\beta|\sin\frac{\pi\tau}{\beta}|}\right]^{\frac{1}{2}} \mathrm{sgn}(\tau)\,. \tag{5.1.14}$$

The retarded propagator is obtained from the finite temperature one through analytic continuation to real time [50]:

$$G_{\beta,R}(t) \equiv \langle\psi(t)\psi(0) + \psi(0)\psi(t)\rangle\theta(t) = b\left[\frac{2\pi}{\beta\sinh\frac{\pi t}{\beta}}\right]^{\frac{1}{2}} \theta(t)\,. \tag{5.1.15}$$

From this expression we get the exponential decay corresponding to the desired quasi-normal behaviour, and we can read off the frequencies of the quasi-normal modes $\omega_n = -i\frac{2\pi}{\beta}(n + 1/4)$.

From the study of the fermion propagators we have showed already two striking properties of melonic models:

- an emergent time-reparameterization symmetry which is spontaneously broken down to $SL(2, R)$ by the power law solution (5.1.6)
- an exponential late-time decay of retarded propagators consistent with quasi-normal behaviour

5.2 Low temperature entropy

It is well established that extremal black holes have a finite entropy at zero temperature, which is proportional to the area of the horizon. Such a property should be shared also by the quantum theory living on the boundary of a spacetime containing such black hole solutions. Since a typical quantum mechanical model is in its ground state at $T = 0$, a large finite entropy can only be obtained if a large number of states becomes indistinguishable from the ground state in the large N limit. It can be shown that this is indeed the case for melonic models. The easiest way to do so is by exploiting the generalization of the SYK model with a q-fermion Hamiltonian defined in (3.3.6). As it was mentioned, in this model we can take the $q \to \infty$, which is well-defined as long as the following combination of λ and q is held fixed:

$$\mathcal{J} \equiv \sqrt{q}\frac{\lambda}{2^{\frac{q-1}{2}}} \,. \tag{5.2.1}$$

In this limit, many simplifications occur. In particular, the free energy of the model can be computed as an expansion in powers of $1/q$ [50]:

$$-\frac{\beta F}{N} = \frac{1}{2}\ln 2 + \frac{1}{q^2}\alpha_2 + O\big(q^{-3}\big) \,. \tag{5.2.2}$$

The coefficient α_2 can be in turn expanded in powers of $(\beta\mathcal{J})^{-1}$, giving:

$$-\frac{\beta F}{N} = \frac{1}{2}\ln 2 + \frac{1}{q^2}\left[\beta\mathcal{J} - \frac{\pi^2}{4} + \frac{\pi^2}{2\beta\mathcal{J}} + \cdots\right] + O\big(q^{-3}\big) \,. \tag{5.2.3}$$

By comparing (5.2.3) with the low temperature expansion of the free energy

$$F = E_0 - \frac{S_0}{\beta} + O(\beta^{-2}) \,, \tag{5.2.4}$$

we obtain that the entropy at zero temperature is given by

$$\frac{S_0}{N} = \frac{1}{2}\ln 2 - \frac{1}{q^2}\frac{\pi^2}{4} + O\big(q^{-3}\big) \,. \tag{5.2.5}$$

This result, which is consistent with finite-q results obtained with other methods [68, 69], tells us that the SYK model has an entropy of order N at low temperature.

5.3 Four-point functions and chaos

We have already used the simple diagrammatic structure of melonic models to compute their two-point functions, by exploiting the fact that they can be obtained through the iteration of the so-called melons. A similar approach can be used to compute four-point functions [70, 50]. In order to keep the number of indices to a minimum, we will present the case of the original SYK model, bearing in mind

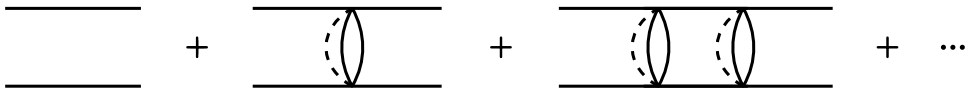

Figure 5.1: The first ladder diagrams contributing to the connected piece of the four point function of melonic models.

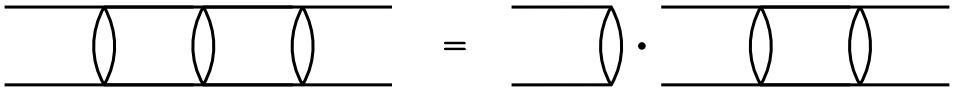

Figure 5.2: Graphical representation of the kernel K, acting on the two-rung ladder diagram.

that the following results apply both to the tensor and matrix melonic models as well. We will consider the following correlator

$$F(\tau_1,\,\tau_2,\,\tau_3,\,\tau_4) = \frac{1}{N^2}\,\langle T\,\chi_i(\tau_1)\chi_i(\tau_2)\chi_j(\tau_3)\chi_j(\tau_4)\rangle\ , \tag{5.3.1}$$

where summation over repeated indices is assumed. The first two contributions to its large N expansion are

$$F(\tau_1,\,\tau_2,\,\tau_3,\,\tau_4) = G(\tau_{12})G(\tau_{34}) + \frac{1}{N}\mathcal{F}(\tau_1,\,\tau_2,\,\tau_3,\,\tau_4) + \dots\,. \tag{5.3.2}$$

The first term is just given by two disconnected dressed propagators, while the first $1/N$ correction is given by the ladder diagrams depicted in Figure 5.1. If we call $\mathcal{F}_n$ the ladder diagram with n rungs, we can write

$$\mathcal{F} = \sum_n \mathcal{F}_n\,. \tag{5.3.3}$$

Much like the O(1) contribution to the four-point function, $\mathcal{F}_0$ is given by a product of disconnected dressed propagators

$$\mathcal{F}_0(\tau_1,\,\tau_2,\,\tau_3,\,\tau_4) = -G(\tau_{13})G(\tau_{24}) + G(\tau_{14})G(\tau_{23})\,. \tag{5.3.4}$$

The ladder diagrams with $n > 0$ can be obtained from $\mathcal{F}_0$ by iterating the diagrammatic structure depicted in Figure 5.2, in the following way

$$\mathcal{F}_{n+1}(\tau_1,\,\tau_2,\,\tau_3,\,\tau_4) = \int d\tau d\tau'\,K(\tau_1,\,\tau_2,\,\tau,\,\tau')\mathcal{F}_n(\tau,\,\tau',\,\tau_3,\,\tau_4)\,, \tag{5.3.5}$$

where the kernel K is given by

$$K(\tau_1,\,\tau_2,\,\tau_3,\,\tau_4) = -3\lambda^2 G(\tau_{13})G(\tau_{24})G(\tau_{34})^2\,. \tag{5.3.6}$$

If we see the integral combination defined in (5.3.5) as a multiplication, $\mathcal{F}$ is given by a geometric series, which can be summed giving

$$\mathcal{F} = \frac{1}{1-K}\mathcal{F}_0\,. \tag{5.3.7}$$

The problem of computing $\mathcal{F}$ translates into the problem of diagonalizing the kernel K. One therefore needs to find a complete set of eigenfunctions of K which satisfy the symmetry properties of the four-point function F. This would allow us to write schematically

$$F = \sum_h \Psi_h \frac{1}{1-k(h)} \frac{\mathcal{F}_0 \cdot \Psi_h}{\langle \Psi_h \cdot \Psi_h \rangle} \,, \tag{5.3.8}$$

where the Ψ_h are functions of two time variables labelled by a number h, such that

$$K \cdot \Psi_h = \int d\tau d\tau' \, K(\tau_1, \, \tau_2, \, \tau, \, \tau') \Psi_h(\tau, \, \tau') = k(h) \Psi_h(\tau_1, \, \tau_2) \,. \tag{5.3.9}$$

In the IR limit, one can exploit the SL(2, $\mathbb{R}$) invariance of the power-law ansatz. By using the following generators of the SL(2, $\mathbb{R}$) algebra:

$$\hat{D} = -\tau \partial_\tau - \frac{1}{4} \qquad \hat{P} = \partial_\tau \qquad \hat{K} = \tau^2 \partial_\tau + \frac{\tau}{2} \,, \tag{5.3.10}$$

one can construct a Casimir operator acting on two times τ_1 and τ_2:

$$C_{1+2} = \big(\hat{D}_1 + \hat{D}_2\big)^2 - \frac{1}{2}\big(\hat{K}_1 + \hat{K}_2\big)\big(\hat{P}_1 + \hat{P}_2\big) - \frac{1}{2}\big(\hat{P}_1 + \hat{P}_2\big)\big(\hat{K}_1 + \hat{K}_2\big) \,. \tag{5.3.11}$$

This Casimir commutes with the kernel K written in terms of the conformal propagator in the following sense

$$C_{1+2} K(\tau_1, \, \tau_2, \, \tau_3, \, \tau_4) = K(\tau_1, \, \tau_2, \, \tau_3, \, \tau_4) C_{3+4} \,. \tag{5.3.12}$$

The eigenfunctions of K must therefore also be eigenfunctions of C. Such functions have the form of conformal three point functions of two fermions with a dimension h operator:

$$\frac{\text{sgn}(\tau_1 - \tau_2)}{|\tau_1 - \tau_0|^h |\tau_2 - \tau_0|^h |\tau_1 - \tau_2|^{\frac{1}{2}-h}} \,, \tag{5.3.13}$$

and the corresponding $k(h)$ can be computed directly, yielding

$$k(h) = -\frac{3}{2} \frac{\tan \frac{\pi(h-1/2)}{2}}{(h-1/2)} \,. \tag{5.3.14}$$

It turns out that the complete set of eigenfunctions respecting the symmetries of the four-point function corresponds to a specific set of h:

$$h = \frac{1}{2} + is \qquad \text{or} \qquad h = 2n \,, \tag{5.3.15}$$

with s and n being a real number and a positive integer respectively. It can be immediately checked that $k(2) = 1$, which makes the expression for the four-point function (5.3.8) divergent. This should not come as a surprise: in order to

obtain the eigenvalues $k(h)$ we used the IR form of the two-point function, which is valid only for $\lambda\tau \gg 0$. This divergence can be dealt with by considering the first correction to the conformal propagator, proportional to the inverse effective coupling $(\beta\lambda)^{-1}$. This produces a shift of the $h = 2$ eigenvalue which results in a contribution to the four-point function proportional to $\beta\lambda$. In the strong coupling limit this contribution is enhanced with respect to all the contributions with $h \neq 2$, and by carefully continuing the four-point function to real time one can check that this enhanced contribution results in an exponential growth of the out-of-time-order four-point function, with a Lyapunov exponent which saturates the chaos bound [50].

5.4 Phase structure of complex melonic models

It was mentioned above that the presence of the mass term in melonic models of complex fermions leads to a richer phase space of the theory. In this section we make this statement more precise, following the results of [64]. The Schwinger-Dyson equation of the SYK model (or equivalently any massless melonic model) involves the resummation of a perturbative series whose starting point is the free fermion propagator:

$$G_{\text{free}}(t) = \frac{1}{2}\text{sgn}(t)\,. \tag{5.4.1}$$

The perturbative regime corresponds to the limit of very small effective coupling $\beta\lambda$. It is important to stress that in such a regime, the system is not in the Fock vacuum as it is customary in perturbation theory. Instead, in that limit the Hamiltonian of the model vanishes and the system is in a state with entropy $S = N(1/2)\ln 2$. In melonic models with no mass term, $\beta\lambda$ is the only dimensionless coupling of the theory, hence this is the only perturbative regime which can be defined. However, as we saw in the definition of the complex fermion generalization of the SYK model and in matrix-vector models, when the degrees of freedom are complex fermions we can add a mass term to the model. The presence of another parameter m allows for a second perturbative regime, corresponding to $\lambda/m \ll 1$ at fixed temperature. This definition of perturbation theory might seem more natural, since it is done around the Fock vacuum. In the second regime, the model has qualitatively different properties with respect to the first one: it behaves like a set of weakly coupled harmonic oscillators and therefore has zero entropy at $T = 0$. Since the choice of the perturbative regime does not influence the diagrammatic structure of the perturbative series of the model, both regimes result in the Schwinger-Dyson equation for massive melonic models:

$$\frac{1}{G_k} = m - i\nu_k + \Sigma_k\,, \qquad \Sigma(t) = \lambda^2 G(t)^2 G(-t)\,. \tag{5.4.2}$$

The difference between the two perturbative regimes can be understood by looking at the finite temperature propagator for a fermionic harmonic oscillator:

$$G_{\text{harm}}(t) = \frac{e^{m(\beta-t)}}{e^{\beta m}+1} \qquad \text{for} \qquad 0 < t < \beta\,, \tag{5.4.3}$$

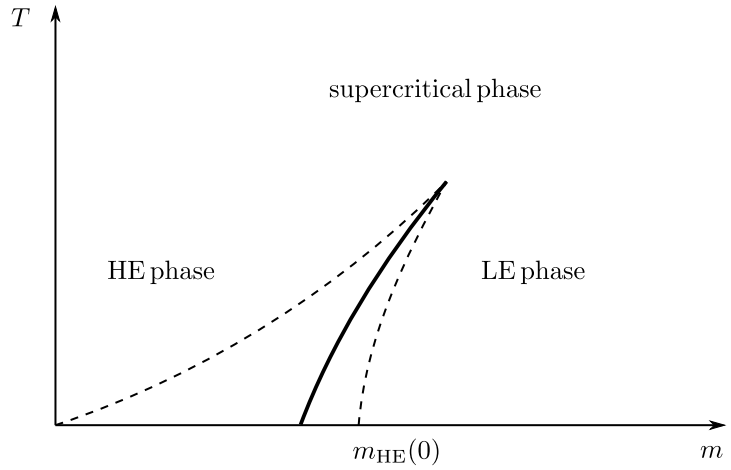

Figure 5.3: Qualitative sketch of the phase diagram of massive melonic models at fixed λ. The plain thick line corresponds to the phase transition between the LE and HE phases. In the region delimited by the dashed lines both the LE and the HE solutions exist.

with $G_{\rm harm}(t)$ given by antiperiodicity for $-\beta < t < 0$. If one takes the $m \to 0$ limit and then the $T \to 0$ limit, the result is the free massless fermion propagator at zero temperature, given in (5.4.1). Using this one as the starting point for the perturbative analysis results in all the properties we reviewed above, including a finite low temperature entropy. On the other hand, by reversing the order of the limits one obtains the small mass limit of the zero temperature propagator for a fermionic hamonic oscillator $\theta(t)e^{-mt}$. It is trivial to check that this form of the propagator solves the zero temperature limit of the Schwinger-Dyson equations (5.4.2), since the presence of the $\theta(t)$ factor implies $\Sigma(t) = 0$. Such a solution clearly encodes different physics with respect to SYK-like solution, in particular it will not feature a finite low temperature entropy. The fact that the two limits do not commute is reflected in the presence of a line of phase transitions when one continuously changes the mass m while keeping the temperature T fixed. Numerical analysis shows that below a critical temperature T_c, the Schwinger-Dyson equations can have two distinct solutions. The SYK-like solution corresponding to a finite low temperature entropy exists for $m < m_{\rm HE}(T)$, the "high entropy" (HE) phase. The solution corresponding to weakly coupled harmonic oscillators exists for $m > m_{\rm LE}(T)$, the "low entropy" (LE) phase. In particular, we have $m_{\rm LE}(T_c) = m_{\rm HE}(T_c)$ and $m_{\rm LE}(0) = 0$. Since $m_{\rm LE}(T) \leq m_{\rm HE}(T)$, there is a mass interval in which both solutions exist. Within this interval, at a specific value of m both solutions have the same free energy, resulting in a line of phase transitions from one phase to the other. Above the critical temperature T_c, instead, only one solution is found and the system is in the "supercritical" phase. The phase structure we just described is depicted in Figure 5.3.

Chapter 6

Quartic matrix-vector models

In the context of melonic models, we mentioned that one can define a model of matrix-vectors with $\mathrm{U}(N)^2\times\mathrm{O}(D)$ symmetry which in the large N, large D limit reproduces the diagrammatic structure, and therefore the physical properties, of the SYK model. It was also stressed that such a model is particularly convenient for the purpose of obtaining information on the gravitational bulk dual, since its degrees of freedom are analogous to those one encounters in D-brane constructions. In this chapter we give a more general definition of these matrix-vector models with quartic interaction terms and we prove that the leading Feynman diagrams in the large N, large D limit are indeed the aforementioned melons. We also perform a probe brane analysis along the lines sketched in Section 3.1.2, obtaining a first non-trivial check on the free energy of the model.

6.1 Definition and properties of the model

Let us consider a model of complex fermionic matrix-vectors with quartic interaction terms, defined in $0+1$ dimensions. The degrees of freedom are $\mathrm{O}(D)$ vectors of $N\times N$ matrices $(\psi_\mu)^a_{\ b}$ and $(\psi^\dagger_\mu)^a_{\ b}=(\psi^a_{\mu\, b})^\dagger$ satisfying the canonical anticommutation relations of fermionic creation and annihilation operators:

$$\left\{\psi^a_{\mu b},\left(\psi^\dagger_\nu\right)^c_{\ d}\right\}=\frac{1}{ND}\delta_{\mu\nu}\delta^a_d\delta^c_b\,. \tag{6.1.1}$$

There are two possible single-trace quartic interaction terms which are consistent with the $\mathrm{U}(N)^2\times\mathrm{O}(D)$ symmetry of the model[1]

$$\begin{aligned} I_{4,1}&=\mathrm{tr}\left(\psi^\dagger_\mu\psi_\mu\psi^\dagger_\nu\psi_\nu\right)\,,\\ I_{4,2}&=\mathrm{tr}\left(\psi_\mu\psi^\dagger_\nu\psi_\mu\psi^\dagger_\nu\right)\,, \end{aligned} \tag{6.1.2}$$

[1]Also a term of the form $\mathrm{tr}\left(\psi_\mu\psi^\dagger_\mu\psi_\nu\psi^\dagger_\nu\right)$ is consistent with the symmetry of the model. Its c-graph can be obtained from the $I_{4,1}$ one by exchanging the red and green lines. Since the diagrammatic structure resulting from adding such an interaction term is essentially the same as the one associated with $I_{4,1}$ we will not consider it.

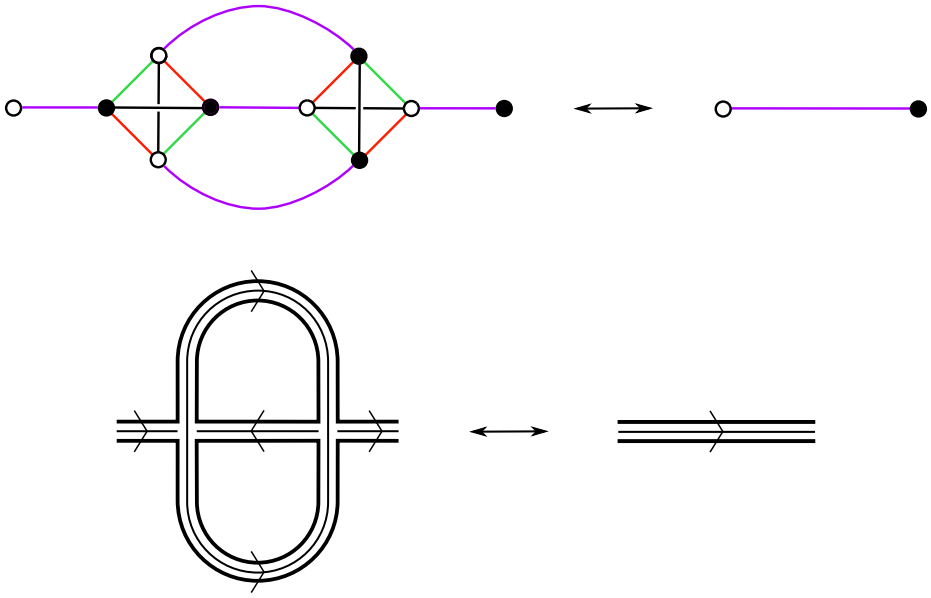

Figure 6.1: Melonic move associated to the tr $\left(X_\mu X_\nu^\dagger X_\mu X_\nu^\dagger\right)$ interaction term in the colored graph (top) and stranded graph (bottom) notations.

whose c-graph, r-graph and s-graph representations are depicted in Figure 4.4. The interaction terms $I_{4,1}$ and $I_{4,2}$ have genera zero and one-half respectively, therefore we choose the following scalings of the coupling constants in the Euclidean action of the model

$$S_N = ND \int_0^\beta dt \,\mathrm{tr}\left(\psi_\mu^\dagger \dot{\psi}_\mu + m\psi_\mu^\dagger \psi_\mu + \frac{\lambda_1}{2}\psi_\mu^\dagger \psi_\mu \psi_\nu^\dagger \psi_\nu + \sqrt{D}\frac{\lambda_2}{2}\psi_\mu \psi_\nu^\dagger \psi_\mu \psi_\nu^\dagger\right), \tag{6.1.3}$$

where the couplings λ_1 and λ_2 are held fixed when taking the large N, large D limits. Note that for full generality, we also included a mass term for the fermions.

6.1.1 Leading diagrams for $\lambda_1 = 0$

Now we would like to show which diagrams contribute to the model at leading order in the large N, large D limit. In order to do so we adapt similar proofs which were obtained for tensor models [59, 58] and in matrix-tensor models [60], which have in general more complicated diagrammatics than the case we are considering. We will further simplify things by considering a model with only the $I_{4,2}$ interaction term: it will become clear later how to include $I_{4,1}$. Let us start from considering the leading vacuum diagrams. We know that any vacuum diagram is proportional to $N^{2-2g}D^{1+g-\ell/2}$, with g being the genus of the ribbon graph. Therefore, leading diagrams correspond to $g = \ell = 0$. Let us consider the melonic move shown in Figure 6.1. It is clear that performing such a move leaves the N and D counting of any diagram unchanged. The genus g of the stranded graph does not change, resulting in the same power of N. Also, with

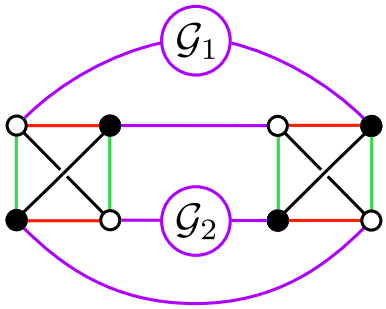

Figure 6.2: Structure of a generic leading diagram.

respect to the diagram on the right, the diagram on the left gets a factor D^{-4} for the propagators, a factor D^3 for the vertices and a factor D for a loop of $\mathrm{O}(D)$ indices: also the power of D stays the same. Now we want to prove that each leading vacuum diagram is a melon diagram, in the sense that it is constructed by iteration of the melonic move. In order to do so we first need to prove a couple of intermediate results. Earlier, we defined a face of the c-graph as a closed loop made of lines of two alternating colors i and j. We can now define its length as the number of 0-lines it is made of. In the case of our model, since the $\mathrm{O}(D)$ lines do not respect the bipartite structure of the c-graphs, (0, 3)-faces can only have even length. Now, because of (4.2.8), a leading diagram satisfies

$$-p+\varphi+\frac{3}{2}v=1\,, \tag{6.1.4}$$

where we have used the fact that in our case we only have one interaction term, with $g(B)=1/2$. Moreover, we can write

$$\sum_k \varphi_{2k}=\varphi \qquad \text{and} \qquad \sum_k 2k\,\varphi_{2k}=p\,, \tag{6.1.5}$$

where φ_{2k} is the number of (0, 3)-faces of length $2k$. By combining (6.1.4) and (6.1.5) we obtain

$$\varphi_2=2+2\sum_{k\geq 2}(\frac{k}{2}-1)\varphi_{2k}\,, \tag{6.1.6}$$

which means that each leading diagram has at least two (0, 3)-faces of length two. This is a crucial result because it implies that a leading diagram must have the structure depicted in Figure 6.2, where we have also used the fact that the diagram must be planar from the point of view of the $\mathrm{U}(N)$ indices. Now, we can prove that all leading diagrams are obtained by recursively applying the melonic move in Figure 6.1 to the vacuum graph depicted in Figure 6.3. This is done by induction: we just need to show that any leading diagram with v vertices contains the elementary melon depicted on the left of Figure 6.1. If that is the case, the melonic move can be performed from left to right to obtain a leading diagram with fewer vertices, and so on. By looking at the general structure of a leading diagram

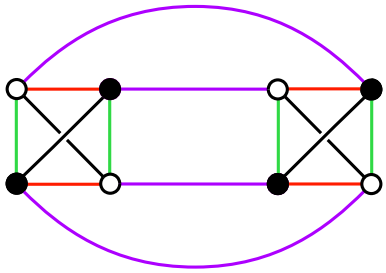

Figure 6.3: Leading vacuum diagram with two vertices.

with v vertices depicted in Figure 6.2 we can immediately notice that if either $\mathcal{G}_1$ or $\mathcal{G}_2$ are the bare two-point function we obtain the elementary melon. Otherwise, since we started from a leading graph, also $\mathcal{G}_1$ and $\mathcal{G}_2$ must be leading graphs. In fact, if that was not the case, by replacing them with the bare two-point function we would obtain a diagram with higher powers of N and/or D. But this is not possible, since we started with a diagram with the highest possible powers of N and D. Now, $\mathcal{G}_1$ and $\mathcal{G}_2$ are leading graphs with a strictly smaller number of vertices than the graph we started from. Hence, by the induction hypothesis they must contain an elementary melon, thus proving the wanted result.

6.1.2 Including the $I_{4,1}$ interaction term

As it was announced above, including the $I_{4,1}$ interaction term in the action does not change dramatically the physics in the large N, large D limit, and it can be taken into account without having to consider the diagrammatics. Let us consider the partition function of the model, given by

$$Z(m,\,\lambda_1\,,\lambda_2) = \int \mathcal{D}\psi\mathcal{D}\psi^\dagger\, e^{-S_N}\,. \tag{6.1.7}$$

One can introduce an auxiliary field Φ^a_b and write an action $\hat{S}_N$ which is equivalent to the action in (6.1.3) on-shell:

$$\hat{S}_N = ND\int_0^\beta dt\,\mathrm{tr}\left(\psi^\dagger_\mu\dot{\psi}_\mu + m\psi^\dagger_\mu\psi_\mu + \Phi\psi^\dagger_\mu\psi_\mu - \frac{1}{2\lambda_1}\Phi^2 + \sqrt{D}\frac{\lambda_2}{2}\psi_\mu\psi^\dagger_\nu\psi_\mu\psi^\dagger_\nu\right)\,. \tag{6.1.8}$$

We now have

$$Z(m,\,\lambda_1\,,\lambda_2) = \int \mathcal{D}\psi\mathcal{D}\psi^\dagger\mathcal{D}\Phi\, e^{-\hat{S}_N}\,. \tag{6.1.9}$$

In fact, it is easy to verify that the equation of motion for the auxiliary field is $\Phi = \lambda_1\psi^\dagger_\mu\psi_\mu$ and that by plugging it back into (6.1.8) one gets the original action (6.1.3). This is a convenient way of rewriting the action because in the large D limit, since Φ does not carry any $\mathrm{O}(D)$ index and its action is proportional to D, the path integral over the auxiliary field does not need to be performed. Instead,

Φ settles to its saddle point value Φ_*, given by:

$$\Phi^a_{*\,b} = \phi_*\,\delta^a_b = \lambda_1 Q\,\delta^a_b\,, \tag{6.1.10}$$

where Q is the fermion number, defined as

$$Q = \frac{1}{N}\big\langle \mathrm{tr}\,\psi^\dagger_\mu\psi_\mu\big\rangle_\beta\,. \tag{6.1.11}$$

At the saddle point, the action can be rewritten as

$$\hat{S}^*_N = -N^2 D\frac{\beta}{2\lambda_1}\phi_*^2 + ND\int_0^\beta dt\,\mathrm{tr}\left(\psi^\dagger_\mu\dot{\psi}_\mu + (m+\phi_*)\psi^\dagger_\mu\psi_\mu + \sqrt{D}\frac{\lambda_2}{2}\psi_\mu\psi^\dagger_\nu\psi_\mu\psi^\dagger_\nu\right), \tag{6.1.12}$$

and we have again to integrate only over the fermionic fields ψ and $\psi^\dagger$:

$$Z(m,\,\lambda_1\,,\lambda_2) = \int \mathcal{D}\psi\mathcal{D}\psi^\dagger\, e^{-\hat{S}^*_N}\,. \tag{6.1.13}$$

Therefore in the large N, large D limit the presence $I_{4,1}$ results only in the shift of the mass m by $\lambda_1 Q$. In this sense, the physics of the $I_{4,1}$ term is analogous to that of the quartic term in the Gross-Neveu model in the large N limit. From this analysis it becomes clear how crucial the $\sqrt{D}$ factor in front of $I_{4,2}$ is. Without it, all diagrams containing such a vertex would be subleading, and only $I_{4,1}$ would contribute, leading to physical properties similar to those of vector models.

6.1.3 Two-point functions

Let us now consider the Euclidean two-point function of the fermions at finite temperature $T = 1/\beta$. It is defined as

$$G(t) \equiv \frac{1}{N}\langle \mathrm{tr}\,\mathrm{T}\,\psi_\mu(t)\psi^\dagger_\mu\rangle_\beta = \frac{1}{\beta}\sum_{k\in\mathbb{Z}+1/2} G_k e^{-i\nu_k t}\,, \tag{6.1.14}$$

where the $\nu_k = 2\pi k/\beta$ are the usual fermionic Matsubara frequencies. The Matsubara coefficients G_k satisfy

$$G_{-k} = G^*_k\,. \tag{6.1.15}$$

As it was shown above, in the large N, large D limit, the leading diagrams contributing to the two-point function at leading order are obtained by iterating the melonic move depicted in Figure 6.1. Such diagrams can be summed, and their sum can be packaged in the following Schwinger-Dyson equation:

$$\begin{aligned} \frac{1}{G_k} &= m_* - i\nu_k + \Sigma_k\,,\\ \Sigma_k(t) &= \lambda_2^2 G(t)^2 G(-t)^2\,. \end{aligned} \tag{6.1.16}$$

In these equations we recognise a generalization of the SYK Schwinger-Dyson equation (4.1.5) to massive complex fermions. The renormalized mass m_* is given by:

$$m_* = m + \phi_* = m + \lambda_1(1 - G(0^+))\,. \tag{6.1.17}$$

6.1.4 Writing the free energy in terms of the Matsubara coefficients G_k

In the SYK model, we showed that in the large N limit it is possible to write the free energy of the model in terms of the G and Σ which solve the Schwinger-Dyson equation. This is done through a path integral computation which relies on the introduction of bilocal auxiliary fields. Such a straightforward computation cannot be performed in the matrix-vector quartic model, but since it shares the same diagrammatics with the SYK model, we expect that a similar rewriting of the free energy in terms of G and Σ should be possible to achieve. The free energy F of the model is obtained from the partition function through the usual formula

$$F(m,\, \lambda_1\,, \lambda_2) = -T \ln\big[Z(m,\, \lambda_1\,, \lambda_2)\big] = N^2 D F_0(m,\, \lambda_1\,, \lambda_2)\,, \tag{6.1.18}$$

where we introduced the notation F_0 for the leading contribution to the free energy in the large N, large D limit. If we turn off the interactions $I_{4,1}$ and $I_{4,2}$, the partition function is just given by $N^2 D$ fermionic harmonic oscillators:

$$\begin{aligned} Z(m,\, \lambda_1 = \lambda_2 = 0) &= \big(1 + e^{-\beta m}\big)^{N^2 D}\,, \\ F(m,\, \lambda_1 = \lambda_2 = 0) &= -N^2 D T \ln\big(1 + e^{-\beta m}\big)\,. \end{aligned} \tag{6.1.19}$$

As it can be deduced from equations (6.1.12) and (6.1.13), turning on I_4^1 only amounts to shifting the mass m by ϕ_* and by multiplying the partition function by a factor $\exp(N^2 D \beta\, \phi_*^2 / 2\lambda_1)$. This results in the following expressions for Z and F:

$$\begin{aligned} Z(m,\, \lambda_1,\, \lambda_2 = 0) &= \left[\big(1 + e^{-\beta(m+\phi_*)}\big) e^{\beta\, \phi_*^2 / 2\lambda_1}\right]^{N^2 D}\,, \\ F(m,\, \lambda_1,\, \lambda_2 = 0) &= -N^2 D \left(T \ln\big(1 + e^{-\beta(m+\phi_*)}\big) + \frac{\phi_*^2}{2\lambda_1}\right), \end{aligned} \tag{6.1.20}$$

where ϕ_* must satisfy (6.1.10). Note that the fermion number Q is given by

$$Q = \frac{1}{N^2 D} \frac{\partial F}{\partial m}\,, \tag{6.1.21}$$

and if we impose $\phi_* = \lambda_1 Q$, it is easy to verify that

$$\frac{\partial F}{\partial \phi_*} = \frac{\partial Z}{\partial \phi_*} = 0\,, \tag{6.1.22}$$

as it should. Now, in order to obtain the full free energy for $\lambda_2 \neq 0$, we first compute

$$\frac{\partial F}{\partial \lambda_2} = \frac{N D^{\frac{3}{2}}}{2} \big\langle \operatorname{tr} \psi_\mu \psi_\nu^\dagger \psi_\mu \psi_\nu^\dagger \big\rangle\,, \tag{6.1.23}$$

and, since we the effect of $I_{4,1}$ is under control, at first we focus on the case $\lambda_1 = 0$. In imaginary time, we have

$$\dot{\psi}_\mu = [H,\, \psi_\mu]\,. \tag{6.1.24}$$

Since we have

$$\big[\mathrm{tr}\,\psi_\nu^\dagger\psi_\nu,\,\psi_\mu\big] = -\frac{1}{ND}\psi_\mu\,,$$
$$[\mathrm{tr}\,\psi_\nu\psi_\sigma^\dagger\psi_\nu\psi_\sigma^\dagger,\,\psi_\mu] = \frac{1}{ND}\big(2\psi_\nu\psi_\mu^\dagger\psi_\nu - \frac{1}{D}\psi_\mu\big)\,,$$

we get

$$\dot\psi_\mu = -\bigg(m + \frac{\lambda_2}{2\sqrt{D}}\bigg)\psi_\mu + \lambda_2\sqrt{D}\,\psi_\nu\psi_\mu^\dagger\psi_\nu\,. \tag{6.1.25}$$

Therefore we can write

$$\lambda_2\sqrt{D}\big\langle\mathrm{tr}\,\big(\psi_\mu\psi_\nu^\dagger\psi_\mu\big)(t)\,\psi_\nu^\dagger\big\rangle = \big(\partial_t + m\big)\langle\mathrm{tr}\,\psi_\mu(t)\psi_\mu^\dagger\rangle\,, \tag{6.1.26}$$

where we discarded the $\lambda_2/2\sqrt{D}$ term in (6.1.25), which is clearly subleading in the large D limit. For $t > 0$, we can finally write

$$\big(\partial_t + m\big)G(t) = \lambda_2\frac{\sqrt{D}}{N}\big\langle\mathrm{tr}\,\big(\psi_\mu\psi_\nu^\dagger\psi_\mu\big)(t)\,\psi_\nu^\dagger\big\rangle\,, \tag{6.1.27}$$

which results in the following relation:

$$\frac{\partial F_0}{\partial\lambda_2} = \frac{1}{2\lambda_2}\big(\partial_t + m\big)G(0^+)\,. \tag{6.1.28}$$

This is the starting point for obtaining an expression for F_0 in terms of the Matsubara coefficients G_k. Since $G(t)$ is discontinuous at $t = 0$, one cannot write $G(0^+)$ in terms of the G_k by simply taking the definition (6.1.14) and imposing $t = 0$. In fact, $\sum_k G_k$ turns out to be divergent. However one can use (6.1.15) to define the following quantity:

$$G(t) + G(-t) = \frac{2}{\beta}\sum_{k\in\mathbb{Z}+1/2}\mathrm{Re}\,G_k e^{-i\nu_k t}\,, \tag{6.1.29}$$

which is continuous at $t = 0$. Using

$$G(0^+) - G(0^-) = 1\,, \tag{6.1.30}$$

which is just the result of the anticommutation relation of the fermions, one obtains

$$G(0^+) = \frac{1}{2} + \frac{1}{\beta}\sum_{k\in\mathbb{Z}+1/2}\mathrm{Re}\,G_k e^{-i\nu_k t}\,. \tag{6.1.31}$$

The computation of $\dot G(0^+)$ requires more care. We have

$$\dot G(t) = -\frac{i}{\beta}\sum_{k\in\mathbb{Z}+1/2}\nu_k\,G_k e^{-i\nu_k t}\,. \tag{6.1.32}$$

The reason why the sum $\sum_k \nu_k G_k$ is divergent is that the coefficients G_k tend to the harmonic oscillator ones for large k. This is related to the discontinuity at $t = 0$, since the high frequency behaviour of the two-point function determines its short time properties. The harmonic oscillator coefficients are given by

$$G_k^{(0)} = \frac{1}{-i\nu_k + m} = \frac{i}{\nu_k} + \frac{m}{\nu_k^2} + O\big(k^{-3}\big)\,, \tag{6.1.33}$$

and it is clear how this translates in the divergence of both $\sum_k G_k$ and $\sum_k \nu_k G_k$. We can however introduce the function $f(t)$, such that

$$f(t) = \frac{1}{\beta} \sum_{k \in \mathbb{Z}+1/2} \left(\frac{i}{\nu_k} + \frac{m}{\nu_k^2} \right) e^{-i\nu_k t}\,. \tag{6.1.34}$$

Using

$$\frac{1}{2}\mathrm{sgn}(t) = \frac{1}{\beta} \sum_{k \in \mathbb{Z}+1/2} \frac{i}{\nu_k} e^{-i\nu_k t}\,, \tag{6.1.35}$$

one obtains

$$f(t) = \frac{1}{2}\mathrm{sgn}(t) - \frac{m}{2} t\,\mathrm{sgn}(t) + \frac{m\beta}{4}\,. \tag{6.1.36}$$

If we now consider the difference $G(t) - f(t)$, we can compute the following quantity:

$$\dot{G}(t) - \dot{f}(t) = -\frac{i}{\beta} \sum_{k \in \mathbb{Z}+1/2} \nu_k \left(G_k - \frac{i}{\nu_k} - \frac{m}{\nu_k^2} \right) e^{-i\nu_k t}\,, \tag{6.1.37}$$

which for $t \to 0^+$ yields an absolutely convergent sum:

$$\dot{G}(0^+) + \frac{m}{2} = -\frac{i}{\beta} \sum_{k \in \mathbb{Z}+1/2} \left(\nu_k G_k - i - \frac{m}{\nu_k} \right). \tag{6.1.38}$$

Since the series is now convergent, we can rearrange the terms as we want, obtaining:

$$\dot{G}(0^+) = -\frac{m}{2} + \frac{1}{\beta} \sum_{k \in \mathbb{Z}+1/2} \big(\nu_k \mathrm{Im}\, G_k - 1 \big)\,. \tag{6.1.39}$$

We can now plug (6.1.31) and (6.1.39) into (6.1.28) to obtain:

$$\begin{aligned} \frac{\partial F_0}{\partial \lambda_2} &= \frac{1}{2\lambda_2} \frac{1}{\beta} \sum_{k \in \mathbb{Z}+1/2} \big(\nu_k \mathrm{Im}\, G_k + m \mathrm{Re}\, G_k - 1 \big) \\ &= \frac{1}{2\lambda_2} \frac{1}{\beta} \sum_{k \in \mathbb{Z}+1/2} \left(\mathrm{Re}\, \frac{G_k}{G_k^{(0)}} - 1 \right), \end{aligned} \tag{6.1.40}$$

where in the last line we used the definition of the Matsubara coefficients of the harmonic oscillator given in (6.1.33). Now we have all the ingredients to proceed

to the construction of the full expression of F_0. First of all we introduce the following operator:

$$\hat{\mathcal{O}}(t_1,\, t_2) = \delta(t_1 - t_2)(\partial_{t_2} + m + \phi) + \Sigma(t_1 - t_2)\,, \tag{6.1.41}$$

which acts on antiperiodic functions. We also introduce the following notations for operations on bilocal functions

$$\begin{aligned} f \cdot g &\equiv \int dt\, f(t_1,\, t) g(t,\, t_2)\,, \\ \mathrm{Tr}\, f &\equiv \int dt\, f(t,\, t)\,. \end{aligned} \tag{6.1.42}$$

In Fourier space, the operator $\hat{\mathcal{O}}$ acts like a standard multiplication on Matsubara coefficients:

$$\left(\hat{\mathcal{O}} \cdot f\right)_k = (-i\nu_k + m + \phi + \Sigma_k) f_k\,. \tag{6.1.43}$$

As a first step in the construction of F_0, we introduce a functional $\mathcal{A}$ of bilocal functions Σ and G such that taking the variation of $\mathcal{A}$ with respect to Σ reproduces the first equation in (6.1.16). It is given by

$$\mathcal{A}(\Sigma,\, G) = \ln \frac{\mathrm{Det}\, \hat{\mathcal{O}}}{\mathrm{Det}\, \hat{\mathcal{O}}_0} - \mathrm{Tr}\, \Sigma \cdot G\,, \tag{6.1.44}$$

where we used the operator $\hat{\mathcal{O}}_0$ given by

$$\hat{\mathcal{O}}_0 = \delta(t_1 - t_2)(\partial_{t_2} + m)\,, \tag{6.1.45}$$

to regularize the logarithm of the functional determinant of $\hat{\mathcal{O}}$. This necessity becomes more appearent if we rewrite (6.1.44) in Fourier space:

$$\mathcal{A}(\Sigma,\, G) = \sum_k \left(\ln \left[1 + \frac{\Sigma_k}{-i\nu_k + m} \right] - \Sigma_k G_k \right). \tag{6.1.46}$$

Since both Σ_k and G_k scale like k^{-1} at large k, the first term in the sum would diverge without the $\mathrm{Det}\, \hat{\mathcal{O}}_0$ at the denominator. It is easy to check that

$$\delta_\Sigma \mathcal{A}(\Sigma,\, G) = 0 \;\Rightarrow G_k^{-1} = -i\nu_k + m + \Sigma_k\,, \tag{6.1.47}$$

as we wanted. Now, in order to obtain a functional whose variation with respect to G results in the second equation in (6.1.16), we just have to introduce

$$\mathcal{S}(\Sigma,\, G) = \mathcal{A}(\Sigma,\, G) + \frac{\lambda_2^2}{4} \int dt_1 dt_2\, G(t_1,\, t_2)^2 G(t_2,\, t_1)^2\,. \tag{6.1.48}$$

We have now constructed a functional whose saddle point equations for Σ and G reproduce the Schwinger-Dyson equations of our model. On the saddle point, we have

$$\frac{\partial \mathcal{S}}{\partial \lambda_2} = \frac{\lambda_2}{2} \int dt_1 dt_2\, G(t_1,\, t_2)^2 G(t_2,\, t_1)^2 = \frac{1}{2\lambda_2} \mathrm{Tr}\, \Sigma \cdot G\,, \tag{6.1.49}$$

were in the second equality we used the Schwinger-Dyson equation which holds at the saddle point. In Fourier space:

$$\frac{\partial \mathcal{S}}{\partial \lambda_2} = \frac{1}{2\lambda_2}\sum_k G_k \Sigma_k = \frac{1}{2\lambda_2}\sum_k \Big(1 - \big(m - i\nu_k\big)G_k\Big) = \frac{1}{2\lambda_2}\sum_k \left(1 - \mathrm{Re}\frac{G_k}{G_k^{(0)}}\right). \tag{6.1.50}$$

By comparison with (6.1.40), we get

$$\frac{\partial \mathcal{S}}{\partial \lambda_2} = -\beta \frac{\partial F_0}{\partial \lambda_2}\,. \tag{6.1.51}$$

Therefore

$$F_0(m,\, \lambda_1 = 0, \lambda_2) = -T\mathcal{S}(m,\, \lambda_2) + \varphi(m)\,, \tag{6.1.52}$$

where the function φ is determined by evaluating both F_0 and $\mathcal{S}$ at $\lambda_2 = 0$. Since $\mathcal{S}(m,\, \lambda_2 = 0) = 0$, we can use (6.1.19) to obtain

$$\varphi(m) = -T \ln\big(1 + e^{-\beta m}\big)\,. \tag{6.1.53}$$

The generalization to $\lambda_1 \neq 0$ is straightforward. Using (6.1.12) and (6.1.13), we just replace m with m^* and subtract $\phi_*^2/2\lambda_1$ from F_0. The complete result is:

$$\begin{aligned} F_0(m,\, \lambda_1, \lambda_2) = &- T\Bigg\{ \sum_k \left(\ln\left[1 + \frac{\Sigma_k}{-i\nu_k + m + \phi_*}\right] - \Sigma_k G_k \right) \\ &+ \frac{\lambda_2^2}{4}\int dt_1 dt_2\, G(t_1,\, t_2)^2 G(t_2,\, t_1)^2 \\ &+ \ln\big(1 + e^{-\beta(m+\phi)}\big) + \beta\frac{\phi_*^2}{2\lambda_1}\Bigg\}\,, \end{aligned} \tag{6.1.54}$$

where both G, Σ and ϕ_* correspond to the saddle point values. The equations they satisfy at the saddle point are summarized below:

$$G_k^{-1} = -i\nu_k + m + \phi_* + \Sigma_k\,, \qquad \Sigma(t) = \lambda_2^2\, G(t)^2 G(-t)\,, \qquad \phi_* = \lambda_1\big(1 - G(0^+)\big)\,. \tag{6.1.55}$$

We can use them, together with (6.1.31), (6.1.49) and (6.1.50), to obtain an expression of F_0 which involves only the Matsubara coefficients G_k.

6.2 Probe analysis

In Section 3.1.2, we sketched a procedure called probe brane analysis which can in principle be carried out for any U(N) gauge theory and which can be used to extract information on the properties of the gravitational bulk dual of the boundary theory we are examining. Now that we have at our disposal matrix models which feature non-trivial properties connected to holography, we can set up the probe brane analysis for the matrix vector-models we defined above.

6.2.1 Generalities

The gauge/gravity duality teaches us that in the large N limit there is a correspondence between the background geometry $\mathcal{B}_N$ generated by a stack of N D-branes and the U(N) gauge theory that lives on their worldvolume [38, 39, 40]. In particular, the following relation between the bulk gravitational action S_g evaluated on $\mathcal{B}_N$ and the partition function Z_N of the boundary gauge theory holds:

$$e^{-S_g^*(N)} = Z_N \,, \tag{6.2.1}$$

where the star notation corresponds to the on-shell gravitational action (i.e. the action evaluated on $\mathcal{B}_N$). Now, if we consider instead a stack of $N+1$ D-branes, the same consideration applies, with a slightly modified background $\mathcal{B}_{N+1}$. Therefore we have

$$-\ln Z_{N+1} = S_g^*(N+1) = S_g^*(N) + \frac{\partial S_g^*(N)}{\partial N} \,, \tag{6.2.2}$$

where to obtain the second equality we used the large N limit. However, we could have given an alternative description of the same system, namely a probe brane moving in the background $\mathcal{B}_N$ generated by the other N branes. If we call S_p^* the on-shell value of the probe action in the gravitational background $\mathcal{B}_N$, we can write

$$-\ln Z_{N+1} = S_g^*(N) + S_p^* \,. \tag{6.2.3}$$

By directly comparing (6.2.2) and (6.2.3), we obtain the following non-trivial statement

$$\frac{\partial S_g^*(N)}{\partial N} = S_p^* \,. \tag{6.2.4}$$

The depth of such a relation lies in the fact that while S_g^* is a bulk quantity, obtained by evaluating a gravitational action on a specific background; S_p^* is a boundary object, in the sense that it is computed by integrating over the worldvolume (or worldline in the case of probe particles) of the probe. In any U(N) gauge theory, we can write the large N expansion of $\ln Z_N$:

$$\ln Z_N = -\sum_{h\geq 0} N^{2-2h} F_h(\lambda) \,, \tag{6.2.5}$$

where $\lambda = 4\pi g_s N$ is the usual 't Hooft coupling. Hence, in the $N \to \infty$ limit we have:

$$S_g^*(N) = N^2 F_0(\lambda) \qquad \text{and} \qquad S_p^* = \frac{\partial N^2 F_0(\lambda)}{\partial N} \tag{6.2.6}$$

which, when we take into account the explicit N dependence of λ, results in the following relation:

$$S_p^* = N\big(2F_0(\lambda) + \lambda F_0'(\lambda)\big) \,. \tag{6.2.7}$$

This makes the on-shell probe action an extremely interesting quantity to compute: on the one hand it encodes all the information on the background geometry the probe moves in. In particular, although as we will see it can be defined purely

in terms of the boundary gauge theory, one should be able to reconstruct the extra coordinates of the bulk space from its computation. On the other hand it is related in a non-trivial way to the planar free energy of the boundary gauge theory. How the probe brane action can be obtained entirely through a boundary gauge theory computation can be understood in the following way. The system composed by the stack of N background branes and the probe brane can be described by a path integral over the worldvolume background fields Φ_b and the worldvolume probe fields Φ_p:

$$\int \mathcal{D}\Phi_b \mathcal{D}\Phi_p \, e^{-A_b - A_p} \,, \tag{6.2.8}$$

where A_b is the low energy worldvolume action on the background branes and A_p is the action for the probe brane fields, including their interactions with the background fields. The gauge/gravity correspondence however states that such a path integral should be equivalent to the following one

$$\int \mathcal{D}\Phi_p \, e^{-S_p} \,, \tag{6.2.9}$$

where S_p in turn describes the motion of the probe brane in the curved geometry generated by the background branes. The equivalence between the two descriptions implies that S_p can be obtained by performing the path integral over the background worldvolume fields in (6.2.8).

6.2.2 A toy example

In order to illustrate how one can construct the probe brane action in a generic U(N) gauge theory, we review the basic steps of such a procedure in a toy example [38], namely the same a zero-dimensional model of $(N+1) \times (N+1)$ matrices which we introduced in Section 3.1.2. Its action is

$$S_{N+1}(M) = \mathrm{tr} \left(\frac{1}{2} M^2 + \frac{g^2}{4} M^4 \right) . \tag{6.2.10}$$

The probe analysis is carried out by splitting the M matrices:

$$M = \begin{pmatrix} V_b^a & \bar{w}^a \\ w_b & v \end{pmatrix} , \tag{6.2.11}$$

which effectively amounts to distinguishing the probe field v from the background fields V, w and $\bar{w}$. This results in a rewriting of the action in terms of the new degrees of freedom:

$$S_{N+1}(M) \to S_{N+1}(V, w, \bar{w}, v) = S_N(V) + S_1(v) + \hat{S}(V, w, \bar{w}, v) \,, \tag{6.2.12}$$

with

$$\hat{S}(V, w, \bar{w}, v) = \bar{w} w + g^2 \left(w V^2 \bar{w} + v^2 \bar{w} w + v w V \bar{w} + \frac{1}{2} \bar{w} w \bar{w} w \right) . \tag{6.2.13}$$

Let us now define the effective action $\mathscr{A}_N$ for the probe field v in the following way:

$$e^{-\mathscr{A}_N(v)} = \frac{e^{-S_1(v)}}{Z_N(g^2)} \int \mathcal{D}V \mathcal{D}w \mathcal{D}\bar{w}\, e^{-S_N(V) - \hat{S}(V,w,\bar{w},v)}\,, \tag{6.2.14}$$

with

$$Z_N(g^2) = \int \mathcal{D}V\, e^{-S_N(V)}\,. \tag{6.2.15}$$

We will now show that from $\mathscr{A}_N$ we can obtain a definition of the on-shell probe action S_p^*. First of all, let us address the problem of performing the path integral over the fundamental and adjoint variables. Although the action for the fundamental fields w and $\bar{w}$ is not quadratic, their path integral can be performed using a standard vector model technique. We can in fact get rid of the quartic vector coupling in (6.2.13) by introducing an auxiliary field ϕ in the following way:

$$\frac{g^2}{2}\bar{w}w\bar{w}w \to \phi\bar{w}w - \frac{1}{2g^2}\phi^2\,. \tag{6.2.16}$$

With the introduction of ϕ, the action for the fundamentals (6.2.13) becomes:

$$\hat{S}(V,\, w,\, \bar{w},\, v,\, \phi) = \bar{w}w + \phi\bar{w}w - \frac{1}{2g^2}\phi^2 + g^2\left(wV^2\bar{w} + v^2\bar{w}w + vwV\bar{w}\right), \tag{6.2.17}$$

and the definition for the action $\mathscr{A}_N$ given in (6.2.14) needs to be upgraded to

$$e^{-\mathscr{A}_N(v,\phi)} = \frac{e^{-S_1(v)}}{Z_N(g^2)} \int \mathcal{D}V \mathcal{D}w \mathcal{D}\bar{w}\, e^{-S_N(V) - \hat{S}(V,w,\bar{w},v,\phi)}\,. \tag{6.2.18}$$

This is a crucial point: in the construction of the effective action for the probe field v, the scalar boson ϕ arises in a natural way. We will see in the next section that this happens even if we start from a model which does not contain bosonic degrees of freedom in the first place. Most importantly, since ϕ does not carry $\mathrm{U}(N)$ indices and its action turns out to be proportional to N, in the large N limit its quantum fluctuations are suppressed, making it a good candidate for an emergent space coordinate. We now need to show the relation between the effective action $\mathscr{A}_N(v,\, \phi)$ and the on-shell probe action S_p^* we defined earlier. From our definition of the effective action for the fields v and ϕ (6.2.14) we have:

$$\int \mathcal{D}v \mathcal{D}\phi\, e^{-\mathscr{A}_N(v,\phi)} = \frac{Z_{N+1}(g^2)}{Z_N(g^2)}\,. \tag{6.2.19}$$

In the large N limit, the path integrals over the scalar fields v and ϕ can be carried out via a saddle point approximation. Both fields settle to their on-shell values v^* and ϕ^* satisfying

$$\frac{\partial \mathscr{A}_N}{\partial v} = \frac{\partial \mathscr{A}_N}{\partial \phi} = 0\,. \tag{6.2.20}$$

Moreover, the $1/N$ expansion of the right hand side of (6.2.19) gives

$$\ln\frac{Z_{N+1}(g^2)}{Z_N(g^2)} = \ln\frac{Z_{N+1}(\lambda)}{Z_N(\frac{N}{N+1}\lambda)} = -2NF_0(\lambda) - N\lambda\frac{\partial F_0(\lambda)}{\partial\lambda}\,, \tag{6.2.21}$$

where we used $\lambda = (N+1)g^2$ as 't Hooft coupling and the large N expansion of $\ln Z_N$ given in (6.2.5). If we now denote by S_p the leading term in the $1/N$ expansion of $\mathscr{A}_N$:

$$\mathscr{A}_N = S_p + O\big(N^0\big)\,, \tag{6.2.22}$$

we can write

$$S_p^* = N\big(2F_0(\lambda) + \lambda F_0'(\lambda)\big)\,, \tag{6.2.23}$$

where the starred notation means that S_p is evaluated at the saddle point values of v and ϕ. The consistency with (6.2.7) shows that this definition of the on-shell probe action obtained entirely in terms of the worldvolume gauge theory matches the on-shell action of a probe moving in the gravitational background of N branes. There is one important subtlety we did not address in this sketch of the construction: the gauge-fixing. In our example, before we distinguished the probe from the N background branes, we had a $\mathrm{U}(N+1)$ gauge theory. After the separation of the probe and the rewriting of the action in terms of the new variables, we ended up with a model with reduced symmetry $\mathrm{U}(N)\times\mathrm{U}(1)$. This should not be seen as a symmetry breaking process, but rather as an equivalent rewriting of the same model. Therefore, in order to properly define the probe effective action, a gauge-fixing fixing procedure is needed [72]. More precisely, we need to partially gauge fix the $\mathrm{U}(N+1)$ symmetry down to $\mathrm{U}(N)\times\mathrm{U}(1)$. However, in the following we will focus on the computation of the on-shell probe action of the quartic matrix-vector model in the large N, large D limit. Whatever gauge-fixing term we might add to the action will be subleading in the large D limit [60], therefore we can ignore this issue for the model under exam.

6.2.3 Probe analysis of the quartic matrix-vector model

We can now directly move on to the probe analysis of the quartic matrix-vector model. The starting point is the action S_N given in (6.1.3). We start from $(N+1)\times(N+1)$ complex fermionic matrices Ψ_μ and $\Psi_\mu^\dagger$ with action S_{N+1}, and perform the following splitting of the matrices:

$$\Psi_\mu = \begin{pmatrix} \psi^a_{\mu b} & \alpha^a_\mu \\ \beta_{\mu b} & \chi_\mu \end{pmatrix} \qquad \text{and} \qquad \Psi_\mu^\dagger = \begin{pmatrix} \psi^{\dagger a}_{\mu b} & \beta^{\dagger a}_\mu \\ \alpha^\dagger_{\mu b} & \chi^\dagger_\mu \end{pmatrix}. \tag{6.2.24}$$

With respect to the toy example we studied above, we notice immediately one important difference: we have two distinct kinds of vector fields α and β. This is related to the fact that the symmetry of our model of complex matrices is $\mathrm{U}(N)^2\times\mathrm{O}(D) = \mathrm{U}(N)_L\times\mathrm{U}(N)_R\times\mathrm{O}(D)$: the two kinds of probes α and β transform in the fundamental representation of the two distinct $\mathrm{U}(N)$ symmetries. The

action, written in terms of the new variables takes the form

$$S_{N+1}(\Psi) = (N+1)\left[\frac{1}{N}S_N(\psi) + S_1(\chi) + S_{N,1}(\psi,\alpha,\beta,\chi)\right], \tag{6.2.25}$$

where $S_{N,1}(\psi,\alpha,\beta,\chi)$ is given by the kinetic terms for the α and β fields, plus different kinds of interaction terms:

$$S_{N,1}(\psi,\alpha,\beta,\chi) = \int dt\, \left(\alpha_\mu^\dagger(\partial_t + m)\alpha_\mu + \beta_\mu^\dagger(\partial_t + m)\beta_\mu + \text{ interactions}\right). \tag{6.2.26}$$

Since the interaction terms are many, and we will have to study them separately, we group them in the following way:

$$\begin{aligned}
I_A =& \frac{\lambda_1}{2}\,\alpha_\mu^\dagger\alpha_\mu\alpha_\nu^\dagger\alpha_\nu\,,\\
I_B =& \frac{\lambda_2}{2}\sqrt{D}\,\Big(\beta_\mu\psi_\nu^\dagger\alpha_\mu\chi_\nu^\dagger + \chi_\mu\alpha_\nu^\dagger\psi_\mu\beta_\nu^\dagger - 2\alpha_\mu^\dagger\alpha_\nu\chi_\mu^\dagger\chi_\nu + 2\beta_\mu\beta_\nu^\dagger\chi_\mu\chi_\nu^\dagger\\
&- \chi_\mu^\dagger\beta_\nu\psi_\mu^\dagger\alpha_\nu - \alpha_\nu^\dagger\psi_\mu\beta_\mu^\dagger\chi_\nu\Big)\\
&+ \frac{\lambda_1}{2}\Big(\chi_\nu^\dagger\beta_{nu}\psi_\mu^\dagger\alpha_\mu + \alpha_\nu^\dagger\psi_\nu\beta_\mu^\dagger\chi_\mu - 2\chi_\mu\chi_\nu^\dagger\beta_\nu\beta_\mu^\dagger + 2\alpha_\mu^\dagger\alpha_\mu\chi_\nu^\dagger\chi_\nu\\
&+ \alpha_\mu^\dagger\psi_\mu\beta_\nu^\dagger\chi_\nu + \chi_\mu^\dagger\beta_\mu\psi_\nu^\dagger\alpha_\nu\Big)\,,\\
I_C =& \frac{1}{2}\Big(\lambda_2\sqrt{D} + \lambda_1\Big)\beta_\mu\beta_\nu^\dagger\beta_\mu\beta_\nu^\dagger + \frac{\lambda_2}{2}\sqrt{D}\,\alpha_\mu^\dagger\alpha_\nu\alpha_\mu^\dagger\alpha_\nu\,,\\
I_D =& \frac{\lambda_1}{2}\,\alpha_\mu^\dagger\psi_\mu\psi_\nu^\dagger\alpha_\nu\,,\\
I_E =& -\lambda_1\,\beta_\nu\psi_\mu^\dagger\psi_\mu\beta_\nu^\dagger\,,\\
I_F =& \lambda_2\sqrt{D}\,\left[\beta_\mu\psi_\nu^\dagger\psi_\mu\beta_\nu^\dagger - \alpha_\mu^\dagger\psi_\nu\psi_\mu^\dagger\alpha_\nu\right].
\end{aligned} \tag{6.2.27}$$

I_A-term

This interaction term is a standard quartic vector coupling of the same kind we encountered in the toy model. Since the U(N) and O(D) indices are contracted in the same way, the leading diagrams in the large N, large D limit are the same as in usual U(N) vectors models. We can deal with this interaction term by introducing an auxiliary field

$$\frac{\lambda_1}{2}\,\alpha_\mu^\dagger\alpha_\mu\alpha_\nu^\dagger\alpha_\nu \;\to\; \varphi\,\alpha_\mu^\dagger\alpha_\mu - \frac{1}{2\lambda_1}\varphi^2\,. \tag{6.2.28}$$

This auxiliary field φ is analogous to the field ϕ we introduced in the toy example described in the previous section. As we had announced in that context, even in a model without bosons like the quartic matrix-vector model, we end up with a scalar boson φ, which can be interpreted as an emergent bulk coordinate. In the computation of the on-shell probe brane action, we will need to set φ to its saddle point value φ^*, which is given by:

$$\varphi_* = \lambda_1\langle\alpha_\mu^\dagger\alpha_\mu\rangle = \lambda_1 Q^{(\alpha)}\,. \tag{6.2.29}$$

I_B-terms

In this context, we are mostly interested in the computation of the effective probe action for the auxiliary field φ, which is obtained by performing the path integral over the scalar fermions χ and $\chi^\dagger$. Such an integration will produce two kinds of contributions: a functional determinant and interaction terms of the form $(\beta\psi^\dagger\alpha)(\alpha^\dagger\psi\beta^\dagger)$. The latter can be easily shown to produce subleading diagrams in the large N limit and can be discarded. The functional determinant as well, since it comes from the integration over a variable which does not carry U(N) indices, will only contribute at order N^0. In the following, we can therefore neglect all contributions from the scalars χ and $\chi^\dagger$, which include all the I_B interaction terms and the $S_1(\chi)$ term in (6.2.25)

I_C-terms

These are, like the I_A-term, quartic interaction terms of the vector fields, but with different O(D) index contractions. Any diagram containing such vertices will be subleading in the large N, large D limit. This can be easily checked with the standard auxiliary field technique:

$$\frac{\lambda_2}{2}\sqrt{D}\,\alpha^\dagger_\mu\alpha_\nu\alpha^\dagger_\mu\alpha_\nu \;\to\; \sqrt{D}\left(A_{\mu\nu}\alpha^\dagger_\mu\alpha_\nu - \frac{1}{2\lambda_2}A_{\mu\nu}A_{\mu\nu}\right). \tag{6.2.30}$$

In the large N limit, since it does not carry U(N) indices, $A_{\mu\nu}$ settles to its saddle point value

$$A^*_{\mu\nu} = \lambda_2\langle\alpha^\dagger_\mu\alpha_\nu\rangle = \lambda_2\frac{\delta_{\mu\nu}}{D}\langle\alpha^\dagger_\mu\alpha_\mu\rangle = \lambda_2\frac{\delta_{\mu\nu}}{D}Q^{(\alpha)}\,, \tag{6.2.31}$$

where $Q^{(\alpha)}$ is the fermionic number of the α fundamentals, and it is a $O(1)$ quantity. By plugging (6.2.31) back into (6.2.30) we get

$$\frac{1}{\sqrt{D}}\left(Q^{(\alpha)}\alpha^\dagger_\mu\alpha_\mu - \frac{1}{2\lambda_2}Q^{(\alpha)\,2}\right), \tag{6.2.32}$$

which, because of the $D^{-1/2}$ prefactor, is a subleading term in the large D limit. An analogous reasoning can be carried out for the quartic term involving the β fundamentals.

I_D-term

This is an interaction term involving both the vectors and the matrices. If we ignore for a moment the O(D) indices, it is analogous to the matrix-vector coupling in the Hamiltonian of the IOP model, which was given in (3.2.29). In the large N limit, therefore, the leading diagrams will be the same as those which contribute to the two-point function of the fundamentals in the IOP model. Those are obtained by iterating a family of diagrammatic units of which the first three are shown in Figure 6.4. If we now consider the D counting, however, it is easy to verify that the presence of any of those units makes the diagram subleading. With respect

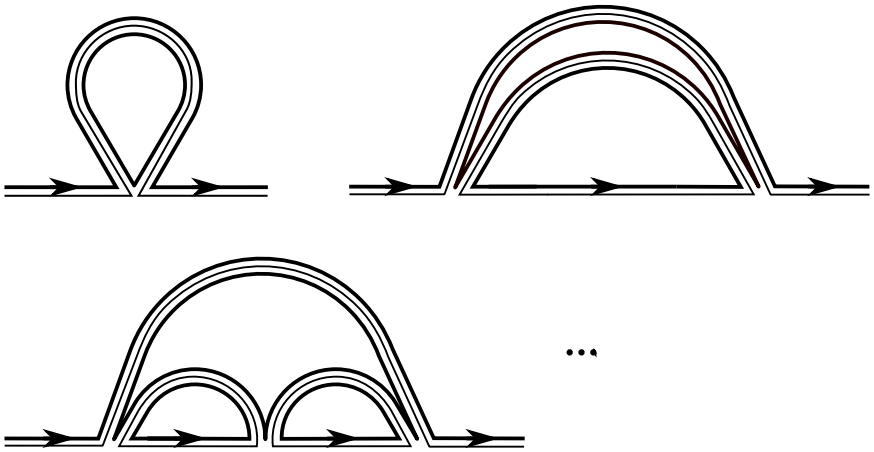

Figure 6.4: The leading large N graphs coming from the I_D-term are obtained by iterating diagrammatic units of this kind.

to the bare propagator, in fact, the n-th unit has: n vertices, $2n$ propagators, n loops of $\mathrm{U}(N)$ indices and $(n-1)$ loops of $\mathrm{O}(D)$ indices. This results in a factor D^{-1}, meaning that in the large N, large D limit, we can discard all diagrams containing the I_D interaction vertex.

I_E-term

This is again an IOP-like interaction term, but its $\mathrm{O}(D)$ index contractions differ from those of the I_D-term. Clearly, the N power counting is the same, and the leading large N diagrammatic units are still those of the IOP model. However, as it can be seen in Figure 6.5, the D power counting turns out to be different from that of the I_D-term. In fact, the n-th unit has: n vertices, $2n$ propagators, n loops of $\mathrm{U}(N)$ indices and one loop of $\mathrm{O}(D)$ indices. This results in a factor of D^{1-n}, which means that only the first diagrammatic unit contributes at leading order. In this sense, the contribution of the I_E-term plays an analogous role to the $I_{4,1}$ interaction term for the matrix fields. It is therefore convenient to deal with it through the introduction of a Lagrange multiplier field L^a_b and an auxiliary field Φ^a_b, in the following way:

$$-2\lambda_1\beta_\nu\psi^\dagger_\mu\psi_\mu\beta^\dagger_\nu \;\to\; \mathrm{tr}\, L\Big(\lambda_1\psi^\dagger_\mu\psi_\mu - \Phi\Big) - \beta_{\mu\,a}\Phi^a_b\beta^{\dagger\,b}_\mu\,. \tag{6.2.33}$$

Both L and Φ do not carry $\mathrm{O}(D)$ indices, therefore in the large D limit we can replace them by their saddle point values:

$$\Phi^a_{*\,b} = \lambda_1\frac{\delta^a_b}{N}\big\langle \mathrm{tr}\,\psi^\dagger_\mu\psi_\mu\big\rangle = \lambda_1\delta^a_b Q^{(\psi)}\,, \qquad L^a_{*\,b} = \delta^a_b\frac{Q^{(\beta)}}{N}\,, \tag{6.2.34}$$

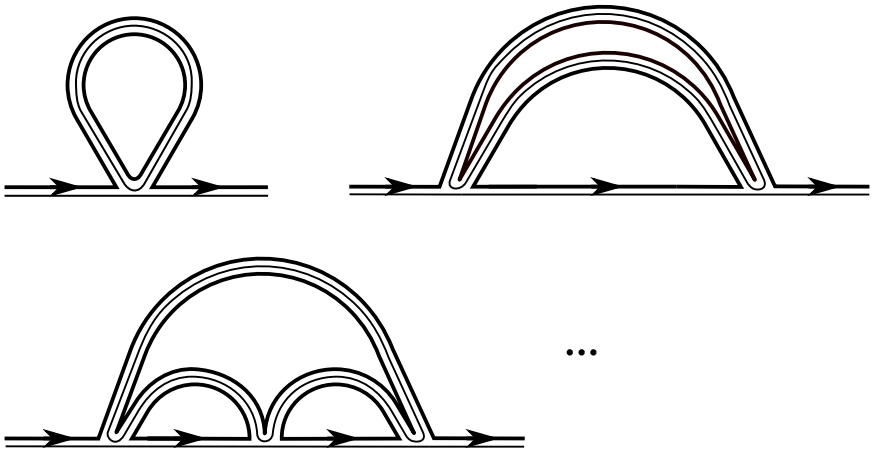

Figure 6.5: The leading large N graphs coming from the I_E-term are obtained by iterating diagrammatic units of this kind.

where $Q^{(\beta)} = \langle \beta^\dagger_\mu \beta_\mu \rangle$ is the fermion number for the β fundamentals. At the saddle point, we therefore have

$$\frac{Q^{(\beta)}}{N} \mathrm{tr}\, \psi^\dagger_\mu \psi_\mu - \lambda_1 Q^{(\psi)} Q^{(\beta)} + \lambda_1 Q^{(\psi)} \beta^\dagger_\mu \beta_\mu \,. \tag{6.2.35}$$

Note that, since $Q^{(\beta)}$ is $O(1)$, the mass term for the matrix fields is subleading at large N.

I_F-terms

The last terms have again the IOP structure, with $\mathrm{O}(D)$ index contractions which differ from both the I_D- and the I_E-terms. The planar diagrams coming from this interaction term are obtained by iterating units of the kind shown in Figure 6.6. In terms of powers of D, one can easily verify that the n-th unit has: n vertices, $2n$ propagators, n loops of $\mathrm{U}(N)$ indices, one loop of $\mathrm{O}(D)$ indices if n is even, otherwise no $\mathrm{O}(D)$ loops. Taking into account that the coupling is enhanced by a factor $\sqrt{D}$, we obtain that the only unit which is leading in the large D limit is the second one, whose iteration produces the well-known melon diagrams.

Final form of the action

After all the previous considerations, we can rewrite the action $S_{N,1}(\psi, \alpha, \beta, \chi)$ by discarding all the interaction terms which lead to subleading diagrams. Also, since our goal is testing the fundamental relation (6.2.7) for the on-shell probe action, we can directly set all the auxiliary fields to their saddle point values and neglect all contributions from the χ and $\chi^\dagger$ scalars. This results in the on-shell

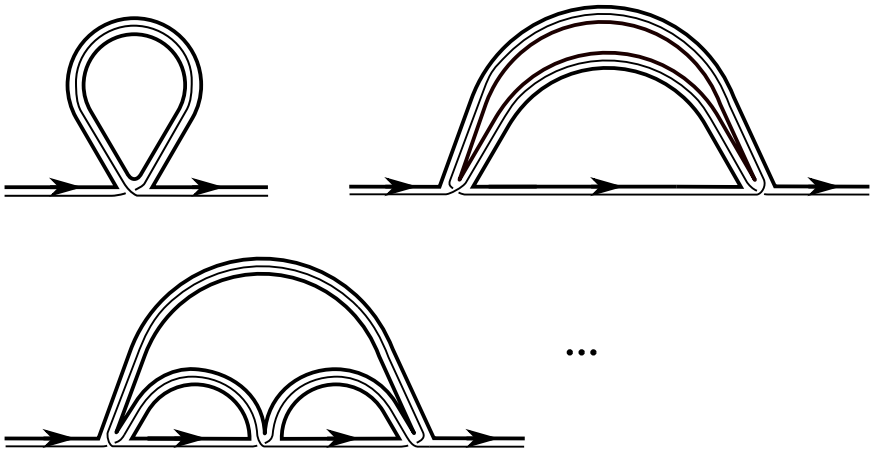

Figure 6.6: The leading large N graphs coming from the I_F-terms are obtained by iterating diagrammatic units of this kind.

action

$$S^*_{N,1}(\psi,\alpha,\beta) = \int dt \left(\alpha^\dagger_\mu \big(\partial_t + m + \lambda_1 Q^{(\alpha)}\big)\alpha_\mu + \beta^\dagger_\mu \big(\partial_t + m + \lambda_1 Q^{(\psi)}\big)\beta_\mu \right.$$
$$\left. + \lambda_2 \sqrt{D} \left[\beta_\mu \psi^\dagger_\nu \psi_\mu \beta^\dagger_\nu - \alpha^\dagger_\mu \psi_\nu \psi^\dagger_\mu \alpha_\nu \right] - \frac{\lambda_1}{2} Q^{(\alpha)\,2} - \lambda_1 Q^{(\psi)} Q^{(\beta)} \right). \tag{6.2.36}$$

It is worth noting that there is a clear difference between the actions for the fundamentals α and β. More precisely, the α fields get a dynamically generated mass term which is proportional to the expectation value of their own number operator, while in the case of the β fields, the mass shift is proportional to the number of the ψ fields. This asymmetry should not come as a surprise, and can in fact be understood by a close examination of the action of the quartic matrix-vector model we started from. In the c-graph representation of the two interaction vertices contained in the action, which is depicted in Figure 4.4, one can immediately see that, while the c-graph for the interaction term $I_{4,2}$ is symmetric under the exchange of green and red lines, the same does not hold for the c-graph of $I_{4,1}$. Since red and green lines are associated to contractions of $\mathrm{U}(N)_L$ and $\mathrm{U}(N)_R$ indices respectively, we can conclude that the $\mathrm{U}(N)_L$ and $\mathrm{U}(N)_R$ symmetries are not interchangeable in the quartic matrix-vector action we chose to study. Since the vectors α and β trasform in the fundamental representations of $\mathrm{U}(N)_L$ and $\mathrm{U}(N)_R$ respectively, this is reflected in an asymmetric action for the two kinds of vector fields.

6.2.4 Test of the fundamental relation for the on-shell probe action

We can now move on to a first non-trivial check of the probe analysis, namely the relation (6.2.7) between the planar free energy of the model and the on-shell probe brane action. In order to obtain it, we use the definition (6.2.18) and perform the path integral over the fundamental and adjoint degrees of freedom. This results in the following expression:

$$e^{-\mathscr{A}_N^*} = \frac{1}{Z_N}\int \mathcal{D}\psi\mathcal{D}\psi^\dagger\mathcal{D}\alpha\mathcal{D}\alpha^\dagger\beta\mathcal{D}\beta^\dagger\, e^{-(N+1)\left(\frac{1}{N}S_N(\psi)-S^*_{N,1}(\psi,\alpha,\beta)\right)}\,. \tag{6.2.37}$$

Now, the path integral over the fundamentals is Gaussian, and can be performed directly, yielding

$$\begin{aligned}\mathscr{A}_N^* \quad &= \quad \left\langle \mathrm{Tr}\ln\left(\partial_t + m + \lambda_1 Q^{(\alpha)}\right) - \lambda_2\sqrt{D}\psi_\mu\psi^\dagger_\nu\right\rangle \\ &\quad + \left\langle \mathrm{Tr}\ln\left(\partial_t + m + \lambda_1 Q^{(\psi)}\right) + \lambda_2\sqrt{D}\psi^\dagger_\mu\psi_\nu\right\rangle \\ &\quad - \frac{\lambda_1}{2}Q^{(\alpha)2} - \lambda_1 Q^{(\psi)}Q^{(\beta)}\,.\end{aligned} \tag{6.2.38}$$

However, the two functional determinants involve a complicated sum of correlators of the ψ matrices. There is an easier way of computing this quantity which relies on a similar technique to the one used in Section 6.1.4 to compute the free energy of the model. We proceed by first defining the finite temperature two-point functions of the vector fields:

$$\begin{aligned}G^{(\alpha)}(t) &\equiv \left\langle \mathrm{T}\alpha^a_\mu(t)\alpha^\dagger_{\mu a}\right\rangle_\beta = \frac{1}{\beta}\sum_{k\in\mathbb{Z}+1/2} G^{(\alpha)}_k e^{-i\nu_k t} \\ G^{(\beta)}(t) &\equiv \left\langle \mathrm{T}\beta_{\mu a}(t)\beta^{\dagger a}_\mu\right\rangle_\beta = \frac{1}{\beta}\sum_{k\in\mathbb{Z}+1/2} G^{(\beta)}_k e^{-i\nu_k t}\end{aligned} \tag{6.2.39}$$

In light of the action (6.2.36) and of the considerations we made on the I_F-terms of the action, we obtain the following Schwinger-Dyson equations:

$$\frac{1}{G^{(\alpha)}_k} = m + \lambda_1 Q^{(\alpha)} - i\nu_k + \Sigma^{(\alpha)}_k\,, \qquad \Sigma^{(\alpha)}_k(t) = \lambda_2^2 G^{(\alpha)}(t)G(t)G(-t)\,, \tag{6.2.40}$$

and

$$\frac{1}{G^{(\beta)}_k} = m + \lambda_1 Q^{(\psi)} - i\nu_k + \Sigma^{(\beta)}_k \qquad \Sigma^{(\beta)}_k(t) = \lambda_2^2 G^{(\beta)}(t)G(t)G(-t)\,, \tag{6.2.41}$$

where $G(t)$ is the two-point function of the ψ_μ matrices, which in turn satisfies (6.1.16). These Schwinger-Dyson equations are solved by

$$\begin{aligned}G^{(\alpha)}_k &= G^{(\beta)}_k = G_k\,, \\ Q^{(\alpha)} &= Q^{(\beta)} = Q^{(\psi)}\,.\end{aligned} \tag{6.2.42}$$

As we did for the computation of the free energy, as a first step we turn off the λ_1 coupling. For simplicity, we also start by focusing on only one kind of probe. The object of interest is of the form $\exp(-\mathcal{F}_1 + \mathcal{F}_2)$, with

$$e^{-\mathcal{F}_1} = \int \mathcal{D}\psi\mathcal{D}\psi^\dagger\mathcal{D}\beta\mathcal{D}\beta^\dagger \exp\Bigg[- ND \int dt \,\mathrm{tr}\left(\psi_\mu^\dagger(\partial_t + m)\psi_\mu + \sqrt{D}\frac{\lambda_a}{2}\psi_\mu\psi_\nu^\dagger\psi_\mu\psi_\nu^\dagger\right) + \beta_\mu^\dagger(\partial_t + m)\beta_\mu + \sqrt{D}\lambda_b\beta_\mu\psi_\nu^\dagger\psi_\mu\beta_\nu^\dagger\Bigg] \tag{6.2.43}$$

and

$$e^{-\mathcal{F}_2} = \int \mathcal{D}\psi\mathcal{D}\psi^\dagger \exp\Bigg[- ND \int dt \,\mathrm{tr}\left(\psi_\mu^\dagger(\partial_t + m)\psi_\mu + \sqrt{D}\frac{\lambda_a}{2}\psi_\mu\psi_\nu^\dagger\psi_\mu\psi_\nu^\dagger\right) . \tag{6.2.44}$$

Now, since in the free energy of the first model the vector fields β always give subleading contributions with respect to the matrix fields ψ, we can write:

$$\frac{\mathcal{F}_1}{N^2 D} = \mathcal{F}_1^{(0)}(\lambda_a) + N^{-1}\mathcal{F}_1^{(1)}(\lambda_a,\, \lambda_b) + O\big(N^{-2}\big) . \tag{6.2.45}$$

Also, since removing the vector contribution from the first model yields the second model, we can also conclude that

$$\mathcal{F}_1^{(0)}(\lambda_a) = \mathcal{F}_2^{(0)}(\lambda_a) . \tag{6.2.46}$$

We therefore obtain that the leading term in the large $1/N$ expansion of the difference between the two free energies is $\mathcal{F}_1^{(1)}(\lambda_a,\, \lambda_b)$. Its computation is carried out by considering the derivative of $\mathcal{F}_1$ with respect to λ_b in the large N, large D limit. We obtain:

$$\frac{\partial\mathcal{F}_1^{(1)}}{\partial\lambda_b} = \sqrt{D}\,\big\langle\beta_\mu\psi_\nu^\dagger\psi_\mu\beta_\nu^\dagger\big\rangle = \frac{1}{\lambda_b}\frac{1}{\beta}\sum_{k\in\mathbb{Z}+1/2}\left(\mathrm{Re}\,\frac{G_k^{(\beta)}}{G_k^{(0)}} - 1\right) , \tag{6.2.47}$$

where to obtain the second equality we carried out the same steps that led to (6.1.40) in Section 6.1.4. Also the following steps of that derivation can be adapted to this new case, leading to

$$\begin{aligned}\mathcal{F}_1^{(1)}(\lambda_a,\, \lambda_b) = &- T\Bigg\{ \sum_k \left(\ln\left[1 + \frac{\Sigma_k^{(\beta)}}{-i\nu_k + m}\right] - \Sigma_k^{(\beta)}G_k^{(\beta)}\right) \\ &+ \frac{\lambda_b^2}{2}\int dt_1 dt_2\, G^{(\beta)}(t_1,\, t_2)G(t_1,\, t_2)G^{(\beta)}(t_2,\, t_1)G(t_2,\, t_1)\cdot \\ &+ \ln\big(1 + e^{-\beta m}\big)\Bigg\}\end{aligned} \tag{6.2.48}$$

This result is the key ingredient for the computation of the on-shell probe brane action. By adding an analogous contribution for the α probe, setting $\lambda_a = \lambda_b = \lambda_2$ and turning on the λ_1 coupling we obtain

$$\begin{aligned}\frac{S_p^*}{ND} = &-\Bigg\{\sum_k\left(\ln\left[1+\frac{\Sigma_k^{(\beta)}}{-i\nu_k+m+\lambda_1 Q^{(\psi)}}\right]-\Sigma_k^{(\beta)}G_k^{(\beta)}\right)\\ &+\sum_k\left(\ln\left[1+\frac{\Sigma_k^{(\alpha)}}{-i\nu_k+m+\lambda_1 Q^{(\alpha)}}\right]-\Sigma_k^{(\alpha)}G_k^{(\alpha)}\right)\\ &+\frac{\lambda_2^2}{2}\int dt_1dt_2\, G^{(\beta)}(t_1,\,t_2)G(t_1,\,t_2)G^{(\beta)}(t_2,\,t_1)G(t_2,\,t_1)\\ &+\frac{\lambda_2^2}{2}\int dt_1dt_2\, G^{(\alpha)}(t_1,\,t_2)G(t_1,\,t_2)G^{(\alpha)}(t_2,\,t_1)G(t_2,\,t_1)\\ &+\ln\left(1+e^{-\beta(m+\lambda_1 Q^{(\psi)})}\right)+\ln\left(1+e^{-\beta(m+\lambda_1 Q^{(\alpha)})}\right)+\lambda_1 Q^{(\psi)}Q^{(\beta)}+\frac{\lambda_1}{2}Q^{(\alpha)2}\Bigg\},\end{aligned} \tag{6.2.49}$$

By using the solutions (6.2.42) of the Schwinger-Dyson equations for $G^{(\alpha)}(t)$ and $G^{(\beta)}(t)$, we can rewrite everything in the following way:

$$\begin{aligned}\frac{S_p^*}{ND} = &-\Bigg\{2\sum_k\left(\ln\left[1+\frac{\Sigma_k}{-i\nu_k+m+\lambda_1 Q^{(\psi)}}\right]-\Sigma_k G_k\right)\\ &+\lambda_2^2\int dt_1dt_2\, G(t_1,\,t_2)^2G(t_2,\,t_1)^2\\ &+2\ln\left(1+e^{-\beta(m+\lambda_1 Q^{(\psi)})}\right)+\frac{3\lambda_1}{2}Q^{(\psi)2}\Bigg\}.\end{aligned} \tag{6.2.50}$$

We now want to compare it with the expression for $2F_0+\lambda_1\partial_{\lambda_1}F_0+\lambda_2\partial_{\lambda_2}F_0$, which can easily be obtained from (6.1.54) and gives

$$\begin{aligned}2F_0+\lambda_1\partial_{\lambda_1}F_0+\lambda_2\partial_{\lambda_2}F_0 = &-\Bigg\{2\sum_k\left(\ln\left[1+\frac{\Sigma_k}{-i\nu_k+m+\lambda_1 Q^{(\psi)}}\right]-\Sigma_k G_k\right)\\ &+\lambda_2^2\int dt_1dt_2\, G(t_1,\,t_2)^2G(t_2,\,t_1)^2\\ &+2\ln\left(1+e^{-\beta(m+\lambda_1 Q^{(\psi)})}\right)+\frac{3\lambda_1}{2}Q^{(\psi)2}\Bigg\},\end{aligned} \tag{6.2.51}$$

thus proving the fundamental relation between the on-shell probe brane effective action and the free energy of the model. This is a first consistency check on the probe analysis of the quartic matrix-vector model and represents a first step in the study of the properties of its gravitational bulk dual.

Part III

Localization in $\mathcal{N} = 2$ SQCD

Chapter 7

Models and observables

7.1 Introduction

As it was explained in Part I, the first realization of the gauge/gravity correspondence featured four-dimensional $\mathcal{N} = 4$ super Yang-Mills (SYM) theory on the gauge theory side of the duality. This is a very special model: it is in fact a superconformal theory, and by virtue of its great amount of symmetry, many of its observables can be computed exactly, allowing for non-trivial tests of the AdS/CFT correspondence. Different techniques allow us to perform such computations, some of which rely on integrability (see [73] for a review) while others, as we will see, exploit localization techniques. It is a very natural step to try and consider models with less supersymmetry: on one hand we get closer to realistic gauge theories like QCD; on the other hand we can obtain more realizations of the gauge/gravity correspondence. In this respect, an interesting model to study is $\mathcal{N} = 2$ SYM in four dimensions. The bulk dual of such a theory is more complicated than the one we described in the $\mathcal{N} = 4$ case: in general it involves the definition of fractional D-branes on orbifolds [74, 75, 76]. Neveretheless, the gauge/gravity correspondence is established for these models as well, and the regime of reliability of the classical supergravity solution is well-understood. In particular, since $\mathcal{N} = 2$ SYM is not in general a conformal theory, there is an energy scale at which the gauge coupling diverges. This phenomenon has a clear interpretation in the bulk theory in terms of the geometric locus, the so-called enhançon, in which probe branes become tensionless. So far we referred exclusively to pure SYM theories, but it is in general possible to couple the pure SU(N) gauge theory to fundamental matter fields. In particular, if we start from pure $\mathcal{N} = 2$ SYM with SU(N) gauge symmetry and couple it to N_f massless hypermultiplets in the fundamental representation of SU(N), there is a specific limit in which the model becomes superconformal. This limit corresponds to the following relation between the rank of the gauge group and the number of fundamental hypermultiplets

$$N_f = 2N\,. \tag{7.1.1}$$

In the following we will refer to this model as $\mathcal{N}=2$ superconformal QCD (SCQCD). The model is of great interest: the conformal symmetry can be used to constrain many observables but, since the model has reduced supersymmetry with respect to $\mathcal{N}=4$ SYM, observables which are protected in the latter theory receive non-trivial quantum corrections in $\mathcal{N}=2$ SCQCD. Moreover, both models can be studied using the powerful tools offered by supersymmetric localization, which allows us to compute several observables in both models for any value of the coupling constant, even taking into account all instanton corrections. This chapter will be devoted to a precise definition of both theories and of the observables of interest, while in Chapter 8 we will introduce the main ideas of localization and use them to compute several observables in $\mathcal{N}=2$ SCQCD.

7.2 $\mathcal{N}=4$ SYM and $\mathcal{N}=2$ SCQCD

In Part I, we gave a definition of the four-dimensional $\mathcal{N}=4$ SYM action which is obtained from the $\mathcal{N}=1$ theory in ten dimensions by dimensional reduction. For the purposes of this section, however, it is more convenient to rewrite it using the four-dimensional $\mathcal{N}=1$ superfield formulation. In terms of $\mathcal{N}=1$ superfields, the $\mathcal{N}=4$ vector multiplet can be seen as being composed of an $\mathcal{N}=1$ vector multiplet V and three chiral multiplets Φ_1, Φ_2 and Φ_3 which transform in the adjoint representation of SU(N). The pure gauge $\mathcal{N}=4$ action is

$$\begin{aligned} S_{\mathcal{N}=4} =& \frac{1}{8g^2}\left(\int d^4x d^2\theta d^2\bar\theta\, \mathrm{tr}\big(W^\alpha W_\alpha\big) + \mathrm{h.c.}\right) \\ &+ 2\sum_{I=1,2,3}\int d^4x d^2\theta d^2\bar\theta\, \mathrm{tr}\big(\mathrm{e}^{-2gV}\Phi_I^\dagger \mathrm{e}^{2gV}\Phi_I\big) \\ &+ \frac{g\sqrt{2}}{3}\sum_{I,J,K=1}^{3}\left[\int d^4x d^2\theta\, \epsilon_{IJK}\mathrm{tr}\big(\Phi_I[\Phi_J,\Phi_K]\big) + \mathrm{h.c.}\right] \\ &- \frac{1}{4}\int d^4x d^2\theta d^2\bar\theta\, \mathrm{tr}\big(\bar D^2 V D^2 V\big)\,, \end{aligned} \tag{7.2.1}$$

where W_α is the chiral superfield-strength of V defined by

$$W_\alpha = -\frac{1}{4}\bar D^2\left(\mathrm{e}^{-2gV} D_\alpha \mathrm{e}^{2gV}\right)\,, \tag{7.2.2}$$

and the covariant derivatives are given by

$$D_\alpha = +\frac{\partial}{\partial\theta^\alpha} + i\sigma^\mu_{\alpha\dot\alpha}\bar\theta^{\dot\alpha}\partial_\mu, \quad \bar D_{\dot\alpha} = -\frac{\partial}{\partial\theta^\alpha} - i\theta^\alpha\sigma^\mu_{\alpha\dot\alpha}\partial_\mu\,. \tag{7.2.3}$$

The last term in the action is a gauge-fixing term which corresponds to the choice of the Fermi-Feynman gauge. Let us now turn to the definition of $\mathcal{N}=2$ SU(N) SYM coupled to N_f hypermultiplets in the fundamental representation (in short, $\mathcal{N}=2$ SQCD). The $\mathcal{N}=2$ vector multiplet can be built in terms of $\mathcal{N}=1$

superfields as the combination of a vector multiplet V and a chiral multiplet Φ. The resulting action for pure $\mathcal{N}=2$ SYM is

$$\begin{aligned} S_{gauge} =& \frac{1}{8g^2}\left(\int d^4x d^2\theta d^2\bar{\theta}\,\mathrm{tr}\big(W^\alpha W_\alpha\big)+\mathrm{h.c.}\right)+2\int d^4x d^2\theta d^2\bar{\theta}\,\mathrm{tr}\big(\mathrm{e}^{-2gV}\Phi^\dagger \mathrm{e}^{2gV}\Phi\big) \\ & -\frac{1}{4}\int d^4x d^2\theta d^2\bar{\theta}\,\mathrm{tr}\big(\bar{D}^2 V D^2 V\big)\,. \end{aligned} \tag{7.2.4}$$

We notice immediately that this action is contained in the $\mathcal{N}=4$ action (7.2.1) if we use the notation $\Phi_1=\Phi$. We call the difference between the two actions S_H:

$$\begin{aligned} S_H = S_{\mathcal{N}=4} - S_{gauge} =& 2\sum_{I=2,3}\int d^4x d^2\theta d^2\bar{\theta}\,\mathrm{tr}\big(\mathrm{e}^{-2gV}\Phi_I^\dagger \mathrm{e}^{2gV}\Phi_I\big) \\ & +\frac{g\sqrt{2}}{3}\sum_{I,J,K=1}^{3}\left[\int d^4x d^2\theta\,\epsilon_{IJK}\mathrm{tr}\big(\Phi_I[\Phi_J,\Phi_K]\big)+\mathrm{h.c.}\right]. \end{aligned} \tag{7.2.5}$$

We now want to couple the pure gauge $\mathcal{N}=2$ action to N_f fundamental massless hypermultiplets. In the language of $\mathcal{N}=1$ superfields, these correspond to N_f pairs of chiral multiplets Q and $\tilde{Q}$ transforming in the fundamental and antifundamental representations of SU(N) respectively. The complete $\mathcal{N}=2$ SQCD action is then obtained by summing the action for the fundamental multiplets to the pure gauge action (7.2.4):

$$S^{(N_f)}_{\mathcal{N}=2} = S_{gauge} + S_Q\,, \tag{7.2.6}$$

with

$$\begin{aligned} S_Q = \sum_{A=1}^{N_f}\Bigg[\int d^4x d^2\theta d^2\bar{\theta}\Big(Q_A^\dagger \mathrm{e}^{2gV}Q_A+\tilde{Q}_A\mathrm{e}^{-2gV}\tilde{Q}_A^\dagger\Big) \\ +\left(\mathrm{i}\sqrt{2}g\int d^4x d^2\theta\,\tilde{Q}_A\Phi Q_A+\mathrm{h.c.}\right)\Bigg]. \end{aligned} \tag{7.2.7}$$

We collected all the propagators we obtain from action (7.2.6) and all the cubic vertices contained in actions (7.2.6) and (7.2.1) in Figures 7.1 and 7.2. We chose to express the actions of both models in terms of $\mathcal{N}=1$ superfields since we are interested in the computation of $\mathcal{N}=2$ SQCD observables, and we will perform such computations by direct comparison with the corresponding $\mathcal{N}=4$ observables. Since from (7.2.5) and (7.2.6) we have

$$S^{(N_f)}_{\mathcal{N}=2} = S_{\mathcal{N}=4} + S_Q - S_H\,, \tag{7.2.8}$$

when we want to compute an $\mathcal{N}=2$ observable A which involves only the fields contained in S_{gauge}, it is often convenient to write it as:

$$A = \widehat{A} + A_Q - A_H\,, \tag{7.2.9}$$

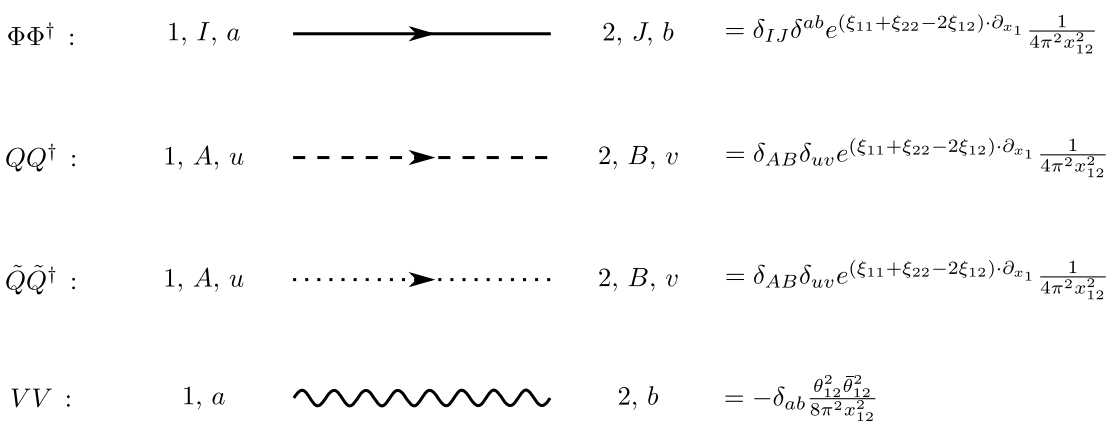

Figure 7.1: The superpropagators in $\mathcal{N}=4$ SYM and $\mathcal{N}=2$ SQCD in configuration superspace. The following notations were used: $x_{ij}=x_i-x_j$, $\theta_{ij}=\theta_i-\theta_j$, $\bar{\theta}_{ij}=\bar{\theta}_i-\bar{\theta}_j$ and $\xi_{ij}=i\theta_i\sigma\bar{\theta}_j$.

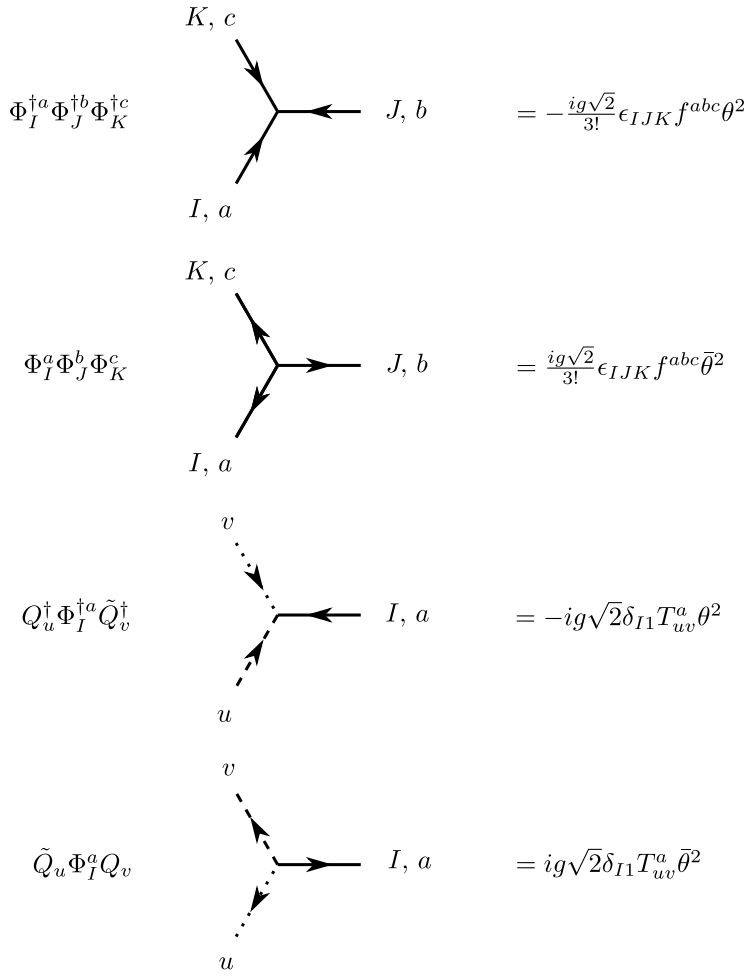

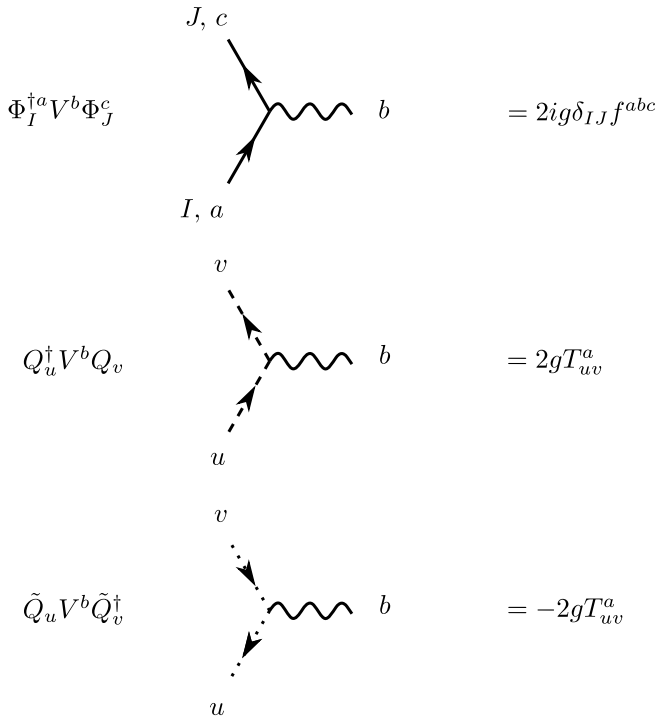

Figure 7.2: The cubic interaction vertices in $\mathcal{N} = 4$ SYM and $\mathcal{N} = 2$ SQCD

where $\widehat{A}$ is the same observable computed in the $\mathcal{N} = 4$ theory. Of the two remaining terms, A_H is the contribution given by Feynman diagrams in which Φ_2 and Φ_3 run in the internal lines, while A_Q is given by all diagrams with Q and $\tilde{Q}$ in their internal lines. This is particularly useful when computing BPS observables: such objects are in fact protected in $\mathcal{N} = 4$ SYM and their expectation values do not receive quantum corrections. For such observables we can therefore substitute $\widehat{A}$ with A_0, namely the tree-level result. The $\mathcal{N} = 2$ observables are therefore computed just by taking

$$A = A_0 + A_Q - A_H \,. \tag{7.2.10}$$

In some of the following computations, we will be interested in observables involving chiral operators, which are in general composite operators constructed using the adjoint complex scalar φ of the $\mathcal{N} = 2$ vector multiplet. The scalar is the lowest component of the chiral superfield Φ, given by

$$\varphi(x) = \Phi(x, \theta, \bar{\theta})|_{\theta=\bar{\theta}=0} = \varphi^a(x) T^a \,, \tag{7.2.11}$$

where the T^a are the generators of SU(N) and a runs from 1 to $(N^2 - 1)$. Equivalently, one can construct anti-chiral operators starting from the conjugate scalar

$$\bar{\varphi}(x) = \Phi^\dagger(x, \theta, \bar{\theta})|_{\theta=\bar{\theta}=0} = \bar{\varphi}^a(x) T^a \,. \tag{7.2.12}$$

Given a totally symmetric n-index tensor of SU(N) $R_{\vec{n}}^{b_1 \dots b_n}$, one can associate it to a gauge invariant chiral operator of dimension n in the following way

$$O_{\vec{n}}(x) = R_{\vec{n}}^{b_1 \dots b_n} \varphi^{b_1}(x) \cdots \varphi^{b_n}(x) \,. \tag{7.2.13}$$

Alternatively, $O_{\vec{n}}$ can be expressed as a multi-trace operator:

$$O_{\vec{n}}(x) = \mathrm{tr}\varphi^{n_1}(x)\cdots\mathrm{tr}\varphi^{n_l}(x)\,, \tag{7.2.14}$$

where the vector of integers $\vec{n} = (n_1, \cdots, n_l)$ satisfies

$$\sum_{k=1}^{l} n_k = n \tag{7.2.15}$$

and labels the different chiral operators. By replacing φ's with $\bar{\varphi}$'s, the corresponding anti-chiral operators are easily obtained. In the special case in which $N_f = 2N$, $\mathcal{N} = 2$ SQCD is a superconformal theory: the β-function of the theory vanishes, and therefore the coupling constant g is not renormalized. In this limit, the chiral operators become conformal primary operators called chiral primary operators (CPOs). Their operator product expansions (OPEs) are non-singular and this results in CPOs being endowed of a ring structure known as the chiral ring. The scaling dimension of a CPO $O_{\vec{n}}$ is fixed to be n at all orders in perturbation theory, and the two point function of a chiral and an anti-chiral operator with the same scaling dimension is fixed by conformal symmetry and takes the form

$$\left\langle O_{\vec{n}}(x_1)\bar{O}^j_{\vec{m}}(x_2)\right\rangle = \frac{A_{\vec{n},\vec{m}}}{(4\pi^2 x_{12}^2)^n}\,, \tag{7.2.16}$$

where $A_{\vec{n},\vec{m}}$ depends on both g and N. As it will be shown in the following, this quantity can be captured by localization computations.

7.3 Supersymmetric Wilson loops

Wilson loops are typical gauge invariant observables which can be defined in gauge theories. They were introduced by Wilson to study quark confinement [77] and carry non-trivial physical information about the model in which they are defined. In general a Wilson loop in the $\mathcal{R}$ representation of the SU(N) gauge group is defined as the holonomy of the gauge connection $A_\mu(x)$ along a closed path C:

$$W(C) = \frac{1}{N}\mathrm{Tr}_{\mathcal{R}}\mathcal{P}\mathrm{exp}\left\{ig\oint_C dx^\mu\, A_\mu(x)\right\} \tag{7.3.1}$$

where the trace is taken in the $\mathcal{R}$ representation and $\mathcal{P}$ denotes the path ordering of the integrals. The same definition can be adapted to open paths and the resulting objects are referred to as Wilson lines. In QCD Wilson loops contain information on the potential between a quark-antiquark pair and can be used as an order parameter in the study of the deconfinement phase transition. In supersymmetric gauge theories, Wilson loops can be generalized to contain couplings with the scalars of the vector multiplet, and can preserve a certain fraction of the supersymmetry. In $\mathcal{N} = 4$ SYM, for example, one can define the Maldacena-Wilson loop which contains the six scalars $\phi_i(x)$ of the $\mathcal{N} = 4$ vector multiplet:

$$W(C) = \frac{1}{N}\mathrm{Tr}_{\mathcal{R}}\mathcal{P}\mathrm{exp}\left\{g\oint_C d\tau\left[iA_\mu(x)\dot{x}^\mu(\tau) + \theta^i(\tau)|\dot{x}(t)|\phi_i(x)\right]\right\} \tag{7.3.2}$$

where $\theta^i(s)$ is a unit six-vector which can be associated to a point on S^5. The path C is parameterized by $x_\mu(\tau)$. It was shown by Maldacena [78] that such a Wilson loop has a counterpart in the holographic dual of $\mathcal{N}=4$ SYM. Its vacuum expectation value (VEV) is in fact computed by the area of the worldsheet of a fundamental string in $AdS_5 \times S^5$. The string worldsheet describes the closed path C at the boundary of AdS_5 and lies on $\theta^i(\tau)$ in S^5. Depending on the choice of the path, such a Wilson loop can partially or completely break supersymmetry. In [79], Zarembo showed that for constant θ^i, the only path which preserves part of $\mathcal{N}=4$ supersymmetry is the straight line. In such a case the Wilson loop commutes with eight out of sixteen $\mathcal{N}=4$ supercharges and therefore is a 1/2-BPS operator. As it was already mentioned, such an operator is protected from quantum corrections in $\mathcal{N}=4$ SYM theory, and therefore its VEV corresponds to the tree-level result

$$\langle W(C) \rangle_{\text{line}} = 1 \,. \tag{7.3.3}$$

From the straight line Wilson loop, one can obtain the circular one through a conformal transformation. Although $\mathcal{N}=4$ SYM is a conformal theory, due to quantum anomalies the VEV of the circular Wilson loop is not trivial as in the case of the straight line [80, 81]. It will in general depend on the coupling g and on the rank of the gauge group N and, as we will see in the following, it can be captured by a matrix model computation.

7.3.1 The circular 1/2 BPS Wilson loop in $\mathcal{N}=2$ SYM

In the rest of the thesis, we will focus on a specific kind of circular Wilson loop, which can be defined both in $\mathcal{N}=4$ and in $\mathcal{N}=2$ SYM theory. It is a circular loop of radius R whose path can be parameterized in the following way

$$x^\mu = R(\cos\tau,\, \sin\tau,\, 0,\, 0) \,. \tag{7.3.4}$$

In the $\mathcal{N}=2$ theory we can define it in a similar way as we defined the Maldacena loop in (7.3.2). The only difference is that, instead of the six $\mathcal{N}=4$ scalars, it contains the two $\mathcal{N}=2$ scalars:

$$W(C) = \frac{1}{N}\text{Tr}_{\mathcal{R}}\mathcal{P}\text{exp}\left\{ g \oint_C d\tau \left[iA_\mu(x)\dot{x}^\mu(\tau) + R\theta^I(\tau)\phi_I(x) \right] \right\} , \tag{7.3.5}$$

with $I = 1, 2$. The same object can be defined in $\mathcal{N}=4$ SYM just by taking the definition (7.3.2) and setting four of the components of $\theta^i(\tau)$ to zero. We also make the choice $\theta^I(\tau) = \delta^{I1}$ and rewrite it in terms of the chiral and anti-chiral complex scalars φ and $\bar{\varphi}$ by using the relations

$$\varphi = \frac{1}{\sqrt{2}}(\phi_1 + i\phi_2) \qquad \text{and} \qquad \bar{\varphi} = \frac{1}{\sqrt{2}}(\phi_1 - i\phi_2) \,. \tag{7.3.6}$$

The resulting expression for the Wilson loop is

$$W(C) = \frac{1}{N}\text{Tr}_{\mathcal{R}}\mathcal{P}\text{exp}\left\{ g \oint_C d\tau \left[iA_\mu(x)\dot{x}^\mu(\tau) + \frac{R}{\sqrt{2}}(\varphi(x) + \bar{\varphi}(x)) \right] \right\} . \tag{7.3.7}$$

The possibility of defining the same object in both the $\mathcal{N} = 2$ and the $\mathcal{N} = 4$ theories is particularly convenient because we can follow the reasoning introduced in Section 7 and obtain perturbative results in $\mathcal{N} = 2$ SQCD by taking the corresponding $\mathcal{N} = 4$ SYM result and adding the diagrammatic difference between the Q and H contributions. Although, as it was stated before, such circular loops in $\mathcal{N} = 4$ SYM are not protected and therefore receive quantum corrections, we will see in the following that their diagrammatic structure is much simpler than in the $\mathcal{N} = 2$ case.

Chapter 8

Localization

8.1 Overview

The basic idea of localization can be traced back to the field of topological quantum field theory [82]: it consists in reducing the infinite-dimensional path integral of a certain theory to finite-dimensional integrals localized on a finite number of fixed points, thus allowing for the computation of the partition function and several other quantities of interest. In the cases of both $\mathcal{N} = 4$ and $\mathcal{N} = 2$ SYM defined on S^4 the path integrals reduce to matrix model integrals, but while for the former it is a simple Gaussian model, the latter is characterized by a more complicated action. The correspondence between the computation of certain observables in $\mathcal{N} = 4$ SYM and analogous Gaussian matrix model computations had been first suggested in [80] and [81] in the context of the computation of circular 1/2-BPS Wilson loops in flat four-dimensional spacetime. They considered a Wilson-Maldacena loop in the fundamental representation of SU(N), defined on a circle C of unit radius. Basing their claims on field theoretical considerations and predictions coming from holographic computations, they conjectured that the expectation value of $W(C)$, was given by the following matrix model computation

$$\langle W(C) \rangle = \frac{1}{N} \frac{\int da \, \mathrm{e}^{-\mathrm{tr} a^2} \mathrm{tr} \, \mathrm{e}^{\frac{g}{\sqrt{2}} a}}{\int da \, \mathrm{e}^{-\mathrm{tr} a^2}} \,, \tag{8.1.1}$$

where a is an SU(N) matrix which can be expanded in terms of the SU(N) generators T^b as $a_b T^b$, with b running from 1 to $(N^2 - 1)$. The integration measure da is then given by

$$da \propto \prod_{b=1}^{N^2-1} da_b \,. \tag{8.1.2}$$

In order to understand how one could prove that such a formula does indeed capture the wanted observable, let us now briefly sketch the basic idea behind supersymmetric localization [83, 84, 85, 86, 87]. Consider a theory with a set of fields Φ and an action $S[\Phi]$. If such a theory has a fermionic symmetry generated by $\mathcal{Q}$, we have that $\mathcal{Q}S = 0$ and that $\mathcal{Q}$ squares either to zero or to the generator

of a bosonic symmetry of the action $\mathcal{P}$. If we introduce a fermionic functional of the fields $V[\Phi]$ such that $\mathcal{P}V = 0$, we can always add a term $t\mathcal{Q}V$ to the action and compute the following path integral

$$\mathcal{Z}(t) = \int \mathcal{D}\Phi \, \mathrm{e}^{-S[\Phi] - t\mathcal{Q}V[\Phi]} \,. \tag{8.1.3}$$

If we can show that such an integral does not depend on t, than $\mathcal{Z}(t)$ is equal to the partition function of the theory $\mathcal{Z}$. Indeed, if we take its derivative with respect to t we obtain

$$\partial_t \mathcal{Z}(t) = -\int \mathcal{D}\Phi \, \mathcal{Q}V \, \mathrm{e}^{-S[\Phi] - t\mathcal{Q}V[\Phi]} = -\int \mathcal{D}\Phi \, \mathcal{Q}\big(V \, \mathrm{e}^{-S[\Phi] - t\mathcal{Q}V[\Phi]}\big) = 0 \,, \tag{8.1.4}$$

where in the last step we assumed the symmetry generated by $\mathcal{Q}$ to be non-anomalous. The same reasoning would apply if we were to use the deformed action in (8.1.3) to compute the expectation value of a supersymmetric observable $O[\Phi]$ such that $\mathcal{Q}O = 0$. The fact that the path integral (8.1.3) is t-independent has a crucial consequence: the partition function (or the vacuum expectation value of O) of the undeformed theory, which corresponds to $t = 0$, can be computed by taking the $t \to \infty$ limit. This greatly simplifies the computation since, if the bosonic part of $\mathcal{Q}V$ is positive semi-definite, in that limit the path integral reduces to field configurations which satisfy $\mathcal{Q}V = 0$, which we will denote by Φ_0. Now, in order to evaluate the path integral in the $t \to \infty$ limit, let us expand the fields around Φ_0 in the following way

$$\Phi = \Phi_0 + t^{-1/2}\delta\Phi \,. \tag{8.1.5}$$

This results in an expansion of the deformed action

$$S[\Phi] + t\mathcal{Q}V[\Phi] = S[\Phi_0] + \frac{1}{2} \left. \frac{\delta^2 \left(\mathcal{Q}V[\Phi]\right)}{\delta\Phi^2} \right|_{\Phi=\Phi_0} \delta\Phi^2 + O\big(t^{-1/2}\big) \,. \tag{8.1.6}$$

In the $t \to \infty$ limit this results in a Gaussian path integral in terms of the fluctuations $\delta\Phi$, which can therefore be integrated out, yielding a one-loop superdeterminant:

$$\mathcal{Z}(t) = \int_{\mathcal{M}} \mathcal{D}\Phi_0 \, \mathrm{e}^{-S[\Phi_0]} \left(\mathrm{SDet} \left[\frac{\delta^2 \left(\mathcal{Q}V[\Phi_0]\right)}{\delta\Phi_0^2} \right] \right)^{-1} \,, \tag{8.1.7}$$

where the integration is now performed over $\mathcal{M}$, the space of zeros of $\mathcal{Q}V$ which is also referred to as the localization locus. The inverse of the superdeterminant in (8.1.7) will be denoted in the following as Z_{1-loop}.

8.1.1 Super Yang-Mills on S^4

These ideas were exploited in [83] to perform computations in $\mathcal{N} = 4$ and $\mathcal{N} = 2$ SYM defined on S^4. In this way, both the partition function and the VEV of

circular Wilson loops were computed by reducing the full path integral to a matrix model integral, thus proving the conjectured expression (8.1.1). Defining the theory on S^4 provides a natural way of regularizing the IR divergencies, which results in a finite partition function. At the same time, it preserves supersymmetry, allowing us to apply the localization technique. To perform the localization, the action is deformed by $t\mathcal{Q}V$, where V can be schematically expressed as

$$V = \sum_{\text{fermions } \Psi} (\mathcal{Q}\Psi)^\dagger \Psi \,, \tag{8.1.8}$$

and $\mathcal{Q}$ is the localizing supercharge. This choice automatically ensures a semi-positive definite bosonic part of $\mathcal{Q}V$. Localization is achieved by taking the $t \to \infty$ limit, which results in the path integral being non-zero only for field configurations such that

$$\mathcal{Q}\Psi = 0 \tag{8.1.9}$$

for all fermions Ψ. Both for $\mathcal{N} = 4$ SYM and $\mathcal{N} = 2$ SQCD the condition (8.1.9) is satisfied by setting the gauge vector A_μ to zero and setting the scalars of the $\mathcal{N} = 2$ vector multiplet to a constant value on S^4:

$$\varphi = \bar{\varphi} = \frac{a}{\sqrt{2}} \,, \tag{8.1.10}$$

where a is a constant SU(N) matrix. Moreover, all the bosonic fields in the $\mathcal{N} = 2$ matter hypermultiplets (N_f fundamental hypermultiplets in the case of $\mathcal{N} = 2$ SQCD, one adjoint hypermultiplet in the case of $\mathcal{N} = 4$ SYM) are set to zero. The path integral effectively reduces to an ordinary integral over the SU(N) matrix a. We get the action for a by plugging the saddle point field configuration back into the original action, and by computing the one-loop superdeterminant. In order to obtain the field configuration (8.1.10), the assumption of smoothness over S^4 was made. If one instead takes into consideration field configurations which are not smooth everywhere on S^4, then also configurations in which the gauge vector takes a non-zero value at the north and south pole of S^4 solve the saddle point equation. Such configurations correspond to instantons and anti-instantons localized at the poles, and they give another contribution to the partition function. The final form of the S^4 partition function is therefore:

$$\mathcal{Z}_{S^4} = \int da \, |Z_{\text{class}}(ia, \tau) Z_{\text{one-loop}}(ia) Z_{\text{inst}}(ia, \tau)|^2 \,. \tag{8.1.11}$$

We have introduced the complexified gauge coupling τ defined by

$$\tau = \frac{\theta}{2\pi} + i\frac{4\pi}{g^2} \tag{8.1.12}$$

and distinguished the three contributions coming from the classical action, the one-loop superdeterminant and instantons. The first contribution is the same for both the $\mathcal{N} = 4$ and the $\mathcal{N} = 2$ theories and corresponds to a Gaussian term

$$|Z_{\text{class}}(ia, g)|^2 = e^{-\frac{8\pi^2}{g^2}\text{tr}a^2} \,. \tag{8.1.13}$$

In $\mathcal{N}=4$ SYM both the one-loop superdeterminant and the instanton configurations do not contribute [88], and the partition function is therefore computed by a Gaussian matrix model:

$$\mathcal{Z}_{\mathcal{N}=4} = \int da\, e^{-\frac{8\pi^2}{g^2}\mathrm{tr}a^2}\,. \tag{8.1.14}$$

Instead, in the case of $\mathcal{N}=2$ SQCD the superdeterminant is non-trivial and is given by the following expression:

$$|Z_{\mathrm{one-loop}}(ia)|^2 = \prod_{u<v=1}^{N} H(ia_{uv})^2 \prod_{u=1}^{N} H(ia_u)^{-N_f} \qquad \text{with} \qquad a_{uv} \equiv a_u - a_v \tag{8.1.15}$$

which is written in terms of the N eigenvalues of a, denoted by a_u. The function $H(x)$ is a product of Barnes G-functions:

$$H(x) = G(x+1)G(1-x)\,. \tag{8.1.16}$$

Also the instanton contribution is non-trivial for $\mathcal{N}=2$ SQCD and it is given by Nekrasov's partition function [89, 90]. However, since in the following we are going to focus on the perturbative regime of the theory, we can set it to one:

$$|Z_{\mathrm{inst}}(ia,\,\tau)|^2 = 1\,. \tag{8.1.17}$$

The H functions appearing in the one-loop partition function can be expanded for small values of their arguments using

$$\log H(x) = -(1+\gamma)x^2 - \sum_{n=2}^{\infty} \zeta(2n-1)\frac{x^{2n}}{n}\,, \tag{8.1.18}$$

where ζ and γ are the Riemann zeta-function and the Euler-Mascheroni constant respectively. Using this formula, we can rewrite the one-loop contribution as

$$|Z_{\mathrm{one-loop}}(ia)|^2 = e^{-S(a)}\,, \tag{8.1.19}$$

with

$$S(a) = -2\sum_{u<v=1}^{N} \log H(ia_{uv}) + N_f \sum_{u=1}^{N} \log(ia_u) = S_2(a) + S_4(a) + \cdots\,. \tag{8.1.20}$$

The $S_n(a)$ are homogeneous polynomials in a of even order n, of which we show the first two

$$\begin{aligned} S_2(a) =& -(1+\gamma)\left(\sum_{u,v=1}^{N} a_{uv}^2 - N_f \sum_{u=1}^{N} a_u^2\right) = -(1+\gamma)(2N-N_f)\mathrm{tr}a^2\,, \\ S_4(a) =& \frac{\zeta(3)}{2}\left(\sum_{u,v=1}^{N} a_{uv}^4 - N_f \sum_{u=1}^{N} a_u^4\right) = \frac{\zeta(3)}{2}\left[(2N-N_f)\mathrm{tr}a^4 + 6(\mathrm{tr}a^2)^2\right]. \end{aligned} \tag{8.1.21}$$

Since in the following we will focus on $\mathcal{N} = 2$ SCQCD, we directly set $N_f = 2N$ in the above expressions, obtaining:

$$\begin{aligned} S_2(a) &= 0\,, \\ S_4(a) &= 3\zeta(3)(\mathrm{tr}a^2)^2\,. \end{aligned} \tag{8.1.22}$$

Rewritten in this way, the one-loop partition function appears as an infinite sum of interaction terms which deform the Gaussian model, which can be canonically normalized using the rescaling

$$a \to \left(\frac{g^2}{8\pi^2}\right)^{\frac{1}{2}} a\,. \tag{8.1.23}$$

After the rewriting of the one-loop term and the rescaling of a, the full partition function becomes

$$\mathcal{Z}_{S^4} = \left(\frac{g^2}{8\pi^2}\right)^{\frac{N^2-1}{2}} \int da\, e^{-\mathrm{tr}a^2 - S_{\mathrm{int}}(a)}\,, \tag{8.1.24}$$

with

$$S_{\mathrm{int}}(a) = \frac{g^2}{8\pi^2} S_2(a) + \left(\frac{g^2}{8\pi^2}\right)^2 S_4(a) + \cdots\,. \tag{8.1.25}$$

The g-dependent prefactor in (8.1.24) plays no role in the computation of observables. With the partition function rewritten in this way, one can put the terms of order g^{2L} in S_{int} in one-to-one correspondence with the quantum field theory computations at L loops in perturbation theory. For this reason, the expansion in powers of g^2 of S_{int} in matrix model computations will also be called a loop expansion. We can now proceed to the computation of observables in the matrix model. First of all, we normalize the integration measure over SU(N) in the following way:

$$da = \prod_{b=1}^{N^2-1} \frac{da_b}{\sqrt{2\pi}}\,, \tag{8.1.26}$$

In this way the partition function for the free Gaussian model is normalized to one:

$$Z_0 = \int da\, e^{-\mathrm{tr}a^2} = 1\,. \tag{8.1.27}$$

With the partition function written as in (8.1.24), we can compute the VEV of any operator $f(a)$

$$\langle f(a)\rangle = \frac{\int da\, e^{-\mathrm{tr}a^2 - S_{\mathrm{int}}(a)} f(a)}{\int da\, e^{-\mathrm{tr}a^2 - S_{\mathrm{int}}(a)}} \tag{8.1.28}$$

which can be expanded in powers of g^2 in a natural way, if we rewrite it in terms of VEVs in the Gaussian model:

$$\langle f(a)\rangle_0 = \frac{1}{Z_0} \int da\, e^{-\mathrm{tr}a^2} f(a)\,. \tag{8.1.29}$$

In the following we will use the notation $\langle\,\cdot\,\rangle_0$ to denote expectation values of operators in the Gaussian model. The VEV of $f(a)$ in the full interacting theory can therefore be rewritten as

$$\langle f(a)\rangle = \frac{\big\langle f(a)\exp(-S_{\rm int}(a))\big\rangle_0}{\big\langle\exp(-S_{\rm int}(a))\big\rangle_0}\,. \tag{8.1.30}$$

The perturbative expansion is easily obtained by making use of (8.1.25) to expand $\exp(-S_{\rm int}(a))$ in powers of g^2. Given this premise, the computation of the wanted VEVs reduces to Gaussian matrix model calculations, which are performed in the following way. First, it is convenient to expand the matrix a in terms of the SU(N) generators as $a = a_b T^b$. With our choice of normalization, they satisfy

$$\mathrm{tr}T^bT^c = \frac{\delta^{bc}}{2}\,,\qquad \mathrm{tr}T^b = 0\,. \tag{8.1.31}$$

Moreover, the normalization we chose for Z_0, results in the following Wick contraction

$$\langle a_b a_c\rangle_0 = \delta_{bc}\,. \tag{8.1.32}$$

The computation of VEVs in the interacting matrix model reduces to computing correlators of n matrices of the following form

$$t_{n_1,n_2,\cdots} = \big\langle \mathrm{tr}a^{n_1}\mathrm{tr}a^{n_2}\cdots\big\rangle_0\,, \tag{8.1.33}$$

with $\sum_p n_p = n$. Using fusion/fission identities

$$\begin{aligned}\mathrm{tr}\big(T^bBT^bC\big) &= \frac{1}{2}\mathrm{tr}B\,\mathrm{tr}C - \frac{1}{2N}\mathrm{tr}\big(BC\big)\,,\\ \mathrm{tr}\big(T^bC\big)\mathrm{tr}\big(T^bC\big) &= \frac{1}{2}\mathrm{tr}\big(BC\big) - \frac{1}{2N}\mathrm{tr}B\,\mathrm{tr}C\,,\end{aligned} \tag{8.1.34}$$

one can relate any such correlator to a sum of correlators of $n-2$ matrices. For example:

$$\begin{aligned}t_n &= \frac{1}{2}\sum_{m=0}^{n-2}\left(t_{m,n-m-2} - \frac{1}{N}t_{n-2}\right),\\ t_{n,n_1} &= \frac{1}{2}\sum_{m=0}^{n-2}\left(t_{m,n-m-2,n_1} - \frac{1}{N}t_{n-2,n_1}\right) + \frac{n_1}{2}\left(t_{n+n_1-2} - \frac{1}{N}t_{n-1,n_1-1}\right).\end{aligned} \tag{8.1.35}$$

Knowing the first few correlators

$$\begin{aligned}t_0 &= \big\langle\mathrm{tr}1\big\rangle_0 = N\,,\qquad t_1 = \big\langle\mathrm{tr}a\big\rangle_0 = 0\,,\\ t_2 &= \big\langle\mathrm{tr}a^2\big\rangle_0 = \mathrm{tr}T^bT^b = \frac{N^2-1}{2}\,,\end{aligned} \tag{8.1.36}$$

one can recursively construct all correlators with an arbitrary number n of matrices. For example we get:

$$\begin{aligned} t_2 =& \frac{N^2-1}{2}\,, \qquad t_{2,2} = \frac{N^4-1}{4}\,, \qquad t_4 = \frac{(N^2-1)(2N^2-3)}{4N}\,, \\ t_6 =& \frac{5(N^2-1)(N^4-3N^2+3)}{8N^2}\,, \qquad t_{3,3} = \frac{3(N^2-1)(N^2-4)}{8N}\,, \\ t_{4,2} =& \frac{(N^2-1)(N^2+3)(2N^2-3)}{8N}\,, \qquad t_{2,2,2} = \frac{(N^4-1)(N^2+3)}{8}\,. \end{aligned} \tag{8.1.37}$$

8.2 Correlators of chiral operators

In this section we show how the results of localization on S^4 can be used to compute the two-point functions of chiral and anti-chiral operators in $\mathcal{N} = 2$ SCQCD defined on $\mathbb{R}_4$. First the localization results are presented, then they are tested against perturbative field theory computations.

8.2.1 From S^4 to $\mathbb{R}_4$

The derivation by Pestun shows how to compute the S^4 partition function and expectation values of circular Wilson loops in $\mathcal{N} = 4$ and $\mathcal{N} = 2$ SYM theories, while it is not immediate to see if more general observables can be extracted from the localization results. Correlation functions of CPOs can be obtained in the following way. We start by deforming the action of the model by source terms for CPOs of the following form

$$\propto \int d^4x d^2\theta d^2\bar{\theta}\, \mathcal{E}\tau_{\mathcal{O}}\mathcal{O} + \text{h.c.}\,, \tag{8.2.1}$$

where $\mathcal{E}$ is the chiral density and $\tau_{\mathcal{O}}$ is the complex coupling associated to the CPO $\mathcal{O}$ [91, 92, 93, 94]. By taking the derivative of the deformed partition function $\mathcal{Z}(\tau_n,\, \bar{\tau}_{\bar{n}})$ with respect to the couplings and making use of a supersymmetric Ward identity [95], we obtain correlators of CPOs. For example we have

$$\frac{1}{\mathcal{Z}(\tau_i,\, \bar{\tau}_j)} \partial_{\tau_i}\partial_{\bar{\tau}_j} \mathcal{Z}(\tau_i,\, \bar{\tau}_j)\Big|_{\tau_i=\bar{\tau}_j=0} = \left\langle \mathcal{O}_i(N)\bar{\mathcal{O}}_j(S)\right\rangle_{S^4}\,, \tag{8.2.2}$$

where the two operators are evaluated at the north and south poles of S^4. This deformation of the theory in general breaks conformal invariance, unless the dimension of $\mathcal{O}$ is two, in which case it is exactly marginal. However, it preserves supersymmetry and the localization argument can be carried out along the same lines as the undeformed case. This allows us to compute the deformed partition function through a matrix model calculation. Let us consider a CPO of the form defined in (7.2.13):

$$O_{\vec{n}}(x) = R_{\vec{n}}^{a_1 a_2 \ldots a_n} \varphi^{a_1}(x)\varphi^{a_2}(x)\ldots\varphi^{a_n}(x)\,. \tag{8.2.3}$$

We can associate to it a multi-trace operator $O_{\vec{n}}(a)$ in the matrix model just by replacing $\varphi(x)$ with a in (8.2.3). The resulting deformed S^4 partition function is obtained from the undeformed one by multiplying $Z_{\text{class}}(ia)$ in (8.1.11) by the following factor

$$\exp\Big(i\tau_{\vec{n}}O_{\vec{n}}(a)\Big)\,. \tag{8.2.4}$$

Taking the double derivative and setting the couplings to zero as shown in (8.2.2), amounts to computing an expectation value in the matrix model:

$$\frac{1}{\mathcal{Z}(\tau_{\vec{n}},\,\bar{\tau}_{\vec{m}})}\partial_{\tau_{\vec{n}}}\partial_{\bar{\tau}_{\vec{m}}}\mathcal{Z}(\tau_{\vec{n}},\,\bar{\tau}_{\vec{m}})\Big|_{\tau_{\vec{n}}=\bar{\tau}_{\vec{m}}=0} = \big\langle O_{\vec{n}}(a)O_{\vec{m}}(a)\big\rangle_{\text{matrix model}}\,. \tag{8.2.5}$$

Since we are dealing with superconformal theories, one might naively expect correlators on S^4 to be trivially related to the ones computed in $\mathbb{R}_4$. However, there is an important subtlety associated to going from $\mathbb{R}_4$ to S^4: due to the conformal anomaly, an operator $\mathcal{O}_\Delta$ of dimension Δ on S^4 has non-vanishing correlators with operators of lower dimensions. Intuitively this can be understood by noting that on the sphere, the presence of a dimensionful Ricci scalar $\mathscr{R}$ allows operators of dimensions differing by an even integer to mix. Therefore, an operator $\mathcal{O}_\Delta$ of dimension Δ on $\mathbb{R}_4$ will in general mix with all operators with dimension $\Delta-2n$ when it is mapped to S^4. Schematically, we can write:

$$\mathcal{O}_\Delta^{\mathbb{R}_4} \to \mathcal{O}_\Delta^{S^4} + \alpha_1\mathscr{R}\mathcal{O}_{\Delta-2}^{S^4} + \alpha_2\mathscr{R}\mathcal{O}_{\Delta-4}^{S^4} + \cdots\,, \tag{8.2.6}$$

for some constants α_i. The fact that on the sphere correlators between operators of different dimensions do not vanish can be easily seen using the matrix model expression (8.2.5). If for example we choose the two operators to be $\text{tr}a^n$ and $\text{tr}a^m$, their correlator at tree-level will be $t_{n,m}$ defined in (8.1.35), which is non-vanishing as long as m and n are both even or both odd integers. In order to reconstruct the flat space two-point function from the sphere one, it is therefore necessary to disentangle each operator on the sphere from all the lower-dimensional ones it is mixed with. In the literature [94, 96, 97, 98] this has been achieved through a Gram-Schmidt orthogonalization procedure. Let us consider an operator $O(a)$ of dimension n. We can always define a basis $\{O_p\}$ of operators with dimensions lower or equal to $(n-2)$, and the matrix of their correlators

$$C_{pq} = \big\langle O_p(a)O_q(a)\big\rangle\,. \tag{8.2.7}$$

We can now introduce the following normal ordering prescription for operator $O(a)$

$$:O(a):_g = O(a) - \sum_{p,q}\big\langle O(a)O_p(a)\big\rangle C^{pq}O_q(a)\,, \tag{8.2.8}$$

where C^{pq} is the inverse of the correlator matrix C_{pq}. The subscript g is used to stress the fact that, since the expectation values in equations (8.2.7) and (8.2.8) are taken in the full interacting theory as it was defined in (8.1.30), this normal ordering procedure results in an explicit dependence on g in the definition of the

operator. Note that the normal-ordered operator $: O(a) :_g$ is by construction orthogonal to all operators with dimension lower than n. This includes also the identity, hence making its one-point function vanish. It is worth noting that this normal ordering amounts to eliminating all self-contractions when one considers correlators involving normal ordered operators. As a simple example, one can consider $O(a) = \mathrm{tr} a^2$. In this case, the basis $\{O_p\}$ contains only the identity, and the result of (8.2.8) is just

$$: \mathrm{tr} a^2 :_g = \mathrm{tr} a^2 - \left\langle \mathrm{tr} a^2 \right\rangle . \tag{8.2.9}$$

When performing perturbative checks, as we will do in the following, one has to consider such an operator order by order in g. In our case we would have

$$: \mathrm{tr} a^2 :_g = \mathrm{tr} a^2 - \frac{N^2-1}{2} + 3\zeta(3)\frac{N^4-1}{2}\left(\frac{g^2}{8\pi^2}\right) + O\big(g^6\big) , \tag{8.2.10}$$

where the term proportional to g^4 comes from the $S_4(a)$ term in $S_{\rm int}(a)$, as it was defined in (8.1.22) and (8.1.25).

8.2.2 Localization results

Now that we have the correct normal ordering prescription for the operators in the matrix model, we turn to the computation of correlators of operators corresponding to the chiral operators defined in (7.2.13). In the expression for the correlator (7.2.16) we just substitute φ and $\bar\varphi$ with a and perform the normal ordering. The correlators we want to focus on are of the form

$$\mathcal{A}_{\vec n,\vec m}(g) \equiv \left\langle : O_{\vec n}(a) :_g : O_{\vec m}(a) :_g \right\rangle = \frac{\left\langle e^{-S_{\rm int}(a)} : O_{\vec n}(a) :_g : O_{\vec m}(a) :_g \right\rangle_0}{\left\langle e^{-S_{\rm int}(a)} \right\rangle_0} . \tag{8.2.11}$$

It should be stressed that in the computation of such a correlator, in the conformal case $N_f = 2N$, the first effect of the g-dependence of the normal ordering appears at order g^6. Since we will check the localization results with standard quantum field theory computations up to two loops, which correspond to order g^4, for our purposes we can use the g-independent normal ordering defined as

$$: O_{\vec n}(a) :_0 = \lim_{g\to 0} : O_{\vec n}(a) :_g \ . \tag{8.2.12}$$

Note however that in the computation of other observables, like correlators between chiral operators and Wilson loops, the g-dependence of the normal ordering is crucial already at two loops [2]. Here we write explicitly the g-independent normal-ordered operators we will use in the following up to dimension four:

$$\begin{aligned}
: O_{(2)} : \ &= : \mathrm{tr}\, a^2 : = \ \mathrm{tr}\, a^2 - \frac{N^2-1}{2} , \\
: O_{(3)} : \ &= : \mathrm{tr}\, a^3 : = \ \mathrm{tr}\, a^3 , \\
: O_{(2,2)} : \ &= : (\mathrm{tr}\, a^2)^2 : = \ (\mathrm{tr}\, a^2)^2 - (N^2+1)\mathrm{tr}\, a^2 + \frac{N^4-1}{4} , \\
: O_{(4)} : \ &= : \mathrm{tr}\, a^4 : = \ \mathrm{tr}\, a^4 - \frac{2N^2-3}{N}\mathrm{tr}\, a^2 + \frac{(N^2-1)(2N^2-3)}{4N} .
\end{aligned} \tag{8.2.13}$$

We can now perform the perturbative expansion of $\mathcal{A}_{\vec{n},\vec{m}}(g)$ up to the order g^4. The tree-level term is simply given by the Gaussian model contribution. Considering the operators are normal-ordered, we get

$$\mathcal{A}_{\vec{n},\vec{m}}(g)\Big|_{\text{tree-level}} = \left\langle : O_{\vec{n}}(a) :: O_{\vec{m}}(a) : \right\rangle_0 = n! R_{\vec{n}\, b_1 b_2 \cdots b_n} R_{\vec{m}}^{b_1 b_2 \cdots b_n} \,. \tag{8.2.14}$$

At order g^2, since $S_2(a) = 0$, we have

$$\mathcal{A}_{\vec{n},\vec{m}}(g)\Big|_{\text{1-loop}} = 0 \,, \tag{8.2.15}$$

for any choice of the operators. The two-loop result is instead given by

$$\mathcal{A}_{\vec{n},\vec{m}}(g)\Big|_{\text{2-loop}} = -\left(\frac{g^2}{8\pi^2}\right)^2 \left\langle : O_{\vec{n}}(a) :: O_{\vec{m}}(a) : \, [S_4(a) - \left\langle S_4(a) \right\rangle_0] \right\rangle_0 \,. \tag{8.2.16}$$

By plugging the explicit expressions for the operators up to dimension four given in (8.2.13) into the tree level and two-loop formulas (8.1) and (8.2.16) we get, up to $O(g^6)$ terms

$$\begin{aligned}
\mathcal{A}_{(2)(2)}(g) =& \frac{N^2-1}{2} - \frac{9(N^4-1)}{2}\zeta(3)\left(\frac{g^2}{8\pi^2}\right)^2 , \\
\mathcal{A}_{(3)(3)}(g) =& \frac{3(N^2-1)(N^2-4)}{8N} - \frac{27(N^2-1)(N^2-4)(N^2+3)}{8N}\zeta(3)\left(\frac{g^2}{8\pi^2}\right)^2 , \\
\mathcal{A}_{(2,2)(2,2)}(g) =& \frac{N^4-1}{2} - 9(N^4-1)(N^2+3)\zeta(3)\left(\frac{g^2}{8\pi^2}\right)^2 , \\
\mathcal{A}_{(4)(4)}(g) =& \frac{(N^2-1)(N^4-6N^2+18)}{4N^2} \\
& - \frac{3(N^2-1)(N^6+2N^4-18N^2+81)}{N^2}\zeta(3)\left(\frac{g^2}{8\pi^2}\right)^2 , \\
\mathcal{A}_{(2,2)(4)}(g) =& \frac{(N^2-1)(2N^2-3)}{2N} - \frac{9(N^2-1)(2N^2-3)(N^2+3)}{N}\zeta(3)\left(\frac{g^2}{8\pi^2}\right)^2 .
\end{aligned} \tag{8.2.17}$$

These results, obtained through simple Gaussian matrix model computations, will be checked against standard perturbative quantum field theory results in the following.

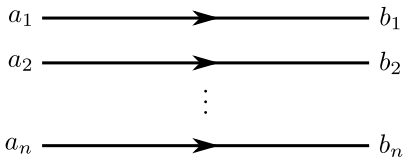

Figure 8.1: The diagram representing the tree-level correlator.

8.2.3 Perturbative checks

In order to make contact with the previous matrix model computations we will consider two-point functions of chiral operators of the form

$$\left\langle O_{\vec{n}}(x_1)\bar{O}_{\vec{m}}(x_2)\right\rangle = \frac{A_{\vec{n},\vec{m}}}{(4\pi^2 x_{12}^2)^n}\,. \tag{8.2.18}$$

Since the coordinate dependence of such a correlator is fixed by conformal invariance, the only thing that remains to be computed is the prefactor $A_{\vec{n},\vec{m}}$, which in turn should match the localization results. The scalars φ and $\bar{\varphi}$ are respectively obtained by the superfields Φ and $\Phi^\dagger$ by setting the Grassmann coordinates to zero, therefore it is easy to obtain their bare propagator from the $\Phi\Phi^\dagger$ one shown in Figure 7.1:

$$\left\langle \varphi^a(x_1)\bar{\varphi}^b(x_2)\right\rangle = \frac{\delta^{ab}}{4\pi^2 x_{12}^2}\,. \tag{8.2.19}$$

From this we can immediately obtain the tree-level contribution to the correlator (8.2.18), which is given by

$$\left\langle O_{\vec{n}}(x_1)\bar{O}_{\vec{m}}(x_2)\right\rangle_{\text{tree-level}} = \frac{n!R_{\vec{n}\,b_1b_2\cdots b_n}R_{\vec{m}}^{b_1b_2\cdots b_n}}{(4\pi^2 x_{12}^2)^n}\,, \tag{8.2.20}$$

where the $n!$ factor accounts for all possible Wick contractions. This tree-level contribution is represented in Figure 8.1. One realizes immediately that the numerator matches the localization result (8.2.14). Now, if we want to move to the computation of quantum corrections it is useful to use the trick introduced in Chapter 7. Therefore, we perform the computations in $\mathcal{N}=2$ SCQCD by taking the $\mathcal{N}=4$ results, adding the contributions for the N_f fundamental hypermultiplets Q and removing the diagrams containing the adjoint hypermultiplets H. Since in $\mathcal{N}=4$ the correlators of chiral operators do not receive quantum corrections, all we have to do is sum the $Q-H$ contributions to the tree level result. At one loop, the $Q-H$ contributions correspond to the one-loop correction to the scalar propagator depicted in Figure 8.2. It is easy to show that such a correction is proportional to (N_f-2N) and therefore vanishes in the conformal case. This was to be expected, since in the conformal $\mathcal{N}=2$ theory the β-function vanishes. The vanishing of the one-loop contribution is in perfect agreement with the localization result (8.2.15). We can now move on to the two-loop computation. At order g^4 we have three kinds of $Q-H$ diagrams. One, depicted in Figure 8.3,

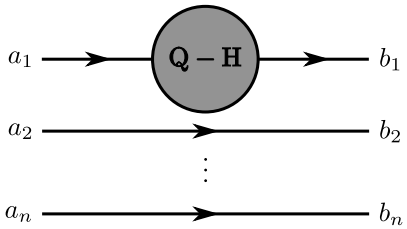

Figure 8.2: The diagram representing the one-loop contribution to the correlator (3.19). The label $Q - H$ in the loop means that this is the difference between the Q and H contributions.

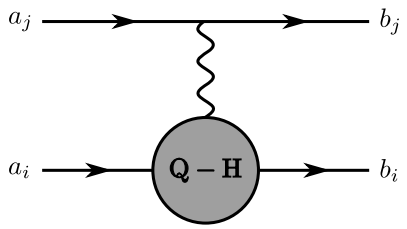

Figure 8.3: A two-loop subdiagram containing the one-loop correction to the gauge coupling that vanishes in the superconformal theory with $N_f = 2N$.

contains the one-loop correction to the three-point coupling. Analogously to the one-loop correction to the propagator, this diagram is proportional to $(N_f - 2N)$ and does not contribute in the conformal theory. The other two, on the other hand, do not vanish. We have a two-loop correction to the propagator, depicted in Figure 8.4, and a two-loop effective quartic vertex which is shown in Figure 8.5. Hence, the sum of these two contributions gives the two-loop piece of the two-point function:

$$\left\langle O_{\vec{n}}(x_1)\bar{O}_{\vec{m}}(x_2)\right\rangle_{2-\text{loop}} = \frac{A_{\vec{n},\vec{m}}\big|_{2-\text{loop}}}{(4\pi^2 x_{12}^2)^n}\,. \tag{8.2.21}$$

Let us start by computing the first contribution. From Figure 7.1 we see that the propagators of the superfields running in the internal lines have the same form for both the Q- and the H-diagrams, therefore the difference between the two must

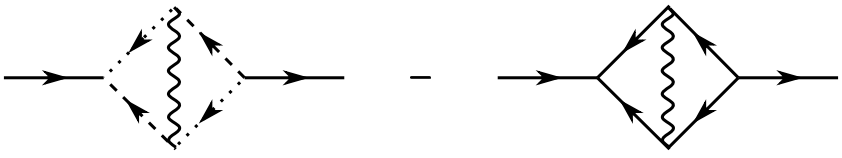

Figure 8.4: The irreducible two-loop correction to the scalar propagator. The left diagram describes the loop of the fundamental superfields Q and $\tilde{Q}$, while the right one accounts for the loop of the adjoint hypermultiplet H.

Figure 8.5: The two-loop diagrams that can contribute to the two-point function (3.19). The left diagram refers to the contribution of the fundamental hypermultiplets while the right diagram refers to the adjoint hypermultiplet H.

come entirely from combinatorial and colour factors. We therefore factorize the $Q-H$ contribution in the following way

$$-8g^4 W_2(x_{12}) C_2^{ab}\,, \tag{8.2.22}$$

where the prefactor $-8g^4$ comes from the vertices, and C_2^{ab} is obtained from the Feynman rules given in Figure 7.2. It therefore takes the form

$$\begin{aligned} C_2^{ab} &= N\mathrm{tr}T^a T^c T^b T^c - f^{ad_4d_1} f^{cd_1d_2} f^{bd_2d_3} f^{cd_3d_4} \\ &= \frac{N^2+1}{2}\delta_{ab}\,. \end{aligned} \tag{8.2.23}$$

The $W_2(x_{12})$ contains all the dependence on the coordinates and it is obtained by integrating over the superspace variables of the internal lines. This integration is performed in [98] and can be expressed as a particular limit of the Usyukina-Davydychev function $\Phi^{(2)}$ [105]. It yields

$$W_2(x_{12}) = -\frac{3\zeta(3)}{\left(16\pi^2\right)^2}\frac{1}{\left(4\pi^2 x_{12}^2\right)}\,. \tag{8.2.24}$$

We proceed in a similar way by writing the contribution due to the diagrams in Figure 8.5 in the following form

$$2g^4 W_4(x_{12}) C_4^{a_1a_2b_1b_2}\,. \tag{8.2.25}$$

The color factor $C_4^{a_1a_2b_1b_2}$ is again obtained from the Feynman rules and gives

$$\begin{aligned} C_4^{a_1a_2b_1b_2} &= N\mathrm{tr}T^{a_1}T^{b_1}T^{a_2}T^{b_2} - f^{a_1d_4d_1} f^{b_1d_1d_2} f^{a_2d_2d_3} f^{b_2d_3d_4} \\ &= -\left(\delta_{a_1b_1}\delta_{a_2b_2} + \delta_{a_1a_2}\delta_{b_1b_2} + \delta_{a_1b_2}\delta_{a_2b_1}\right). \end{aligned} \tag{8.2.26}$$

Analogously to the previous case, also for the two-loop effective quartic vertex the superspace integral on the internal lines reduces to a limit of the Usyukina-Davydychev function $\Phi^{(2)}$ and gives the following result:

$$W_4(x_{12}) = \frac{6\zeta(3)}{\left(16\pi^2\right)^2}\frac{1}{\left(4\pi^2 x_{12}^2\right)^2}\,. \tag{8.2.27}$$

We can now combine the two contributions for specific choices of the operators, obtaining:

$$A_{(2)(2)}\big|_{2-\text{loop}} = -\frac{9(N^4-1)}{2}\zeta(3)\left(\frac{g^2}{8\pi^2}\right)^2,$$

$$A_{(3)(3)}\big|_{2-\text{loop}} = -\frac{27(N^2-1)(N^2-4)(N^2+3)}{8N}\zeta(3)\left(\frac{g^2}{8\pi^2}\right)^2,$$

$$A_{(2,2)(2,2)}\big|_{2-\text{loop}} = -9(N^4-1)(N^2+3)\zeta(3)\left(\frac{g^2}{8\pi^2}\right)^2, \tag{8.2.28}$$

$$A_{(4)(4)}\big|_{2-\text{loop}} = -\frac{3(N^2-1)(N^6+2N^4-18N^2+81)}{N^2}\zeta(3)\left(\frac{g^2}{8\pi^2}\right)^2,$$

$$A_{(2,2)(4)}\big|_{2-\text{loop}} = -\frac{9(N^2-1)(2N^2-3)(N^2+3)}{N}\zeta(3)\left(\frac{g^2}{8\pi^2}\right)^2.$$

These results, checked against the localization results (8.2.17), show again perfect agreement.

8.3 1/2-BPS circular Wilson loops

As it was mentioned above, the first observables computed through supersymmetric localization techniques were circular 1/2-BPS Wilson loops in $\mathcal{N}=2$ SYM. In $\mathcal{N}=4$ SYM, the fact that the VEV of such Wilson loops could be captured by a Gaussian matrix model had been conjectured before the rigorous proof through localization by Pestun [80, 81]. The conjecture was motivated by holographic computations [78, 99, 100, 101], and confirmed by perturbative field theory results, which we review in the following.

8.3.1 Localization results in $\mathcal{N}=4$ SYM and their interpretation

Using the localization prescription (8.1.10), we obtain that in $\mathcal{N}=4$ SYM the VEV of the Maldacena-Wilson loop defined in (7.3.2) is obtained through the following matrix model computation

$$\langle W(C)\rangle = \frac{1}{N}\frac{\int da\, e^{-\text{tr}a^2}\text{tr}\, e^{\frac{g}{\sqrt{2}}a}}{\int da\, \mathrm{e}^{-\text{tr}a^2}} = \frac{1}{N}\left\langle \text{tr}\, e^{\frac{g}{\sqrt{2}}a}\right\rangle_0. \tag{8.3.1}$$

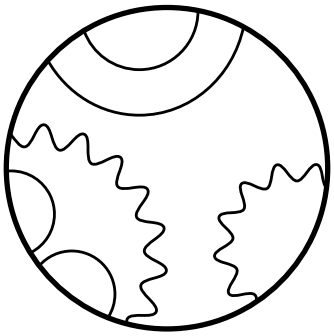

Figure 8.6: An example of rainbow diagram contributing to the expectation value of the Maldacena-Wilson loop. The thick line represents the Wilson loop, while the thin straight and wiggly lines represent the scalar and gluon propagators respectively.

By expanding the exponential we obtain

$$\langle W(C)\rangle = \frac{1}{N}\sum_{k=0}^{\infty}\frac{g^k}{2^{\frac{k}{2}}k!}\big\langle \mathrm{tr} a^k\big\rangle_0 = \frac{1}{N}\sum_{k=0}^{\infty}\frac{g^k}{2^{\frac{k}{2}}k!}t_k\,. \tag{8.3.2}$$

This series can be computed with the orthogonal polynomial technique [81] and yields the following result

$$\begin{aligned}\langle W(C)\rangle &= 1 + g^2\frac{N^2-1}{8N} + g^4\frac{(N^2-1)(2N^2-3)}{384N^2} + \cdots \\ &= \frac{1}{N}L^1_{N-1}\Big(-\frac{g^2}{4}\Big)\exp\Big[\frac{g^2}{8}\Big(1-\frac{1}{N}\Big)\Big]\,,\end{aligned} \tag{8.3.3}$$

where L_n^m is the generalized Laguerre polynomial of degree n. In the large N limit, we have

$$\begin{aligned}\langle W(C)\rangle_{\text{planar}} &= 1 + \frac{\lambda}{8} + \frac{\lambda^2}{192} + \cdots \\ &= \frac{2}{\sqrt{\lambda}}I_1(\sqrt{\lambda})\,,\end{aligned} \tag{8.3.4}$$

where we have introduced the 't Hooft coupling $\lambda = g^2N$ and I_n is the modified Bessel function of the first kind. In the strong coupling limit we have

$$\langle W(C)\rangle_{\text{planar}} = \frac{e^{\sqrt{\lambda}}}{(\pi/2)^{1/2}\lambda^{3/4}}\,, \tag{8.3.5}$$

which matches the AdS/CFT prediction [100, 101]:

$$\langle W(C)\rangle_{\text{AdS/CFT}} \sim e^{\sqrt{\lambda}}\,. \tag{8.3.6}$$

This result can be captured by a perturbative field theory computation, which corresponds to the sum over all the planar diagrams with no internal vertices

Figure 8.7: Any planar rainbow diagram with $n+1$ internal lines can be uniquely decomposed in a subdiagram with k internal lines and one with $n-k$ internal lines, separated by one internal line. The thick line represents the Wilson loop, while the thin line is an internal propagator.

[80]. Such diagrams are referred to as rainbow diagrams in the literature and an example is depicted in Figure 8.6. Let us start by considering the second term in the Taylor expansion of the Wilson loop:

$$\frac{g^2}{N}\int_0^{2\pi} d\tau_1 \int_0^{\tau_1} d\tau_2 \,\mathrm{tr}\Big[\big\langle \varphi(x_1)\bar{\varphi}(x_2)\big\rangle - \big\langle (A_\mu(x_1)\dot{x}^\mu(\tau_1)A_\nu(x_2)\dot{x}^\nu(\tau_2)\big\rangle\Big] \,. \tag{8.3.7}$$

By substituting the propagators for the gauge vector and the scalars, and taking the trace over the colour indices, we obtain:

$$\frac{g^2(N^2-1)}{8\pi^2 N}\int_0^{2\pi} d\tau_1 \int_0^{\tau_1} d\tau_2 \,\frac{1-\dot{x}(\tau_1)\cdot\dot{x}(\tau_2)}{|x(\tau_1)-x(\tau_2)|^2} = \frac{g^2(N^2-1)}{8N}\,, \tag{8.3.8}$$

where in the last step we used the fact that, by using the parameterization of the circle defined in (7.3.4), we obtain a constant integrand. First of all, we notice immediately that this result is consistent with the expression obtained from localization (8.3.3). Secondly, it is easy to convince ourselves that if we restrict ourselves to diagrams with no internal vertices, we will always encounter integrals of the kind we obtained in (8.3.8). At the planar level, there is a straightforward way of performing the sum over all such diagrams. First of all, because of the above considerations, we realize that at te $2n$-th order in perturbation theory the contribution coming from planar rainbow diagrams will be of the form

$$\frac{\big(\lambda/4\big)^n}{(2n)!}\chi_n\,, \tag{8.3.9}$$

where χ_n is the number of planar rainbow diagrams with n propagators. The counting can be done by exploiting the fact that each diagram of this kind always admits a unique decomposition like the one depicted in Figure 8.7. In terms of χ_n this implies

$$\chi_{n+1} = \sum_{k=0}^{n} \chi_{n-k}\chi_k \,. \tag{8.3.10}$$

We can now introduce the function $f(z)$ such that

$$f(z) = \sum_{n=0}^{\infty} \chi_n z^n \,. \tag{8.3.11}$$

The recursion relation (8.3.10) results in

$$zf^2(z) = f(z) - 1\,, \tag{8.3.12}$$

which is solved by

$$f(z) = \frac{1-\sqrt{1-4z}}{2z} = \sum_{n=0}^{\infty} \frac{(2n)!}{(n+1)!n!} z^n\,. \tag{8.3.13}$$

The sign of the square root is imposed by the condition $\chi_0 = 1$. Therefore, we obtain that the total contribution to the Wilson loop due to planar rainbow diagrams is given by

$$\langle W(C)\rangle_{\text{rainbow}} = \sum_{n=0}^{\infty} \frac{(\lambda/4)^n}{(n+1)!n!} = \frac{2}{\sqrt{\lambda}} I_1(\lambda) \tag{8.3.14}$$

By comparison with (8.3.4), we see that the localization result is matched by the rainbow diagram contribution: this means that all diagrams with internal vertices must cancel.

8.3.2 Localization results in $\mathcal{N} = 2$ SCQCD and their interpretation

In $\mathcal{N} = 2$ SCQCD, as one might expect, things get more complicated, both at the level of the localization results and at the level of perturbative computations. However, since the results in $\mathcal{N} = 4$ SYM are well established, we can consider the same Wilson loop in both theories and compute the difference between the two results, both in the matrix model and in quantum field theory. The Wilson loop we will consider is the circular 1/2-BPS Wilson loop defined in (7.3.7). In the perturbative expansion of the localization results, the first term that appears in the difference between $\mathcal{N} = 2$ and $\mathcal{N} = 4$ is at order g^6:

$$\begin{aligned} \left\langle W(C)\right\rangle_{\mathcal{N}=2} - \left\langle W(C)\right\rangle_{\mathcal{N}=4} &= -\frac{g^6}{\left(8\pi^2\right)^2}\frac{1}{4}\Big\langle \text{tr}a^2[S_4(a) - \left\langle S_4(a)\right\rangle_0]\Big\rangle_0 \\ &= -g^6\frac{3\zeta(3)}{\left(8\pi^2\right)^2}\frac{N^4-1}{8N} + O(g^8)\,. \end{aligned} \tag{8.3.15}$$

In [102], a perturbative quantum field theory test of this contribution was performed. We start by realizing that two particular classes of diagrams always cancel in the difference between $\mathcal{N} = 2$ and $\mathcal{N} = 4$. We call these classes tree-type diagrams and one-loop corrected tree-type diagrams, and an example for both types is depicted in Figure 8.8. Tree-type diagrams are diagrams which do not contain any internal loop. These diagrams always vanish in the difference between the two theories because the fields which appear in the definition of the Wilson loop

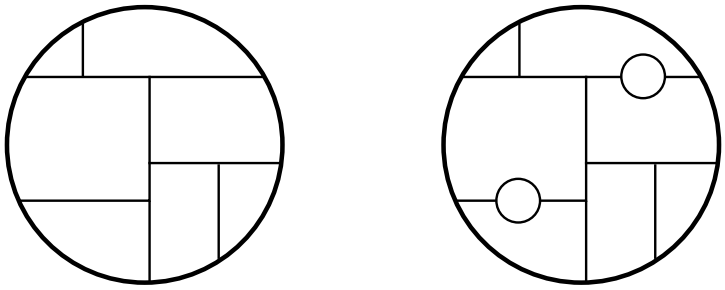

Figure 8.8: An example of tree-type diagram (left) and of one-loop corrected tree-type diagram (right).The internal lines can be both scalar or gluon propagators. Both types of diagrams cancel in the difference between $\mathcal{N} = 2$ and $\mathcal{N} = 4$.

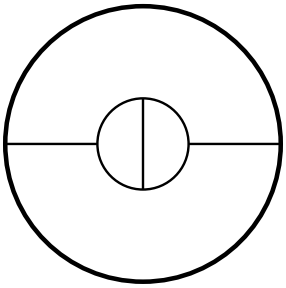

Figure 8.9: The diagram which accounts for the order g^6 contribution predicted by localization.

are the same both for $\mathcal{N} = 2$ and $\mathcal{N} = 4$. From tree-type diagrams we can construct one-loop corrected tree-type diagrams, by performing a one-loop correction on any of the propagators of the diagrams. As it was explained in the computation of the difference between the one-loop correction to the scalar propagator in $\mathcal{N} = 4$ SYM and the one in $\mathcal{N} = 2$ SCQCD is proportional to $(N_f - 2N)$ and therefore vanishes. The same can be said about the one-loop correction to the gluon propagator. Since only diagrams belonging to these two classes contribute to the Wilson loop up to order g^4, we can conclude that the first contribution to the difference between the two theories must appear at higher orders. At order g^6, we already know from our previous considerations a kind of diagram which can produce the $\zeta(3)$ factor predicted by localization. It is the two-loop correction to the internal scalar or gluon propagator depicted in Figure 8.9. We already encountered this diagram topology in Section 8.2.3, and from equations (8.2.22), (8.2.23) and (8.2.24) we can conclude that performing this correction to the scalar propagator amounts to multiplying the bare propagator by the following factor:

$$\mathcal{W}_2 = -g^4 \frac{3\zeta(3)}{\left(8\pi^2\right)^2}(N^2+1)\,. \tag{8.3.16}$$

By supersymmetry, the same applies to the two-loop correction to the gluon propagator. Therefore the total contribution due to the diagram in Figure 8.9 can be obtained by taking the $O(g^2)$ contribution to the $\mathcal{N} = 4$ Wilson loop which was

obtained in (8.3.8), and multiplying it by $\mathcal{W}_2$. The result is

$$-g^6\frac{3\zeta(3)}{\left(8\pi^2\right)^2}\frac{N^4-1}{8N}\,, \tag{8.3.17}$$

which means that the localization result is captured by this diagram alone. In fact, it can be showed that all other diagrams at order g^6 either belong to the tree-type and one-loop corrected tree-type categories, or give no contribution because of symmetry considerations.

8.4 Correlators between Wilson loop and chiral operators in $\mathcal{N}=2$ conformal gauge theories

This section contains a summary of the original results of [2], which can be found attached in Appendix B. The paper focuses on the computation of one-point functions of chiral operators in the presence of a 1/2-BPS Wilson loop in $\mathcal{N}=2$ superconformal SQCD. On one hand, the computation is carried out by generalizing the localization formulas used for the VEV of Wilson loops and for correlators of chiral operators to the observables of interest. On the other hand, the localization results are checked against direct perturbative QFT computations performed up to two loops. In the large N limit, a class of Feynman diagrams whose amplitude is proportional to $\zeta(3)$ is identified and given an interpretation in light of the localization computations.

8.4.1 Wilson loop and its correlators with chiral operators

The 1/2-BPS circular wilson loop of radius R that will be considered in the paper is defined as

$$W(C)=\frac{1}{N}\mathrm{tr}\mathcal{P}\mathrm{exp}\left\{g\oint_C d\tau\left[iA_\mu(x)\dot{x}^\mu(\tau)+\frac{R}{\sqrt{2}}\big(\varphi(x)+\bar{\varphi}(x)\big)\right]\right\} \tag{8.4.1}$$

Using known results in conformal field theories with defects, the correlator between the Wilson loop and a chiral operator $O_{\vec{n}}$ of order n is cast in the form

$$\langle W(C)O_{\vec{n}}(x)\rangle=\frac{A_{\vec{n}}}{\left(2\pi\left\|x\right\|_C\right)^n} \tag{8.4.2}$$

where

$$\left\|x\right\|_C=\frac{\sqrt{(R^2-x^2)^2+4L^2R^2}}{R} \tag{8.4.3}$$

contains all the dependence on the position of the operator. Since the functional dependence on x is entirely fixed by conformal symmetry, the only quantity that remains to be computed is $A_{\vec{n}}$, which is captured by the localization results.

8.4.2 The matrix model approach

The main result of localization is that the observable of interest can be computed using the same matrix model used for the correlators of chiral operators defined in (8.1.24). In this matrix model, the operator corresponding to the Wilson loop is

$$\mathcal{W}(a) = \frac{1}{N}\mathrm{tr}\exp\left(\frac{g}{\sqrt{2}}a\right) \tag{8.4.4}$$

while the chiral operators have to undergo the same g-dependent normal ordering procedure which was outlined in the case of correlators of chiral operators. It is important to stress that, while in all previous examples considered in the literature the g-dependence in the normal ordering did not play any role, in our case it is actually crucial in order to match the field theory results. Using the aforementioned matrix model technology, correlators of the Wilson loop and normal ordered chiral operators of the form

$$\left\langle \mathcal{W}(a)\widehat{\mathcal{O}}_{\vec{n}}(a)\right\rangle \tag{8.4.5}$$

can be evaluated. The results are shown for the $\mathcal{N}=4$ and superconformal $\mathcal{N}=2$ theories, both at finite N and in the planar limit.

8.4.3 Perturbative checks in field theory

The localization results are checked against field theory computations in $\mathcal{N}=2$ SCQCD defined on $\mathbb{R}_4$. This is done, following a strategy already exploited in [98] and [102], by direct evaluation of the Feynman diagrams that appear in the difference between the $\mathcal{N}=2$ and $\mathcal{N}=4$ theories. At finite N, this difference is computed up to two loops in perturbation theory and for operators of order $n \leq 4$. All the results match perfectly the corresponding matrix model computations. At large N, a special class of diagrams containing a particular two-loop structure is identified. These diagrams, which can appear at arbitrarily high orders in perturbation theory, are always proportional to $\zeta(3)$. Analogously to rainbow diagrams in the $\mathcal{N}=4$ theory, their complete resummation can be performed and can be matched with the $\zeta(3)$-proportional term obtained in the large N limit of the matrix model, yielding another direct check of the localization results.

Appendix A

Publication I: More on the new large D limit of matrix models

Annals of Physics 393 (2018) 308–326

Contents lists available at ScienceDirect

Annals of Physics

journal homepage: www.elsevier.com/locate/aop

More on the new large D limit of matrix models

Tatsuo Azeyanagi [a], Frank Ferrari [a,b], Paolo Gregori [a,c], Lætitia Leduc [a], Guillaume Valette [a,*]

[a] *Service de Physique Théorique et Mathématique, Université Libre de Bruxelles (ULB) and International Solvay Institutes, Campus de la Plaine, CP 231, B-1050 Bruxelles, Belgique*

[b] *Fields, Gravity and Strings, Center for the Theoretical Physics of the Universe, Institute for Basic Sciences, Daejeon, 34047, South Korea*

[c] *Università di Torino, Dipartimento di Fisica and I. N. F. N. - sezione di Torino, Via P. Giuria 1, I-10125 Torino, Italy*

ARTICLE INFO

Article history:
Received 17 January 2018
Accepted 4 April 2018
Available online 21 April 2018

Keywords:
Matrix models
Large N field theories
SYK-like models

ABSTRACT

In this paper, we extend the recent analysis of the new large D limit of matrix models to the cases where the action contains arbitrary multi-trace interaction terms as well as to arbitrary correlation functions. We discuss both the cases of complex and Hermitian matrices, with $\mathrm{U}(N)^2 \times \mathrm{O}(D)$ and $\mathrm{U}(N) \times \mathrm{O}(D)$ symmetries respectively. In the latter case, the new large D limit is consistent for planar diagrams; at higher genera, it crucially requires the tracelessness condition. For similar reasons, the large N limit of tensor models with reduced symmetries is typically inconsistent already at leading order without the tracelessness condition. We also further discuss some interesting properties of purely bosonic models pointed out recently and explain that the standard argument predicting a non-trivial IR behavior in fermionic models à la SYK does not work for bosonic models. Finally, we explain that the new large D scaling is consistent with linearly realized supersymmetry.

1. Introduction and summary

In a series of recent developments, interesting toy models for quantum black holes have been built and studied. The first class of models is based on large N fermionic systems with quenched disorder

* Corresponding author.
E-mail addresses: tatsuo.azeyanagi@ulb.ac.be (T. Azeyanagi), frank.ferrari@ulb.ac.be (F. Ferrari), paolo.gregori@ulb.ac.be (P. Gregori), laetitia.leduc@ulb.ac.be (L. Leduc), guillaume.valette@ulb.ac.be (G. Valette).

https://doi.org/10.1016/j.aop.2018.04.010
0003-4916/

and was proposed by Kitaev [1], building on previous studies in the condensed matter literature by Sachdev, Ye and others [2]. The second class of models is based on large N tensor theories and were first proposed by Witten in [3], building on the tensor model technology developed by Gurau and collaborators [4]. There is a rapidly growing literature on this subject, see e.g. [5–7]. These models are able to capture very non-trivial properties of black holes, including the quasi-normal behavior and chaos [8]. The advantage of the tensor models over models with quenched disorder is that they are genuine quantum theories at finite N; in particular, there is no need to limit the investigations to self-averaging quantities.

Both models with quenched disorder and tensors remain, however, rather exotic. String theory, via the open/closed string duality, singles out unambiguously matrix models in the 't Hooft's large N limit as being the favored candidates to describe quantum black holes. Matrix models are ubiquitous in string theory simply because the two indices of the matrices are the Chan-Paton factors associated with the two end points of open strings. It is very difficult to find a similar interpretation for tensors of rank three or higher.

The models originating from D-brane constructions always involve several bosonic matrices X_μ, $1 \leq \mu \leq D$, which describe motion transverse to the brane worldvolume. The index μ naturally transforms in the fundamental representation of $\mathrm{O}(D)$, which is the rotation group in the directions orthogonal to the branes. The full symmetry is usually $\mathrm{U}(N) \times \mathrm{O}(D)$, the $\mathrm{U}(N)$ part being gauged. These models must be studied in the planar $N \to \infty$ limit and superficially seem to be much more difficult to solve than models with quenched disorder or tensors.

Recently, it was shown in [9] that the above-mentioned large N, $\mathrm{O}(D)$-invariant matrix models have a new large D limit which is both analytically tractable and captures the essential physics associated with the sum over planar diagrams. The limit is "new" in the sense that it does not coincide with the well-known large D limit of $\mathrm{O}(D)$-invariant vector models because, crucially, the large D scaling of some coupling constants is enhanced.[1] This implies that many more Feynman diagrams contribute at large D than what one would find in a vector model and the result yields the expected continuous spectrum of states and chaotic behavior. As explained in [9], the new large D limit could also be related to the large space–time dimension limit of general relativity studied in [11].

The consistency of the new large D limit is ensured by remarkable and unexpected constraints the genus of a Feynman diagram puts on the highest possible power of D the diagram can be proportional to. The technology involved to prove some of these results is directly imported from the tensor model literature [12], which may not be surprising since our matrices are objects with three indices $X^a_{\mu b}$. However, there are important differences, both conceptual and technical, with the tensor models. The fact that the matrix indices a, b on the one hand and μ on the other hand transform with respect to different groups is conceptually fundamental, since the group associated with the matrix indices must always be gauged in string theory. Moreover, the large D expansion does not coincide with the large N expansion of tensor models, because it is made at fixed genus. In particular, the large N and large D limits do not commute, the large N limit must always be taken first.

The purpose of the present note is to complement the analysis of [9], both at the technical level and on the possible applications of the models. First, we generalize the discussion to arbitrary multi-trace interaction terms and to arbitrary multiply-connected interaction bubbles.[2] Multi-trace terms have been shown to be important in holographic contexts [13], but the analogue of this useful generalization does not seem to have been studied before in the context of tensor models. The results we obtain also play a role in the new large N and large D limits for general matrix–tensor models studied in [14].[3] We also discuss the general structure of the large N and large D expansions of arbitrary correlation functions. We emphasize the special features of models with reduced symmetry $\mathrm{U}(N) \times \mathrm{O}(D)$ instead of $\mathrm{U}(N)^2 \times \mathrm{O}(D)$. The large D limit remains well-defined for planar diagrams. However, without any further constraint on the matrices, it is inconsistent at higher genera; similarly, models involving symmetrized tensors, proposed recently in the literature [15,16], do not have a

[1] For the use of the standard large D limit with no enhancement in the context of matrix models, see for example [10].

[2] See below for definitions.

[3] The results of the present note relevant for [14] were obtained before the development of the general theory presented in [14].

consistent large N limit. Interestingly, when the tracelessness condition is added on the matrices and/or the tensors, the basic obstructions to the existence of the limits are waived. Finally, we emphasize that our results apply to a very wide and interesting class of matrix theories in space–time dimensions $0 \leq d \leq 3$. In particular, the new large D scaling of coupling constants is consistent with ordinary linearly realized supersymmetry. We also explain some crucial differences between the well-studied fermionic models à la SYK and bosonic models, giving more details on some properties first pointed out in [17].

2. Definition of the models

Our models are O(D)-invariant matrix theories. The basic variables are complex or Hermitian matrices X_μ transforming in the fundamental representation of O(D). When we deal explicitly with complex matrices, we always assume that the models are also invariant under a $\mathrm{U}(N)_{\mathrm{L}} \times \mathrm{U}(N)_{\mathrm{R}}$ symmetry acting as $X_\mu \mapsto U_{\mathrm{L}} X_\mu U_{\mathrm{R}}^{-1}$. In the purely Hermitian case, this symmetry is reduced down to a single U(N) factor and the matrices transform in the adjoint representation. The matrices X_μ may carry additional "flavor" labels, may be bosonic or fermionic and may live in various number of space–time dimensions. This additional information is irrelevant for our purposes.

For many applications, it is important to gauge the U(N) symmetries of the models, whereas the O(D) symmetry is ungauged. The explicit gauging can be straightforwardly performed and does not change our discussion in any non-trivial way, so we shall not mention it any further in the following. Note that, in the leading large N and large D approximations, the gauging is altogether irrelevant.

Our results can be straightforwardly generalized to other types of symmetries and matrix ensembles. For example, a special case of our analysis corresponds to models invariant under U(D) instead of O(D); similar methods can be applied to models of real matrices with orthogonal or symplectic gauge symmetries and O(D) vector symmetry, etc. A completely general formalism is described in [14].

The Lagrangian of the models are of the form

$$L = ND\Big(\text{Kinetic Term} - \sum_a N^{1-t(\mathcal{B}_a)} \tau_a I_{\mathcal{B}_a}(X)\Big)\,. \tag{2.1}$$

The kinetic term is $\mathrm{tr}\, X_\mu \mathscr{D} X_\mu^\dagger$ for some wave operator $\mathscr{D}$ that does not act on the U(N) or O(D) indices. The $I_{\mathcal{B}_a}(X)$ are O(D) invariant $t(\mathcal{B}_a)$-trace interaction terms, labeled by $\mathcal{B}_a$, with associated 't Hooft's coupling constants τ_a. They can be written as

$$I_{\mathcal{B}_a}(X) = \prod_{i=1}^{t(\mathcal{B}_a)} \mathrm{tr}\big(X_{\mu_{1,i}} X^\dagger_{\mu_{2,i}} \cdots X_{\mu_{2r_i-1,i}} X^\dagger_{\mu_{2r_i,i}}\big)\,, \tag{2.2}$$

where the $O(D)$ indices are contracted pairwise and summed over. In particular, the degree of an interaction vertex, which is the number of matrices X and $X^\dagger$ entering in (2.2), is always even. Note that the models studied in [9] correspond to single-trace interactions $t(\mathcal{B}_a) = 1$.

3. Vertices and graphs

As in [9], we use two graphical representations for each interaction vertex $\mathcal{B}_a$: the standard stranded fat graph representation and the three-colored bubble graph representation. We shall often denote by $\mathcal{B}_a$ either the interaction term itself or the associated three-colored graph. Our detailed conventions are exactly the same as in [9] and we shall not repeat them here. Simply note that the colors (green, red, black) are also denoted by (1, 2, 3). To any interaction vertex $\mathcal{B}_a$, we assign: the number of connected components $c(\mathcal{B}_a)$ of the bubble; the number of traces $t(\mathcal{B}_a)$, which is also the number of (12)-faces of the associated bubble, $t(\mathcal{B}_a) = F_{12}(\mathcal{B}_a)$ and the genus $g(\mathcal{B}_a)$ of the interaction, given by Euler's formula in terms of the total number of faces $F(\mathcal{B}_a) = F_{12}(\mathcal{B}_a) + F_{13}(\mathcal{B}_a) + F_{23}(\mathcal{B}_a)$ and vertices $V(\mathcal{B}_a)$ of the bubble, $2c(\mathcal{B}_a) - 2g(\mathcal{B}_a) = F(\mathcal{B}_a) - \frac{1}{2}V(\mathcal{B}_a)$. A typical interaction term is depicted in Fig. 1. When an interaction vertex has several connected components, as it is the case in the figure, we insert it in a dashed rectangular box to emphasize the fact that it represents a unique Feynman diagram vertex.

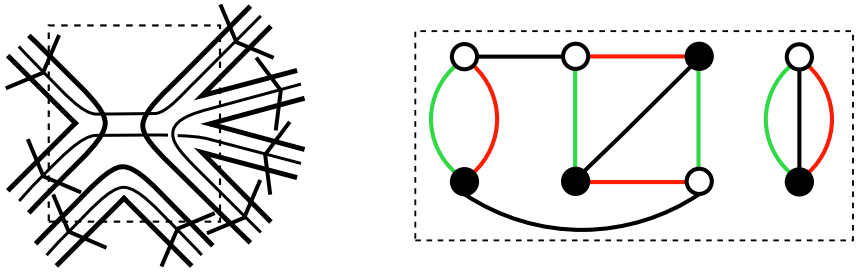

Fig. 1. Fat graph and colored graph for the interaction vertex $tr\, X_\mu X_\nu^\dagger\, tr\, X_\mu X_\rho^\dagger X_\nu X_\rho^\dagger\, tr\, X_\sigma X_\sigma^\dagger$, with $c = 2$, $t = 3$ and $g = 1/2$. (For interpretation of the references to color in this figure legend, the reader is referred to the web version of this article.)

Similar to the interaction vertices, the Feynman diagrams can also be represented either by a stranded graph or by a four-colored graph. The colored Feynman graphs are obtained by representing the propagators as lines of a new color, say violet (or 0). In the case of complex matrix models, the fat graph propagators are oriented, say from $X^\dagger$ to X and this implies that the violet lines of the colored graph respect the bipartite structure of the graph (i.e. they join vertices of different types). In the case of Hermitian matrices, the fat graph propagators are no longer oriented and thus in general, the violet lines of the colored graph do not respect the bipartite structure. However, as explained in [9], if the fat graph is planar, then it is always possible to assume that they do respect the bipartite structure.[4] This is a crucial property that allows one to extend the results obtained in the complex case to the planar Hermitian case.

4. The large *N* and large *D* limits

To define the large N and large D limits of our models, we introduce new couplings λ_a, related to the couplings τ_a appearing in the Lagrangian (2.1) by

$$\tau_a = D^{t(\mathcal{B}_a)-c(\mathcal{B}_a)+g(\mathcal{B}_a)}\lambda_a\,, \tag{4.1}$$

and we decide to keep λ_a fixed. The large N limit defined this way is the usual 't Hooft's limit, suitably generalized to the case of multi-trace interactions; note in particular that both τ_a and λ_a are fixed at large N but finite D. The large D limit has the enhancement factor $D^{g(\mathcal{B}_a)}$ with respect to the standard vector model large D scaling, as in [9], together with a new additional factor $D^{t(\mathcal{B}_a)-c(\mathcal{B}_a)}$ that takes into account both the multi-trace structure and the fact that the interaction bubbles may be disconnected. In this section, we show that the free energy has well-defined large N and large D limits with the scalings (4.1). This result extends to correlation functions, whose study is postponed to Section 5.

Let us consider an arbitrary vacuum Feynman diagram. We denote by p, v, f and φ the number of propagators, vertices, U(N) and O(D) faces, respectively. With the Lagrangian (2.1) and the scaling (4.1), the amplitude of the diagram is proportional to

$$N^{-p+2v-\sum_a t(\mathcal{B}_a)+f} D^{-p+v+\sum_a (t(\mathcal{B}_a)-c(\mathcal{B}_a)+g(\mathcal{B}_a))+\varphi} = N^{2-h} D^{1+\frac{h}{2}-\frac{\ell}{2}}\,, \tag{4.2}$$

where we introduced the parameters h and ℓ defined by

$$h = 2 + p - 2v + \sum_a t(\mathcal{B}_a) - f\,, \tag{4.3}$$

$$\frac{\ell}{2} = 2 + \frac{3}{2}p - 2v - \frac{1}{2}\sum_a t(\mathcal{B}_a) + \sum_a c(\mathcal{B}_a) - \sum_a g(\mathcal{B}_a) - \frac{1}{2}f - \varphi\,. \tag{4.4}$$

[4] The argument in [9] applies without change to the more general case of multi-trace interactions considered here and thus will not be repeated.

4.1. Counting the power of N

To study the power of N of a given Feynman diagram $\mathcal{B}$, we consider the matrix model fat graph obtained by removing the O(D) lines in the stranded representation. In the colored representation, it amounts to studying the three-bubble $\mathcal{B}^{(3)}$ obtained by removing the edges of color 3. Since we deal with multi-trace interactions, the resulting fat graph may be disconnected. Indeed, each multi-trace vertex effectively leads to $t(\mathcal{B}_a)$ single-trace vertices in the fat graph. We denote by $\tilde{v}$ the total number of effective single-trace vertices so that $\tilde{v} = \sum_a t(\mathcal{B}_a)$. Besides, the number of connected components of the fat graph is the same as the number of connected components $B^{(3)}$ of the three-bubble $\mathcal{B}^{(3)}$. The genus g of the fat graph[5] is then given by the usual Euler's formula

$$2B^{(3)} - 2g = -p + f + \tilde{v} = -p + f + \sum_a t(\mathcal{B}_a)\,. \tag{4.5}$$

We can obtain a similar relation by studying the corresponding three-bubble $\mathcal{B}^{(3)}$, whose genus is given by the relation

$$\begin{aligned} 2B^{(3)} - 2g(\mathcal{B}^{(3)}) &= -\frac{1}{2}V(\mathcal{B}^{(3)}) + F(\mathcal{B}^{(3)}) \\ &= -\frac{1}{2}V(\mathcal{B}) + F_{01}(\mathcal{B}) + F_{02}(\mathcal{B}) + F_{12}(\mathcal{B})\,. \end{aligned} \tag{4.6}$$

By using the following identities that connect the quantities characterizing $\mathcal{B}$ in the stranded and colored representations,

$$2p = V(\mathcal{B})\,, \quad f = F_{01}(\mathcal{B}) + F_{02}(\mathcal{B})\,, \quad \sum_a t(\mathcal{B}_a) = F_{12}(\mathcal{B})\,, \tag{4.7}$$

it is straightforward to check that the genera of the fat graph and the colored graph coincide,

$$g = g(\mathcal{B}^{(3)})\,. \tag{4.8}$$

Using the above formulas, we can rewrite h in (4.3) as

$$\frac{h}{2} = g + \sum_a \big(t(\mathcal{B}_a) - 1\big) - B^{(3)} + 1\,, \tag{4.9}$$

which importantly shows that h is non-negative since it is given by the sum of two non-negative terms,

$$g \geq 0\,, \quad 1 + \sum_a \big(t(\mathcal{B}_a) - 1\big) - B^{(3)} \geq 0\,. \tag{4.10}$$

The second inequality comes from the fact that each $t(\mathcal{B}_a)$-trace interaction vertex can increase the number of connected components of the fat graph by $t(\mathcal{B}_a)-1$ at most. The non-negativity of h ensures that the large N limit à la 't Hooft of models with multi-trace interactions is well-defined. For single-trace interactions, $t(\mathcal{B}_a) = 1$ and $B^{(3)} = 1$ so that $h = 2g$ as usual.

4.2. Counting the power of D

By generalizing the proof for the single-trace models found in [9], we want to express ℓ given in (4.4) as the sum of non-negative terms. The Euler's formula (4.6) for the three-bubble $\mathcal{B}^{(3)}$ generalizes straightforwardly to the three other three-bubbles $\mathcal{B}^{(0)}$, $\mathcal{B}^{(1)}$ and $\mathcal{B}^{(2)}$. We write them in a unified way as

$$2B^{(i)} - 2g(\mathcal{B}^{(i)}) = -\frac{1}{2}V(\mathcal{B}) + \sum_{\substack{j<k \\ j,k\neq i}} F_{jk}(\mathcal{B})\,, \tag{4.11}$$

[5] We always implicitly define the genus of a multiply-connected graph as the sum of the genus of each connected component.

where $i = \{0, 1, 2, 3\}$ and $B^{(i)}$ is the number of connected components of the three-bubble $\mathcal{B}^{(i)}$. By summing these equations for $i = 0, 1, 2$ and using the following identities that complement the ones in (4.7),

$$\varphi = F_{03}(\mathcal{B}) \,, \quad \sum_a c(\mathcal{B}_a) = B^{(0)} \,, \quad \sum_a g(\mathcal{B}_a) = g(\mathcal{B}^{(0)}) \,, \tag{4.12}$$

one obtains the following relation

$$\begin{aligned} &g(\mathcal{B}^{(1)}) + g(\mathcal{B}^{(2)}) + \left(B^{(01)} - B^{(1)} - B^{(0)} + B\right) + \left(B^{(02)} - B^{(2)} - B^{(0)} + B\right) \\ &\quad = 2B + \frac{3}{2}p - \frac{1}{2}\sum_a t(\mathcal{B}_a) - \sum_a c(\mathcal{B}_a) - \sum_a g(\mathcal{B}_a) - \frac{1}{2}f - \varphi \,, \end{aligned} \tag{4.13}$$

where B in the number of effective connected components of $\mathcal{B}$ and $B^{(01)} = F_{23}(\mathcal{B})$, $B^{(02)} = F_{13}(\mathcal{B})$. Comparing (4.13) with (4.4), we get

$$\begin{aligned} \frac{\ell}{2} &= g(\mathcal{B}^{(1)}) + g(\mathcal{B}^{(2)}) + \left(B^{(01)} - B^{(1)} - B^{(0)} + B\right) + \left(B^{(02)} - B^{(2)} - B^{(0)} + B\right) \\ &\quad + 2\left(1 + \sum_a \left(c(\mathcal{B}_a) - 1\right) - B\right) . \end{aligned} \tag{4.14}$$

The first two terms on the right hand side are manifestly non-negative. The third and fourth terms are also non-negative using the connectivity inequality

$$B^{(ij)} - B^{(i)} - B^{(j)} + B \geq 0 \,, \tag{4.15}$$

which is proven in [9] for the case $B = 1$, the case $B > 0$ being a straightforward generalization (see also the discussion in [14]). Finally, the last term is also non-negative,

$$1 + \sum_a \left(c(\mathcal{B}_a) - 1\right) - B \geq 0 \,, \tag{4.16}$$

because each interaction vertex with $c(\mathcal{B}_a)$ connected components increases the number of effective connected components of $\mathcal{B}$ by $c(\mathcal{B}_a) - 1$ at most (Eq. (4.16) can also be viewed as a consequence of a connectivity inequality of the form (4.15), see [14]).

In conclusion, we have shown that ℓ is a non-negative integer. This proves that the large D expansion is well-defined at any fixed power of N. In the case of single-trace interactions only, we have that $c(\mathcal{B}_a) = 1$ and $B = 1$ so that the expression (4.14) for ℓ matches the one found in [9].

4.3. Form of the expansions and leading order graphs

The large N expansion of the free energy reads

$$F = \sum_{h \in \mathbb{N}} F_h N^{2-h} \,, \tag{4.17}$$

where the F_h are N-independent coefficients. Each F_h is itself expanded at large D in powers of $1/\sqrt{D}$ as

$$F_h = \sum_{\ell \in \mathbb{N}} F_{h,\ell} D^{1+\frac{h}{2}-\frac{\ell}{2}} \,, \tag{4.18}$$

with D-independent coefficients $F_{h,\ell}$. In particular, we see that the highest possible power of D for diagrams of given h is bounded above by $1 + h/2$. It is this crucial property that makes the limit exist. However, if diagrams of arbitrary h are considered, there is no such upper bound. This implies that the limit $N \to \infty$ must always be taken first and then the $D \to \infty$ limit next, at each order in the $1/N$ expansion. The non-commutativity of the two limits is a central property of the new large D limit introduced in [9].

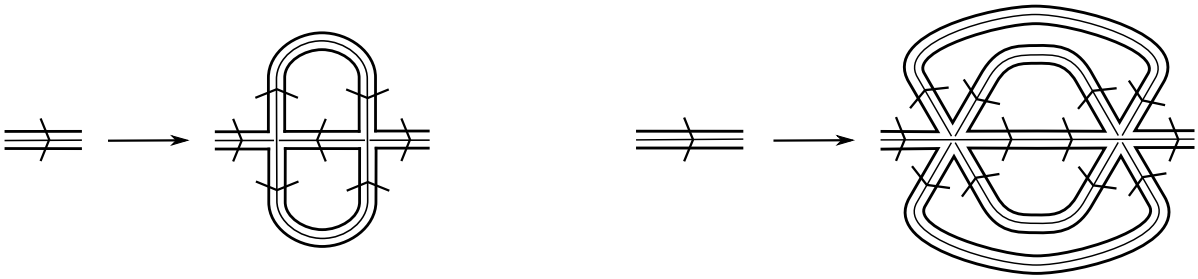

Fig. 2. Melonic moves for the $tr\, X_\mu X_\nu^\dagger X_\mu X_\nu^\dagger$ and $tr\, X_\mu X_\nu^\dagger X_\rho X_\mu^\dagger X_\nu X_\rho^\dagger$ interactions.

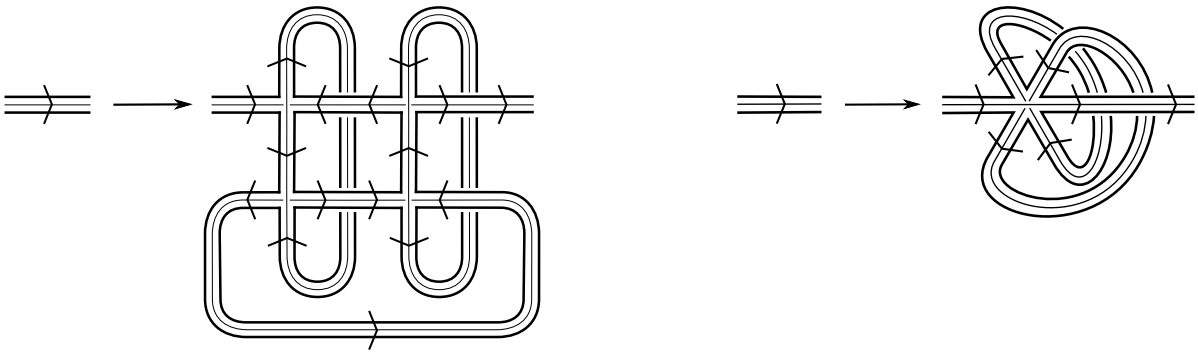

Fig. 3. Moves increasing the genus by one unit at fixed ℓ for the $tr\, X_\mu X_\nu^\dagger X_\mu X_\nu^\dagger$ and $tr\, X_\mu X_\nu^\dagger X_\rho X_\mu^\dagger X_\nu X_\rho^\dagger$ interactions.

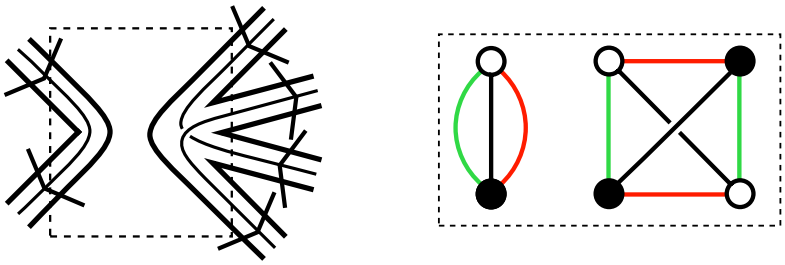

Fig. 4. Stranded graph and colored graph for the interaction vertex $tr\, X_\rho X_\rho^\dagger\ tr\, X_\mu X_\nu^\dagger X_\mu X_\nu^\dagger$ discussed in the main text, with $c = 2$, $t = 2$ and $g = 1/2$. (For interpretation of the references to color in this figure legend, the reader is referred to the web version of this article.)

Leading order graphs, called generalized melons in [14], must have $h = 0$ and $\ell = 0$. These conditions require in particular the planarity of the three-colored graphs $\mathcal{B}^{(1)}$, $\mathcal{B}^{(2)}$ and $\mathcal{B}^{(3)}$. Typically, they can be built by applying an arbitrary number of so-called melonic moves, which amounts to replacing internal lines by a more complicated structure, starting from the one-loop ring vacuum graph. Examples of melonic moves for the interactions $\mathrm{tr}\, X_\mu X_\nu^\dagger X_\mu X_\nu^\dagger$ and $\mathrm{tr}\, X_\mu X_\nu^\dagger X_\rho X_\mu^\dagger X_\nu X_\rho^\dagger$ are depicted on Fig. 2. We let the reader check explicitly that these moves do not change the powers of N and D (i.e. the values of h and ℓ).

Leading order graphs at fixed genus $g > 0$, on the other hand, are planar only with respect to the colors 0, 1, 3 and 0, 2, 3. For single-trace interactions they are proportional to D^{1+g}. Families of leading graphs at fixed genus can be obtained, for example, using the moves depicted on Fig. 3 an arbitrary number of times. It is easy to check that these moves increase the genus by one unit but leave ℓ unchanged. One can of course also use the moves of Fig. 2 to generate more leading graphs at fixed g.

To illustrate the case of a multi-trace interaction, consider the interaction vertex depicted in Fig. 4. The leading order graphs $h = \ell = 0$ must be maximally disconnected and each connected component must be a leading order graph for the model involving the effective single-trace interactions $\mathrm{tr}\, X_\rho X_\rho^\dagger$

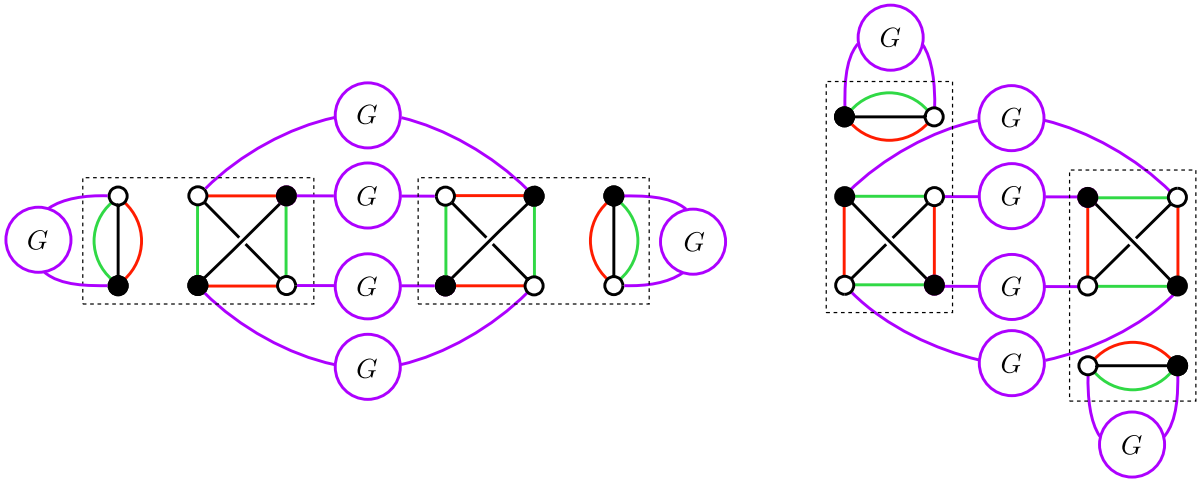

Fig. 5. Structure of the leading order vacuum graphs for the multi-trace model with interaction vertex $tr\, X_\rho X_\rho^\dagger\, tr\, X_\mu X_\nu^\dagger X_\mu X_\nu^\dagger$. G is the leading two-point function.

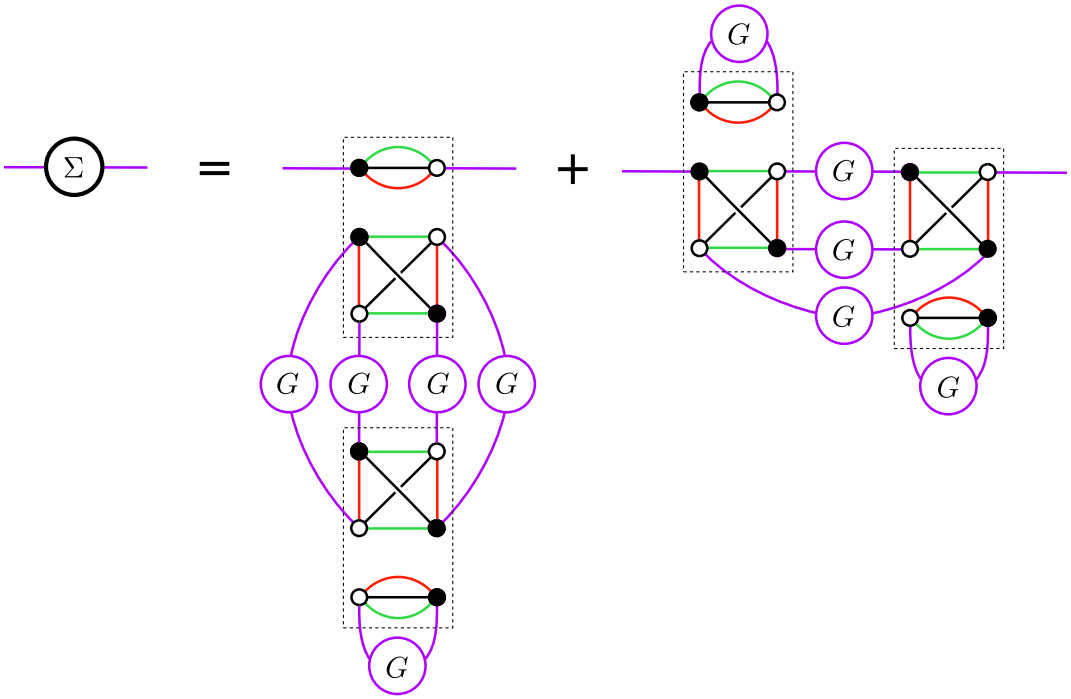

Fig. 6. Diagrammatic representation of the Schwinger–Dyson equation (4.19).

and $\mathrm{tr}\, X_\mu X_\nu^\dagger X_\mu X_\nu^\dagger$. We can then straightforwardly apply the results of [12]. The leading vacuum graphs have the structure depicted in Fig. 5, the two-point function being determined by the Schwinger–Dyson equation with the self-energy given by Fig. 6 or, equivalently, in terms of the equation (in the quantum mechanical case)

$$\begin{aligned}\Sigma(t-t') = (-1)^\sigma 2\lambda^2 \delta(t-t') \int dt_1\, G^2(t_1) G^2(-t_1)\, G(0) \\ + (-1)^\sigma 4\lambda^2\, G^2(t-t') G(-t+t')\, G^2(0)\,. \end{aligned} \tag{4.19}$$

In this equation, Σ is the self-energy and $\sigma = 0$ or 1 depending on whether we are dealing with complex fermions or bosons.

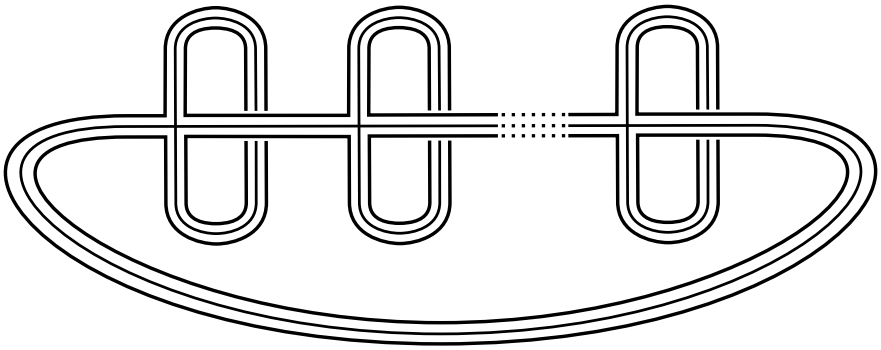

Fig. 7. Example of graphs at genus one in the Hermitian models (or real symmetric models) that are proportional to an arbitrarily high power of D.

4.4. On cases with reduced symmetry

Up to now, we have focused on models with $\mathrm{U}(N)^2 \times \mathrm{O}(D)$ symmetry. The fact that a symmetry group is associated with each individual index is crucial in the standard tensor model technology, for which $D = N$. An interesting question is whether non-trivial and consistent large N and large D limits exist in models with reduced symmetry.

The first rigorous argument showing that this is the case was given in [9], where the example of Hermitian matrices was studied. For Hermitian matrices, the symmetry group is reduced from $\mathrm{U}(N)^2 \times \mathrm{O}(D)$ down to $\mathrm{U}(N) \times \mathrm{O}(D)$ and all the usual tools based on colored graphs superficially seem to break down. But the argument in [9], which generalizes straightforwardly to the multi-trace interactions considered in the present paper, showed that the large D limit is still well-defined for the sum over *planar* diagrams. The same argument would also work for real symmetric or antisymmetric matrices, again at the planar level.

However, it is not difficult to prove that the large D limit for general Hermitian matrices does not exist for diagrams of genera $g \geq 1$ (which also invalidates the tensor large $N = D$ limit). Indeed, for any $g \geq 1$, one can construct diagrams which are proportional to an arbitrarily high power of D. For example, consider the genus one graphs depicted in Fig. 7, with interaction vertices $\mathrm{tr}\, X_\mu X_\nu X_\mu X_\nu$. Note that these graphs are allowed in the Hermitian case but are forbidden in the complex case, because the self-contractions of the vertices would violate the orientation of the propagators. It is straightforward to check that the graph containing q interaction vertices is proportional to $D^{1+q/2}$. There is thus no upper bound for the power of D. The graphs of Fig. 7 can be straightforwardly generalized by using the melonic move depicted on the left of Fig. 2. In particular, we can build in this way a large class of graphs with no self-contractions on the vertices[6] that make the large D limit inconsistent. It is also very easy to build similar graphs at any genus, by inserting the basic structure of the genus one graph in a larger graph.

Another closely related example is the $\mathrm{O}(N)^3$-symmetric Carrozza–Tanasa model, or the similar $\mathrm{O}(N)^2 \times \mathrm{O}(D)$-symmetric model of real matrices with an interaction term $\mathrm{tr}\, X_\mu X_\nu^T X_\mu X_\nu^T$. In the fat graph representation, the XX and XX^T propagators are twisted and untwisted ribbons respectively. The graphs of Fig. 7 are thus not allowed. There are similar allowed graphs, represented in the left inset of Fig. 8, but these are never greater than N^2 and are thus harmless in the large $N = D$ limit. On the other hand, if one breaks the $\mathrm{O}(N)^2 \times \mathrm{O}(D)$ symmetry down to $\mathrm{O}(N) \times \mathrm{O}(D)$ by imposing that the matrices X_μ are symmetric, or down to $\mathrm{O}(N)$ by imposing the complete symmetry between the three indices in the tensor case $N = D$, as was suggested in [15], then the XX and XX^T propagators can both be either twisted or untwisted. The graphs of Fig. 7 are then allowed, together with the more general graphs depicted on the right inset of Fig. 8. These are proportional to $N^{1+q/2}$ for any q, showing that the large N limit of such models does not exist.

---

[6] If only graphs with self-contractions were harmful, it would be easy to get rid of them in some cases, for example by using a normal-ordered interaction at zero temperature, or dimensional regularization in massless models in space–time dimension $d \geq 2$.

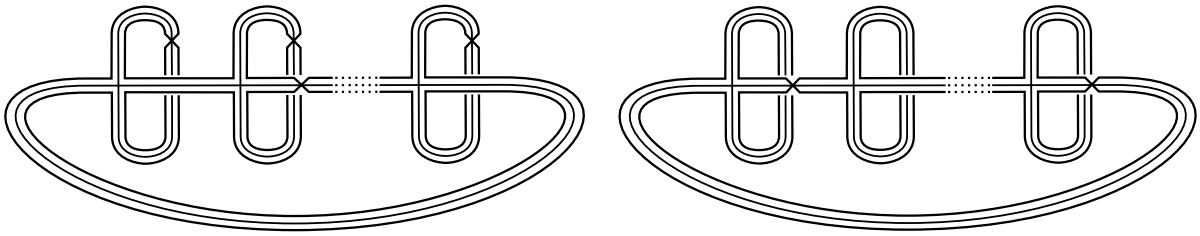

Fig. 8. Graphs for the real rank three tensor models studied in [15]. Left inset: graphs allowed in the $O(N)^3$ Carrozza–Tanasa model, which are at most proportional to N^2. The graph with q interaction vertices must have q mod 2 twisted "horizontal" ribbons, whereas all the self-contractions come with twisted ribbons. Right inset: similar graphs allowed when the symmetry is broken down to $O(N)^2$ or $O(N)$ by imposing a symmetry constraint on the tensor; these graphs are proportional to an arbitrarily high power of N and the large N limit does not exist for these models.

A common feature of all the "bad" graphs mentioned above, including their most general versions obtained by applying the melonic moves of Fig. 2 on the internal edges an arbitrary number of times, is that they all contain so-called *singular* edges. A singular edge is defined [18] to be an edge in the graph which is traversed twice by the same face. In other words, in the ribbon representation, the two borders of the ribbon associated with a singular edge belong to the same face. A simple and elegant way to eliminate all such graphs is to impose a tracelessness condition on the matrices, since singular edges are automatically associated with the contraction of two indices of the same matrix (or tensor). This yields the natural conjecture that *traceless* symmetric or Hermitian models could have well-defined large D limits *at all genera.* Support for this conjecture is given in the recent work [16], which constructs and checks numerically a large class of graphs in the symmetrized Carrozza–Tanasa model.[7] It is unknown whether this conjecture will turn out to be true in full generality, for all types of interaction terms, which would suggest that a general conceptual proof, in the spirit of [9,14], could be devised, or whether it will work only for some very specific models. For example, a detailed discussion of an interesting bipartite model can be found in [19]. This model is very special because the bipartite structure actually implies that the tracelessness condition is not needed.

5. On correlation functions

5.1. General remarks

Based on the results derived in Section 4 for the free energy, we can analyze some properties of the large N and large D expansions of correlation functions in our models.

Let us consider correlation functions of general multi-trace operators. These operators may be included in the Lagrangian (2.1) as interaction terms $I_{\mathcal{B}_a}$. They can be obtained in the usual way by taking the derivative of the free energy with respect to the associated coupling constant λ_a, taking into account the scalings in the Lagrangian (2.1) and in (4.1),

$$N^{2-t(\mathcal{B}_a)}D^{1+t(\mathcal{B}_a)-c(\mathcal{B}_a)+g(\mathcal{B}_a)}\langle I_{\mathcal{B}_a}\rangle = \frac{\partial F}{\partial \lambda_a}\,. \tag{5.1}$$

The expansions (4.17) and (4.18) for the free energy thus yield

$$\langle I_{\mathcal{B}_a}\rangle \sim \frac{1}{N^{2-t(\mathcal{B}_a)}D^{1+t(\mathcal{B}_a)-c(\mathcal{B}_a)+g(\mathcal{B}_a)}} \sum_{h\in\mathbb{N},\,\ell\in\mathbb{N}} N^{2-h}D^{1+\frac{h}{2}-\frac{\ell}{2}}\,. \tag{5.2}$$

Let us consider a multiply-connected interaction term $I_{\mathcal{B}} = I_{\mathcal{B}_1}I_{\mathcal{B}_2}\ldots I_{\mathcal{B}_c}$, with $c(\mathcal{B}) = c > 1$, $t(\mathcal{B}_i) = t_i$, $c(\mathcal{B}_i) = 1$ and $g(\mathcal{B}_i) = g_i$ for $i = 1,\ldots,c$. By definition, we have $t(\mathcal{B}) = \sum_i t_i$ and

[7] We would like to thank Igor Klebanov for a fruitful exchange about this point. The harmful graphs of Figs. 7 and 8 that we communicated to the authors of [16] made them realize that the consistency of the large N limit required, and might be achieved by, the tracelessness condition.

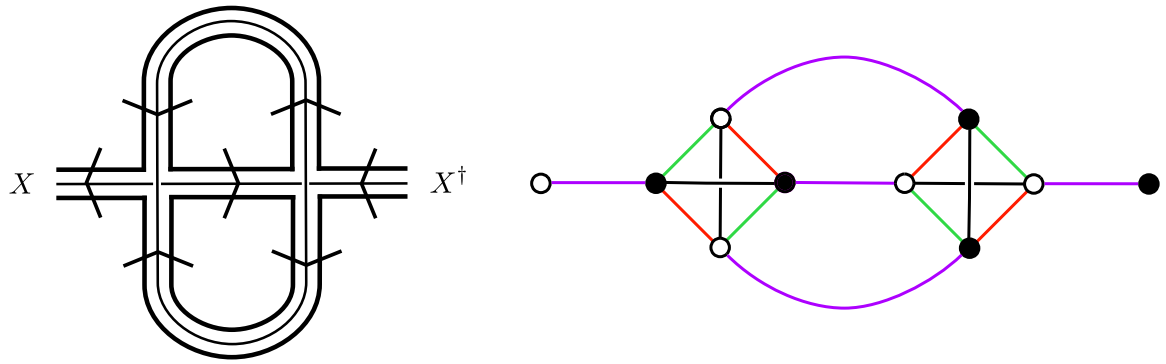

Fig. 9. Example of a Feynman graph with two external legs, in the stranded and colored representations. (For interpretation of the references to color in this figure legend, the reader is referred to the web version of this article.)

$g(\mathcal{B}) = \sum_i g_i$. The expectation value $\langle I_{\mathcal{B}} \rangle$ is given by (5.2). Moreover,

$$N^{2c-t(\mathcal{B})} D^{t(\mathcal{B})+g(\mathcal{B})} \langle I_{\mathcal{B}_1} \rangle \langle I_{\mathcal{B}_2} \rangle \dots \langle I_{\mathcal{B}_c} \rangle = \frac{\partial F}{\partial \lambda_1} \frac{\partial F}{\partial \lambda_2} \cdots \frac{\partial F}{\partial \lambda_c} , \tag{5.3}$$

which is consistent with factorization at leading order,

$$\langle I_{\mathcal{B}} \rangle = \langle I_{\mathcal{B}_1} \rangle \langle I_{\mathcal{B}_2} \rangle \dots \langle I_{\mathcal{B}_c} \rangle \sim N^{t(\mathcal{B})} D^{c-t(\mathcal{B})-g(\mathcal{B})} . \tag{5.4}$$

On the other hand, the connected correlation function is given by

$$N^{2c-t(\mathcal{B})} D^{t(\mathcal{B})+g(\mathcal{B})} \langle I_{\mathcal{B}} \rangle_{\mathrm{c}} = \frac{\partial^c F}{\partial \lambda_1 \dots \partial \lambda_c} , \tag{5.5}$$

yielding at leading order

$$\langle I_{\mathcal{B}} \rangle_{\mathrm{c}} \sim N^{2-2c+t(\mathcal{B})} D^{1-t(\mathcal{B})-g(\mathcal{B})} . \tag{5.6}$$

Of course, the graphs contributing to $\langle I_{\mathcal{B}} \rangle_{\mathrm{c}}$ cannot be maximally disconnected and the connected expectation value is thus suppressed compared to $\langle I_{\mathcal{B}} \rangle$ at leading order.

5.2. Connected 2n-point correlation functions

In this section, we examine the large N and large D expansions of the connected $2n$-point correlation functions of the form

$$\left\langle (X_{\mu_1})^{\alpha_1}_{\beta_1} (X^\dagger_{\mu_2})^{\alpha_2}_{\beta_2} \dots (X_{\mu_{2n-1}})^{\alpha_{2n-1}}_{\beta_{2n-1}} (X^\dagger_{\mu_{2n}})^{\alpha_{2n}}_{\beta_{2n}} \right\rangle_{\mathrm{c}} . \tag{5.7}$$

The Feynman graphs that contribute to these correlation functions have $2n$ external legs. In the colored graph representation, the external legs correspond to "external" vertices of valency one, to which only a line of color 0 is attached. The external vertices are, as usual, unfilled or filled depending on whether they correspond to X or $X^\dagger$. An example is depicted on Fig. 9. We denote by $V_{\mathrm{ext}} = 2n$ the number of external vertices in the colored graph, by V_{int} the number of standard internal vertices and by $V = V_{\mathrm{ext}} + V_{\mathrm{int}}$ the total number of vertices.

The amplitude for a Feynman diagram with $2n$ external legs is obtained from the Lagrangian (2.1) and the scalings (4.1) and is proportional to

$$N^{-p+2v-\sum_a t(\mathcal{B}_a)+f} D^{-p+v+\sum_a (t(\mathcal{B}_a)-c(\mathcal{B}_a)+g(\mathcal{B}_a))+\varphi} = N^{2-2n-h'} D^{1-\frac{3}{2}n+\frac{h'}{2}-\frac{\ell'}{2}} , \tag{5.8}$$

where we have defined the parameters h' and ℓ' as

$$h' = 2 + p - 2v + \sum_a t(\mathcal{B}_a) - f - 2n , \tag{5.9}$$

$$\frac{\ell'}{2} = 2 + \frac{3}{2}p - 2v - \frac{1}{2}\sum_a t(\mathcal{B}_a) + \sum_a c(\mathcal{B}_a) - \sum_a g(\mathcal{B}_a) - \frac{1}{2}f - \varphi - \frac{5}{2}n\,. \tag{5.10}$$

These definitions are convenient because, as we shall prove, $h' \geq 0$ and $\ell' \geq 0$. The formulas (5.9) and (5.10) are of course very similar to (4.3) and (4.4), with additional contributions depending on n.

5.2.1. Counting the power of N

We follow the same strategy as in Section 4.1: we remove the O(D) lines in the stranded representation and we consider the resulting matrix model fat graph. The difference is that the fat graph is now dual to a surface with boundaries because of the external insertion points. The relevant Euler's formula is

$$2B^{(3)} - 2g - b = -p + \tilde{v} + 2n + f = -p + \sum_a t(\mathcal{B}_a) + 2n + f\,, \tag{5.11}$$

where g is the genus of the fat graph, b its number of boundaries and $\tilde{v} = \sum_a t(\mathcal{B}_a)$ its number of internal effective single-trace vertices. Note that using the relations (4.7), which are still valid here, together with

$$2E(\mathcal{B}^{(3)}) = 3V_{\text{int}}(\mathcal{B}) + V_{\text{ext}}(\mathcal{B}) = 3V_{\text{int}}(\mathcal{B}) + 2n\,, \tag{5.12}$$

where $E(\mathcal{B}^{(3)})$ is the number of edges of $\mathcal{B}^{(3)}$, a similar Euler's formula can be written for the colored graph,

$$\begin{aligned} 2B^{(3)} - 2g(\mathcal{B}^{(3)}) - b(\mathcal{B}^{(3)}) &= F(\mathcal{B}^{(3)}) - E(\mathcal{B}^{(3)}) + V(\mathcal{B}^{(3)}) \\ &= -\frac{1}{2}V_{\text{int}}(\mathcal{B}) + \frac{1}{2}V_{\text{ext}}(\mathcal{B}) + F_{01}(\mathcal{B}) + F_{02}(\mathcal{B}) + F_{12}(\mathcal{B}) \\ &= 2B^{(3)} - 2g - b\,. \end{aligned} \tag{5.13}$$

Finally, (5.9) together with (5.11) yields

$$\frac{h'}{2} = g + \frac{b}{2} + \sum_a \big(t(\mathcal{B}_a) - 1\big) - B^{(3)} + 1\,, \tag{5.14}$$

generalizing (4.9) and showing that $h' \geq 0$ in all cases, with actually $h' \geq 1$ as soon as $n \neq 0$ since then, $b \geq 1$. As a result, we get a well-defined large N expansion, the leading graphs with respect to N corresponding as usual to maximally disconnected planar graphs with a single boundary component.

5.2.2. Counting the power of D

Following Section 4.2, we consider $\mathcal{B}^{(1)}$ and $\mathcal{B}^{(2)}$, which are open three-colored graphs just like $\mathcal{B}^{(3)}$, so that the corresponding Euler's formulas read

$$2B^{(i)} - 2g(\mathcal{B}^{(i)}) - b(\mathcal{B}^{(i)}) = -\frac{1}{2}V_{\text{int}}(\mathcal{B}) + \frac{1}{2}V_{\text{ext}}(\mathcal{B}) + \sum_{\substack{j<k \\ j,k\neq i}} F_{jk}(\mathcal{B})\,. \tag{5.15}$$

On the other hand, the three-bubble $\mathcal{B}^{(0)}$ remains a closed colored graph, with a standard Euler's formula. Summing these three Euler's identities and using (4.12), we can rewrite ℓ' in (5.10) as

$$\begin{aligned} \frac{\ell'}{2} &= g(\mathcal{B}^{(1)}) + g(\mathcal{B}^{(2)}) + \frac{1}{2}\big(b(\mathcal{B}^{(1)}) + b(\mathcal{B}^{(2)})\big) + \big(B^{(01)} - B^{(1)} - B^{(0)} + B\big) \\ &\quad + \big(B^{(02)} - B^{(2)} - B^{(0)} + B\big) + 2\Big(1 + \sum_a \big(c(\mathcal{B}_a) - 1\big) - B\Big)\,. \end{aligned} \tag{5.16}$$

As soon as $n \neq 0$, $b(\mathcal{B}^{(i)}) \geq 1$ for $i = 1, 2$ and thus we get $\ell' \geq 2$.

The above results show that the connected $2n$-point correlation functions (5.7) have well-defined large N and large D expansions of the form

$$\sum_{h'\in\mathbb{N}_{\geq 1},\, \ell'\in\mathbb{N}_{\geq 2}} N^{2-2n-h'} D^{1-\frac{3}{2}n+\frac{h'}{2}-\frac{\ell'}{2}} \,. \tag{5.17}$$

The leading order contribution is proportional to $N^{1-2n}D^{\frac{1}{2}-\frac{3}{2}n}$, which corresponds to $h' = 1$ and $\ell' = 2$.

Let us finally note that the correlation functions of $\mathrm{U}(N)^2$ or $\mathrm{U}(N)^2 \times \mathrm{O}(D)$ invariant operators can be obtained from (5.7) by contracting the free indices. This amounts to sewing together the external legs of the Feynman graphs. We let the reader rederive Eq. (5.6) in this way, starting from (5.17).

6. Model building

The class of matrix–tensor models that can be built using the above ideas is very large and their strongly coupled physics is likely to display a wide variety of interesting new effects. On top of the SYK-like behavior [1], which is associated with a non-trivial IR limit and a macroscopic degeneracy of the ground state, it was recently discovered in [17] that many other phenomena can occur and that the phase diagrams of the models can have a rich structure. Clearly, only the surface of this subject has been scratched and many examples, in various dimensions, remain to be studied. The aim of the present section is to provide a brief overview, emphasizing a few models that we find particularly interesting. In particular, we provide more details on some of the results for bosonic models announced in [17]. We also explain that our new large D limit, with the scaling (4.1), is compatible with linearly realized supersymmetry. The detailed study of the physics and the phase diagrams of supersymmetric models in various dimensions is an outstanding research avenue for the future.

6.1. Unstable bosonic models

6.1.1. Simple models

The simplest purely bosonic and non-trivial quantum mechanical model one can study is based on the Lagrangian

$$L = ND\,\mathrm{tr}\Big(\frac{1}{2}\dot{X}_\mu\dot{X}_\mu - \frac{m^2}{2}X_\mu X_\mu - \frac{\lambda^3}{4}\sqrt{D}\,X_\mu X_\nu X_\mu X_\nu\Big)\,, \tag{6.1}$$

where the matrices X_μ are Hermitian. There are obvious generalizations is any number of space–time dimension $d \leq 4$ (for $d > 4$, the model is not renormalizable). This model is solvable because the leading order graphs can be fully classified following [9,12]. A very similar model, which has exactly the same physics at leading order, is based on real matrices $X_{\mu ab}$ and a potential proportional to $\mathrm{tr}\, X_\mu X_\nu^T X_\mu X_\nu^T$. When $N = D$, this coincides with a special case of the Carrozza–Tanasa model [12] and is also discussed in [15,20].

At leading $N \to \infty$ and $D \to \infty$ order, the solution of the model is governed by the finite temperature $T = 1/\beta$ Euclidean two-point function

$$G(t) = \frac{1}{N}\big\langle \mathrm{tr}\, \mathrm{T} X_\mu(t) X_\mu\big\rangle_\beta\,, \tag{6.2}$$

which can be expanded in terms of Fourier–Matsubara modes as

$$G(t) = \frac{1}{\beta}\sum_{k\in\mathbb{Z}} G_k e^{-i\nu_k t}\,. \tag{6.3}$$

The Matsubara frequencies are defined by

$$\nu_k = 2\pi k T\,. \tag{6.4}$$

The structure of the dominating generalized melonic graphs implies the following Schwinger–Dyson equations,

$$\frac{1}{G_k} = \nu_k^2 + m^2 + \Sigma_k \tag{6.5}$$

$$\Sigma(t) = -\lambda^6 G(t)^3 \,. \tag{6.6}$$

The self-energy $\Sigma(t)$ is expanded in Fourier series with coefficients Σ_k in a way similar to (6.3). At zero temperature, (6.3) and (6.5) are replaced by

$$G(t) = \frac{1}{2\pi}\int_{-\infty}^{+\infty} \tilde{G}(\omega) e^{-i\omega t}\, \mathrm{d}\omega \tag{6.7}$$

and

$$\frac{1}{\tilde{G}(\omega)} = \omega^2 + m^2 + \tilde{\Sigma}(\omega) \,. \tag{6.8}$$

6.1.2. Why the naive analysis is wrong

The Eqs. (6.5) and (6.6) look very similar to the Schwinger–Dyson equations governing the solution of fermionic models, like the original SYK model [1]. Naively, one may thus expect that the resulting physics would be very similar, but this turns out to be erroneous [17].

To understand in a simple way where the problem comes from, let us consider the case $m = 0$ and let us try to perform the usual analysis of the IR limit of Eqs. (6.8) and (6.6) at zero temperature,

$$\frac{1}{\tilde{G}(\omega)} = \tilde{\Sigma}(\omega) \,, \quad \Sigma(t) = -\lambda^6 G(t)^3 \,. \tag{6.9}$$

Using naively the Fourier transform formula

$$\int_{-\infty}^{+\infty} \frac{e^{i\omega t}}{|t|^{2\Delta}}\, \mathrm{d}t = \frac{2\Gamma(1-2\Delta)}{|\omega|^{1-2\Delta}} \sin(\pi\Delta) \tag{6.10}$$

and seeking power-law solutions to (6.9), $G(t) = b/|t|^{2\Delta}$ and $\Sigma(t) = b'/|t|^{2\Delta'}$, we get

$$\Delta' = 1 - \Delta \,, \quad \frac{1}{4bb'} = \Gamma(1-2\Delta)\Gamma(1-2\Delta')\sin(\pi\Delta)\sin(\pi\Delta') \tag{6.11}$$

from the first equation in (6.9) and

$$\Delta' = 3\Delta \,, \quad b' = -\lambda^6 b^3 \tag{6.12}$$

from the second equation in (6.9). This yields

$$\Delta = \frac{1}{4} \,, \quad \Delta' = \frac{3}{4} \,, \quad b = \frac{1}{(4\pi\lambda^6)^{1/4}} \tag{6.13}$$

and produce the following "solution",

$$\begin{aligned} G(t) &= \frac{1}{(4\pi\lambda^6)^{1/4}} \frac{1}{\sqrt{|t|}} \,, \quad \tilde{G}(\omega) = \left(\frac{\pi}{\lambda^6}\right)^{\frac{1}{4}} \frac{1}{\sqrt{|\omega|}} \,, \\ \Sigma(t) &= -\lambda^6 \frac{1}{(4\pi\lambda^6)^{3/4}} \frac{1}{|t|^{\frac{3}{2}}} \,, \quad \tilde{\Sigma}(\omega) = \left(\frac{\lambda^6}{\pi}\right)^{\frac{1}{4}} \sqrt{|\omega|} \,. \end{aligned} \tag{6.14}$$

However, this result is inconsistent. On the one hand, it predicts $\tilde{G}(\omega) > 0$ and $\tilde{\Sigma}(\omega) > 0$, whereas the Fourier transform of the second equation in (6.9),

$$\tilde{\Sigma}(\omega) = -\frac{\lambda^6}{4\pi^2} \int \tilde{G}(\omega_1)\tilde{G}(\omega_2)\tilde{G}(\omega-\omega_1-\omega_2)\, \mathrm{d}\omega_1 \mathrm{d}\omega_2 \,, \tag{6.15}$$

clearly shows that $\tilde{G}(\omega) > 0$ implies that $\tilde{\Sigma}(\omega) < 0$. There is no way (6.14) could be a meaningful solution of (6.9).

The mistake comes from the fact that the above reasoning, albeit standard in the literature, involves formal manipulations of divergent integrals. The Fourier transform formula (6.10) makes sense only if $\Delta > 0$ to avoid IR divergences and $\Delta < 1/2$ to avoid UV divergences. The analysis however assumes that one can use (6.10) to compute the Fourier transforms of both G and Σ; this is clearly incompatible with the first equation in (6.11), since $\Delta < 1/2$ implies that $\Delta' = 1 - \Delta > 1/2$.[8]

One may think that the difficulty comes from the use of the IR limit of the exact Schwinger–Dyson equation (6.8), but this is not the case. It is easy to see that the full set of Eqs. (6.5) cannot have consistent solutions when $m \to 0$. The argument uses unitarity. It is straightforward to show, using the spectral decomposition of the two-point function (6.2), that the Fourier coefficients G_k must be real and strictly positive. But when $m \to 0$, (6.5) implies that $\Sigma_0 > 0$ too. One then obtains a contradiction with (6.6), which shows that Σ_0 is a sum of strictly negative terms.

Let us note that the above conclusions are not restricted to the case of quantum mechanics. The discussion can indeed be straightforwardly generalized to the case of higher dimensional field theories, of the type considered for example in [20].

6.1.3. The physics

The physics associated with the above phenomenon is explained in [17] and the reader is invited to look into this reference for detailed explanations; see also [21]. Let us simply very briefly recall the main points here. The difference between bosonic models like (6.1) and SYK-like fermionic models is twofold. First, unlike in the fermionic cases, the large temperature limit of bosonic models is not weakly coupled in general. For instance, the model (6.1) at $m = 0$ is always strongly coupled, even when the dimensionless "coupling" $\beta\lambda$ is very small. An SYK-like high temperature perturbation theory thus simply does not exist for bosonic models. Second, models like (6.1) are unstable. The leading large N and large D limits still make sense, but only as long as the effective dimensionless coupling is not too strong. The particular point $T = 0$, $m \to 0$ in parameter space discussed in Section 6.1.2 belongs to a larger strongly coupled region where the Eqs. (6.5) and (6.6) do not have a solution, see Fig. 5 in Ref. [17].

6.2. Stable bosonic models

One can easily build stable purely bosonic models, for which the large N and large D limits are still dominated by generalized melonic diagrams and can thus be exactly solved. These models are interesting for several reasons. For example, one would like to investigate whether the absence of a non-trivial IR limit for the model (6.1) is due to its instability or to other qualitative differences with the fermionic models, such as the absence of a high temperature perturbation theory à la SYK.

A simple Lagrangian with Hermitian matrices and a stable potential is

$$L = ND\,\mathrm{tr}\Big(\frac{1}{2}\dot{X}_\mu\dot{X}_\mu - \frac{m^2}{2}X_\mu X_\mu - \frac{\lambda^4}{2}D\,X_\rho X_\mu X_\rho X_\sigma X_\mu X_\sigma\Big)\,. \tag{6.16}$$

The scaling with D of the interaction term is according to (4.1). The potential is manifestly positive, since it can be rewritten as $(1/2)\,\mathrm{tr}\,A_\mu A_\mu$ where

$$A_\mu = \sqrt{D}\lambda^2 X_\rho X_\mu X_\rho \tag{6.17}$$

is Hermitian. The leading Feynman graphs can be easily classified by introducing an auxiliary field F_μ and noting that (6.16) is equivalent to

$$L = ND\,\mathrm{tr}\Big(\frac{1}{2}\dot{X}_\mu\dot{X}_\mu - \frac{m^2}{2}X_\mu X_\mu + \frac{1}{2}F_\mu F_\mu - \lambda^2\sqrt{D}\,F_\mu X_\nu X_\mu X_\nu\Big)\,. \tag{6.18}$$

[8] This problem does not occur, e.g., in the usual SYK model, because G and Σ are then odd functions of time and the Fourier transforms involve the integrals of $|t|^{-2\Delta}\sin(\omega t)$ and $|t|^{-2\Delta'}\sin(\omega t)$, which are not UV divergent.

The interaction tr $F_\mu X_\nu X_\mu X_\nu$ is of the same general form as in (6.1). Moreover, the scaling with D that results from going from (6.16) to (6.18) is nicely consistent with (4.1). This is a general fact whose generalization has nice consequences in supersymmetric models, as we will explain below. We can thus use the results of [9,12] to get the leading graphs. Introducing the Euclidean two-point functions $G_X(t)$, $G_F(t)$ and the associated self-energies and Fourier transforms, the Schwinger–Dyson equations read, in obvious notations,

$$\frac{1}{G_{X,k}} = \nu_k^2 + m^2 + \Sigma_{X,k}\,, \quad \frac{1}{G_{F,k}} = -1 + \Sigma_{F,k}\,, \tag{6.19}$$

$$\Sigma_X(t) = -3\lambda^4 G_X(t)^2 G_F(t)\,, \quad \Sigma_F(t) = -\lambda^4 G_X(t)^3\,. \tag{6.20}$$

Note that the Fourier coefficients $G_{A,k}$ for the two-point function of the operator A_μ defined in (6.17) are simply given by $G_{A,k} = G_{F,k} + 1$.

We can proceed to analyze (6.19) and (6.20) in the usual way. A naive solution of the IR limit of the equations with non-trivial scaling dimensions $1/6$ and $1/2$ associated with the two-point functions G_X and G_A can be found straightforwardly. However, a careful analysis shows that this solution actually does not exist, that is to say, it is *not* the IR limit of a solution to the full set of Eqs. (6.19) and (6.20) [17,21]. This result is surprising. At least when $m \to 0$, it would have been natural to guess that the model (6.16) could develop a non-trivial IR behavior, with a non-zero zero temperature entropy, etc.; pretty much in the same way as the fermionic SYK-like models do. The fact that it does not shows that there is an important qualitative difference between purely fermionic and purely bosonic models, *even when the bosonic models are stable and dominated by the same type of generalized melonic diagrams as the fermionic models.* To the best of our knowledge, no purely bosonic model with SYK behavior has been found up to now.

6.3. Supersymmetric models

Supersymmetric theories are extremely natural to look at, in particular if one wishes to devise models with a gravitational dual. Up to now, most studies have focused on models with quenched disorder and/or a non-linear realization of supersymmetry where all fundamental degrees of freedom are fermions, see e.g. [6]. Here we point out that our matrix–tensor models have standard linearly realized supersymmetric versions with two or four supercharges.[9]

There is one possible obstruction to build models with linearly realized supersymmetry: supersymmetry relates several interaction terms together and this is not obviously consistent with the large D scaling (4.1). Our simple goal in the present subsection is to display explicitly how supersymmetry acts on the bubble representing the interaction terms and check that this action is consistent with the scaling (4.1). Note that another way to understand the consistency of supersymmetry with (4.1) is to use a supergraph formulation of the Feynman rules.

We focus on $\mathcal{N} = 2$ supersymmetric matrix quantum mechanics for concreteness. The case $\mathcal{N} = 4$ and higher space–time dimensions are very similar. The $\mathcal{N} = 2$ models contain traceless Hermitian bosonic matrices X_μ and complex fermionic matrices ψ_μ transforming in the adjoint representation of U(N). The real superpotential can be written in parallel with the interaction terms in the Lagrangian, see Eqs. (2.1) and (2.2), in the form

$$W(X) = \sum_a N^{1-t(\mathcal{B}_a)} \tau_a \mathcal{I}_{\mathcal{B}_a}(X)\,. \tag{6.21}$$

The bubbles $\mathcal{B}_a$ encode the term $\mathcal{I}_{\mathcal{B}_a}(X)$ in the usual way. The superpotential yields two types of interaction terms in the Lagrangian.

The terms coupling the fermions and the bosons read

$$L_1 = -ND\,\bar\psi_\mu{}^\alpha{}_\beta \frac{\partial^2 W}{\partial X_\mu{}^\alpha{}_\beta \partial X_\nu{}^\gamma{}_\delta} \psi_\nu{}^\gamma{}_\delta = -ND \sum_a N^{1-t(\mathcal{B}_a)} \tau_a I_{\mathcal{B}_a}(X, \psi, \bar\psi)\,, \tag{6.22}$$

[9] See also [15] for linearly realized supersymmetrization of an SYK-like tensor model.

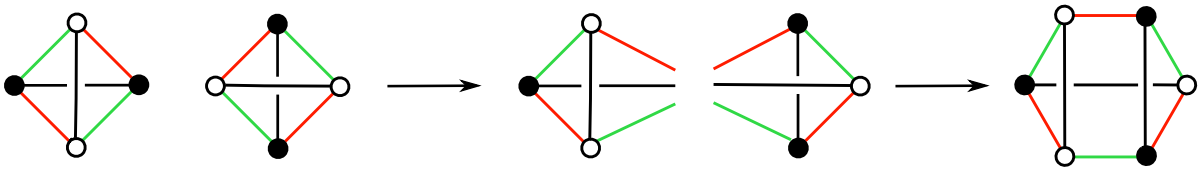

Fig. 10. Construction of the bubble associated with the potential term (6.24) (right inset) from the bubble associated with the superpotential (6.21) (left inset) in the case $W(X) = \tau\, tr\, X_\mu X_\nu X_\mu X_\nu$, as described below Eq. (6.26).

where

$$I_{\mathcal{B}_a}(X, \psi, \bar{\psi}) = \bar{\psi}_\mu{}^\alpha{}_\beta \frac{\partial^2 \mathcal{I}_{\mathcal{B}_a}}{\partial X_\mu{}^\alpha{}_\beta \partial X_\nu{}^\gamma{}_\delta} \psi_\nu{}^\gamma{}_\delta \,. \tag{6.23}$$

Each term in $I_{\mathcal{B}_a}$ is obtained from $\mathcal{I}_{\mathcal{B}_a}$ by substituting two matrices X_μ and X_ν by ψ_μ and $\bar{\psi}_\nu$. They are thus all labeled by the same bubble $\mathcal{B}_a$ and in particular, the coupling constants τ_a must scale as in (4.1) at large N and large D.

The potential term contributes as

$$L_2 = -\frac{1}{2} ND \frac{\partial W}{\partial X_\mu{}^\alpha{}_\beta} \frac{\partial W}{\partial X_\mu{}^\beta{}_\alpha} = -\frac{1}{2} ND \sum_{a,b} N^{2-t(\mathcal{B}_a)-t(\mathcal{B}_b)} \tau_{ab} I_{ab}(X) \,, \tag{6.24}$$

where

$$\tau_{ab} = \tau_a \tau_b \tag{6.25}$$

and

$$I_{ab}(X) = \frac{\partial \mathcal{I}_{\mathcal{B}_a}}{\partial X_\mu{}^\alpha{}_\beta} \frac{\partial \mathcal{I}_{\mathcal{B}_b}}{\partial X_\mu{}^\beta{}_\alpha} \,. \tag{6.26}$$

The interaction terms appearing in I_{ab} are described by many different bubbles, which we denote collectively by $\mathcal{B}_{ab}$, obtained from $\mathcal{B}_a$ and $\mathcal{B}_b$ in the following way: we remove one vertex from $\mathcal{B}_a$ and one vertex from $\mathcal{B}_b$ and then join together the edges that were attached to these two vertices in a way consistent with the coloring. In the tensor model literature, this operation is called a "one-dipole contraction". An example is depicted in Fig. 10. Since one connected component of $\mathcal{B}_a$ is connected to one connected component of $\mathcal{B}_b$ under the contraction, we have

$$c(\mathcal{B}_{ab}) = c(\mathcal{B}_a) + c(\mathcal{B}_b) - 1 \,. \tag{6.27}$$

Moreover, the vertices we remove belong to (12)-faces in $\mathcal{B}_a$ and $\mathcal{B}_b$ and under the contraction these two faces merge into one, which yields

$$t(\mathcal{B}_{ab}) = t(\mathcal{B}_a) + t(\mathcal{B}_b) - 1 \,. \tag{6.28}$$

By considering similarly the (13)- and (23)-faces passing through the vertices that are removed, we get

$$F_{13}(\mathcal{B}_{ab}) = F_{13}(\mathcal{B}_a) + F_{13}(\mathcal{B}_b) - 1 \,, \quad F_{23}(\mathcal{B}_{ab}) = F_{23}(\mathcal{B}_a) + F_{23}(\mathcal{B}_b) - 1 \,. \tag{6.29}$$

Using (6.27), (6.28), (6.29) together with

$$V(\mathcal{B}_{ab}) = V(\mathcal{B}_a) + V(\mathcal{B}_b) - 2 \,, \tag{6.30}$$

we then obtain

$$g(\mathcal{B}_{ab}) = g(\mathcal{B}_a) + g(\mathcal{B}_b) \,. \tag{6.31}$$

According to the general formulas (2.1) and (4.1), the overall powers of N and D in front of $I_{ab}(X)$ in (6.24) must thus be

$$\begin{aligned} &ND \times N^{1-t(\mathcal{B}_{ab})} \times D^{t(\mathcal{B}_{ab})-c(\mathcal{B}_{ab})+g(\mathcal{B}_{ab})} = \\ &\quad ND \times N^{2-t(\mathcal{B}_a)-t(\mathcal{B}_b)} \times D^{t(\mathcal{B}_a)+t(\mathcal{B}_b)-c(\mathcal{B}_a)-c(\mathcal{B}_b)+g(\mathcal{B}_a)+g(\mathcal{B}_b)} . \end{aligned} \tag{6.32}$$

Comparing with (6.24), we see that the coupling τ_{ab} must scale as

$$D^{t(\mathcal{B}_a)-c(\mathcal{B}_a)+g(\mathcal{B}_a)} \times D^{t(\mathcal{B}_b)-c(\mathcal{B}_b)+g(\mathcal{B}_b)} . \tag{6.33}$$

This is precisely matching the scaling implied by the supersymmetric relation (6.25) between couplings and by (4.1), as was to be shown.

Acknowledgments

We would like to thank Igor Klebanov for discussions. This work is supported in part by the Belgian Fonds National de la Recherche Scientifique FNRS (convention IISN 4.4503.15 and CDR grant J.0088.15 "Quantum Models of Black Holes") and the Fédération Wallonie-Bruxelles (Advanced ARC project "Holography, Gauge Theories and Quantum Gravity"). G. V. is a Research Fellow at the Belgian F.R.S.-FNRS. T. A. would like to thank Centro de Ciencias de Benasque Pedro Pascual for hospitality during his stay for the workshop "Gravity — New perspectives from strings and higher dimensions". The work of P.G. is partially supported by the Compagnia di San Paolo contract "MAST:Modern Applications of String Theory" TO-Call3-2012-0088.

References

[1] A. Kitaev, A Simple Model of Quantum Holography, KITP Program "Entanglement in Strongly-Correlated Quantum Matter," unpublished; see http://online.kitp.ucsb.edu/online/entangled15/.
[2] S. Sachdev, J. Ye, Phys. Rev. Lett. 70 (1993) 3339, cond-mat/9212030;
S. Sachdev, Phys. Rev. Lett. 105 (2010) 151602. arXiv:1006.3794;
O. Parcollet, A. Georges, Phys. Rev. B 59 (1999) 5341–5360.
[3] E. Witten, An SYK-Like Model Without Disorder. arXiv:1610.09758 [hep-th].
[4] R. Gurau, Ann. H. Poincaré 12 (2011) 829. arXiv:1011.2726;
R. Gurau, V. Rivasseau, Europhys. Lett. 95 (2011) 50004. arXiv:1101.4182;
R. Gurau, Ann. H. Poincaré 13 (2012) 399. arXiv:1102.5759;
V. Bonzom, R. Gurau, A. Riello, V. Rivasseau, Nucl. Phys. B 853 (2011) 174. arXiv:1105.3122;
R. Gurau, J.P. Ryan, SIGMA 8 (2012) 020. arXiv:1109.4812;
R. Gurau, Ann. Inst. Henry Poincaré Probab. Statist. 50 (2014) 1474. arXiv:1111.0519;
V. Bonzom, R. Gurau, V. Rivasseau, Phys. Rev. D 85 (2012) 084037. arXiv:1202.3637;
S. Dartois, V. Rivasseau, A. Tanasa, Ann. H. Poincaré 15 (2014) 965. arXiv:1301.1535;
A. Tanasa, SIGMA 12 (2016) 056. arXiv:1512.0208;
R. Gurau, Random Tensors, Oxford University Press, 2016. SIGMA special issue "Tensor Models, Formalism and Applications".
[5] J. Polchinski, V. Rosenhaus, J. High Energy Phys. 04 (2016) 001. arXiv:1601.06768;
J. Maldacena, D. Stanford, Phys. Rev. D 94 (2016) 106002. arXiv:1604.07818;
A. Jevicki, K. Suzuki, J. Yoon, J. High Energy Phys. 07 (2016) 007. arXiv:1603.06246;
A. Jevicki, K. Suzuki, J. High Energy Phys. 11 (2016) 046. arXiv:1608.07567;
D.J. Gross, V. Rosenhaus, A Generalization of Sachdev-Ye-Kitaev, arXiv:1610.01569.
[6] W. Fu, D. Gaiotto, J. Maldacena, S. Sachdev, Supersymmetric SYK models, arXiv:1610.08917;
T. Nishinaka, S. Terashima, arXiv:1611.10290 [hep-th];
C. Peng, M. Spradlin, A. Volovich, J. High Energy Phys. 05 (2017) 062. arXiv:1612.03851;
T. Li, J. Liu, Y. Xin, Y. Zhou, J. High Energy Phys. 06 (2017) 111. arXiv:1702.01738;
T. Kanazawa, T. Wettig, Complete random matrix classification of SYK models with $\mathcal{N}$ = 0, 1 and 2 supersymmetry, arXiv:1706.03044;
J. Murugan, D. Stanford, E. Witten, More on Supersymmetric and 2d Analogs of the SYK Model, arXiv:1706.05362;
C. Peng, M. Spradlin, A. Volovich, Correlators in the N = 2 Supersymmetric SYK Model, arXiv:1706.06078;
J. Yoon, Supersymmetric SYK Model: Bi-local Collective Superfield/Supermatrix Formulation, arXiv:1706.05914;
C. Peng, M. Spradlin, A. Volovich, arXiv:1706.06078 [hep-th].
[7] R. Gurau, The complete $1/N$ expansion of a SYK-like tensor model, arXiv:1611.04032;
C. Krishnan, S. Sanyal, P.N.B. Subramanian, Quantum Chaos and Holographic Tensor Models, arXiv:1612.06330;
V. Bonzom, L. Lionni, A. Tanasa, J. Math. Phys. 58 (2017) 052301. arXiv:1702.06944;

C. Krishnan, K.V.P. Kumar, S. Sanyal, J. High Energy Phys. 06 (2017) 036. arXiv:1703.08155.
[8] J.M. Maldacena, J. High Energy Phys. 04 (2003) 021, hep-th/0106112;
G. Festuccia, H. Lu, J. High Energy Phys. 12 (2007) 027, hep-th/0611098;
S. Shenker, D. Stanford, J. High Energy Phys. 12 (2014) 046. arXiv:1312.3296;
J. Maldacena, S.H. Shenker, D. Stanford, J. High Energy Phys. 08 (2016) 106. arXiv:1503.01409.
[9] F. Ferrari, Ann. H.Poincaré D (2018) (in press). arXiv:1701.01171.
[10] T. Hotta, J. Nishimura, A. Tsuchiya, Nuclear Phys. B 545 (1999) 543, hep-th/9811220;
G. Mandal, M. Mahato, T. Morita, J. High Energy Phys. 02 (2010) 034. arXiv:0910.4526;
T. Morita, J. High Energy Phys. 08 (2010) 015. arXiv:1005.2181.
[11] R. Emparan, R. Suzuki, K. Tanabe, J. High Energy Phys. 06 (2013) 009. arXiv:1302.6382;
R. Emparan, K. Tanabe, Phys. Rev. D 89 (2014) 064028. arXiv:1401.1957;
R. Emparan, R. Suzuki, K. Tanabe, J. High Energy Phys. 06 (2014) 106. arXiv:1402.6215;
R. Emparan, R. Suzuki, K. Tanabe, J. High Energy Phys. 04 (2015) 085. arXiv:1502.02820;
S. Bhattacharyya, A. De, S. Minwalla, R. Mohan, A. Saha, J. High Energy Phys. 04 (2016) 076, arXiv:1504.06613 [hep-th];
R. Emparan, T. Shiromizu, R. Suzuki, K. Tanabe, T. Tanaka, J. High Energy Phys. 06 (2015) 159. arXiv:1504.06489.
[12] S. Carrozza, A. Tanasa, Lett. Math. Phys. 106 (2016) 1531. arXiv:1512.06718.
[13] O. Aharony, M. Berkooz, E. Silverstein, J. High Energy Phys. 0108 (2001) 006, hep-th/0105309;
O. Aharony, M. Berkooz, E. Silverstein, Phys. Rev. D 65 (2002) 106007, hep-th/0112178;
E. Witten, Multitrace operators, boundary conditions, and AdS / CFT correspondence, hep-th/0112258.
[14] F. Ferrari, V. Rivasseau, G. Valette, A New Large N Expansion for General Matrix-Tensor Models, arXiv:1707.07366.
[15] I.R. Klebanov, G. Tarnopolsky, Uncolored Random Tensors, Melon Diagrams, and the SYK Models. arXiv:1611.08915.
[16] I.R. Klebanov, G. Tarnoplosky, On Large N Limit of Symmetric Traceless Tensor Models. rXiv:1706.00839.
[17] T. Azeyanagi, F. Ferrari, F.I. Schaposnik Massolo, Phase Diagram of Planar Matrix Quantum Mechanics, Tensor and SYK Models. arXiv:1707.03431.
[18] B. Mohar, C. Thomassen, Graphs on Surfaces, The Johns Hopkins University Press, 2001.
[19] R. Gurau, The $1/N$ expansion of tensor models with two symmetric tensors. arXiv:1706.05328.
[20] S. Giombi, I.R. Klebanov, G. Tarnopolsky, Bosonic Tensor Models at Large N and Small ϵ, arXiv:1707.03866.
[21] F. Ferrari, F.I. Schaposnik Massolo, More on the Phase Diagram of Planar Matrix Quantum Mechanics, in preparation.

Appendix B

Publication II: Correlators between Wilson loop and chiral operators in $\mathcal{N} = 2$ conformal gauge theories

Published for SISSA by Springer

Received: March 15, 2018
Accepted: March 27, 2018
Published: March 30, 2018

Correlators between Wilson loop and chiral operators in $\mathcal{N} = 2$ conformal gauge theories

M. Billò,[a,b] **F. Galvagno,**[a,b] **P. Gregori**[a,c] **and A. Lerda**[d,b]

[a] *Dipartimento di Fisica and Arnold-Regge Center, Università di Torino, Via P. Giuria 1, I-10125 Torino, Italy*

[b] *I.N.F.N. — sezione di Torino, Via P. Giuria 1, I-10125 Torino, Italy*

[c] *Service de Physique Théorique et Mathématique, Université Libre de Bruxelles and International Solvay Institutes, Campus de la Plaine, CP 231, B-1050 Bruxelles, Belgium*

[d] *Dipartimento di Scienze e Innovazione Tecnologica and Arnold-Regge Center, Università del Piemonte Orientale, Viale T. Michel 11, I-15121 Alessandria, Italy*

E-mail: billo@to.infn.it, galvagno@to.infn.it, pgregori@ulb.ac.be, lerda@to.infn.it

Abstract: We consider conformal $\mathcal{N} = 2$ super Yang-Mills theories with gauge group SU(N) and $N_f = 2N$ fundamental hypermultiplets in presence of a circular 1/2-BPS Wilson loop. It is natural to conjecture that the matrix model which describes the expectation value of this system also encodes the one-point functions of chiral scalar operators in presence of the Wilson loop. We obtain evidence of this conjecture by successfully comparing, at finite N and at the two-loop order, the one-point functions computed in field theory with the vacuum expectation values of the corresponding normal-ordered operators in the matrix model. For the part of these expressions with transcendentality $\zeta(3)$, we also obtain results in the large-N limit that are exact in the 't Hooft coupling λ.

Keywords: Extended Supersymmetry, Wilson, 't Hooft and Polyakov loops, Conformal Field Theory, Supersymmetric Gauge Theory

ArXiv ePrint: 1802.09813

https://doi.org/10.1007/JHEP03(2018)193

JHEP03(2018)193

Contents

1 Introduction **1**

2 Wilson loop and its correlators with chiral operators **3**

3 The matrix model approach **5**
3.1 Wilson loop and chiral operators in the matrix model 8

4 Matrix model correlators in presence of a Wilson loop **10**
4.1 The $\mathcal{N} = 4$ theory 10
4.2 The $\mathcal{N} = 2$ superconformal theory 12
4.3 The large-N limit 14

5 Perturbative checks in field theory **17**
5.1 Tree-level 18
5.2 Loop corrections 20
5.3 Planar limit 25

6 Conclusions **28**

A One-point functions from defect conformal field theory **29**

B Calculation of $\delta A_{(4)}$ and $\delta A_{(2,2)}$ at two loops **30**

C Group theory identities **34**

JHEP03(2018)193

1 Introduction

The study of defects and of their properties may improve our understanding of quantum field theories. Wilson loops represent a class of gauge-invariant line defects which is of paramount relevance in gauge theories.

In general, Wilson loops receive perturbative and non-perturbative corrections and their exact evaluation is a difficult task. It is therefore important to find classes of theories and of Wilson loops for which it is possible to make progress in this direction. In this perspective, much work has been devoted to the study of Wilson loops in supersymmetric gauge theories, in theories which possess integrable sectors and in theories enjoying conformal symmetry. Furthermore, a powerful angle of approach to the strong coupling behavior is furnished by correspondences of the AdS/CFT type.

$\mathcal{N} = 4$ super Yang-Mills (SYM) theory is maximally supersymmetric, it is conformal and many sectors of its observables are integrable. Moreover, it is the theory for which

the AdS/CFT correspondence was originally conjectured and for which it is best established. In this theory important results, many of which are exact, have been obtained regarding Wilson loop operators which preserve at least a fraction of the supersymmetry. In particular the 1/2-BPS circular Wilson loop has been evaluated exactly in terms of a Gaussian matrix model in [1–3]. Wilson loops preserving fewer supersymmetries [4], such as the 1/4-BPS circular loop [5] and particular classes of 1/8-BPS loops [6–8], have been classified and analyzed. Correlators among such Wilson loops, or between Wilson loops and local operators have also been considered [9–11]; in particular, correlators of a 1/8-BPS circular loop and chiral primaries in $\mathcal{N} = 4$ SYM theory have been computed [12–16], mapping them to multi-matrix models. Also correlators with local chiral operators and Wilson loops in higher representations have been discussed [17, 18]. Often these results have been successfully compared, at least in the large-N limit, with AdS/CFT [17–19] and with the outcome of the integrability approach [20].

$\mathcal{N} = 4$ SYM is a superconformal theory, and Wilson loops that preserve a subgroup of the superconformal symmetry are instances [21] of a defect conformal field theory (DCFT) [22–25]. The spectrum and the structure constants of operators defined on the defect represent an extra important piece of conformal data; correlators of certain such operators have been considered both directly [26, 27] and via integrability [28]. Also the correlators of the Wilson loop defect with bulk operators, such as the chiral primaries, are constrained by the residual symmetry.

Similar progress has been made also in $\mathcal{N} = 2$ SYM theories, mainly thanks to localization techniques [29, 30]. These techniques, relying on supersymmetry, yield exact results for the field theory partition function in a deformed space-time geometry by localizing it on a finite set of critical points and expressing it as a matrix model. This procedure was extended by Pestun in a seminal paper [3] to compute the expectation value of a circular Wilson loop in a S^4 sphere background, reducing the path integral computation to a matrix model which is a simple modification of the one for the partition function. In the $\mathcal{N} = 4$ SYM case the matrix model is Gaussian, in agreement with the field theory results [1, 2] mentioned above, while in the $\mathcal{N} = 2$ theory it receives both one-loop and instanton corrections.

Pestun's results on circular Wilson loops have opened several directions in the study of gauge theories and allowed us to deepen our knowledge about the AdS/CFT duality in the $\mathcal{N} = 2$ setting [31–33], as well as to provide exact results for some observables directly related to the Wilson loop, such as the Bremsstrahlung function [34–38].

When the $\mathcal{N} = 2$ theory is conformal, as it is the case for $\mathcal{N} = 2$ SQCD with $N_f = 2N$, it has been shown that the matrix model for the partition function on S_4 also contains information about correlators of chiral operators on $\mathbb{R}^4$ [39–43], provided one disentangles the operator mixing induced by the map from S^4 to $\mathbb{R}^4$ [44–46]. In [47] this disentangling of operators has been realized as a normal-ordering procedure and the relation between field theory and matrix model correlators has been shown to hold also in non-conformal situations for a very special class of operators.

It is natural to conjecture that, as it is the case in the $\mathcal{N} = 4$ theory, also in superconformal $\mathcal{N} = 2$ theories the matrix model for the circular Wilson loop on S_4 may contain

JHEP03(2018)193

information on correlators of chiral operators in the presence of a circular loop in $\mathbb{R}^4$. In particular, from DCFT we know that the functional form of the one-point function in presence of a Wilson loop is completely fixed up to a coefficient depending on the coupling constant g; this coefficient can be encoded in the Pestun matrix model.

In this paper, neglecting non-perturbative instanton contributions, we deal with the determinant factor in the matrix model definition, which can be expanded in powers of g. We work at finite and generic N. Following [47], we identify the matrix model counterparts of chiral operators in the field theory through a normal-ordering prescription, and compute the one-point functions of such operators in the matrix model. We then compare them with the corresponding field theory one-point functions in presence of the Wilson loop computed in standard perturbation theory up to two loops for finite N, and to all orders in perturbation theory in planar limit for the $\zeta(3)$ dependent part. We heavily rely on the $\mathcal{N} = 4$ results in that we consider the diagrammatic difference between $\mathcal{N} = 4$ and $\mathcal{N} = 2$ [48]; this procedure massively reduces the number of Feynman diagrams to be computed. We find complete agreement between the matrix model and field theory results; we believe that this represent compelling evidence for the conjecture.

The paper is structured as follows. We introduce our set-up in section 2. In sections 3 and 4 we perform the matrix model computation, reviewing first the $\mathcal{N} = 4$ case and then moving to the superconformal $\mathcal{N} = 2$ theory. We also derive large-N results which are exact in $\lambda = gN^2$ for the $\mathcal{N} = 4$ part of these one-point functions and for the extra part in the $\mathcal{N} = 2$ theory which has $\zeta(3)$ transcendentality. The diagrammatic evaluation of the correlators in field theory is performed in section 5, up to two loops for finite N. We also show how the large-N results derived in the matrix model approach arise diagrammatically. Finally, section 6 contains our conclusions, while some more technical material is contained in three appendices.

2 Wilson loop and its correlators with chiral operators

We consider a $\mathcal{N} = 2$ SYM theory on $\mathbb{R}^4$ with gauge group SU(N) and N_f fundamental flavours. As is well-known, when $N_f = 2N$ this theory is superconformal invariant, even at the quantum level. In the following we will restrict to this case.

We place a 1/2-BPS Wilson loop in a representation $\mathcal{R}$ along a circle C of radius R inside $\mathbb{R}^4$. Such operator, which we denote $W_{\mathcal{R}}(C)$, measures the holonomy of the gauge field and the adjoint scalars around C and represents a (conformal) defect in the theory. The explicit expression of $W_{\mathcal{R}}(C)$ is

$$W_{\mathcal{R}}(C) = \frac{1}{N}\mathrm{Tr}_{\mathcal{R}}\,\mathcal{P}\exp\left\{g\oint_C d\tau\left[\mathrm{i}\,A_\mu(x)\,\dot{x}^\mu(\tau) + R\,\theta^I(\tau)\phi_I(x)\right]\right\} \tag{2.1}$$

with $I = 1, 2$. Here g is the gauge coupling constant, A_μ is the gauge field and ϕ_I are the two (real) scalar fields of the $\mathcal{N} = 2$ vector multiplet, while $\mathcal{P}$ denotes the path-ordering and $\mathrm{Tr}_{\mathcal{R}}$ the trace in the representation $\mathcal{R}$ of SU(N). If we take $\theta^I(\tau) = \delta^{I1}$, which is the standard choice for the scalar coupling, and introduce the chiral and anti-chiral

JHEP03(2018)193

combinations

$$\varphi = \frac{1}{\sqrt{2}}\big(\phi_1 + \mathrm{i}\,\phi_2\big)\,, \quad \bar\varphi = \frac{1}{\sqrt{2}}\big(\phi_1 - \mathrm{i}\,\phi_2\big)\,, \tag{2.2}$$

the Wilson loop (2.1) becomes

$$W_{\mathcal{R}}(C) = \frac{1}{N}\mathrm{Tr}_{\mathcal{R}}\,\mathcal{P}\exp\left\{g\oint_C d\tau\left[\mathrm{i}\,A_\mu(x)\,\dot x^\mu(\tau) + \frac{R}{\sqrt{2}}\big(\varphi(x)+\bar\varphi(x)\big)\right]\right\}. \tag{2.3}$$

For definiteness, from now on we will take the representation $\mathcal{R}$ to be the fundamental of SU(N) and denote the corresponding Wilson loop simply as $W(C)$. Furthermore, we will use the symbol "tr" for the trace in the fundamental representation.

We are interested in computing the correlators between the Wilson loop and the chiral operators of the SYM theory. The latter are labeled by a vector of integers $\vec n = (n_1, n_2, \cdots, n_\ell)$ and take a multi-trace expression of the form

$$O_{\vec n}(x) = \mathrm{tr}\,\varphi^{n_1}(x)\,\mathrm{tr}\,\varphi^{n_2}(x)\cdots\mathrm{tr}\,\varphi^{n_\ell}(x)\,. \tag{2.4}$$

In our model, these are protected chiral primary operators with a conformal dimension n given by

$$n = \sum_{k=1}^{\ell} n_k\,, \tag{2.5}$$

and obey chiral ring relations. Equivalently, by expanding $\varphi(x) = \varphi^b(x)\,T^b$, where T^b are the generators of SU(N) in the fundamental representation normalized in such a way that

$$\mathrm{tr}\,\big(T^bT^c\big) = \frac{1}{2}\,\delta^{bc}\,, \quad \mathrm{tr}\,T^b = 0 \quad \text{with} \quad b,c = 1,\cdots,N^2-1\,, \tag{2.6}$$

we can write

$$O_{\vec n}(x) = R_{\vec n}^{\,b_1\ldots b_n}\,\varphi^{b_1}(x)\ldots\varphi^{b_n}(x) \tag{2.7}$$

where $R_{\vec n}^{\,b_1\ldots b_n}$ is a totally symmetric n-index tensor whose expression is encoded[1] in (2.4).

The quantity of interest is the one-point function

$$\big\langle\, W(C)\,O_{\vec n}(x)\,\big\rangle\,. \tag{2.8}$$

To evaluate it, we can proceed as follows. Firstly, without any loss of generality, we can place the circle C in the plane $(x^1, x^2) \subset \mathbb{R}^4$. The points on the loop C can then be parameterized as

$$x^\mu(\tau) = R\,\big(\cos\tau, \sin\tau, 0, 0\,\big) \tag{2.9}$$

with $\tau \in [\,0, 2\pi\,]$. Secondly, using the standard results of defect conformal field theory [24], we can fix the functional dependence of the one-point function (2.8). Indeed, splitting the coordinates x^μ into parallel and transverse components, namely $x^\mu \to (x^a; x^i)$ with $a = 1, 2$

[1] Explicitly,

$$R_{\vec n}^{\,b_1\ldots b_n} = \mathrm{tr}\,\big(T^{(b_1}\cdots T^{b_{n_1}}\big)\;\mathrm{tr}\,\big(T^{b_{n_1+1}}\cdots T^{b_{n_1+n_2}}\big)\ldots\mathrm{tr}\,\big(T^{b_{n_1+\ldots+n_{\ell-1}+1}}\cdots T^{b_n)}\big)$$

where the indices are symmetrized with strength 1.

JHEP03(2018)193

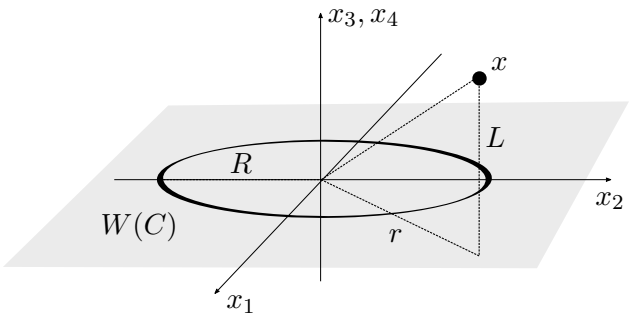

Figure 1. The geometric set-up for the configuration we consider.

and $i = 3, 4$, and denoting $x^a x_a = r^2$ and $x^i x_i = L^2$, so that $x^2 = r^2 + L^2$ (see figure 1), we see that

$$\|x\|_C = \frac{\sqrt{(R^2 - x^2)^2 + 4L^2R^2}}{R} \tag{2.10}$$

is the "distance" between x and C, which is invariant under the $\mathrm{SO}(1,2) \times \mathrm{SO}(3)$ subgroup of the conformal symmetry that is preserved by the Wilson loop (see appendix A for details). When $x \to 0$, we have $\|x\|_c \to R$.

Because of conformal invariance, the correlator (2.8) takes the form

$$\left\langle W(C)\, O_{\vec{n}}(x) \right\rangle = \frac{A_{\vec{n}}}{\left(2\pi \|x\|_C\right)^n} \tag{2.11}$$

where $A_{\vec{n}}$ is a g-dependent constant which corresponds to the one-point function evaluated in the origin:

$$A_{\vec{n}} = (2\pi R)^n \left\langle W(C)\, O_{\vec{n}}(0) \right\rangle . \tag{2.12}$$

In the next sections we will compute this function in two different ways: one by using the matrix model approach suggested by localization, and the other by using standard perturbative field theory methods. As anticipated in the Introduction, these two approaches lead to the same results.

3 The matrix model approach

The vacuum expectation value of the Wilson loop can be expressed and computed in terms of a matrix model, as shown in [3] using localization methods. In the following we extend this approach to compute also the correlators between the Wilson loop and the chiral correlators in $\mathcal{N} = 2$ superconformal theories, but before we briefly review the matrix model and introduce our notations, relying mainly on [47].

The matrix model in question corresponds to putting the $\mathcal{N} = 2$ SYM theory on a sphere $\mathcal{S}_4$ and writing the corresponding partition function as follows:

$$\mathcal{Z}_{\mathcal{S}_4} = \int \prod_{u=1}^{N} da_u \; \Delta(a) \left| Z(\mathrm{i}a) \right|^2 \delta\left(\sum_{v=1}^{N} a_v \right) . \tag{3.1}$$

JHEP03(2018)193

Here a_u are the eigenvalues of a traceless $N \times N$ matrix a which are integrated over the real line; $\Delta(a)$ is the Vandermonde determinant and $Z(\mathrm{i}a)$ is the gauge theory partition function on $\mathbb{R}^4$. The latter is computed using the localization techniques as in [49, 50], with the assumption that the adjoint scalar $\varphi(x)$ of the vector multiplet has a purely imaginary vacuum expectation value given by $\langle\varphi\rangle = \mathrm{i}\, a$, and that the Ω-deformation parameters are $\epsilon_1 = \epsilon_2 = 1/R$ where R is the radius of $\mathcal{S}_4$ which from now on we take to be 1 for simplicity. This partition function is a product of the classical, 1-loop and instanton contributions, namely:

$$Z(\mathrm{i}a) = Z_{\mathrm{class}}(\mathrm{i}a)\, Z_{1-\mathrm{loop}}(\mathrm{i}a)\, Z_{\mathrm{inst}}(\mathrm{i}a)\,. \tag{3.2}$$

The classical part provides a Gaussian term in the matrix model:

$$\left|Z_{\mathrm{class}}(\mathrm{i}a)\right|^2 = \mathrm{e}^{-\frac{8\pi^2}{g^2}\,\mathrm{tr}\,a^2}\,, \tag{3.3}$$

while the 1-loop contribution is

$$\left|Z_{1-\mathrm{loop}}(\mathrm{i}a)\right|^2 = \prod_{u<v=1}^{N} H(\mathrm{i}a_{uv})^2 \prod_{u=1}^{N} H(\mathrm{i}a_u)^{-N_f} \tag{3.4}$$

where $a_{uv} = a_u - a_v$, and

$$H(x) = G(1+x)\, G(1-x) \tag{3.5}$$

with $G(x)$ being the Barnes G-function. In the weak-coupling limit $g \ll 1$, where instantons are exponentially suppressed, we can set

$$\left|Z_{\mathrm{inst}}(\mathrm{i}a)\right|^2 = 1\,. \tag{3.6}$$

Moreover, in this limit the integral (3.1) is dominated by the region of small a_u, and thus we can expand the functions H appearing in (3.4) using

$$\log H(x) = -(1+\gamma)\, x^2 - \sum_{n=2}^{\infty} \zeta(2n-1)\, \frac{x^{2n}}{n} \tag{3.7}$$

where $\zeta(n)$ is the Riemann zeta-function and γ is the Euler-Mascheroni constant. In this way the one-loop contribution can be viewed as an interaction term in a free matrix model:

$$\left|Z_{1-\mathrm{loop}}(\mathrm{i}a)\right|^2 = e^{-S_{\mathrm{int}}(a)} \tag{3.8}$$

where $S_{\mathrm{int}}(a)$ is a sum of homogeneous polynomials S_n in a of order n. The first few are:

$$\begin{aligned}
S_2(a) &= -(1+\gamma)\,(2N - N_f)\,\mathrm{tr}\,a^2 = 0\,,\\
S_4(a) &= \frac{\zeta(3)}{2}\left[(2N-N_f)\,\mathrm{tr}\;a^4 + 6\left(\mathrm{tr}\,a^2\right)^2\right] = 3\,\zeta(3)\left(\mathrm{tr}\,a^2\right)^2\,,\\
S_6(a) &= -\frac{\zeta(5)}{3}\left[(2N-N_f)\,\mathrm{tr}\,a^6 + 30\,\mathrm{tr}\,a^4\,\mathrm{tr}\,a^2 - 20\,\left(\mathrm{tr}\;a^3\right)^2\right]\\
&= -\frac{10\,\zeta(5)}{3}\left[3\,\mathrm{tr}\,a^4\,\mathrm{tr}\,a^2 - 2\,\left(\mathrm{tr}\,a^3\right)^2\right]
\end{aligned} \tag{3.9}$$

JHEP03(2018)193

where the last step in each line follow from the superconformal condition $N_f = 2N$. After the rescaling

$$a \to \left(\frac{g^2}{8\pi^2}\right)^{\frac{1}{2}} a\,, \tag{3.10}$$

the matrix model gets a canonically normalized Gaussian factor and the sphere partition function becomes

$$\mathcal{Z}_{\mathcal{S}_4} = \left(\frac{g^2}{8\pi^2}\right)^{\frac{N^2-1}{2}} \int \prod_{u=1}^{N} da_u\ \Delta(a)\, \mathrm{e}^{-\mathrm{tr}\, a^2 - S_{\mathrm{int}}(a)}\, \delta\left(\sum_{v=1}^{N} a_v\right) \tag{3.11}$$

with

$$S_{\mathrm{int}}(a) = \frac{3\,\zeta(3)\,g^4}{(8\pi^2)^2}\,\left(\mathrm{tr}\, a^2\right)^2 - \frac{10\,\zeta(5)\,g^6}{3(8\pi^2)^3}\left[3\,\mathrm{tr}\, a^4\,\mathrm{tr}\, a^2 - 2\,\left(\mathrm{tr}\, a^3\right)^2\right] + \cdots\,. \tag{3.12}$$

Exploiting the Vandermonde determinant $\Delta(a)$ and writing $a = a^b\, T^b$, we can alternatively express the integral (3.11) using a flat integration measure da over all matrix components a^b as follows

$$\mathcal{Z}_{\mathcal{S}_4} = c_N \left(\frac{g^2}{8\pi^2}\right)^{\frac{N^2-1}{2}} \int da\ \mathrm{e}^{-\mathrm{tr}\, a^2 - S_{\mathrm{int}}(a)} \tag{3.13}$$

where c_N is a g-independent constant and $da \propto \prod_b da_b$. The overall factor c_N and the normalization of the flat measure da are clearly irrelevant for the computation of the vacuum expectation value of any quantity $f(a)$, which is defined as

$$\left\langle\, f(a)\,\right\rangle = \frac{\displaystyle\int da\ \mathrm{e}^{-\mathrm{tr}\, a^2 - S_{\mathrm{int}}(a)}\, f(a)}{\displaystyle\int da\ \mathrm{e}^{-\mathrm{tr}\, a^2 - S_{\mathrm{int}}(a)}} = \frac{\left\langle\, \mathrm{e}^{-S_{\mathrm{int}}(a)}\, f(a)\,\right\rangle_0}{\left\langle\, \mathrm{e}^{-S_{\mathrm{int}}(a)}\,\right\rangle_0}\,. \tag{3.14}$$

Here we have denoted with a subscript 0 the expectation value in the Gaussian matrix model, namely

$$\left\langle\, f(a)\,\right\rangle_0 = \frac{\displaystyle\int da\ \mathrm{e}^{-\mathrm{tr}\, a^2}\, f(a)}{\displaystyle\int da\ \mathrm{e}^{-\mathrm{tr}\, a^2}}\,. \tag{3.15}$$

This Gaussian model is the matrix model that is appropriate to describe the $\mathcal{N} = 4$ SYM theory. In this case, in fact, the field content of the theory is such that the 1-loop partition function $Z_{1-\mathrm{loop}}$ and the instanton partition function Z_{inst} are both equal to 1, implying that $S_{\mathrm{int}} = 0$.

Notice that if we normalize the flat measure as

$$da = \prod_{b=1}^{N^2-1} \frac{da^b}{\sqrt{2\pi}}\,, \tag{3.16}$$

then the denominator of (3.15) becomes 1 and we simply have

$$\left\langle\, f(a)\,\right\rangle_0 = \int da\ \mathrm{e}^{-\mathrm{tr}\, a^2}\, f(a)\,. \tag{3.17}$$

JHEP03(2018)193

Using this, we can easily see that the basic Wick contraction in the Gaussian model is

$$\left\langle a^b\, a^c \right\rangle_0 = \delta^{bc}\,. \tag{3.18}$$

Introducing the notation

$$t_{n_1,n_2,\dots} = \left\langle \operatorname{tr} a^{n_1} \operatorname{tr} a^{n_2} \cdots \right\rangle_0 \tag{3.19}$$

and using (2.6), we evidently have

$$t_0 = \left\langle \operatorname{tr} 1 \right\rangle_0 = N\,, \quad t_1 = \left\langle \operatorname{tr} a \right\rangle_0 = 0\,, \quad t_2 = \left\langle \operatorname{tr} a^2 \right\rangle_0 = \frac{N^2-1}{2}\,. \tag{3.20}$$

Higher order traces can be computed performing consecutive Wick contractions with (3.18) and using the fusion/fission identities

$$\begin{aligned} \operatorname{tr}\left(T^b B\, T^b C\right) &= \frac{1}{2}\operatorname{tr} B\, \operatorname{tr} C - \frac{1}{2N}\operatorname{tr}\left(B\, C\right), \\ \operatorname{tr}\left(T^b C\right)\, \operatorname{tr}\left(T^b C\right) &= \frac{1}{2}\operatorname{tr}\left(B\, C\right) - \frac{1}{2N}\operatorname{tr} B\, \operatorname{tr} C\,, \end{aligned} \tag{3.21}$$

which hold for any two matrices B and C. In this way we can build recursion relations and, for example, get:

$$\begin{aligned} t_n &= \frac{1}{2}\sum_{m=0}^{n-2}\left(t_{m,n-m-2} - \frac{1}{N}\, t_{n-2}\right), \\ t_{n,n_1} &= \frac{1}{2}\sum_{m=0}^{n-2}\left(t_{m,n-m-2,n_1} - \frac{1}{N}\, t_{n-2,n_1}\right) + \frac{n_1}{2}\left(t_{n+n_1-2} - \frac{1}{N}\, t_{n-1,n_1-1}\right), \\ t_{n,n_1,n_2} &= \frac{1}{2}\sum_{m=0}^{n-2}\left(t_{m,n-m-2,n_1,n_2} - \frac{1}{N}\, t_{n-2,n_1,n_2}\right) + \frac{n_1}{2}\left(t_{n+n_1-2,n_2} - \frac{1}{N}\, t_{n-1,n_1-1,n_2}\right) \\ &\quad + \frac{n_2}{2}\left(t_{n+n_2-2,n_1} - \frac{1}{N} t_{n-1,n_1,n_2-1}\right), \end{aligned} \tag{3.22}$$

and so on. These relations, together with the initial conditions (3.20), give an efficient way to obtain multi-trace vacuum expectation values in the Gaussian model and will be the basic ingredients for the computations of the correlators in the $\mathcal{N}=2$ superconformal theory.

3.1 Wilson loop and chiral operators in the matrix model

As shown in [3], in the matrix model the Wilson loop (2.3) in the fundamental representation and on a circle of radius $R=1$ is given by the following operator

$$\mathcal{W}(a) = \frac{1}{N}\operatorname{tr}\exp\left(\frac{g}{\sqrt{2}}\, a\right) = \frac{1}{N}\sum_{k=0}^{\infty}\frac{g^k}{2^{\frac{k}{2}}\, k!}\operatorname{tr} a^k\,. \tag{3.23}$$

On the other hand, to any multi-trace chiral operator $O_{\vec{n}}(x)$ of the SYM theory defined as in (2.4), it would seem natural to associate a matrix operator $O_{\vec{n}}(a)$ with precisely the same expression but with the field $\varphi(x)$ replaced by the matrix a, namely

$$O_{\vec{n}}(a) = \operatorname{tr} a^{n_1} \operatorname{tr} a^{n_2} \cdots \operatorname{tr} a^{n_\ell} = R_{\vec{n}}^{b_1\dots b_n}\; a^{b_1}\, a^{b_2} \cdots a^{b_n}\,. \tag{3.24}$$

JHEP03(2018)193

However, since the field theory propagator only connects φ with $\bar{\varphi}$, all operators $O_{\vec{n}}(x)$ have no self-contractions, whereas the operators $O_{\vec{n}}(a)$ defined above do not share this property. This means that the dictionary between the SYM theory and the matrix model is more subtle. Indeed, we have to subtract from $O_{\vec{n}}(a)$ all its self-contractions by making it orthogonal to all the lower dimensional operators, or equivalently by making it normal-ordered. As discussed in [47], given any operator $O(a)$ we can define its normal-ordered version $\mathcal{O}(a)$ as follows. Let be Δ the dimension of $O(a)$ and $\{O_p(a)\}$ a basis of in the finite-dimensional space of matrix operators with dimension smaller than Δ. Denoting by C_Δ the (finite-dimensional) matrix of correlators

$$\big(C_\Delta\big)_{pq} = \big\langle\, O_p(a)\, O_q(a)\,\big\rangle \tag{3.25}$$

which are computed according to (3.14), we define the normal-ordered operator

$$\mathcal{O}(a) = :O(a):_g \,=\, O(a) - \sum_{p,q} \big\langle\, O(a)\, O_p(a)\,\big\rangle\, (C_\Delta^{-1})^{pq}\, O_q(a)\,. \tag{3.26}$$

As emphasized by the notation, the normal-ordered operators are g-dependent, since the correlators in the right hand side of (3.26) are computed in the interacting $\mathcal{N}=2$ matrix model using (3.12).

Using these definitions, the correspondence between field theory and matrix model operators takes the following simple form

$$O_{\vec{n}}(x) \;\to\; \mathcal{O}_{\vec{n}}(a) = :O_{\vec{n}}(a):_g \;. \tag{3.27}$$

Let us give some explicit examples by considering the first few low-dimensional operators. At level $n=2$ we have just one operator:

$$\mathcal{O}_{(2)}(a) = :\mathrm{tr}\, a^2:_g = \mathrm{tr}\, a^2 - \frac{N^2-1}{2} + \frac{3\,\zeta(3)\,g^4}{(8\pi^2)^2}\,\frac{(N^2-1)(N^2+1)}{2} + O(g^6)\,. \tag{3.28}$$

Similarly, at level $n=3$ we have one operator, which in the SU(N) theory does not receive any correction:

$$\mathcal{O}_{(3)}(a) = :\mathrm{tr}\, a^3:_g = \mathrm{tr}\, a^3\,. \tag{3.29}$$

At level $n=4$, we have instead two independent operators corresponding to $\vec{n}=(4)$ and $\vec{n}=(2,2)$. Their normal-ordered expressions are given, respectively, by

$$\begin{aligned}\mathcal{O}_{(4)}(a) &= :\mathrm{tr}\, a^4:_g \\ &= \mathrm{tr}\, a^4 - \frac{2N^2-3}{N}\,\mathrm{tr}\, a^2 + \frac{(N^2-1)(2N^2-3)}{4N} \\ &\quad + \frac{3\zeta(3)\,g^4}{(8\pi^2)^2}\left[\frac{(2N^2-3)(N^2+5)}{N}\,\mathrm{tr}\, a^2 - \frac{2(N^2-1)(N^2+4)(2N^2-3)}{4N}\right] + O(g^6)\,,\end{aligned} \tag{3.30}$$

and

$$\begin{aligned}\mathcal{O}_{(2,2)}(a) &= :\big(\mathrm{tr}\, a^2\big)^2:_g \\ &= \big(\mathrm{tr}\, a^2\big)^2 - (N^2-1)\,\mathrm{tr}\, a^2 + \frac{N^4-1}{4} \\ &\quad + \frac{3\,\zeta(3)\,g^4}{(8\pi^2))^2}\left[(N^2-1)(N^2+5)\,\mathrm{tr}\, a^2 - \frac{(N^4-1)(N^2+4)}{2}\right] + \mathcal{O}(g^6)\,.\end{aligned} \tag{3.31}$$

JHEP03(2018)193

Up to the order g^6 we have considered, it is easy to check that these operators satisfy

$$\begin{aligned} \langle\, \mathcal{O}_{\vec{n}}(a) \,\rangle &= 0\,, \\ \langle\, \mathcal{O}_{\vec{n}}(a)\, \mathcal{O}_{\vec{m}}(a) \,\rangle &= 0\,, \end{aligned} \tag{3.32}$$

for $n \neq m$. Normal-ordered operators of higher dimension can be constructed without any problem along these same lines.

We observe that the g-independent parts of the above expressions correspond to the normal-ordered operators in the Gaussian model, *i.e.* in the $\mathcal{N} = 4$ theory. Since we will often compare our $\mathcal{N} = 2$ results with those of the $\mathcal{N} = 4$ theory, we find convenient to introduce a specific notation for the $g \to 0$ limit of the normal ordering and write

$$\widehat{\mathcal{O}}_{\vec{n}}(a) \equiv \lim_{g\to 0} \mathcal{O}_{\vec{n}}(a) = :O_{\vec{n}}(a):\,, \tag{3.33}$$

so that most of the formulas will look simpler.

In the following section we will explicitly compute the one-point functions between the Wilson loop and the chiral operators in the $\mathcal{N} = 2$ matrix model, namely

$$\mathcal{A}_{\vec{n}} = \langle\, \mathcal{W}(a)\, \mathcal{O}_{\vec{n}}(a) \,\rangle \tag{3.34}$$

which will later compare with the field theory amplitudes defined in (2.12).

4 Matrix model correlators in presence of a Wilson loop

Our main goal here is the computation of $\mathcal{A}_{\vec{n}}$ in the interacting matrix model described above. As a warming-up, but also for later applications, we begin by presenting the results in the Gaussian matrix model, *i.e.* in the $\mathcal{N} = 4$ theory.

4.1 The $\mathcal{N} = 4$ theory

In this case we should consider the operators $\widehat{\mathcal{O}}_{\vec{n}}(a)$ defined in (3.33) and compute

$$\widehat{\mathcal{A}}_{\vec{n}} = \langle\, \mathcal{W}(a)\, \widehat{\mathcal{O}}_{\vec{n}}(a) \,\rangle_0 \tag{4.1}$$

using the definition (3.17).

The simplest example is the amplitude with the identity ($\vec{n} = (0)$), which yields the vacuum expectation value of the Wilson loop operator (3.23):

$$\widehat{\mathcal{A}}_{(0)} = \langle\, \mathcal{W}(a) \,\rangle_0 = \frac{1}{N} \sum_{k=0}^{\infty} \frac{g^k}{2^{\frac{k}{2}}\, k!}\, t_k \tag{4.2}$$

with t_k defined in (3.19). Using the explicit expressions given in (3.20) and (3.22), we find

$$\widehat{\mathcal{A}}_{(0)} = 1 + g^2\, \frac{N^2-1}{8N} + g^4\, \frac{(N^2-1)(2N^2-3)}{384N^2} + g^6\, \frac{(N^2-1)(N^4-3N^2+3)}{9216N^3} + \cdots \tag{4.3}$$

This perturbative series can be resummed into

$$\widehat{\mathcal{A}}_{(0)} = \frac{1}{N}\, L^1_{N-1}\left(-\frac{g^2}{4}\right) \exp\left[\frac{g^2}{8}\left(1 - \frac{1}{N}\right)\right] \tag{4.4}$$

JHEP03(2018)193

where L_n^m is the generalized Laguerre polynomial of degree n. This is the SU(N) version of the well-known result of [2], originally derived for U(N).

Next we consider the amplitude between the Wilson loop and the operator $\widehat{\mathcal{O}}_{(2)}(a)$ at level 2. This is given by

$$\widehat{\mathcal{A}}_{(2)} = \left\langle \mathcal{W}(a) \ :\mathrm{tr}\, a^2: \right\rangle_0 = \frac{1}{N} \sum_{k=0}^{\infty} \frac{g^k}{2^{\frac{k}{2}}\, k!} \left(t_{k,2} - \frac{N^2-1}{2}\, t_k \right). \tag{4.5}$$

The recursion relations (3.22) imply

$$t_{k,2} = \left(\frac{k}{2} + \frac{N^2-1}{2} \right) t_k \,, \tag{4.6}$$

and thus the amplitude (4.5) becomes

$$\widehat{\mathcal{A}}_{(2)} = \frac{1}{N} \sum_{k=0}^{\infty} \frac{k}{2}\, \frac{g^k}{2^{\frac{k}{2}}\, k!}\, t_k = \frac{g}{2}\, \partial_g \widehat{\mathcal{A}}_{(0)} \,. \tag{4.7}$$

Expanding for small g, we get

$$\widehat{\mathcal{A}}_{(2)} = g^2\, \frac{N^2-1}{8N} + g^4\, \frac{(N^2-1)(2N^2-3)}{192N^2} + g^6\, \frac{(N^2-1)(N^4-3N^2+3)}{3072N^3} + \cdots . \tag{4.8}$$

This same procedure can be used to compute the amplitudes $\widehat{\mathcal{A}}_{\vec{n}}$ for any $\vec{n}$. The remarkable fact is that, thanks to the recursion relations (3.22), it is always possible to obtain compact expressions in terms of $\widehat{\mathcal{A}}_{(0)}$ and its derivatives that are exact, *i.e.* valid for any N and any g. For example, at level $n = 3$ we find

$$\widehat{\mathcal{A}}_{(3)} = \frac{g}{\sqrt{2}}\, \partial_g^2 \widehat{\mathcal{A}}_{(0)} - \frac{g^2}{4\sqrt{2}N}\, \partial_g \widehat{\mathcal{A}}_{(0)} - \frac{g(N^2-1)}{4\sqrt{2}N}\, \widehat{\mathcal{A}}_{(0)} \,, \tag{4.9}$$

while at level $n = 4$ we have

$$\widehat{\mathcal{A}}_{(4)} = g\, \partial_g^3 \widehat{\mathcal{A}}_{(0)} + \frac{g^2}{4N}\, \partial_g^2 \widehat{\mathcal{A}}_{(0)} + \frac{g^3 - 4gN(2N^2-3)}{16N^2}\, \partial_g \widehat{\mathcal{A}}_{(0)} + \frac{g^2(N^2-1)}{16N^2}\, \widehat{\mathcal{A}}_{(0)} \,, \tag{4.10}$$

and

$$\widehat{\mathcal{A}}_{(2,2)} = \frac{g^2}{4}\, \partial_g^2 \widehat{\mathcal{A}}_{(0)} - \frac{g}{4}\, \partial_g \widehat{\mathcal{A}}_{(0)} \,. \tag{4.11}$$

We have performed similar calculations for higher dimensional operators, but we do not report the results since they would not add much to what we have already exhibited. Instead, we point out that the lowest order term in the small g expansion of $\widehat{\mathcal{A}}_{\vec{n}}$, which we call "tree-level term", can be compactly written as

$$\begin{aligned} \widehat{\mathcal{A}}_{\vec{n}}\Big|_{\text{tree-level}} &= \frac{g^n}{N\, 2^{\frac{n}{2}}\, n!}\, R_{\vec{n}}^{b_1 \dots b_n} \left\langle \mathrm{tr}\, a^n \ :a^{b_1} \dots a^{b_n}: \right\rangle_0 \\ &= \frac{g^n}{N\, 2^{\frac{n}{2}}}\, R_{\vec{n}}^{b_1 \dots b_n}\, \mathrm{tr}\left(T^{b_1} \dots T^{b_n} \right) \end{aligned} \tag{4.12}$$

where $R_{\vec{n}}^{b_1 \dots b_n}$ is the symmetric tensor associated to the operator $O_{\vec{n}}(a)$ according to (3.24). For later convenience, in table 1 we collect the explicit expressions of $\widehat{\mathcal{A}}_{\vec{n}}\big|_{\text{tree-level}}$ for all operators up to level $n = 4$.

JHEP03(2018)193

$\vec{n}$	$\widehat{\mathcal{A}}_{\vec{n}}\big\vert_{\text{tree-level}}$
(2)	$g^2\frac{N^2-1}{8N}$
(3)	$g^3\frac{(N^2-1)(N^2-4)}{32\sqrt{2}N^2}$
(4)	$g^4\frac{(N^2-1)(N^4-6N^2+18)}{384N^3}$
(2, 2)	$g^4\frac{(N^2-1)(2N^2-3)}{192N^2}$

Table 1. The tree-level contribution to $\widehat{\mathcal{A}}_{\vec{n}}$ for operators up to order $n = 4$.

4.2 The $\mathcal{N} = 2$ superconformal theory

Let us now return to our main goal, namely the computation of the one-point amplitudes in the interacting matrix model that describes the $\mathcal{N} = 2$ superconformal theory. Comparing $\mathcal{A}_{\vec{n}}$ with the $\mathcal{N} = 4$ amplitudes $\widehat{\mathcal{A}}_{\vec{n}}$, we see two main differences:

1. the normal-ordered operators $\mathcal{O}_{\vec{n}}$ explicitly contain g-dependent terms;

2. the vacuum expectation value is computed in a g-dependent matrix model.

Both effects arise from the interaction terms of $S_{\text{int}}(a)$ given in (3.12); thus we can write

$$\mathcal{A}_{\vec{n}} = \widehat{\mathcal{A}}_{\vec{n}} + \delta\mathcal{A}_{\vec{n}} \tag{4.13}$$

with

$$\delta\mathcal{A}_{\vec{n}} = \frac{3\,\zeta(3)\,g^4}{(8\pi^2)^2}\,\mathcal{X}_{\vec{n}} - \frac{10\,\zeta(5)\,g^6}{3(8\pi^2)^3}\,\mathcal{Y}_{\vec{n}} + \cdots \tag{4.14}$$

where the ellipses stand for terms of higher transcendentality, proportional to $\zeta(7)$, $\zeta(3)^2$ and so on. The quantities $\mathcal{X}_{\vec{n}}$, $\mathcal{Y}_{\vec{n}}$ and the analogous ones at higher transcendentality depend on the coupling constant g and can be expressed using vacuum expectation values in the Gaussian model and, eventually, $\widehat{\mathcal{A}}_{(0)}$ and its derivatives in a compact way. Since $\delta\mathcal{A}_{\vec{n}}$ starts at order g^4, *i.e.* at two loops, we clearly have

$$\delta\mathcal{A}_{\vec{n}}\Big|_{\text{tree-level}} = 0 \qquad \text{and} \qquad \delta\mathcal{A}_{\vec{n}}\Big|_{1-\text{loop}} = 0 \tag{4.15}$$

for any $\vec{n}$. In the following we will restrict our analysis to the first correction $\mathcal{X}_{\vec{n}}$ for which we will provide explicit formulas in several examples.

Let us start with the Wilson loop, *i.e.* with the identity operator ($n = 0$). In this case there is no normal-ordering to do and thus the only contribution to $\mathcal{X}_{(0)}$ comes from the interactions in the matrix model. Focusing on the $\zeta(3)$-term which is proportional to $\big(\operatorname{tr} a^2\big)^2$, after some straightforward algebra we get

$$\mathcal{X}_{(0)} = -\left\langle\, \mathcal{W}(a)\,\big(\operatorname{tr} a^2\big)^2\,\right\rangle_0 + \left\langle\, \mathcal{W}(a)\,\right\rangle_0 \left\langle\, \big(\operatorname{tr} a^2\big)^2\,\right\rangle_0 . \tag{4.16}$$

JHEP03(2018)193

Evaluating the vacuum expectation values by means of the recursion relations (3.22) and expressing the results in terms of the $\mathcal{N}=4$ Wilson loop, we can rewrite the above expression as

$$\mathcal{X}_{(0)} = -\frac{g^2}{4}\,\partial_g^2\widehat{\mathcal{A}}_{(0)} - \frac{g(2N^2+1)}{4}\,\partial_g\widehat{\mathcal{A}}_{(0)}\,. \tag{4.17}$$

Using (4.4) and expanding for small g, we easily get

$$\begin{aligned}\mathcal{X}_{(0)} = &-g^2\,\frac{(N^2-1)(N^2+1)}{8N} - g^4\,\frac{(N^2-1)(2N^2-3)(N^2+2)}{192N^2}\\ &- g^6\,\frac{(N^2-1)(N^4-3N^2+3)(N^2+3)}{8N} + \cdots\,.\end{aligned} \tag{4.18}$$

Therefore, in the difference $\delta\mathcal{A}_{(0)}$ the leading term, which is a 2-loop effect induced by the g^4-part of $S_{\rm int}(a)$ proportional to $\zeta(3)$, turns out to be

$$\delta\mathcal{A}_{(0)}\Big|_{2-\text{loop}} = -g^6\,\frac{\zeta(3)}{(8\pi^2)^2}\,\frac{3(N^2-1)(N^2+1)}{8N}\,. \tag{4.19}$$

This expression has been successfully checked in [48] against an explicit perturbative 2-loop calculation in field theory.

Let us now consider the operator $\mathcal{O}_{(2)}$ at level $n=2$. In this case we have

$$\begin{aligned}\mathcal{X}_{(2)} = &-\big\langle\,\mathcal{W}(a)\,\widehat{\mathcal{O}}_{(2)}(a)\,\big(\operatorname{tr}a^2\big)^2\,\big\rangle_0 + \big\langle\,\mathcal{W}(a)\,\widehat{\mathcal{O}}_{(2)}(a)\,\big\rangle_0\,\big\langle\big(\operatorname{tr}a^2\big)^2\,\big\rangle_0\\ &+\frac{(N^2-1)(N^2+1)}{2}\,\big\langle\,\mathcal{W}(a)\,\big\rangle_0\end{aligned} \tag{4.20}$$

where the last term is due to the normal-ordering procedure in the interacting theory which indeed yields a part proportional to $(N^2-1)(N^2+1)/2$ (see (3.28)). Evaluating the vacuum expectation values, this expression becomes

$$\mathcal{X}_{(2)} = -\frac{g^3}{8}\,\partial_g^3\widehat{\mathcal{A}}_{(0)} - \frac{g^2(2N^2+7)}{8}\,\partial_g^2\widehat{\mathcal{A}}_{(0)} - \frac{5g(2N^2+1)}{8}\,\partial_g\widehat{\mathcal{A}}_{(0)}\,, \tag{4.21}$$

while its perturbative expansion is

$$\begin{aligned}\mathcal{X}_{(2)} = &-g^2\,\frac{3(N^2-1)(N^2+1)}{8N} - g^4\,\frac{(N^2-1)(2N^2-3)(N^2+2)}{48N^2}\\ &- g^6\,\frac{5(N^2-1)(N^4-3N^2+3)(N^2+3)}{3072N^3} + \cdots\,.\end{aligned} \tag{4.22}$$

The leading term tells us that the 2-loop correction to the $\mathcal{N}=2$ amplitude $\mathcal{A}_{(2)}$ is

$$\delta\mathcal{A}_{(2)}\Big|_{2-\text{loop}} = -g^6\,\frac{\zeta(3)}{(8\pi^2)^2}\,\frac{9(N^2-1)(N^2+1)}{8N}\,. \tag{4.23}$$

This procedure can be easily applied to operators of higher dimensions. For example, skipping the intermediate steps, at level $n=3$ we find

$$\begin{aligned}\mathcal{X}_{(3)} = &-g^3\,\frac{3(N^2-1)(N^2-4)(N^2+3)}{32\sqrt{2}N^2} - g^5\,\frac{(N^2-1)(N^2-4)(N^4+2N^2-8)}{128\sqrt{2}N^3}\\ &- g^7\,\frac{(N^2-1)(N^2-4)(3N^6+5N^4-35N^2+75)}{12288\sqrt{2}N^4} + \cdots\,,\end{aligned} \tag{4.24}$$

JHEP03(2018)193

$\vec{n}$	$\delta\mathcal{A}_{\vec{n}}\big\vert_{2-\text{loop}}$
(2)	$-g^6\frac{\zeta(3)}{(8\pi^2)^2}\frac{9(N^2-1)(N^2+1)}{8N}$
(3)	$-g^7\frac{\zeta(3)}{(8\pi^2)^2}\frac{9(N^2-1)(N^2-4)(N^2+3)}{32\sqrt{2}N^2}$
(4)	$-g^8\frac{\zeta(3)}{(8\pi^2)^2}\frac{(N^2-1)(N^6+2N^4-18N^2+81)}{32N^3}$
(2, 2)	$-g^8\frac{\zeta(3)}{(8\pi^2)^2}\frac{3(N^2-1)(2N^2-3)(N^2+3)}{32N^2}$

Table 2. The 2-loop contribution to the difference $\delta\mathcal{A}_{\vec{n}}$ between the $\mathcal{N}=2$ and the $\mathcal{N}=4$ amplitudes for operators up to order $n=4$.

while at level $n=4$ we get

$$\begin{aligned}\mathcal{X}_{(4)} = &-g^4\,\frac{(N^2-1)(N^6+2N^4-18N^2+81)}{96N^3}\\ &-g^6\frac{(N^2-1)(2N^8+5N^6-41N^4+270N^2-486)}{3072N^4}\\ &-g^8\,\frac{(N^2-1)(2N^{10}+9N^8-53N^6+270N^4-960N^2+1710)}{122880N^5}+\cdots,\end{aligned}\tag{4.25}$$

and

$$\begin{aligned}\mathcal{X}_{(2,2)} = &-g^4\,\frac{(N^2-1)(2N^2-3)(N^2+3)}{32N^2}-g^6\frac{(N^2-1)(7N^2+27)(N^4-3N^2+3)}{1536N^3}\\ &-g^8\,\frac{(N^2-1)(4N^2+19)(2N^6-8N^4+15N^2-15)}{61440N^4}+\cdots.\end{aligned}\tag{4.26}$$

Multiplying the leading terms in these expansions by $\frac{3\zeta(3)\,g^4}{(8\pi^2)^2}$, we obtain the 2-loop corrections to the amplitudes $\mathcal{A}_{\vec{n}}$, whose explicit expressions are collected in table 2 for all operators up to dimension $n=4$.

It should be clear by now that this procedure can be used to find $\mathcal{X}_{\vec{n}}$ for any $\vec{n}$, and also that it can be straightforwardly generalized to obtain the exact expressions of the corrections with higher transcendentality, like for example $\mathcal{Y}_{\vec{n}}$ in (4.14). Of course, the resulting formulas become longer and longer when one goes higher and higher in n or in transcendentality; however this approach, which is essentially based on the use of the recursion relations (3.22), provides a systematic way to obtain exact expressions to any desired order.

4.3 The large-N limit

We now study the behavior of the matrix model amplitudes in the planar limit $N\to\infty$ with the 't Hooft coupling

$$\lambda = g^2N\tag{4.27}$$

kept fixed. We begin with the $\mathcal{N}=4$ theory and later turn to the superconformal $\mathcal{N}=2$ model.

JHEP03(2018)193

$\vec{n}$	Expansion of $g^{n-2\ell}\,\widehat{\mathcal{A}}_{\vec{n}}\big\vert_{\text{planar}}$	Exact expression of $g^{n-2\ell}\,\widehat{\mathcal{A}}_{\vec{n}}\big\vert_{\text{planar}}$
(2)	$\frac{\lambda}{8}+\frac{\lambda^2}{96}+\frac{\lambda^3}{3072}+\cdots$	$I_2\big(\sqrt{\lambda}\big)$
(3)	$\frac{\lambda^2}{32\sqrt{2}}+\frac{\lambda^3}{512\sqrt{2}}+\frac{\lambda^4}{20480\sqrt{2}}+\cdots$	$\frac{3\sqrt{\lambda}}{2\sqrt{2}}\,I_3\big(\sqrt{\lambda}\big)$
(4)	$\frac{\lambda^3}{384}+\frac{\lambda^4}{7680}+\frac{\lambda^5}{368640}+\cdots$	$\lambda\,I_4\big(\sqrt{\lambda}\big)$
(2, 2)	$\frac{\lambda^2}{96}+\frac{\lambda^3}{1536}+\frac{\lambda^4}{61440}+\cdots$	$\frac{\sqrt{\lambda}}{2}\,I_3\big(\sqrt{\lambda}\big)$

Table 3. Results for the $\mathcal{N}=4$ matrix model in the planar limit. As explained in the text, n is the sum of the components of $\vec{n}$ while ℓ is the number of these components.

The $\mathcal{N}=4$ theory. Taking the planar limit of the expectation value of the Wilson loop, from (4.3) we get

$$\widehat{\mathcal{A}}_{(0)}\Big\vert_{\text{planar}}=1+\frac{\lambda}{8}+\frac{\lambda^2}{192}+\frac{\lambda^3}{9216}+\cdots=\frac{2}{\sqrt{\lambda}}\,I_1\big(\sqrt{\lambda}\big) \tag{4.28}$$

where I_n is the modified Bessel function of the first kind. This is a well-known and established result [1].

Next, let us consider the amplitude between the Wilson loop and the operator at level $n=2$ given in (4.8). In the planar limit it becomes

$$\widehat{\mathcal{A}}_{(2)}\Big\vert_{\text{planar}}=\frac{\lambda}{8}+\frac{\lambda^2}{96}+\frac{\lambda^3}{3072}+\cdots=I_2\big(\sqrt{\lambda}\big)\,. \tag{4.29}$$

Also this is a known result [9].

Proceeding systematically in this way and using the explicit results in the Gaussian matrix model, it is not difficult to find the weak-coupling expansion of the amplitude $\widehat{\mathcal{A}}_{\vec{n}}$ in the planar limit for a generic operator, and also to obtain its exact resummation in terms of Bessel functions. Indeed, for a generic vector $\vec{n}$ one can show that

$$g^{n-2\ell}\,\widehat{\mathcal{A}}_{\vec{n}}\Big\vert_{\text{planar}}=\frac{\big(\sqrt{\lambda}\big)^{n-\ell-1}}{2^{\frac{n}{2}+\ell-1}}\,I_{n-\ell+1}\big(\sqrt{\lambda}\big)\prod_{i=1}^{\ell}n_i \tag{4.30}$$

where n is, as usual, the sum of the components of $\vec{n}$ (see (2.5)), while ℓ is the number of these components, namely the number of traces that appear in the corresponding operator. We have verified the validity of this formula by explicitly computing the planar limit of the amplitudes between the Wilson loop and all operators up to dimension $n=7$. In table 3 we collect our results up to level $n=4$. We point out that for $\ell=1$, *i.e.* for the single trace operators, our formula (4.30) agrees with the findings of [9].

JHEP03(2018)193

$\vec{n}$	Expansion of the $\zeta(3)$-term of $g^{n-2\ell}\,\delta\mathcal{A}_{\vec{n}}\big\vert_{\text{planar}}$	Exact expression of the $\zeta(3)$-term of $g^{n-2\ell}\,\delta\mathcal{A}_{\vec{n}}\big\vert_{\text{planar}}$
(2)	$-\frac{3\,\zeta(3)\,\lambda^2}{(8\pi^2)^2}\left(\frac{3\lambda}{8}+\frac{4\lambda^2}{96}+\frac{5\lambda^3}{3072}+\cdots\right)$	$-\frac{3\,\zeta(3)\,(\sqrt{\lambda})^5}{2(8\pi^2)^2}\left(I_1\big(\sqrt{\lambda}\big)+\frac{2}{\sqrt{\lambda}}I_2\big(\sqrt{\lambda}\big)\right)$
(3)	$-\frac{3\,\zeta(3)\,\lambda^2}{(8\pi^2)^2}\left(\frac{3\lambda^2}{32\sqrt{2}}+\frac{4\lambda^3}{512\sqrt{2}}+\frac{5\lambda^4}{20480\sqrt{2}}+\cdots\right)$	$-\frac{9\,\zeta(3)\,\lambda^3}{4\sqrt{2}(8\pi^2)^2}\,I_2\big(\sqrt{\lambda}\big)$
(4)	$-\frac{3\,\zeta(3)\,\lambda^2}{(8\pi^2)^2}\left(\frac{4\lambda^3}{384}+\frac{5\lambda^4}{7680}+\frac{6\lambda^5}{368640}+\cdots\right)$	$-\frac{3\,\zeta(3)\,(\sqrt{\lambda})^7}{2(8\pi^2)^2}\,I_3\big(\sqrt{\lambda}\big)$
(2, 2)	$-\frac{3\,\zeta(3)\,\lambda^2}{(8\pi^2)^2}\left(\frac{6\lambda^2}{96}+\frac{7\lambda^3}{1536}+\frac{8\lambda^4}{61440}+\cdots\right)$	$-\frac{3\,\zeta(3)\,\lambda^3}{4(8\pi^2)^2}\left(I_2\big(\sqrt{\lambda}\big)+\frac{6}{\sqrt{\lambda}}I_3\big(\sqrt{\lambda}\big)\right)$

Table 4. Results for the $\mathcal{N}=2$ superconformal matrix model in the planar limit. As before, n is the sum of the components of $\vec{n}$ while ℓ is their number.

The $\mathcal{N}=2$ superconformal theory. Multiplying (4.16) by $\frac{3\,\zeta(3)\,g^4}{(8\pi^2)^2}$ and then taking the large N limit, it is straightforward to obtain[2]

$$\delta\mathcal{A}_{(0)}\Big\vert_{\text{planar}}=-\frac{3\,\zeta(3)\,\lambda^2}{(8\pi^2)^2}\left(\frac{\lambda}{8}+\frac{2\lambda^2}{192}+\frac{3\lambda^3}{9216}+\cdots\right)+\cdots=-\frac{3\,\zeta(3)\,\lambda^2}{(8\pi^2)^2}\,I_2\big(\sqrt{\lambda}\big)+\cdots \tag{4.31}$$

where the last ellipses stand for terms of higher transcendentality.

In a similar way, from (4.22) we easily get

$$\delta\mathcal{A}_{(2)}\Big\vert_{\text{planar}}=-\frac{3\,\zeta(3)\,\lambda^2}{(8\pi^2)^2}\left(\frac{3\lambda}{8}+\frac{4\lambda^2}{96}+\frac{5\lambda^3}{3072}+\cdots\right)+\cdots\,. \tag{4.32}$$

It is interesting to observe that if one compares this expression with the expansion of the planar limit of the $\mathcal{N}=4$ amplitude $\widehat{\mathcal{A}}_{(2)}$ given in (4.29), one sees that each term of the latter proportional to λ^k gets multiplied by

$$-\frac{3\,\zeta(3)\,\lambda^2}{(8\pi^2)^2}\,(k+2)\,. \tag{4.33}$$

As we will see in section 5, this fact has a simple and nice diagrammatic interpretation. The expansion (4.32) can be resummed in terms of modified Bessel functions as follows

$$\delta\mathcal{A}_{(2)}\Big\vert_{\text{planar}}=-\frac{3\,\zeta(3)\,(\sqrt{\lambda})^5}{2(8\pi^2)^2}\left(I_1\big(\sqrt{\lambda}\big)+\frac{2}{\sqrt{\lambda}}I_2\big(\sqrt{\lambda}\big)\right)+\cdots\,. \tag{4.34}$$

Taking into account the different normalization of the operator $\mathcal{O}_{(2)}(a)$ we have used, our result agrees with [46].

Proceeding in this way and using (4.24)–(4.26), it is not difficult to obtain the weak-coupling expansions of $\delta\mathcal{A}_{(3)}$, $\delta\mathcal{A}_{(4)}$ and $\delta\mathcal{A}_{(2,2)}$ in the planar limit, and eventually their exact expressions. In table 4 we have collected our findings for the terms proportional to $\zeta(3)$ in $\delta\mathcal{A}_{\vec{n}}$ for all operators up to dimension $n=4$.

[2]See also [51].

JHEP03(2018)193

From these explicit results it is possible to infer the following general formula

$$g^{n-2\ell}\,\delta\mathcal{A}_{\vec{n}}\Big|_{\text{planar}} = -\frac{3\,\zeta(3)}{(8\pi^2)^2}\,\frac{\left(\sqrt{\lambda}\right)^{n-\ell+4}}{2^{\frac{n}{2}+\ell}}\left\{\left[I_{n-\ell}\big(\sqrt{\lambda}\big)+\frac{2(\ell-1)}{\sqrt{\lambda}}\,I_{n-\ell+1}\big(\sqrt{\lambda}\big)\right]\prod_{k=1}^{\ell}n_k\right.$$
$$\left.+\quad\left(\sum_{i=1}^{\ell}\delta_{n_i,2}\right)\frac{2}{\sqrt{\lambda}}\,I_{n-\ell+1}\big(\sqrt{\lambda}\big)\prod_{k=1}^{\ell}n_k\right\}+\cdots \tag{4.35}$$

which we have verified in all cases up to $n = 7$. We observe that there is a contribution, represented by the second line above, which occurs only when the operator $\mathcal{O}_{\vec{n}}(a)$ contains at least a factor of the type $\operatorname{tr} a^2$. This fact has a precise diagrammatic counterpart, as we will see in the next section.

Comparing the two exact expressions (4.35) and (4.30) and using the properties of the modified Bessel functions, it is not difficult to realize that

$$g^{n-2\ell}\,\delta\mathcal{A}_{\vec{n}}\Big|_{\text{planar}} = -\frac{3\,\zeta(3)\,\lambda^2}{(8\pi^2)^2}\left(\lambda\,\frac{\partial}{\partial\lambda}+\ell+\sum_{i=1}^{\ell}\delta_{n_i,2}\right)\left(g^{n-2\ell}\,\widehat{\mathcal{A}}_{\vec{n}}\Big|_{\text{planar}}\right)+\cdots \tag{4.36}$$

where, as usual, the ellipses stand for terms of higher transcendentality. Such a relation implies that if we multiply each term λ^k in the weak-coupling expansion of $g^{n-2\ell}\,\widehat{\mathcal{A}}_{\vec{n}}\big|_{\text{planar}}$ by

$$-\frac{3\,\zeta(3)\,\lambda^2}{(8\pi^2)^2}\left(k+\ell+\sum_{i=1}^{\ell}\delta_{n_i,2}\right), \tag{4.37}$$

then we obtain the expansion of the $\zeta(3)$-correction of the corresponding $\mathcal{N}=2$ planar amplitude $g^{n-2\ell}\,\delta\mathcal{A}_{\vec{n}}\big|_{\text{planar}}$. Also this formula, which generalizes (4.33) to any $\vec{n}$, has a simple and nice interpretation in terms of field theory diagrams, as we will see in the next section.

5 Perturbative checks in field theory

We now consider the direct field theory computation of the expectation values of chiral operators with a circular BPS Wilson loop in a superconformal $\mathcal{N}=2$ theory defined on $\mathbb{R}^4$.

As explained in section 2, conformal invariance implies that all information about these expectation values is contained in the amplitudes $A_{\vec{n}}$ defined in (2.12). The conjecture we want to test is that these amplitudes match the corresponding ones $\mathcal{A}_{\vec{n}}$ in the matrix model that we introduced in (3.34), namely we want to show that

$$A_{\vec{n}} = \mathcal{A}_{\vec{n}}\,. \tag{5.1}$$

The diagrammatic evaluation in field theory of the correlators $A_{\vec{n}}$ beyond tree-level is in general quite complicated. However, it becomes tractable if one only computes the difference between the $\mathcal{N}=2$ result and the one we would have in the $\mathcal{N}=4$ theory. This is the same strategy utilized in [48] to check the matrix model expression (4.19) for the $\mathcal{N}=2$ Wilson loop itself, as well as in [47] to compute chiral-antichiral two-point functions in absence of Wilson loops. We now briefly recall the main steps of this approach.

JHEP03(2018)193

We first split the $\mathcal{N}=2$ action as:

$$S^{(N_f)}_{\mathcal{N}=2} = S_{\text{gauge}} + S_Q\,, \tag{5.2}$$

separating the pure gauge term, S_{gauge}, with the $\mathcal{N}=2$ vector multiplet from the matter term, S_Q, which contains N_f hypermultiplets Q in the fundamental representation of the gauge group. Then, we view the $\mathcal{N}=4$ vector multiplet as a combination of a $\mathcal{N}=2$ vector with an adjoint $\mathcal{N}=2$ hypermultiplet H; in this way the $\mathcal{N}=4$ SYM action can be written as:

$$S_{\mathcal{N}=4} = S_{\text{gauge}} + S_H\,, \tag{5.3}$$

so that

$$S^{(N_f)}_{\mathcal{N}=2} = S_{\mathcal{N}=4} + S_Q - S_H\,. \tag{5.4}$$

All terms in the right hand side of (5.4) have a well-established $\mathcal{N}=1$ superfield formulation, which allows us to easily write down the Feynman rules in configuration space. For this we refer to section 3.1 of [47], whose notations and conventions we consistently use in the following.

From (5.4) we deduce that any correlator $A_{\vec{n}}$ of the $\mathcal{N}=2$ theory can be written as:

$$A_{\vec{n}} = \widehat{A}_{\vec{n}} + A_{\vec{n},Q} - A_{\vec{n},H} \tag{5.5}$$

where $\widehat{A}_{\vec{n}}$ is the correlator in the $\mathcal{N}=4$ theory, while $A_{\vec{n},H}$ and $A_{\vec{n},Q}$ are the contributions from diagrams in which the adjoint hypermultiplet H and the fundamental hypermultiplets Q run in the internal lines. Therefore the difference between the $\mathcal{N}=2$ and the $\mathcal{N}=4$ amplitudes is

$$\delta A_{\vec{n}} = A_{\vec{n}} - \widehat{A}_{\vec{n}} = A_{\vec{n},Q} - A_{\vec{n},H}\,. \tag{5.6}$$

Performing this diagrammatic difference in the perturbative field theory computations leads to remarkable simplifications, since all diagrams without Q or H internal lines do not need to be considered.

Starting from this set up, what we shall check, up to two loops, is in fact the following equality:

$$\delta A_{\vec{n}} = \delta\mathcal{A}_{\vec{n}}\,, \tag{5.7}$$

where $\delta\mathcal{A}_{\vec{n}}$ is the difference between the $\mathcal{N}=2$ and $\mathcal{N}=4$ matrix model results introduced in (4.13).

5.1 Tree-level

At the lowest order in g the $\mathcal{N}=2$ and $\mathcal{N}=4$ amplitudes coincide:

$$A_{\vec{n}}\Big|_{\text{tree-level}} = \widehat{A}_{\vec{n}}\Big|_{\text{tree-level}}\,; \tag{5.8}$$

in other words,

$$\delta A_{\vec{n}}\Big|_{\text{tree-level}} = 0\,. \tag{5.9}$$

Also in the matrix model this difference vanishes at the lowest order, see (4.15). Thus, the equality (5.7) is satisfied at tree level.

JHEP03(2018)193

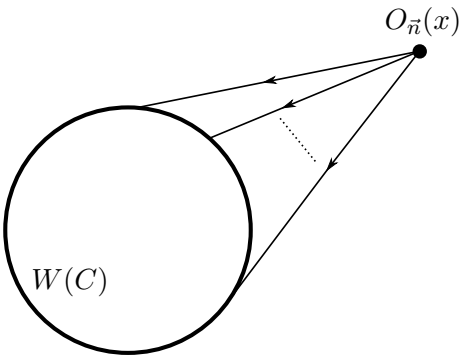

Figure 2. At the lowest perturbative order, the operator $O_{\vec{n}}(x)$ is connected to the Wilson loop by n scalar propagators. Exploiting conformal invariance, we can place the operator in the origin, *i.e.* in the center of the Wilson loop. Nevertheless, in this and in the following pictures we will continue to place it outside the loop to avoid graphical clutter.

Actually, in this case it is easy (and also convenient for later purposes) to check directly the validity of (5.1). Performing this check is helpful also to establish some facts that will be useful at higher orders; in particular, the way the path-ordered integration over the Wilson loop simplifies in the tree-level case will be exploited also in the two-loop order computations. Thus, for later convenience we briefly show some details. At the lowest order in g, the n chiral fields φ appearing in the operator $O_{\vec{n}}$ must be contracted with the n antichiral fields present in the term of order n in the expansion on the Wilson loop operator (2.3). This is represented by the diagram in figure 2.

Thus, we have

$$\left\langle W(C)\, O_{\vec{n}}(0)\right\rangle\Big|_{\text{tree-level}} = \frac{1}{N}\,\frac{g^n}{n!}\left\langle \mathcal{P}\,\mathrm{tr}\left(\prod_{i=1}^{n}\oint_C d\tau_i\,\frac{R}{\sqrt{2}}\,\bar\varphi(x_i)\right) O_{\vec{n}}(0)\right\rangle \tag{5.10}$$

where we have denoted by $x_i = x(\tau_i)$ the positions along the Wilson loop C. Using (2.7), we rewrite this expression as

$$\begin{aligned}\left\langle W(C)\, O_{\vec{n}}(0)\right\rangle\Big|_{\text{tree-level}} = \frac{1}{N}\,\frac{g^n\,R^n}{2^{\frac{n}{2}}\,n!}\,\mathcal{P}\prod_{i=1}^{n}\oint_C d\tau_i\,\mathrm{tr}\left(T^{a_1}\cdots T^{a_n}\right) R_{\vec{n}}^{b_1\ldots b_n}\\ \times\left\langle\bar\varphi^{a_1}(x_1)\cdots\bar\varphi^{a_n}(x_n)\,\varphi^{b_1}(0)\cdots\varphi^{b_n}(0)\right\rangle.\end{aligned} \tag{5.11}$$

The vacuum expectation value in the second line above is computed using the free scalar propagator

$$\left\langle\bar\varphi^a(x_i)\,\varphi^b(0)\right\rangle = \frac{\delta^{ab}}{4\pi^2\,x_i^2} = \frac{\delta^{ab}}{4\pi^2 R^2} \tag{5.12}$$

where we have exploited the fact that $x_i = x(\tau_i)$ belongs to the circle C of radius R and thus can be parameterized as in (2.9). In view of this, when we apply Wick's theorem in (5.11) we obtain an integrand that does not depend on the variables τ_i. The path ordering becomes therefore irrelevant and, from the integration over τ_i, we simply get a factor of $(2\pi)^n$. Moreover the $n!$ different contraction patterns all yield the same expression,

JHEP03(2018)193

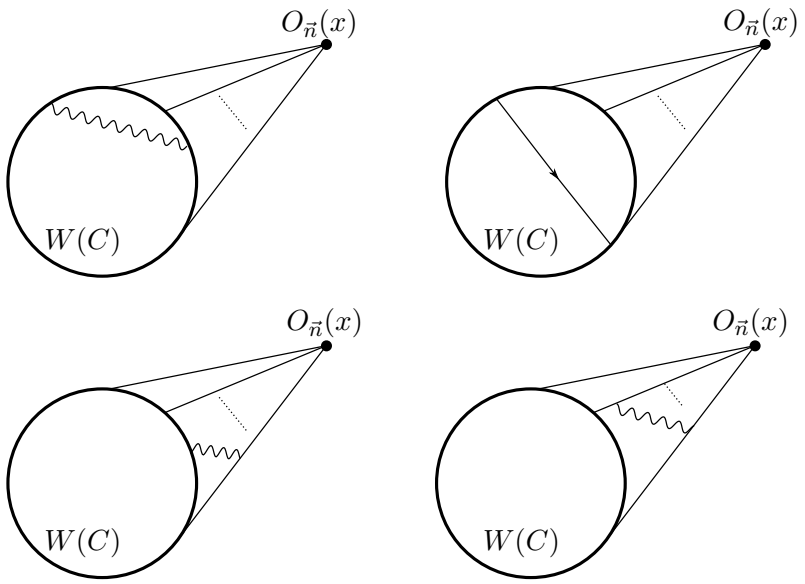

Figure 3. Diagrams which do not contain interaction vertices including H or Q hypermultiplets and which therefore vanish in the difference between the $\mathcal{N}=2$ and the $\mathcal{N}=4$ theory. Here there are some examples of diagrams which appear at order g^2 with respect to the tree-level amplitude $A_{\vec{n}}$, but vanish in the difference $\delta A_{\vec{n}}$.

due to the symmetry of the tensor $R_{\vec{n}}$. Taking all this into account, we get

$$\langle\, W(C)\, O_{\vec{n}}(0)\,\rangle\Big|_{\text{tree-level}} = \frac{1}{N}\,\frac{g^n}{2^{\frac{n}{2}}}\,\frac{1}{(2\pi R)^n}\,R_{\vec{n}}^{b_1\dots b_n}\,\mathrm{tr}\left(T_{b^1}\dots T^{b_n}\right), \tag{5.13}$$

which implies that

$$A_{\vec{n}}\Big|_{\text{tree-level}} = \widehat{A}_{\vec{n}}\Big|_{\text{tree-level}} = \frac{g^n}{N\,2^{\frac{n}{2}}}\,R_{\vec{n}}^{b_1\dots b_n}\,\mathrm{tr}\left(T^{b_1}\dots T^{b_n}\right), \tag{5.14}$$

in full agreement with the matrix model result (4.12).

5.2 Loop corrections

At higher orders in g we concentrate on the difference $\delta A_{\vec{n}}$. As we already pointed out, the number of diagrams which contribute to this difference is massively reduced. For example, all diagrams represented in figure 3 yield a g^2 correction with respect to the tree-level amplitude $A_{\vec{n}}$ but they should not be considered in the computation of $\delta A_{\vec{n}}$ since they do not contain internal lines with H or Q hypermultiplets.

One loop. It is easy to see that in the $\mathcal{N}=2$ superconformal theory there are no corrections of order g^2 with respect to the tree-level result. In fact, at this order the only possible diagrams containing H and Q hypermultiplets arise from the one-loop correction of the external scalar propagators as shown in figure 4. This one-loop correction is due to the two diagrams represented in figure 5. Using the Feynman rules and conventions spelled out in detail in [47], one can easily see that the sum of these two diagrams is proportional to

$$N_f\,\mathrm{tr}\left(T^b T^a\right) - \left(\mathrm{i}\,f^{bcd}\right)\left(\mathrm{i}\,f^{adc}\right) = \left(\frac{N_f}{2} - N\right)\delta^{ab}, \tag{5.15}$$

JHEP03(2018)193

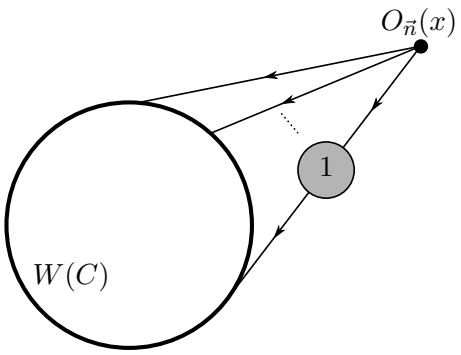

Figure 4. The only diagrams that yield a g^2 correction to the tree-level amplitude $A_{\vec{n}}$ and contain Q and H hypermultiplets arise from the one-loop correction of the external scalar propagators.

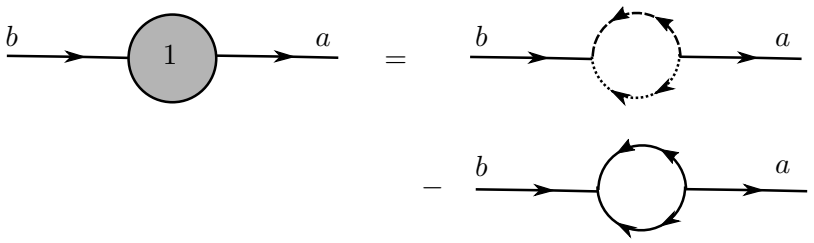

Figure 5. The one-loop correction to the scalar propagator. The first diagram on the right hand side is the Q-contribution due the fundamental hypermultiplets; the second diagram is the H-contribution due the adjoint hypermultiplet and so it comes with a minus sign.

which vanishes for $N_f = 2N$. Therefore, in the superconformal $\mathcal{N} = 2$ theory we have

$$\delta A_{\vec{n}}\Big|_{1-\text{loop}} = 0\,, \tag{5.16}$$

in full agreement with the matrix model result (see (4.15)).

Two loops. Let us now consider the two-loop corrections, *i.e.* those at order g^4 with respect to the tree-level amplitudes, and focus on the difference $\delta A_{\vec{n}}$. The H or Q diagrams which contribute at this order can be divided into two classes. The first one is formed by those diagrams which contain a sub-diagram with the one-loop correction to the scalar propagator, or to the gluon propagator or to the 3-point vertex. Some examples of such diagrams are shown in figure 6. All these diagrams vanish in the $\mathcal{N} = 2$ superconformal theory. Indeed, both the one-loop correction to the gluon propagator and the one-loop correction to the 3-point vertex are proportional to $(N_f - 2N)$, just like the one-loop correction to the scalar propagator as we have seen in (5.15)

The second class of diagrams that can contribute to $\delta A_{\vec{n}}$ at two loops in the superconformal theory are those of the type displayed in figure 7. They contain either the irreducible two-loop correction of the scalar propagator represented in figure 8, or the two-loop effective vertex represented in figure 9. Thus, we can write

$$\delta A_{\vec{n}}\Big|_{2-\text{loop}} = I_{\vec{n}} + J_{\vec{n}} \tag{5.17}$$

where $I_{\vec{n}}$ and $J_{\vec{n}}$ correspond, respectively, to the diagrams of type (**i**) and (**j**).

JHEP03(2018)193

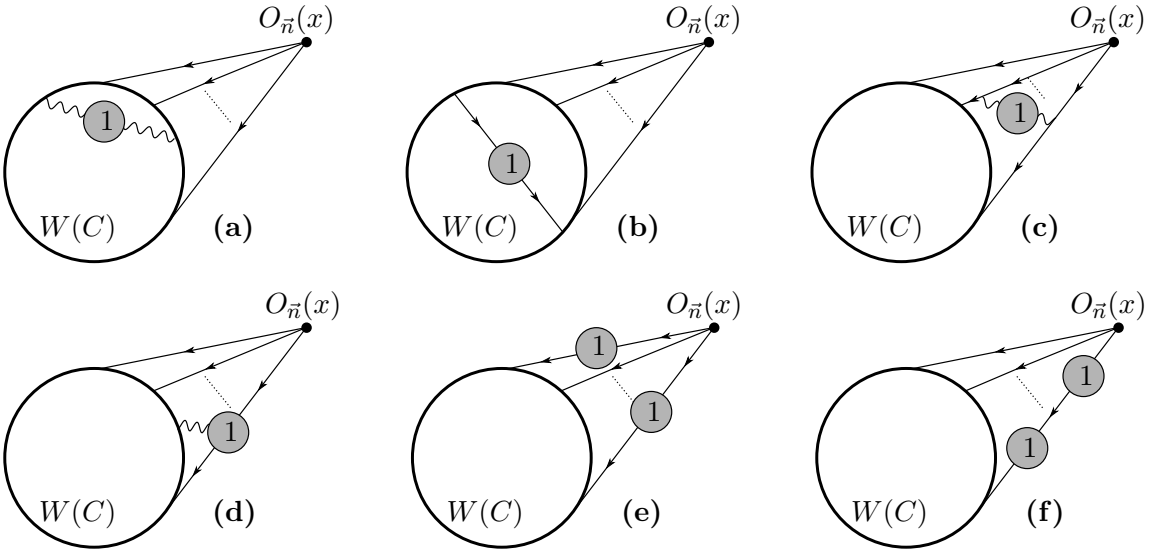

Figure 6. Some examples of diagrams contributing to $\delta A_{\vec{n}}$ at two loops. Diagrams (**a**) and (**c**) contain the one-loop correction of the gluon propagator, diagram (**d**) contains the one-loop correction to the 3-point vertex, while diagrams (**b**), (**e**) and (**f**) contain the one-loop correction to the scalar propagator. All these diagrams vanish in the superconformal theory since they are proportional to $(N_f - 2N)$. Beside these, one should also consider the one-loop diagrams of figure 3 in which one of the external scalar propagators is corrected at one loop. Also such diagrams vanish in the superconformal theory.

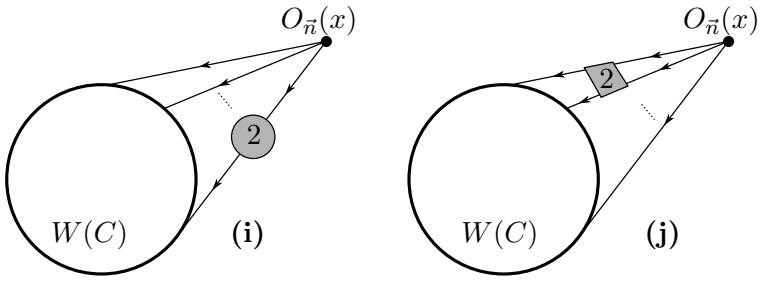

Figure 7. Diagrams that contribute to $\delta A_{\vec{n}}$ at two loops in the $\mathcal{N} = 2$ superconformal theory. Diagram (**i**) on the left contains the irreducible two-loop correction of the scalar propagator represented in figure 8, while diagram (**j**) on the right contains the two-loop effective vertex depicted in figure 9.

Let us first consider the irreducible two-loop correction[3] of the scalar propagator drawn in figure 8. In configuration space this correction has been computed in [47] to which we refer for details, and the result is[4]

$$-8\, g^4\, C_2^{ba}\, W_2(x_1, x_2) \tag{5.18}$$

[3]Notice that in the superconformal theory the only diagrams that contribute to the scalar propagator at two loops are those represented in figure 8. Indeed, all other two-loop diagrams that correct the propagators are proportional to $(N_f - 2N)$.

[4]See eq. (3.24) of [47].

JHEP03(2018)193

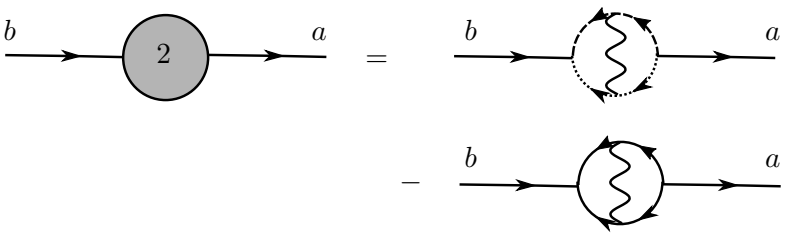

Figure 8. The irreducible two-loop correction to the scalar propagator in the $\mathcal{N}=2$ superconformal theory. The first diagram on the right hand side is the Q-contribution involving the fundamental hypermultiplets, while the second diagram is the H-contribution due to the adjoint hypermultiplet which therefore comes with a minus sign.

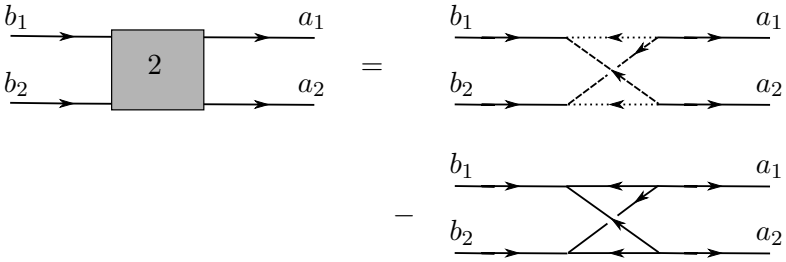

Figure 9. The two-loop effective vertex that can contribute to the amplitude $A_{\vec{n}}$ in the $\mathcal{N}=2$ superconformal theory. The first diagram on the right hand side is the Q-contribution involving the fundamental hypermultiplets, while the second diagram is the H-contribution due to the adjoint hypermultiplet and thus comes with a minus sign.

where the colour factor is

$$\begin{aligned} C_2^{ba} &= N_f \,\mathrm{tr}\left(T^b T^c T^a T^c\right) - f^{bd_4d_1}\, f^{cd_1d_2}\, f^{ad_2d_3}\, f^{cd_3d_4} \\ &= -\Big(\frac{N_f}{2N} + N^2\Big)\mathrm{tr}\left(T^b T^a\right) = -\frac{N^2+1}{2}\,\delta^{ab}\,, \end{aligned} \tag{5.19}$$

while the superspace integral yields

$$W_2(x_1,x_2) = -\frac{3\,\zeta(3)}{(16\pi^2)^2}\,\frac{1}{4\pi^2(x_1-x_2)^2}\,. \tag{5.20}$$

Putting everything together, we find that the two-loop correction of the scalar propagator is

$$-\,g^4\,\frac{3\,\zeta(3)}{(8\pi^2)^2}\left[\frac{\delta^{ab}}{4\pi^2(x_1-x_2)^2}\right](N^2+1) \tag{5.21}$$

where the expression in square brackets is the tree-level propagator. Therefore, when we compute the amplitude $I_{\vec{n}}$ corresponding to the diagram (**i**) of figure 7, we simply obtain an expression which is proportional to the tree-level result (5.14). Indeed we get

$$I_{\vec{n}} = -n\,g^4\,\frac{3\,\zeta(3)}{(8\pi^2)^2}\left[\frac{g^n}{N\,2^{\frac{n}{2}}}\,R_{\vec{n}}^{b_1\ldots b_n}\,\mathrm{tr}\left(T^{b_1}\ldots T^{b_n}\right)\right](N^2+1) \tag{5.22}$$

JHEP03(2018)193

where the overall factor of n is due to the fact that the two-loop correction (5.21) can be inserted in any of the n external propagators.

Let us now consider the two-loop diagram (**j**) of figure 7. To compute the corresponding amplitude $J_{\vec{n}}$, we have to perform all contractions as in the tree-level diagram but with two scalar propagators replaced by the sub-structure corresponding to the two-loop effective vertex of figure 9. The latter has been analyzed in [47] to which we refer again for details. Considering that the two external legs with colour indices b_1 and b_2 are inserted at the point x where the operator $O_{\vec{n}}$ is located, and the other two external legs with indices a_1 and a_2 are inserted at two points x_1 and x_2 on the circular Wilson loop, the relevant expression is[5]

$$2\, g^4\, C_4^{b_1 b_2 a_1 a_2}\, W_4(x, x; x_1, x_2) \tag{5.23}$$

where the colour factor is

$$\begin{aligned} C_4^{b_1 b_2 a_1 a_2} &= N_f \,\mathrm{tr}\left(T^{b_1} T^{a_1} T^{b_2} T^{a_2}\right) - f^{b_1 d_4 d_1}\, f^{a_1 d_1 d_2}\, f^{b_2 d_2 d_3}\, f^{a_2 d_3 d_4} \\ &= -\frac{1}{2}\left(\delta^{b_1 a_1}\,\delta^{b_2 a_2} + \delta^{b_1 b_2}\,\delta^{a_1 a_2} + \delta^{b_1 a_2}\,\delta^{b_2 a_1}\right), \end{aligned} \tag{5.24}$$

while the superspace integral leads to

$$W_4(x, x; x_1, x_2) = \frac{6\,\zeta(3)}{(16\pi^2)^2}\left[\frac{1}{4\pi^2 (x - x_1)^2}\,\frac{1}{4\pi^2 (x - x_2)^2}\right]. \tag{5.25}$$

As is clear from the expression in square brackets, we still recover the same space dependence of two scalar propagators as in the tree-level computation, even if the colour structure of the C_4 tensor is different. Exploiting conformal invariance to set $x = 0$ and recalling the parametrization (2.9) for points on a circle, the above square brackets simply becomes $1/(2\pi R)^4$; thus the path-ordering and the integration over the Wilson loop become trivial to perform, just as they were in the tree-level amplitude. Putting everything together and replacing any pair of external scalar propagators with this effective two-loop vertex in all possible ways, we obtain

$$\begin{aligned} J_{\vec{n}} = g^4\, \frac{3\,\zeta(3)}{(8\pi^2)^2}\, &\left[\frac{g^n}{N\, 2^{\frac{n}{2}}}\, R_{\vec{n}}^{b_1 \ldots b_n}\,\mathrm{tr}\left(T^{a_1} \ldots T^{a_n}\right)\right] \\ &\times 2 \sum_{p \in S_{n-1}} C_4^{b_1 b_2 a_{p(1)} a_{p(2)}}\, \delta^{b_3 a_{p(3)}} \ldots \delta^{b_{n-1} a_{p(n-1)}}\, \delta^{b_n a_n} \end{aligned} \tag{5.26}$$

where $p \in S_{n-1}$ are the permutations of $(n-1)$ elements. We observe that the $1/n!$ coming from the expansion of the Wilson loop operator at order g^n is compensated by a factor of $n!$ that arises when we take into account the complete symmetry of the tensor $R_{\vec{n}}$ and the cyclic symmetry of the trace factor in the square bracket. Furthermore the factor of 2 in the last line of (5.26) is a combinatorial factor due to the multiplicity of the two-loop box diagram of figure 9.

[5] See eq. (3.33) of [47].

JHEP03(2018)193

Summing $I_{\vec{n}}$ and $J_{\vec{n}}$, we get

$$\delta A_{\vec{n}}\Big|_{2-\text{loop}} = -g^4\,\frac{3\,\zeta(3)}{(8\pi^2)^2}\left[\frac{g^n}{N\,2^{\frac{n}{2}}}\,R_{\vec{n}}^{b_1\ldots b_n}\,\mathrm{tr}\left(T^{a_1}\ldots T^{a_n}\right)\right] \tag{5.27}$$
$$\times\left[n\,(N^2{+}1)\,\delta^{b_1a_1}\ldots\delta^{b_na_n} - 2\sum_{p\in S_{n-1}} C_4^{b_1b_2a_{p(1)}a_{p(2)}}\,\delta^{b_3a_{p(3)}}\ldots\delta^{b_{n-1}a_{p(n-1)}}\,\delta^{b_na_n}\right].$$

This is the final result of our diagrammatic computation of the two-loop correction to the amplitude $A_{\vec{n}}$ in the $\mathcal{N}=2$ superconformal theory.

As an example, we work out the explicit expression for the lowest dimensional operator $O_{(2)}$. In this case, we simply have

$$R_{(2)}^{b_1b_2} = \mathrm{tr}\left(T^{b_1}T^{b_2}\right) = \frac{1}{2}\,\delta^{b_1b_2}\,. \tag{5.28}$$

Thus, the contribution from the diagram (**i**) is (see (5.22)):

$$I_{(2)} = -2\,g^4\,\frac{3\,\zeta(3)}{(8\pi^2)^2}\left[\frac{g^2}{2\,N}\,\frac{(N^2-1)}{4}\right](N^2+1)\,, \tag{5.29}$$

while from the diagram (**j**) we get (see (5.26)):

$$J_{(2)} = -g^4\,\frac{3\,\zeta(3)}{(8\pi^2)^2}\left[\frac{g^2}{2\,N}\,\frac{(N^2-1)}{4}\right](N^2+1)\,. \tag{5.30}$$

Note that in this case both diagrams (**i**) and (**j**) provide colour contributions with the same leading power of N. This is a specific feature of this operator and it does not hold for higher dimensional operators unless they contain a factor of $\mathrm{tr}\,\phi^2$ (see appendix B where we discuss the cases corresponding to $\vec{n}=(4)$ and $\vec{n}=(2,2)$ in which this property is clearly exhibited). This fact will have important consequences for the planar limit as we will see in the following subsection. Summing (5.29) and (5.30), we finally get

$$\delta A_{(2)}\Big|_{2-\text{loop}} = -g^6\,\frac{\zeta(3)}{(8\pi^2)^2}\,\frac{9(N^2-1)(N^2+1)}{8N}\,, \tag{5.31}$$

in perfect agreement with the matrix model result (4.23).

We have explicitly performed similar checks for many operators of higher dimension and always found a precise match between the field theory expression (5.27) and the matrix model results summarized in table 2, thus confirming the validity of (5.7) up to two loops. The details of the calculation in the cases $\vec{n}=(4)$ and $\vec{n}=(2,2)$ are given in appendix B.

5.3 Planar limit

All the above checks are easily extended in the planar limit by keeping the highest power of N and performing the substitution $g^2N=\lambda$. In this limit the number of diagrams which contribute to the correlator is drastically reduced, and thus such checks can be pushed to higher orders in perturbation theory without much effort. Let us first review the well-known $\mathcal{N}=4$ case [9–11].

JHEP03(2018)193

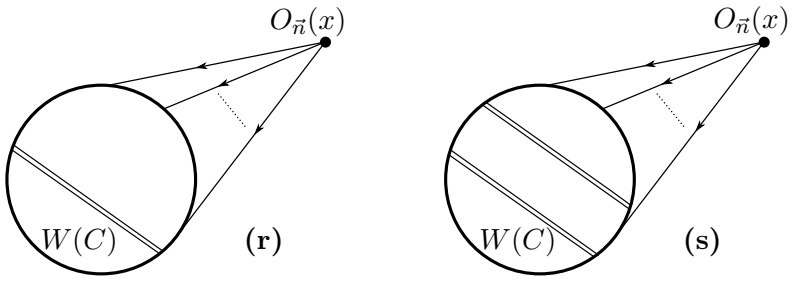

Figure 10. In the planar limit of the $\mathcal{N}=4$ theory, the tree-level expression encoded in figure 2 gets corrected only by the so-called "rainbow" diagrams, the first two of which are represented here. We have used a double line to denote the sum of the gluon and the scalar propagator, which always occur together when attached to the Wilson loop and yield the simple expression given in (5.35).

The $\mathcal{N}=4$ theory. At leading order, using the tree-level result (5.14) that corresponds to the diagram of figure 2, one easily finds

$$g^{n-2\ell}\,\widehat{A}_{\vec{n}}\Big|_{\text{tree-level,planar}} = \lim_{N\to\infty}\frac{g^{2n-2\ell}}{N\,2^{\frac{n}{2}}}\,R_{\vec{n}}^{b_1\ldots b_n}\,\mathrm{tr}\left(T^{b_1}\ldots T^{b_n}\right) = c_{\vec{n},0}\,\lambda^{n-\ell} \tag{5.32}$$

where $c_{\vec{n},0}$ are numerical coefficients which can be deduced from table 1. In particular we have:

$$c_{(2),0} = \frac{1}{8}\,,\quad c_{(3),0} = \frac{1}{32\sqrt{2}}\,,\quad c_{(4),0} = \frac{1}{384}\,,\quad c_{(2,2),0} = \frac{1}{96}\,. \tag{5.33}$$

In [9] it was argued that all diagrams with internal vertices cancel at the next order and it was conjectured that analogous cancellations should occur at all orders in perturbation theory. Thus, only the "rainbow" diagrams of the type represented in figure 10 contribute to the amplitude $\widehat{A}_{\vec{n}}$ in the planar limit.

The evaluation of these "rainbow" diagrams is particularly simple in the case of a circular Wilson loop. Indeed, if we denote by $w^a(x)$ the combination of gluons and scalars that appears inside the path-ordered exponential in (2.3), namely

$$w^a(x) = \mathrm{i}\,A_\mu^a(x)\,\dot{x}^\mu + \frac{R}{\sqrt{2}}\Big(\varphi^a(x) + \bar{\varphi}^a(x)\Big) \tag{5.34}$$

with x being a point on the circle C, then we have

$$\left\langle w^a(x_1)\,w^b(x_2)\right\rangle = \frac{\delta^{ab}}{4\pi^2}\,\frac{1-\dot{x_1}\cdot\dot{x_2}}{(x_1-x_2)^2} = \frac{\delta^{ab}}{8\pi^2 R^2} \tag{5.35}$$

where in the last step we have used the parameterization (2.9). Thus, the contribution of the internal propagators, represented by double lines in figure 10, is constant and similar to the one of the external scalar propagators (see (5.12)) so that only combinatorial coefficients have to be computed. For example, the diagram (**r**) yields a contribution of the form

$$c_{\vec{n},1}\,\lambda^{n-\ell+1} \tag{5.36}$$

with

$$c_{(2),1} = \frac{1}{96}\,,\quad c_{(3),1} = \frac{1}{512\sqrt{2}}\,,\quad c_{(4),1} = \frac{1}{7680}\,,\quad c_{(2,2),1} = \frac{1}{1536}\,. \tag{5.37}$$

JHEP03(2018)193

Similarly, the diagram (**s**) leads to

$$c_{\vec{n},2}\,\lambda^{n-\ell+2} \tag{5.38}$$

with

$$c_{(2),2}=\frac{1}{3072}\,,\quad c_{(3),2}=\frac{1}{24480\sqrt{2}}\,,\quad c_{(4),2}=\frac{1}{368640}\,,\quad c_{(2,2),2}=\frac{1}{61440}\,. \tag{5.39}$$

From these results it is possible to infer the following resummed expression

$$g^{n-2\ell}\,\widehat{A}_{\vec{n}}\Big|_{\text{planar}}=\sum_{j=0}^{\infty}c_{\vec{n},j}\,\lambda^{n-\ell+j}=\frac{\big(\sqrt{\lambda}\big)^{n-\ell-1}}{2^{\frac{n}{2}+\ell-1}}\,I_{n-\ell+1}\big(\sqrt{\lambda}\big)\prod_{i=1}^{\ell}n_i \tag{5.40}$$

which agrees with the matrix model result (4.30).

The $\mathcal{N}=2$ theory. In this case we focus on the planar limit of the difference $\delta A_{\vec{n}}$ and in particular on the terms proportional to $\zeta(3)$. To obtain the result at the lowest order, one simply has to take the two-loop result (5.27) and evaluate it in the large-N limit. As we have seen in the previous subsection, there are two types of terms: one corresponding to the diagram (**i**) of figure 7 and one corresponding to the diagram (**j**), which arise from the two-loop contributions depicted, respectively, in figure 8 and 9. The correction to the scalar propagator gives rise to a contribution that always survives in the planar; in fact in (5.21) it was proved to be proportional to $g^4(N^2+1)$, which in the planar limit reduces to λ^2. On the other hand, the two-loop effective vertex does not always contribute in the planar limit, since it is leading for $N\to\infty$ only when it is attached to $\operatorname{tr}\varphi^2$. This can be realized by noticing that in this case such a diagram, because of (5.24), always produces the structure

$$\operatorname{tr}\big(T^{b_1}T^{b_2}\big)\delta^{b_1b_2}\,\delta^{a_1a_2}=\frac{1}{2}(N^2-1)\delta^{a_1a_2}\,, \tag{5.41}$$

with the N^2 factor making the contribution leading. Thus, the diagrams of type (**i**) always contribute in the planar limit, while the diagrams of type (**j**) are sub-leading unless some of the components of the vector $\vec{n}$ are equal to 2. This fact can be checked in the explicit computations for $O_{(2)}$ (see (5.29) and (5.30)) and for $O_{(4)}$ and $O_{(2,2)}$ reported in appendix B. These simple considerations give a nice field theory interpretation to some of the matrix model results presented in section 4.3.

Building on the idea that all diagrams with internal vertices cancel at all orders in perturbation theory, like in the $\mathcal{N}=4$ model [9], one can construct a class of $\zeta(3)$-proportional diagrams, starting from the $\mathcal{N}=4$ "rainbow" diagrams and performing on them one of the aforementioned planar two-loop corrections. This can be done either by correcting one of the external scalar propagators, or by correcting one of the internal double-line propagators[6] or by including the two-loop effective vertex if $O_{\vec{n}}$ contains at least a factor $\operatorname{tr}\varphi^2$. The result of performing any of these corrections is always equal to the original $\mathcal{N}=4$ "rainbow" diagram multiplied by $-\frac{3\zeta(3)\,\lambda^2}{(8\pi^2)^2}$. This analysis tells us how to get the $\mathcal{N}=2$ correction proportional to $\zeta(3)$ in the planar limit starting from the $\mathcal{N}=4$ amplitude. In

[6] Since these internal propagators and the scalar propagators are proportional to each other (see (5.35) and (5.12)), also their planar two-loop corrections are proportional.

JHEP03(2018)193

fact, expanding (5.40) for small λ, the term of order k corresponds to a sum over "rainbow" diagrams with $(k-n+\ell)$ internal propagators and n external ones. Using the method we just described, any such diagram can be corrected once for every internal propagator, once for every external propagator and once for every factor $\operatorname{tr}\varphi^2$ appearing in $O_{\vec{n}}$, giving a total of

$$(k-n+\ell)+n+\sum_{i=1}^{\ell}\delta_{n_i,2}=k+\ell+\sum_{i=1}^{\ell}\delta_{n_i,2} \tag{5.42}$$

corrections proportional to $-\frac{3\,\zeta(3)\,\lambda^2}{(8\pi^2)^2}$. This result precisely matches the matrix model expression (4.37) and suggests that this class of diagrams reconstructs the full $\zeta(3)$-term of the $\mathcal{N}=2$ correlator at all orders in perturbation theory, just like the "rainbow" diagrams make up the full $\mathcal{N}=4$ correlator.

6 Conclusions

We have verified up to two loops in the $\mathcal{N}=2$ superconformal theory that the one-point amplitude $\mathcal{A}_{\vec{n}}$ of a chiral operator in presence of a circular Wilson loop computed using the matrix model exactly matches the amplitude $A_{\vec{n}}$ computed using standard field theory methods with (super) Feynman diagrams. We have also discussed the planar limit of the amplitudes and found a perfect agreement between the two approaches also in this case. We have performed our checks in many examples with operators of dimensions up to $n=7$, even if here we have explicitly reported our results only for the low-dimensional operators up to $n=4$ for brevity.

We would like to remark that in order to obtain this agreement, an essential ingredient on the matrix model side is the g-dependent normal ordering of the chiral operators introduced in [47]. This normal ordering prescription is equivalent to the Gram-Schmidt orthogonalization algorithm discussed in [44] and later in [43, 45, 46, 52] in both $\mathcal{N}=4$ and $\mathcal{N}=2$ cases. In the $\mathcal{N}=4$ theory, however, this procedure actually does not introduce any g-dependence, while in the $\mathcal{N}=2$ examples considered so far in the literature, the g-dependent terms of the normal-ordered operators could not be really tested since they affect only higher-loop subleading terms which have not been computed. This is the case, for instance, of the two-point functions of chiral operators investigated in [44] for the superconformal theory, or in [47] for the superconformal theory and for a special class of operators in the non-conformal case. On the contrary, for the one-point functions in presence of a Wilson loop that we have studied in this paper, such g-dependence already shows up at two loops, and thus its crucial role for the agreement with the field theory results could be tested in our two-loop calculations.

Several extensions and generalizations are possible. For example, one could compute the one-point functions of chiral operators in presence of Wilson loops that are more general than the circular one we have considered and that preserve a smaller amount of supersymmetry. Another interesting possibility would be to study the two-point functions in presence of a Wilson loop (as in [53]) and see what kind of information could be extracted from the matrix model in this case. An even more challenging development would be to

JHEP03(2018)193

consider non-conformal $\mathcal{N}=2$ theories [54] and check whether also in this case the matrix model can be used to obtain the field theory amplitudes. As is clear from our discussion in section 3, there is no obstruction to define and compute amplitudes in non-conformal $\mathcal{N}=2$ theories. One simply has to take into account the fact that several cancellations do not occur any longer when $N_f \neq 2N$ and thus more terms have to be considered. On the field theory side, instead, one has deal with delicate issues related to the renormalization of the coupling constant, of the wave-function and of the composite operators, and also to the appearance of a dynamically generated scale at the quantum level. We believe that making some progress in this direction would be very interesting since the matrix model approach is technically much more amenable than the diagrammatic one and allows one to obtain results at high perturbative orders in a more efficient way.

Acknowledgments

We thank M. Frau, F. Fucito, R.R. John, G. Korchemski, E. Lauria, L. Magnea and J.F. Morales for many useful discussions.

The work of M.B. and A.L. is partially supported by the MIUR PRIN Contract 2015 MP2CX4 "Non-perturbative Aspects Of Gauge Theories And Strings".

A One-point functions from defect conformal field theory

In a conformal field theory, the functional form of the one-point function of a conformal operator $O(x)$ in presence of a circular defect $W(C)$ of radius R is completely determined. One way to obtain this form is to use the embedding formalism, in which a point $x \in \mathbb{R}^4$ is associated in a projective way to a null section P in the embedding space $\mathbb{M}^{1,5}$ of the form

$$P = \left(\frac{R^2 + x^2}{2R}, \frac{R^2 - x^2}{2R}, x^\mu \right), \tag{A.1}$$

which satisfies $P^2 \equiv P^T \eta\, P = 0$ with $\eta = \mathrm{diag}(-1,1,1,1,1,1)$. Scalar operators $O(x)$ of dimension Δ are associated to operators $\hat{O}(P)$ which are homogeneous of degree Δ, namely such that $\widehat{O}(\lambda P) = \lambda^{-\Delta}\, \widehat{O}(P)$.

In absence of defects, the conformal group $\mathrm{SO}(1,5)$ is the isometry group of the embedding space and acts linearly on P. In presence of the Wilson loop, we can split the spacetime coordinates into "parallel" and "transverse" ones: $x^\mu \to (x^a, x^i)$, where $a = 1,2$ and $i = 3,4$. We will denote $x^a x_a = r^2$ and $x^i x_i = L^2$, so that $x^2 = r^2 + L^2$. The symmetry is reduced according to the pattern

$$\mathrm{SO}(1,5) \to \mathrm{SO}(1,2) \times \mathrm{SO}(3)\,, \tag{A.2}$$

with $\mathrm{SO}(1,2)$ and $\mathrm{SO}(3)$ linearly acting, respectively, on

$$P_\parallel = \left(\frac{R^2 + x^2}{2R}, x^a \right) \quad \text{and} \quad P_\perp = \left(\frac{R^2 - x^2}{2R}, x^i \right). \tag{A.3}$$

JHEP03(2018)193

There are two scalar products invariant with respect to the two symmetry factors, which we denote as

$$P \bullet P \equiv P_\parallel^T \eta\, P_\parallel \quad \text{with } \eta = \mathrm{diag}(-1,1,1) \qquad \text{and} \qquad P \circ P \equiv P_\perp^T\, P_\perp \,. \tag{A.4}$$

They are not independent, since $P \bullet P + P \circ P = P^2 = 0$. Therefore, we can take as the single independent invariant the quantity

$$\|x\|_C \equiv 2\sqrt{P \circ P} = \frac{\sqrt{(R^2 - x^2)^2 - 4R^2 L^2}}{R} \,. \tag{A.5}$$

The one-point function $\langle\, W(C) O(x) \,\rangle = \langle\, W(C)\, \widehat{O}(P) \,\rangle$ must depend on $\|x\|_C$, and must be homogeneous of degree Δ in it; thus it must necessarily be of the form

$$\langle\, W(C)\, \widehat{O}(P) \,\rangle = \frac{A_O}{(2\pi \|x\|_C)^\Delta} \,. \tag{A.6}$$

The 2π factor is inserted for convenience and the constant A_O is related to the value of the correlator at $x = 0$, *i.e.* at $P = P_0 = (\frac{R}{2}, \frac{R}{2}, \vec{0})$ where $\|x\|_C \to R$, so that

$$\langle\, W(C)\, \widehat{O}(P_0) \,\rangle = \frac{A_O}{(2\pi R)^\Delta} \,. \tag{A.7}$$

B Calculation of $\delta A_{(4)}$ and $\delta A_{(2,2)}$ at two loops

We provide some details for the calculation of the color factor in the amplitude $\delta A_{(4)}$ and $\delta A_{(2,2)}$ at two loops.

$\delta A_{(4)}$ at two loops. When $\vec{n} = (4)$, the tensor $R_{(4)}$ associated to the chiral operator $O_{(4)}$ can be written as a normalized sum over all permutations of the generators in $\mathrm{tr}\left(T^{b_1} T^{b_2} T^{b_3} T^{b_4}\right)$, up to cyclic rearrangements, namely (see also footnote 1)

$$R_{(4)}^{b_1 b_2 b_3 b_4} = \frac{1}{4!}\, 4 \sum_{p \in S_3} \mathrm{tr}\left(T^{b_{p(1)}} T^{b_{p(2)}} T^{b_{p(3)}} T^{b_4}\right) . \tag{B.1}$$

Using this, we can easily compute the tree-level amplitude $A_{(4)}\big|_{\text{tree-level}}$ given in (5.14):

$$A_{(4)}\Big|_{\text{tree-level}} = \frac{g^4}{4N}\, \mathrm{tr}\left(T^{b_1} T^{b_2} T^{b_3} T^{b_4}\right) R_{(4)}^{b_1 b_2 b_3 b_4} \,. \tag{B.2}$$

Using the explicit form (B.1), one can realize that $\mathrm{tr}\left(T^{b_1} T^{b_2} T^{b_3} T^{b_4}\right) R_{(4)}^{b_1 b_2 b_3 b_4}$ contains six terms that have three different structures. The first one is

$$\begin{aligned} &\frac{1}{6}\, \mathrm{tr}\left(T^{b_1} T^{b_2} T^{b_3} T^{b_4}\right) \mathrm{tr}\left(T^{b_1} T^{b_2} T^{b_3} T^{b_4}\right) \\ &\quad = \frac{1}{6}\left[\frac{1}{8}\left(d^{b_1 b_2 e} + \mathrm{i} f^{b_1 b_2 e}\right)\left(d^{b_3 b_4 e} + \mathrm{i} f^{b_3 b_4 e}\right) + \frac{1}{4N}\, \delta^{b_1 b_2} \delta^{b_3 b_4}\right]^2 \\ &\quad = \frac{(N^2-1)(N^2+3)}{96 N^2} \end{aligned} \tag{B.3}$$

where the last equality follows from the group theory identities in appendix C. The second type of structure is

$$\begin{aligned}
&\frac{1}{6}\,\mathrm{tr}\left(T^{b_1}T^{b_2}T^{b_3}T^{b_4}\right)\mathrm{tr}\left(T^{b_2}T^{b_1}T^{b_3}T^{b_4}\right)\\
&\quad=\frac{1}{6}\left[\frac{(N^2-1)(N^2+3)}{16N^2}+\mathrm{i}f^{b_2b_1c}\,\mathrm{tr}\left(T^cT^{b_3}T^{b_4}\right)\mathrm{tr}\left(T^{b_1}T^{b_2}T^{b_3}T^{b_4}\right)\right]\\
&\quad=-\frac{(N^2-1)(N^2-3)}{96N^2}\,.
\end{aligned}\tag{B.4}$$

Up to relabeling of the indices, we have four such terms. Finally, the third structure is

$$\begin{aligned}
&\frac{1}{6}\,\mathrm{tr}\left(T^{b_1}T^{b_2}T^{b_3}T^{b_4}\right)\mathrm{tr}\left(T^{b_3}T^{b_2}T^{b_1}T^{b_4}\right)\\
&\quad=\frac{1}{6}\left[-\frac{(N^2-1)(N^2-3)}{16N^2}+\mathrm{i}f^{b_4b_3c}\,\mathrm{tr}\left(T^cT^{b_2}T^{b_1}\right)\mathrm{tr}\left(T^{b_1}T^{b_2}T^{b_3}T^{b_4}\right)\right]\\
&\quad=\frac{(N^2-1)(N^4-3N^2+3)}{96N^2}\,.
\end{aligned}\tag{B.5}$$

Summing these contributions and plugging the result in (B.2), we get

$$A_{(4)}\Big|_{\text{tree-level}}=g^4\frac{(N^2-1)(N^4-6N^2+18)}{384N^3}\,,\tag{B.6}$$

which precisely matches the matrix model expression reported in the last-but-one row of table 1.

Now let us consider the two-loop correction $\delta A_{(4)}\big|_{2-\text{loop}}$. From (5.27), we have

$$\begin{aligned}
\delta A_{(4)}\Big|_{2-\text{loop}}=&-g^4\,\frac{3\zeta(3)}{(8\pi^2)^2}\left[\frac{g^4}{4N}\,R_{(4)}^{b_1b_2b_3b_4}\,\mathrm{tr}\left(T^{a_1}T^{a_2}T^{a_3}T^{a_4}\right)\right]\\
&\times\left[4\,(N^2+1)\,\delta^{b_1a_1}\,\delta^{b_2a_2}\,\delta^{b_3a_3}\,\delta^{b_4a_4}-2\sum_{p\in S_3}C_4^{\,b_1b_2a_{p(1)}a_{p(2)}}\,\delta^{b_3a_{p(3)}}\,\delta^{b_4a_4}\right].
\end{aligned}\tag{B.7}$$

The first term in the square brackets, which corresponds to the sub-amplitude $I_{(4)}$ associated to the diagram (**i**) of figure 7, is proportional to the tree-level result (B.6) and is given by

$$I_{(4)}=-g^4\,\frac{\zeta(3)}{(8\pi^2)^2}\left[g^4\frac{(N^2-1)(N^2+1)(N^4-6N^2+18)}{32N^3}\right].\tag{B.8}$$

The second term in the square brackets of (B.7), corresponding to the sub-amplitude $J_{(4)}$ associated to the diagram (**j**) of figure 7, is a bit lengthy to compute, since it is no more proportional to the tree-level expression (B.6). However, looking at the explicit form of the tensor C_4 which we rewrite here for convenience

$$C_4^{\,b_1b_2a_1a_2}=-\frac{1}{2}\left(\delta^{b_1a_1}\,\delta^{b_2a_2}+\delta^{b_1a_2}\,\delta^{b_2a_1}+\delta^{b_1b_2}\,\delta^{a_1a_2}\right),\tag{B.9}$$

we can realize that

$$\frac{g^4}{4N}\,R_{(4)}^{b_1b_2b_3b_4}\,\mathrm{tr}\left(T^{a_1}T^{a_2}T^{a_3}T^{a_4}\right)\delta^{b_1a_{p(1)}}\,\delta^{b_2a_{p(2)}}\,\delta^{b_3a_{p(3)}}\delta^{b_4a_4}=A_{(4)}\Big|_{\text{tree-level}}\tag{B.10}$$

JHEP03(2018)193

for any permutation $p \in S_3$, thanks to the symmetry of $R_{(4)}$. Thus, the first two terms of C_4 produce color structures that are proportional to the tree-level one for each permutation p. We can therefore write

$$J_{(4)} = -g^4 \frac{3\,\zeta(3)}{(8\pi^2)^2} \Bigg[12\, A_{(4)}\Big|_{\text{tree-level}} + \frac{g^4}{4N} R_{(4)}^{b_1b_2b_3b_4} \operatorname{tr}\left(T^{a_1}T^{a_2}T^{a_3}T^{a_4}\right) \sum_{p\in S_3} \delta^{b_1 b_2}\, \delta^{a_{p(1)}a_{p(2)}}\, \delta^{b_3 a_{p(3)}}\, \delta^{b_4 a_4} \Bigg] . \tag{B.11}$$

The last term must be computed explicitly. To do so we use the fact that

$$R_{(4)}^{aabc} = \frac{2N^2-3}{12N}\,\delta^{bc}\,, \tag{B.12}$$

so that

$$\begin{aligned} J_{(4)} &= -g^4 \frac{3\,\zeta(3)}{(8\pi^2)^2} \Bigg[12\, A_{(4)}\Big|_{\text{tree-level}} + \frac{g^4}{4N} \frac{2N^2-3}{12N} \Big(4 \operatorname{tr}\left(T^aT^aT^bT^b\right) + 2\operatorname{tr}\left(T^aT^bT^aT^b\right)\Big) \Bigg] \\ &= -g^8 \frac{3\,\zeta(3)}{(8\pi^2)^2} \frac{1}{4N} \left[\frac{(N^2-1)(N^4-6N^2+18)}{8N^2} + \frac{(N^2-1)(2N^2-3)^2}{24N^2} \right] \\ &= -g^8 \frac{\zeta(3)}{(8\pi^2)^2} \frac{(N^2-1)(7N^4-30N^2+63)}{32N^3}\,. \end{aligned} \tag{B.13}$$

Notice that in the large-N limit, $J_{(4)}$ is subleading with respect to $I_{(4)}$. Summing the two contributions, we find that the total amplitude $\delta A_{(4)}\big|_{2-\text{loops}}$ is

$$\delta A_{(4)}\Big|_{2-\text{loops}} = I_{(4)} + J_{(4)} = -g^8 \frac{\zeta(3)}{(8\pi^2)^2} \frac{(N^2-1)(N^6+2N^4-18N^2+81)}{32N^3} \tag{B.14}$$

which exactly matches the matrix model expression reported in the last-but-one row of table 2.

$\delta A_{(2,2)}$ at two loops. In a similar way we perform the computation for the other 4-dimensional operator, namely $O_{(2,2)}$, defined by the tensor

$$R_{(2,2)}^{b_1b_2b_3b_4} = \frac{1}{4!}\, 4 \sum_{p\in S_3} \operatorname{tr}\left(T^{b_{p(1)}}T^{b_{p(2)}}\right) \operatorname{tr}\left(T^{b_{p(3)}}T^{b_4}\right) = \frac{1}{12}\left(\delta^{b_1b_2}\delta^{b_3b_4} + \delta^{b_1b_3}\delta^{b_2b_4} + \delta^{b_2b_3}\delta^{b_1b_4}\right). \tag{B.15}$$

Then, from (5.14) the tree-level amplitude:

$$\begin{aligned} A_{(2,2)}\Big|_{\text{tree-level}} &= \frac{g^4}{4N} \operatorname{tr}\left(T^{b_1}T^{b_2}T^{b_3}T^{b_4}\right) R_{(2,2)}^{b_1b_2b_3b_4} \\ &= \frac{g^4}{4N} \frac{1}{12} \left[2 \operatorname{tr}\left(T^aT^aT^bT^b\right) + \operatorname{tr}\left(T^aT^bT^aT^b\right)\right] \\ &= \frac{g^4}{4N} \frac{(N^2-1)(2N^2-3)}{48N}\,. \end{aligned} \tag{B.16}$$

JHEP03(2018)193

We can see that this matches the matrix model expression reported in the last row of table 1.

Let us then consider the two-loop correction $\delta A_{(2,2)}\big|_{2-\text{loop}}$. According to (5.27):

$$\delta A_{(2,2)}\Big|_{2-\text{loop}} = -g^4\,\frac{3\,\zeta(3)}{(8\pi^2)^2}\,\left[\frac{g^4}{4N}\,R^{b_1b_2b_3b_4}_{(2,2)}\,\text{tr}\left(T^{a_1}T^{a_2}T^{a_3}T^{a_4}\right)\right] \times\left[4\,(N^2+1)\,\delta^{b_1a_1}\,\delta^{b_2a_2}\,\delta^{b_3a_3}\,\delta^{b_4a_4} - 2\sum_{p\in S_3} C_4^{\,b_1b_2a_{p(1)}a_{p(2)}}\,\delta^{b_3a_{p(3)}}\,\delta^{b_4a_4}\right]. \tag{B.17}$$

The first term in the square brackets of the last line, which corresponds to the diagram of type (**i**) in figure 7, is manifestly proportional to the tree-level result (B.16) and is given by

$$I_{(2,2)} = -g^4\,\frac{\zeta(3)}{(8\pi^2)^2}\left[g^4\frac{(N^2-1)(N^2+1)(2N^2-3)}{16N^2}\right]. \tag{B.18}$$

The second term of the last line of (B.17) corresponds to the sub-amplitude $J_{(2,2)}$ associated to the diagram of type (**j**) in figure 7. Exploiting the symmetry properties of C_4 and $R_{(2,2)}$, we can immediately write it as

$$J_{(2,2)} = -g^4\,\frac{3\,\zeta(3)}{(8\pi^2)^2}\left[12\,A_{(2,2)}\Big|_{\text{tree-level}} + \frac{g^4}{4N}\,R^{b_1b_2b_3b_4}_{(2,2)}\,\text{tr}\left(T^{a_1}T^{a_2}T^{a_3}T^{a_4}\right)\sum_{p\in S_3}\delta^{b_1b_2}\,\delta^{a_{p(1)}a_{p(2)}}\,\delta^{b_3a_{p(3)}}\,\delta^{b_4a_4}\right]. \tag{B.19}$$

Differently from $J_{(4)}$, the form of

$$R^{aabc}_{(2,2)} = \frac{N^2+1}{12}\,\delta^{bc} \tag{B.20}$$

implies that also $J_{(2,2)}$ is proportional to the tree-level amplitude. Indeed,

$$\begin{aligned} J_{(2,2)} &= -g^4\,\frac{3\,\zeta(3)}{(8\pi^2)^2}\left[12\,+2\,(N^2+1)\right]A_{(2,2)}\Big|_{\text{tree-level}} \\ &= -g^4\,\frac{\zeta(3)}{(8\pi^2)^2}\left[g^4\frac{(N^2-1)(N^2+7)(2N^2-3)}{32N^2}\right]. \end{aligned} \tag{B.21}$$

We explicitly notice that in this case both $I_{(2,2)}$ and $J_{(2,2)}$ contribute to the leading order in the large-N limit. In total we get:

$$\delta A_{(2,2)}\Big|_{2-\text{loops}} = I_{(2,2)} + J_{(2,2)} = -g^8\,\frac{\zeta(3)}{(8\pi^2)^2}\,\frac{3\,(N^2-1)(2N^2-3)(N^2+3)}{32N^2} \tag{B.22}$$

which matches the matrix model expression reported in the last row of table 2.

JHEP03(2018)193

C Group theory identities

Here we collect some group theory formulas that are useful to perform explicit calculations and check our results. We take the generators T^a of SU(N) to be Hermitean and normalized as

$$\mathrm{tr}\left(T^a T^b\right) = \frac{1}{2}\,\delta^{ab}\,, \tag{C.1}$$

and define the structure constants f^{abc} by

$$\left[T^a\,,\,T^b\right] = \mathrm{i}\,f^{abc}\,T^c\,, \tag{C.2}$$

and the d^{abc}-symbols by

$$\left\{T^a\,,\,T^b\right\} = \frac{1}{N}\,\delta^{ab} + d^{abc}\,T^c\,. \tag{C.3}$$

Then one has

$$\mathrm{tr}\left(T^a T^b T^c\right) = \frac{1}{4}\left(d^{abc} + \mathrm{i}\,f^{abc}\right), \tag{C.4}$$

$$\mathrm{tr}\left(T^a T^b T^c T^d\right) = \frac{1}{8}\left(d^{abe} + \mathrm{i}\,f^{abe}\right)\left(d^{cde} + \mathrm{i}\,f^{cde}\right) + \frac{1}{4N}\,\delta^{ab}\,\delta^{cd}\,, \tag{C.5}$$

and

$$f^{abe}\,f^{cde} = \frac{2}{N}\left(\delta^{ac}\,\delta^{bd} + \delta^{ad}\,\delta^{bc}\right) + d^{ace}\,d^{bde} - d^{ade}\,d^{bce}\,, \tag{C.6}$$

$$d^{abc}\,d^{abd} = \frac{N^2-4}{N}\,\delta^{dc}\,, \tag{C.7}$$

$$f^{abc}\,f^{abd} = N\,\delta^{dc}\,, \tag{C.8}$$

$$f^{abc}\,d^{abd} = 0\,. \tag{C.9}$$

References

[1] J.K. Erickson, G.W. Semenoff and K. Zarembo, *Wilson loops in $N = 4$ supersymmetric Yang-Mills theory*, *Nucl. Phys.* **B 582** (2000) 155 [hep-th/0003055] [INSPIRE].

[2] N. Drukker and D.J. Gross, *An Exact prediction of $N = 4$ SUSYM theory for string theory*, *J. Math. Phys.* **42** (2001) 2896 [hep-th/0010274] [INSPIRE].

[3] V. Pestun, *Localization of gauge theory on a four-sphere and supersymmetric Wilson loops*, *Commun. Math. Phys.* **313** (2012) 71 [arXiv:0712.2824] [INSPIRE].

[4] K. Zarembo, *Supersymmetric Wilson loops*, *Nucl. Phys.* **B 643** (2002) 157 [hep-th/0205160] [INSPIRE].

[5] N. Drukker, *1/4 BPS circular loops, unstable world-sheet instantons and the matrix model*, *JHEP* **09** (2006) 004 [hep-th/0605151] [INSPIRE].

[6] N. Drukker, S. Giombi, R. Ricci and D. Trancanelli, *Wilson loops: From four-dimensional SYM to two-dimensional YM*, *Phys. Rev.* **D 77** (2008) 047901 [arXiv:0707.2699] [INSPIRE].

JHEP03(2018)193

[7] N. Drukker, S. Giombi, R. Ricci and D. Trancanelli, *More supersymmetric Wilson loops*, *Phys. Rev.* **D 76** (2007) 107703 [arXiv:0704.2237] [INSPIRE].

[8] N. Drukker, S. Giombi, R. Ricci and D. Trancanelli, *Supersymmetric Wilson loops on S^3*, *JHEP* **05** (2008) 017 [arXiv:0711.3226] [INSPIRE].

[9] G.W. Semenoff and K. Zarembo, *More exact predictions of SUSYM for string theory*, *Nucl. Phys.* **B 616** (2001) 34 [hep-th/0106015] [INSPIRE].

[10] V. Pestun and K. Zarembo, *Comparing strings in $AdS_5 \times S^5$ to planar diagrams: An Example*, *Phys. Rev.* **D 67** (2003) 086007 [hep-th/0212296] [INSPIRE].

[11] G.W. Semenoff and D. Young, *Exact 1/4 BPS Loop: Chiral primary correlator*, *Phys. Lett.* **B 643** (2006) 195 [hep-th/0609158] [INSPIRE].

[12] S. Giombi and V. Pestun, *Correlators of local operators and 1/8 BPS Wilson loops on S^2 from 2d YM and matrix models*, *JHEP* **10** (2010) 033 [arXiv:0906.1572] [INSPIRE].

[13] S. Giombi and V. Pestun, *Correlators of Wilson Loops and Local Operators from Multi-Matrix Models and Strings in AdS*, *JHEP* **01** (2013) 101 [arXiv:1207.7083] [INSPIRE].

[14] A. Bassetto, L. Griguolo, F. Pucci, D. Seminara, S. Thambyahpillai and D. Young, *Correlators of supersymmetric Wilson-loops, protected operators and matrix models in $N = 4$ SYM*, *JHEP* **08** (2009) 061 [arXiv:0905.1943] [INSPIRE].

[15] A. Bassetto, L. Griguolo, F. Pucci, D. Seminara, S. Thambyahpillai and D. Young, *Correlators of supersymmetric Wilson loops at weak and strong coupling*, *JHEP* **03** (2010) 038 [arXiv:0912.5440] [INSPIRE].

[16] M. Bonini, L. Griguolo and M. Preti, *Correlators of chiral primaries and 1/8 BPS Wilson loops from perturbation theory*, *JHEP* **09** (2014) 083 [arXiv:1405.2895] [INSPIRE].

[17] S. Giombi, R. Ricci and D. Trancanelli, *Operator product expansion of higher rank Wilson loops from D-branes and matrix models*, *JHEP* **10** (2006) 045 [hep-th/0608077] [INSPIRE].

[18] J. Gomis, S. Matsuura, T. Okuda and D. Trancanelli, *Wilson loop correlators at strong coupling: From matrices to bubbling geometries*, *JHEP* **08** (2008) 068 [arXiv:0807.3330] [INSPIRE].

[19] D.E. Berenstein, R. Corrado, W. Fischler and J.M. Maldacena, *The Operator product expansion for Wilson loops and surfaces in the large N limit*, *Phys. Rev.* **D 59** (1999) 105023 [hep-th/9809188] [INSPIRE].

[20] N. Drukker, *Integrable Wilson loops*, *JHEP* **10** (2013) 135 [arXiv:1203.1617] [INSPIRE].

[21] A. Kapustin, *Wilson-'t Hooft operators in four-dimensional gauge theories and S-duality*, *Phys. Rev.* **D 74** (2006) 025005 [hep-th/0501015] [INSPIRE].

[22] D.M. McAvity and H. Osborn, *Energy momentum tensor in conformal field theories near a boundary*, *Nucl. Phys.* **B 406** (1993) 655 [hep-th/9302068] [INSPIRE].

[23] D.M. McAvity and H. Osborn, *Conformal field theories near a boundary in general dimensions*, *Nucl. Phys.* **B 455** (1995) 522 [cond-mat/9505127] [INSPIRE].

[24] M. Billò, V. Gonçalves, E. Lauria and M. Meineri, *Defects in conformal field theory*, *JHEP* **04** (2016) 091 [arXiv:1601.02883] [INSPIRE].

[25] A. Gadde, *Conformal constraints on defects*, arXiv:1602.06354 [INSPIRE].

JHEP03(2018)193

[26] M. Cooke, A. Dekel and N. Drukker, *The Wilson loop CFT: Insertion dimensions and structure constants from wavy lines*, *J. Phys.* **A 50** (2017) 335401 [arXiv:1703.03812] [INSPIRE].

[27] M. Kim, N. Kiryu, S. Komatsu and T. Nishimura, *Structure Constants of Defect Changing Operators on the* 1/2 *BPS Wilson Loop*, *JHEP* **12** (2017) 055 [arXiv:1710.07325] [INSPIRE].

[28] A. Cavaglià, N. Gromov and F. Levkovich-Maslyuk, *Quantum Spectral Curve and Structure Constants in* $N = 4$ *SYM: Cusps in the Ladder Limit*, arXiv:1802.04237 [INSPIRE].

[29] J. Teschner, *Exact results on* $N = 2$ *supersymmetric gauge theories*, arXiv:1412.7145.

[30] V. Pestun et al., *Localization techniques in quantum field theories*, *J. Phys.* **A 50** (2017) 440301 [arXiv:1608.02952] [INSPIRE].

[31] S.-J. Rey and T. Suyama, *Exact Results and Holography of Wilson Loops in* $N = 2$ *Superconformal (Quiver) Gauge Theories*, *JHEP* **01** (2011) 136 [arXiv:1001.0016] [INSPIRE].

[32] F. Passerini and K. Zarembo, *Wilson Loops in* $N = 2$ *Super-Yang-Mills from Matrix Model*, *JHEP* **09** (2011) 102 [*Erratum ibid.* **10** (2011) 065] [arXiv:1106.5763] [INSPIRE].

[33] J.G. Russo and K. Zarembo, *Localization at Large* N, in *Proceedings, 100th anniversary of the birth of I.Ya. Pomeranchuk (Pomeranchuk 100)*, Moscow, Russia, June 5–6, 2013, pp. 287–311 (2014) [DOI:10.1142/9789814616850_0015] [arXiv:1312.1214] [INSPIRE].

[34] D. Correa, J. Henn, J. Maldacena and A. Sever, *An exact formula for the radiation of a moving quark in* $N = 4$ *super Yang-Mills*, *JHEP* **06** (2012) 048 [arXiv:1202.4455] [INSPIRE].

[35] D. Correa, J. Maldacena and A. Sever, *The quark anti-quark potential and the cusp anomalous dimension from a TBA equation*, *JHEP* **08** (2012) 134 [arXiv:1203.1913] [INSPIRE].

[36] A. Lewkowycz and J. Maldacena, *Exact results for the entanglement entropy and the energy radiated by a quark*, *JHEP* **05** (2014) 025 [arXiv:1312.5682] [INSPIRE].

[37] B. Fiol, E. Gerchkovitz and Z. Komargodski, *Exact Bremsstrahlung Function in* $N = 2$ *Superconformal Field Theories*, *Phys. Rev. Lett.* **116** (2016) 081601 [arXiv:1510.01332] [INSPIRE].

[38] M. Bonini, L. Griguolo, M. Preti and D. Seminara, *Bremsstrahlung function, leading Lüscher correction at weak coupling and localization*, *JHEP* **02** (2016) 172 [arXiv:1511.05016] [INSPIRE].

[39] M. Baggio, V. Niarchos and K. Papadodimas, tt^* *equations, localization and exact chiral rings in* $4d$ $\mathcal{N} = 2$ *SCFTs*, *JHEP* **02** (2015) 122 [arXiv:1409.4212] [INSPIRE].

[40] M. Baggio, V. Niarchos and K. Papadodimas, *Exact correlation functions in* SU(2) $\mathcal{N} = 2$ *superconformal QCD*, *Phys. Rev. Lett.* **113** (2014) 251601 [arXiv:1409.4217] [INSPIRE].

[41] E. Gerchkovitz, J. Gomis and Z. Komargodski, *Sphere Partition Functions and the Zamolodchikov Metric*, *JHEP* **11** (2014) 001 [arXiv:1405.7271] [INSPIRE].

[42] M. Baggio, V. Niarchos and K. Papadodimas, *On exact correlation functions in* SU(N) $\mathcal{N} = 2$ *superconformal QCD*, *JHEP* **11** (2015) 198 [arXiv:1508.03077] [INSPIRE].

[43] M. Baggio, V. Niarchos, K. Papadodimas and G. Vos, *Large-N correlation functions in* $\mathcal{N} = 2$ *superconformal QCD*, *JHEP* **01** (2017) 101 [arXiv:1610.07612] [INSPIRE].

JHEP03(2018)193

[44] E. Gerchkovitz, J. Gomis, N. Ishtiaque, A. Karasik, Z. Komargodski and S.S. Pufu, *Correlation Functions of Coulomb Branch Operators*, *JHEP* **01** (2017) 103 [arXiv:1602.05971] [INSPIRE].

[45] D. Rodriguez-Gomez and J.G. Russo, *Large N Correlation Functions in Superconformal Field Theories*, *JHEP* **06** (2016) 109 [arXiv:1604.07416] [INSPIRE].

[46] D. Rodriguez-Gomez and J.G. Russo, *Operator mixing in large N superconformal field theories on S^4 and correlators with Wilson loops*, *JHEP* **12** (2016) 120 [arXiv:1607.07878] [INSPIRE].

[47] M. Billò, F. Fucito, A. Lerda, J.F. Morales, Ya.S. Stanev and C. Wen, *Two-point Correlators in $N = 2$ Gauge Theories*, *Nucl. Phys.* **B 926** (2018) 427 [arXiv:1705.02909] [INSPIRE].

[48] R. Andree and D. Young, *Wilson Loops in $N = 2$ Superconformal Yang-Mills Theory*, *JHEP* **09** (2010) 095 [arXiv:1007.4923] [INSPIRE].

[49] N.A. Nekrasov, *Seiberg-Witten prepotential from instanton counting*, *Adv. Theor. Math. Phys.* **7** (2003) 831 [hep-th/0206161] [INSPIRE].

[50] N. Nekrasov and A. Okounkov, *Seiberg-Witten theory and random partitions*, *Prog. Math.* **244** (2006) 525 [hep-th/0306238] [INSPIRE].

[51] E. Sysoeva, *Wilson loops and its correlators with chiral operators in $\mathcal{N} = 2, 4$ SCFT at large N*, arXiv:1712.10297 [INSPIRE].

[52] S. Giombi and S. Komatsu, *Exact Correlators on the Wilson Loop in $\mathcal{N} = 4$ SYM: Localization, Defect CFT and Integrability*, arXiv:1802.05201 [INSPIRE].

[53] E.I. Buchbinder and A.A. Tseytlin, *Correlation function of circular Wilson loop with two local operators and conformal invariance*, *Phys. Rev.* **D 87** (2013) 026006 [arXiv:1208.5138] [INSPIRE].

[54] M. Beccaria, S. Giombi and A. Tseytlin, *Non-supersymmetric Wilson loop in $\mathcal{N} = 4$ SYM and defect 1d CFT*, *JHEP* **03** (2018) 131 [arXiv:1712.06874] [INSPIRE].

JHEP03(2018)193

Bibliography

[1] T. Azeyanagi, F. Ferrari, P. Gregori, L. Leduc, and G. Valette, *More on the New Large D Limit of Matrix Models*, *Annals Phys.* **393** (2018) 308–326, [arXiv:1710.07263].

[2] M. Billo, F. Galvagno, P. Gregori, and A. Lerda, *Correlators between Wilson loop and chiral operators in $\mathcal{N} = 2$ conformal gauge theories*, *JHEP* **03** (2018) 193, [arXiv:1802.09813].

[3] J. D. Bekenstein, *Black holes and the second law*, *Lett. Nuovo Cim.* **4** (1972) 737–740.

[4] J. D. Bekenstein, *Black holes and entropy*, *Phys. Rev.* **D7** (1973) 2333–2346.

[5] J. M. Bardeen, B. Carter, and S. W. Hawking, *The Four laws of black hole mechanics*, *Commun. Math. Phys.* **31** (1973) 161–170.

[6] S. W. Hawking, *Particle Creation by Black Holes*, *Commun. Math. Phys.* **43** (1975) 199–220. [,167(1975)].

[7] G. 't Hooft and M. J. G. Veltman, *One loop divergencies in the theory of gravitation*, *Ann. Inst. H. Poincare Phys. Theor.* **A20** (1974) 69–94.

[8] M. H. Goroff and A. Sagnotti, *The Ultraviolet Behavior of Einstein Gravity*, *Nucl. Phys.* **B266** (1986) 709–736.

[9] V. E. Hubeny, *The AdS/CFT Correspondence*, *Class. Quant. Grav.* **32** (2015), no. 12 124010, [arXiv:1501.00007].

[10] G. T. Horowitz and J. Polchinski, *Gauge/gravity duality*, gr-qc/0602037.

[11] G. 't Hooft, *Dimensional reduction in quantum gravity*, *Conf. Proc.* **C930308** (1993) 284–296, [gr-qc/9310026].

[12] L. Susskind, *The World as a hologram*, *J. Math. Phys.* **36** (1995) 6377–6396, [hep-th/9409089].

[13] G. 't Hooft, *A Planar Diagram Theory for Strong Interactions*, *Nucl. Phys.* **B72** (1974) 461. [,337(1973)].

[14] J. Polchinski, *Tasi lectures on D-branes*, in *Fields, strings and duality. Proceedings, Summer School, Theoretical Advanced Study Institute in Elementary Particle Physics, TASI'96, Boulder, USA, June 2-28, 1996*, pp. 293–356, 1996. hep-th/9611050.

[15] D. Tong, *String Theory*, arXiv:0908.0333.

[16] J. Polchinski, *String Theory: Volume 1, An Introduction to the Bosonic String*. Cambridge Monographs on Mathematical Physics. Cambridge University Press, 1998.

[17] J. M. Maldacena, *The Large N limit of superconformal field theories and supergravity*, *Int. J. Theor. Phys.* **38** (1999) 1113–1133, [hep-th/9711200]. [Adv. Theor. Math. Phys.2,231(1998)].

[18] T. Banks, W. Fischler, S. H. Shenker, and L. Susskind, *M theory as a matrix model: A Conjecture*, *Phys. Rev.* **D55** (1997) 5112–5128, [hep-th/9610043]. [,435(1996)].

[19] N. Itzhaki, J. M. Maldacena, J. Sonnenschein, and S. Yankielowicz, *Supergravity and the large N limit of theories with sixteen supercharges*, *Phys. Rev.* **D58** (1998) 046004, [hep-th/9802042].

[20] J. Maldacena and A. Milekhin, *To gauge or not to gauge?*, arXiv:1802.00428.

[21] E. Berkowitz, M. Hanada, and J. Maltz, *A microscopic description of black hole evaporation via holography*, *Int. J. Mod. Phys.* **D25** (2016), no. 12 1644002, [arXiv:1603.03055].

[22] E. Berkowitz, E. Rinaldi, M. Hanada, G. Ishiki, S. Shimasaki, and P. Vranas, *Precision lattice test of the gauge/gravity duality at large-N*, *Phys. Rev.* **D94** (2016), no. 9 094501, [arXiv:1606.04951].

[23] G. Festuccia and H. Liu, *The Arrow of time, black holes, and quantum mixing of large N Yang-Mills theories*, *JHEP* **12** (2007) 027, [hep-th/0611098].

[24] G. Festuccia and H. Liu, *Excursions beyond the horizon: Black hole singularities in Yang-Mills theories. I.*, *JHEP* **04** (2006) 044, [hep-th/0506202].

[25] C. V. Vishveshwara, *Stability of the schwarzschild metric*, *Phys. Rev.* **D1** (1970) 2870–2879.

[26] W. H. Press, *Long Wave Trains of Gravitational Waves from a Vibrating Black Hole*, *Astrophys. J.* **170** (1971) L105–L108.

[27] G. T. Horowitz and V. E. Hubeny, *Quasinormal modes of AdS black holes and the approach to thermal equilibrium*, *Phys. Rev.* **D62** (2000) 024027, [hep-th/9909056].

[28] U. H. Danielsson, E. Keski-Vakkuri, and M. Kruczenski, *Black hole formation in AdS and thermalization on the boundary*, *JHEP* **02** (2000) 039, [hep-th/9912209].

[29] M. Kleban, M. Porrati, and R. Rabadan, *Poincare recurrences and topological diversity*, *JHEP* **10** (2004) 030, [hep-th/0407192].

[30] A. I. Larkin and Y. N. Ovchinnikov, *Quasiclassical Method in the Theory of Superconductivity*, .

[31] D. A. Roberts, D. Stanford, and L. Susskind, *Localized shocks*, *JHEP* **03** (2015) 051, [arXiv:1409.8180].

[32] J. Polchinski, *Chaos in the black hole S-matrix*, arXiv:1505.08108.

[33] J. Maldacena, S. H. Shenker, and D. Stanford, *A bound on chaos*, *JHEP* **08** (2016) 106, [arXiv:1503.01409].

[34] F. Ferrari, *Emergent Space and the Example of $AdS_5 \times S^5$*, *Nucl. Phys.* **B869** (2013) 31–55, [arXiv:1207.0886].

[35] F. Ferrari, M. Moskovic, and A. Rovai, *Examples of Emergent Type IIB Backgrounds from Matrices*, *Nucl. Phys.* **B872** (2013) 184–212, [arXiv:1301.3738].

[36] F. Ferrari and M. Moskovic, *Emergent D4-Brane Background from D-Particles*, *Phys. Lett.* **B723** (2013) 455–458, [arXiv:1301.7062].

[37] F. Ferrari and A. Rovai, *Emergent D5-brane Background from D-strings*, *Phys. Lett.* **B724** (2013) 121–126, [arXiv:1303.7254].

[38] F. Ferrari, *D-Brane Probes in the Matrix Model*, *Nucl. Phys.* **B880** (2014) 290–320, [arXiv:1311.4520].

[39] F. Ferrari and A. Rovai, *Gravity and On-Shell Probe Actions*, *JHEP* **08** (2016) 047, [arXiv:1602.07177].

[40] F. Ferrari, *Gauge Theories, D-Branes and Holography*, *Nucl. Phys.* **B880** (2014) 247–289, [arXiv:1310.6788].

[41] N. Iizuka and J. Polchinski, *A Matrix Model for Black Hole Thermalization*, *JHEP* **10** (2008) 028, [arXiv:0801.3657].

[42] N. Iizuka, T. Okuda, and J. Polchinski, *Matrix Models for the Black Hole Information Paradox*, *JHEP* **02** (2010) 073, [arXiv:0808.0530].

[43] F. Ferrari, *Black Hole Horizons and Bose-Einstein Condensation*, arXiv:1601.08120.

[44] B. Michel, J. Polchinski, V. Rosenhaus, and S. J. Suh, *Four-point function in the IOP matrix model*, *JHEP* **05** (2016) 048, [arXiv:1602.06422].

[45] A. Kitaev, "A simple model of quantum holography." KITP strings seminar and Entanglement 2015 program, 2015.

[46] S. Sachdev and J. Ye, *Gapless spin fluid ground state in a random, quantum Heisenberg magnet*, *Phys. Rev. Lett.* **70** (1993) 3339, [cond-mat/9212030].

[47] T. Castellani and A. Cavagna, *Spin-glass theory for pedestrians*, *Journal of Statistical Mechanics: Theory and Experiment* **2005** (2005), no. 05 P05012.

[48] S. Sachdev, *Bekenstein-Hawking Entropy and Strange Metals*, *Phys. Rev.* **X5** (2015), no. 4 041025, [arXiv:1506.05111].

[49] K. Bulycheva, *A note on the SYK model with complex fermions*, *JHEP* **12** (2017) 069, [arXiv:1706.07411].

[50] J. Maldacena and D. Stanford, *Remarks on the Sachdev-Ye-Kitaev model*, *Phys. Rev.* **D94** (2016), no. 10 106002, [arXiv:1604.07818].

[51] W. Fu, D. Gaiotto, J. Maldacena, and S. Sachdev, *Supersymmetric Sachdev-Ye-Kitaev models*, *Phys. Rev.* **D95** (2017), no. 2 026009, [arXiv:1610.08917]. [Addendum: Phys. Rev.D95,no.6,069904(2017)].

[52] E. Witten, *An SYK-Like Model Without Disorder*, arXiv:1610.09758.

[53] R. Gurau, *The 1/N expansion of colored tensor models*, *Annales Henri Poincare* **12** (2011) 829–847, [arXiv:1011.2726].

[54] V. Bonzom, R. Gurau, and V. Rivasseau, *Random tensor models in the large N limit: Uncoloring the colored tensor models*, *Phys. Rev.* **D85** (2012) 084037, [arXiv:1202.3637].

[55] R. Gurau, *The complete 1/N expansion of colored tensor models in arbitrary dimension*, *Annales Henri Poincare* **13** (2012) 399–423, [arXiv:1102.5759].

[56] V. Bonzom, R. Gurau, A. Riello, and V. Rivasseau, *Critical behavior of colored tensor models in the large N limit*, *Nucl. Phys.* **B853** (2011) 174–195, [arXiv:1105.3122].

[57] R. Gurau and J. P. Ryan, *Colored Tensor Models - a review*, *SIGMA* **8** (2012) 020, [arXiv:1109.4812].

[58] I. R. Klebanov and G. Tarnopolsky, *Uncolored Random Tensors, Melon Diagrams, and the SYK Models*, *Phys. Rev.* **D95** (2017), no. 4 046004, [arXiv:1611.08915].

[59] S. Carrozza and A. Tanasa, *$O(N)$ Random Tensor Models*, *Lett. Math. Phys.* **106** (2016), no. 11 1531–1559, [arXiv:1512.06718].

[60] F. Ferrari, *The Large D Limit of Planar Diagrams*, arXiv:1701.01171.

[61] R. Emparan, R. Suzuki, and K. Tanabe, *The large D limit of General Relativity*, *JHEP* **06** (2013) 009, [arXiv:1302.6382].

[62] R. Emparan and K. Tanabe, *Universal quasinormal modes of large D black holes*, *Phys. Rev.* **D89** (2014), no. 6 064028, [arXiv:1401.1957].

[63] S. Bhattacharyya, A. De, S. Minwalla, R. Mohan, and A. Saha, *A membrane paradigm at large D*, *JHEP* **04** (2016) 076, [arXiv:1504.06613].

[64] T. Azeyanagi, F. Ferrari, and F. I. Schaposnik Massolo, *Phase Diagram of Planar Matrix Quantum Mechanics, Tensor, and Sachdev-Ye-Kitaev Models*, *Phys. Rev. Lett.* **120** (2018), no. 6 061602, [arXiv:1707.03431].

[65] I. R. Klebanov and G. Tarnopolsky, *On Large N Limit of Symmetric Traceless Tensor Models*, *JHEP* **10** (2017) 037, [arXiv:1706.00839].

[66] R. Gurau, *The $1/N$ expansion of tensor models with two symmetric tensors*, *Commun. Math. Phys.* **360** (2018), no. 3 985–1007, [arXiv:1706.05328].

[67] A. Jevicki, K. Suzuki, and J. Yoon, *Bi-Local Holography in the SYK Model*, *JHEP* **07** (2016) 007, [arXiv:1603.06246].

[68] A. Georges, O. Parcollet, and S. Sachdev, *Quantum fluctuations of a nearly critical heisenberg spin glass*, *Phys. Rev. B* **63** (Mar, 2001) 134406.

[69] G. Sárosi, *AdS2 holography and the SYK model*, *PoS* **Modave2017** (2018) 001, [arXiv:1711.08482].

[70] J. Polchinski and V. Rosenhaus, *The Spectrum in the Sachdev-Ye-Kitaev Model*, *JHEP* **04** (2016) 001, [arXiv:1601.06768].

[71] F. Ferrari, V. Rivasseau, and G. Valette, *A New Large N Expansion for General Matrix-Tensor Models*, arXiv:1709.07366.

[72] F. Ferrari, *Partial Gauge Fixing and Equivariant Cohomology*, *Phys. Rev.* **D89** (2014), no. 10 105018, [arXiv:1308.6802].

[73] N. Beisert et al., *Review of AdS/CFT Integrability: An Overview*, *Lett. Math. Phys.* **99** (2012) 3–32, [arXiv:1012.3982].

[74] M. Bertolini, P. Di Vecchia, M. Frau, A. Lerda, R. Marotta, and I. Pesando, *Fractional D-branes and their gauge duals*, *JHEP* **02** (2001) 014, [hep-th/0011077].

[75] M. Bertolini, P. Di Vecchia, M. Frau, A. Lerda, and R. Marotta, *N=2 gauge theories on systems of fractional D3/D7 branes*, *Nucl. Phys.* **B621** (2002) 157–178, [hep-th/0107057].

[76] J. Polchinski, *N=2 Gauge / gravity duals*, *Int. J. Mod. Phys.* **A16** (2001) 707–718, [hep-th/0011193]. [,67(2000)].

[77] K. G. Wilson, *Confinement of Quarks*, *Phys. Rev.* **D10** (1974) 2445–2459. [,319(1974)].

[78] J. M. Maldacena, *Wilson loops in large N field theories*, *Phys. Rev. Lett.* **80** (1998) 4859–4862, [hep-th/9803002].

[79] K. Zarembo, *Supersymmetric Wilson loops*, *Nucl. Phys.* **B643** (2002) 157–171, [hep-th/0205160].

[80] J. K. Erickson, G. W. Semenoff, and K. Zarembo, *Wilson loops in N=4 supersymmetric Yang-Mills theory*, *Nucl. Phys.* **B582** (2000) 155–175, [hep-th/0003055].

[81] N. Drukker and D. J. Gross, *An Exact prediction of N=4 SUSYM theory for string theory*, *J. Math. Phys.* **42** (2001) 2896–2914, [hep-th/0010274].

[82] E. Witten, *Topological Quantum Field Theory*, *Commun. Math. Phys.* **117** (1988) 353.

[83] V. Pestun, *Localization of gauge theory on a four-sphere and supersymmetric Wilson loops*, *Commun. Math. Phys.* **313** (2012) 71–129, [arXiv:0712.2824].

[84] K. Hosomichi, $\mathcal{N} = 2$ *SUSY gauge theories on* S^4, *J. Phys.* **A50** (2017), no. 44 443010, [arXiv:1608.02962].

[85] S. Cremonesi, *An Introduction to Localisation and Supersymmetry in Curved Space*, *PoS* **Modave2013** (2013) 002.

[86] J. Teschner, *Exact Results on* $\mathcal{N} = 2$ *Supersymmetric Gauge Theories*, in *New Dualities of Supersymmetric Gauge Theories* (J. Teschner, ed.), pp. 1–30. 2016. arXiv:1412.7145.

[87] V. Pestun et al., *Localization techniques in quantum field theories*, *J. Phys.* **A50** (2017), no. 44 440301, [arXiv:1608.02952].

[88] T. Okuda and V. Pestun, *On the instantons and the hypermultiplet mass of N=2* super Yang-Mills on* S^4, *JHEP* **03** (2012) 017, [arXiv:1004.1222].

[89] N. A. Nekrasov, *Seiberg-Witten prepotential from instanton counting*, *Adv. Theor. Math. Phys.* **7** (2003), no. 5 831–864, [hep-th/0206161].

[90] N. Nekrasov and A. Okounkov, *Seiberg-Witten theory and random partitions*, *Prog. Math.* **244** (2006) 525–596, [hep-th/0306238].

[91] M. Baggio, V. Niarchos, and K. Papadodimas, *Exact correlation functions in $SU(2)\mathcal{N} = 2$ superconformal QCD*, *Phys. Rev. Lett.* **113** (2014), no. 25 251601, [arXiv:1409.4217].

[92] M. Baggio, V. Niarchos, and K. Papadodimas, *tt^* equations, localization and exact chiral rings in 4d $\mathcal{N}$ =2 SCFTs*, *JHEP* **02** (2015) 122, [arXiv:1409.4212].

[93] E. Gerchkovitz, J. Gomis, and Z. Komargodski, *Sphere Partition Functions and the Zamolodchikov Metric*, *JHEP* **11** (2014) 001, [arXiv:1405.7271].

[94] E. Gerchkovitz, J. Gomis, N. Ishtiaque, A. Karasik, Z. Komargodski, and S. S. Pufu, *Correlation Functions of Coulomb Branch Operators*, *JHEP* **01** (2017) 103, [arXiv:1602.05971].

[95] J. Gomis and N. Ishtiaque, *Kähler potential and ambiguities in 4d $\mathcal{N}$ = 2 SCFTs*, *JHEP* **04** (2015) 169, [arXiv:1409.5325]. [JHEP04,169(2015)].

[96] D. Rodriguez-Gomez and J. G. Russo, *Large N Correlation Functions in Superconformal Field Theories*, *JHEP* **06** (2016) 109, [arXiv:1604.07416].

[97] D. Rodriguez-Gomez and J. G. Russo, *Operator mixing in large N superconformal field theories on S^4 and correlators with Wilson loops*, *JHEP* **12** (2016) 120, [arXiv:1607.07878].

[98] M. Billo, F. Fucito, A. Lerda, J. F. Morales, Ya. S. Stanev, and C. Wen, *Two-point Correlators in N=2 Gauge Theories*, *Nucl. Phys.* **B926** (2018) 427–466, [arXiv:1705.02909].

[99] S.-J. Rey and J.-T. Yee, *Macroscopic strings as heavy quarks in large N gauge theory and anti-de Sitter supergravity*, *Eur. Phys. J.* **C22** (2001) 379–394, [hep-th/9803001].

[100] D. E. Berenstein, R. Corrado, W. Fischler, and J. M. Maldacena, *The Operator product expansion for Wilson loops and surfaces in the large N limit*, *Phys. Rev.* **D59** (1999) 105023, [hep-th/9809188].

[101] N. Drukker, D. J. Gross, and H. Ooguri, *Wilson loops and minimal surfaces*, *Phys. Rev.* **D60** (1999) 125006, [hep-th/9904191].

[102] R. Andree and D. Young, *Wilson Loops in N=2 Superconformal Yang-Mills Theory*, *JHEP* **09** (2010) 095, [arXiv:1007.4923].

[103] G. W. Semenoff and K. Zarembo, *More exact predictions of SUSYM for string theory*, *Nucl. Phys.* **B616** (2001) 34–46, [hep-th/0106015].

[104] V. Pestun and K. Zarembo, *Comparing strings in AdS(5) x S**5 to planar diagrams: An Example*, *Phys. Rev.* **D67** (2003) 086007, [hep-th/0212296].

[105] N. I. Usyukina and A. I. Davydychev, *Exact results for three and four point ladder diagrams with an arbitrary number of rungs*, *Phys. Lett.* **B305** (1993) 136–143.